KU Leuven
Biomedical Sciences Group
Faculty of Medicine
Department of Neuroscience
Laboratory of proteolytic mechanisms
mediating neurodegeneration

KU LEUVEN

DOCTORAL SCHOOL
BIOMEDICAL SCIENCES

MECHANISTIC INSIGHTS INTO THE FOUNDATIONS OF ALZHEIMER'S DISEASE PATHOGENESIS AND ITS VALUE FOR THERAPEUTIC DEVELOPMENT

Dieter PETIT

Dissertation presented in partial fulfilment of the requirements for the degree of Doctor in Biomedical Sciences

Jury:

Supervisor:	Prof. Lucía Chávez-Gutiérrez
Chair examining committee:	Prof. Tassos Economou
Chair public defense:	Prof. Patrick Dupont
Jury members:	Prof. John Hardy
	Prof. Matthew Freeman
	Prof. Chris Ulens
	Prof. Joost Schymkowitz

September 2020

Acknowledgements

"Even the smallest (French translation: le plus **petit**) person can change the course of the future." With these words, Galadriel encouraged Frodo Baggins to believe that no matter how hard the challenge may seem, any person can make the difference if he/she is willing to commit to overcome it (in the book "the lord of the rings" by J.R.R. Tolkien). With this thought in mind, I decided to start a PhD in the field of Alzheimer's disease, one of the most challenging medical conditions in modern day societies, with the ambition to make a difference for science as well as for patients. Similar to Frodo, however, I was not alone in this "quest". Therefore, I would like to give special thanks to all the members of my "fellowship".

First of all, I would like to like to thank my promoter Lucia. Your mentorship has undoubtedly shaped me to the scientist I am today. You taught me to not only think about the current question, but also the next questions and that curiosity will take your science to the next level. I still did not figure out where you keep getting all your ideas from, but they have served as a major source of inspiration during my PhD. I would also like to thank my former co-supervisor Bart De Strooper, for giving me the opportunity to start my scientific career in his lab and in that way allowing all the amazing things I have experienced during my PhD. Furthermore, I would like to thank the jury members of my thesis. My internal jury members, professors Chris Ulens and Joost Schymkowitz for their critical and supportive evaluation of my performance and progress during the PhD. My external jury members, professors John Hardy and Matthew Freeman: I'm truly honoured that you dedicated your time to evaluate my work and shared your expert opinions on its broader impact.

Special thanks goes out to all the current and past members of the 'LCG' lab. Together we philosophized (about science and many other topics), laughed and shared difficult moments. All of you have made this PhD such a unique experience. Sam – my 'lunch buddy', thank you for sharing your wisdom about cloning, prepping, purifying … and football. I wish you all the best in your coaching aspirations and your further career in the lab. Maria – thank you for being a true friend and a source of both

inspiration and information (about the 'ins and outs' of the lab). I already miss being 'infected' by your excitement upon learning important updates in the field. Matthias – I do not know whether I should define you as a scientist or a cook. Anyway, thank you for allowing me to 'degust' from your many ideas/hypotheses as well as your culinary escapades. Kasia – your warm and kind personality far exceeds your physical stature. Thank you for all your spontaneous help with analysing/interpreting complex data and revising my first paper as well as my thesis manuscript. Ivica – your 'no nonsense' attitude of working inspired me to focus on the 'essentials' of my own work. Thank you for teaching me about the complex but fascinating world of structural biology. Thomas – thanks for sharing some tips and tricks to make 3D plots in R as well as enlightening me about the power of mass spectrometry. Sara, Laetitia, Ruggiero and Jonathan – my conclusion in the lab is your start, may your journeys be as interesting and fruitful as mine.

Of course, my PhD did not restrict itself to the borders of the LCG lab. Therefore, I would like to thank all the people from the VIB/KUL with whom I interacted throughout these past 5 years. Certain persons merit a special mention. Sulieman and Sriram – my two other regular lunch companions. Thank you for many amusing discussions and expanding my cultural perception of the world (through sharing your thoughts about the latest series/movies/documentaries as well as obscure conspiracy theories). Dries – the 'creative centipede' of the department, thank you for your help in the lab and sharing your sometimes hard to believe travel adventures. Isabel and Eliane – thank you for the administrative support throughout the years. An, Annerieke, Katleen, Katrien, Leen, Lutgarde, Tom, Yessica – thank you for your advice about experiments and the small talk during endless hours of cell culture.

I would also like to express my deepest gratitude to my family and friends for their relentless support. My friends – Nathan, Bert, Nicolas, Lien, Bart, Michael and Stef, thank you for helping me to take my mind of science and PhD struggles when necessary and replacing it with fun and laughter. My family 'in law' – Hilde, Louis, Inez, Jarne, Natasja and Andy, thank you for giving me such a warm welcome into your

family and allowing me to become a part of the amazing Rock Werchter festival community. My family – Myriam, Koen, Cedric, Lotte and Sarah, thank you for showing me the immense value and strength of a close family bond which has shaped me to be the person I am today. Our book of memorable family moments is already richly filled, but I hope to write many more chapters together with you. I would like to give a very special thanks to my parents for igniting my passion for science throughout my youth and therefore being the driving force behind my scientific career.

Finally – my wife Liesbeth, THE most significant 'achievement' of my PhD. You gave this PhD experience a completely new dimension. Thank you so much for your never ending support and being so considerate when I again came home late from work. I can honestly say that you have kept me going through the difficult moments that are inherent to each PhD. Together with you I feel ready to face any future challenge that will cross our path.

I would like to close this word of thanks the way I opened it, with a suitable quote from the books of Tolkien: "Don't adventures ever have an end? I suppose not. Someone else always has to carry on the story." I hope the same applies for the results of my scientific PhD research, as the 'quest' to cure/treat Alzheimer's disease is far from complete.

Dieter

Table of Contents

Table of Contents 6
List of abbreviations 8
Synopsis 10
Samenvatting 13
1 Introduction 16
1.1 Alzheimer's disease 16
1.2 Sporadic AD 17
1.3 The "cause" of SAD: a pleiotropy of theories 19
1.4 Autosomal dominant (familial) AD 20
1.4.1 Proteolytic processing of APP 21
1.4.2 The γ-secretase complex, a member of the iCLIP family 24
1.4.2.1 GSEC: a dynamic multimeric complex in the membrane 24
1.4.2.2 The complex cleavage scheme of GSEC processing of APP 27
1.4.3 How do pathogenic mutations in *PSEN/APP* lead to early-onset AD? 28
1.4.3.1 APP mutations highlight Aβ as driver of pathogenesis 29
1.4.3.2 How does secreted Aβ trigger disease? 30
1.5 AD clinical trials targeting Aβ: a path of failures or a road to success? 32
1.5.1 Strategies targeting Aβ clearance 32
1.5.2 Strategies targeting Aβ production 33
1.5.3 What did we learn from the clinical trials? 34
2 Aims of the thesis 36
3 Extracellular interface between APP and Nicastrin regulates Aβ length and response to γ-secretase modulators 38
3.1 Synopsis 39
3.2 Abstract 39
3.3 Introduction 40
3.4 Materials and methods 42
3.5 Results 48
3.6 Discussion 66
3.7 Supplementary figures 72
3.8 Acknowledgements and author contributions 78
4 Aβ profiles generated by Alzheimer's disease-causing *PSEN1* variants determine pathogenicity and linearly correlate with disease onset 79
4.1 Abstract 80
4.2 Introduction 80

4.3 Materials and methods 83
4.4 Results 86
4.5 Discussion 96
4.6 Supplementary figures 101
4.7 Acknowledgements and author contributions 103
5 Characterization of the binding pocket and mode of interaction of γ-secretase stabilizers 104
5.1 Abstract 105
5.2 Introduction 105
5.3 Materials and methods 107
5.4 Results 112
5.5 Discussion 131
5.6 Supplementary figures 135
5.7 Acknowledgements and author contributions 140
6 General discussion 142
6.1 The APP N-terminal anchor secures GSEC-APP/Aβn stability 142
6.2 The molecular 'footprint' of a FAD *PSEN1* mutation: link with AD onset 145
6.3 Stabilizing GSEC-APP/Aβn interaction: a novel strategy for AD therapy 149
6.4 A critical reflection of using a FAD model to study AD pathogenesis 152
7 Conclusions 154
8 References 155
9 Acknowledgements, Personal Contribution and Conflict of Interest statements 184
9.1 Scientific acknowledgements 184
9.2 Personal contributions 185
9.3 Conflict of interest 186
10 Curriculum Vitae 187

List of abbreviations

AAO – Age At Alzheimer's disease Onset
Aβ – Amyloid-β
AβO – Amyloid-β Oligomer
ACH – Amyloid Cascade Hypothesis
AD – Alzheimer's Disease
ADAD – Autosomal Dominant Alzheimer's Disease
ADAM – Proteins containing A Disintegrin and A Metalloprotease domain
AICD – APP Intracellular Domain
ANOVA – ANalysis Of VAriance
APOE – Apolipoprotein E
APH1 – Anterior Pharynx defective 1
APP – Amyloid Precursor Protein
BACE – β-site APP Cleaving Enzyme 1
BBB – Blood-Brain Barrier
BMPS – N-β-MaleimidoPropyl-oxySuccinimide ester
BME –β-MercaptoEthanol
CAA – Cerebral Amyloid Angiopathy
CHAPSO – 3-([3-Cholamidopropyl]dimethylammonio)-2-hydroxy-1-propane sulfonate
CI – Confidence Intervals
CSF – Cerebrospinal Fluid
CTF – Carboxy-Terminal Fragment
dKO – Double Knock-out
DDM – n-Dodecyl β-D-Maltoside
DMEM – Dulbecco's Modified Eagle Medium
DMSO – DiMethylSulfOxide
E – Enzyme
EDTA – EthyleneDiamine Tetraacetic Acid
ELISA – Enzyme-Linked ImmunoSorbent Assay
EOAD – Early Onset Alzheimer's Disease
FAD – Familial Alzheimer's Disease
FBS – Fetal Bovine Serum
FDG-PET – Fluorodeoxyglucose (18F) Position Emission Tomography
GFP – Green Fluorescent Protein
GOF – Gain Of Function
GSEC – γ-Secretase
GSI – γ-Secretase Inhibitor
GSM – γ-Secretase Modulator

GSS – γ-Secretase Stabilizer
GWAS – Genome-Wide Association Study
HEK – Human Embryonic Kidney
iPSC – Induced Pluripotent Stem Cell
kDa – kilo Dalton
KO – Knock-Out
LOAD – Late-Onset Alzheimer's Disease
LOF – Loss Of Function
MAB – Monoclonal Antibody
Mb – Membrane
MD – Molecular Dynamics
MEF – Mouse Embryonic Fibroblast
MES – 2-(N-Morpholino)EthaneSulfonic acid
MMPBSA – Molecular Mechanics Poisson-Boltzmann Surface Area (MMPBSA)
MSD – Meso Scale Discovery
MW – Molecular Weight
NCT – Nicastrin
NGS – Next Generation Sequencing
NFT – NeuroFibrillary Tangle
NTF – N-Terminal Fragment
PBS – Phosphate Buffered Saline
PCR – Polymerase Chain Reaction
PEN-2 – Presenilin Enhancer 2
PI – Protease Inhibitors
PIPES – PIPerazine-N, N'-bis(2-EthaneSulfonic acid)
PSEN – Presenilin
S – Substrate
SAD – Sporadic Alzheimer's Disease
sAPPα – soluble APP N-terminal fragment generated by cleavage at the α-site
sAPPβ – soluble APP N-terminal fragment generated by cleavage at the β-site
SCAM – Substituted Cysteine Accessibility Method
SD – Standard Deviation
SDM – Site-Directed Mutagenesis
SDS-PAGE – Sodium Dodecyl Sulfate PolyAcrylamide Gel Electrophoresis
SNP – Single Nucleotide Polymorphism
TMD – Transmembrane Domain
VaD – Vascular Dementia
WES – Whole Exome Sequencing
WGS – Whole Genome Sequencing
WT – Wild Type

Synopsis

γ-Secretases (GSECs) are a family of multimeric intramembrane proteases involved in a wide variety of physiological processes and implicated in Alzheimer's disease (AD). Presenilin (PSEN, catalytic subunit), Nicastrin (NCT), Presenilin Enhancer 2 (PEN-2) and Anterior Pharynx Defective 1 (APH1) are essential subunits of GSECs. The identification of AD-causing mutations in *PSEN1/2* and the Amyloid Precursor Protein (*APP*) genes, encoding the catalytic subunit of the APP cleaving enzyme (GSEC) and the substrate from which amyloid-β (Aβ) peptides are generated, respectively, has provided the basis for the amyloid cascade hypothesis. This hypothesis proposes that toxic Aβ triggers AD.

State-of-the-art:

Discovery of AD-linked mutations in *PSEN1/2* and *APP* enabled the generation of genetically-validated models of the molecular mechanisms operating in AD pathogenesis. It has been shown that these mutations destabilize GSEC-APP/Aβn interactions during the sequential GSEC proteolytic cleavage on APP, and thus enhance the production of longer, incompletely "digested" Aβ peptides, which may elicit neurotoxicity.

Aims of the research:

I Elucidation of the molecular strategies that stabilize GSEC-APP/Aβn during the sequential proteolysis

II Characterization of the molecular composition of secreted Aβ profiles generated by pathogenic GSEC variants and definition of its relationship with the age at AD onset (AAO)

III Determination of the mode of action and the binding pocket of GSEC modulators (GSMs)

Results and discussion:

I) Based on previous data from the laboratory, we proposed that an extracellular interaction between the APP substrate (S) and the GSEC enzyme (E) secures the E-S assembly during the sequential cleavage process. Guided by the novel GSEC structures, we hypothesized that NCT ectodomain (residues 240-245) interacts with the N-terminal part of APP, and that this interaction stabilizes the protease-substrate complex. Our studies reveal that a short-range (~ 2Å) interaction between the NCT ectodomain and APP_{C99} (residue Lys28) critically influences the stability of GSEC-APP/Aβn assemblies, and thereby modulates Aβ product length. The data thus uncover a key, active role for the NCT subunit in the regulation of APP processing and suggests a link between potential, yet to be discovered, single nucleotide variants in *NCSTN* and AD risk.

II) The magnitude of the destabilizing effects that AD-linked *PSEN1* mutations exert on the stability of GSEC-APP/Aβn correlates linearly with the AAO. Here, we hypothesized that the changes in the molecular composition of Aβ profiles generated by AD-causing variants drive the disease. Our analysis of a set of *PSEN1* familial AD (FAD) causing mutations, associated with a broad AAO range, showed a remarkable linear correlation between the molecular composition of secreted Aβ profiles (Aβ(38+40)/(42+43) ratio) and AAO. Therefore, the Aβ(38+40)/(42+43) ratio may serve as an indicator of the pathogenicity of novel, potential FAD-causing *PSEN1* mutations and can be used for the interpolation of the AAO in their carriers.

III) GSEC modulators (GSMs) lower Aβ42 production. Despite their relevance as potential therapeutics, their mode of action and binding pocket remain unknown. Based on the published data and our recent findings, we hypothesized that GSMs target the GSEC (NCT-PSEN)-APP interface and stabilize the E-S interactions. Guided by structural data, we performed extensive functional analysis and *in silico* molecular dynamics (MD) simulations to challenge this hypothesis. Our studies located the binding pocket of potent GSMs/GSEC stabilizers and defined their binding mode. Our ongoing

efforts focus on the elucidation of the structural mechanisms underlying their modulatory effects.

Conclusions:

The work conducted in this thesis identified a crucial extracellular "anchor" in GSEC-APP/Aβn assemblies that governs their stability and regulates the length of Aβn peptides produced. Moreover, it demonstrated that this "anchor" represents the target of (stabilizing) compounds, known to allosterically modulate the GSEC mediated cleavage of APP and alter Aβn length. Finally, the uncovered correlation between the Aβ(38+40)/(42+43) ratio and the AAO of AD-linked *PSEN1* variants strongly supports that a shift in Aβ production – towards longer (≥ Aβ42) peptides – drives AD pathogenesis. Collectively, these studies provide substantial new insights into the molecular mechanisms underlying AD pathogenesis and provide a solid basis for future structure-based drug discovery efforts aiming at developing safe therapeutics to tackle AD.

Samenvatting

γ-Secretases (GSECs) zijn een familie van multimere intramembraanproteasen betrokken in een breed scala aan fysiologische processen alsook in de ziekte van Alzheimer (AD). Preseniline (PSEN, katalytische subeenheid), Nicastrin (NCT), “Presenilin Enhancer 2” (PEN-2) en “Anterior Pharynx Defective 1” (APH1) zijn de essentiële subeenheden van GSEC. De identificatie van AD-veroorzakende mutaties in de genen coderend voor PSEN1/2 en het Amyloïde precursor eiwit (APP), respectievelijk het enzym en het substraat verantwoordelijk voor de productie van amyloïde-β (Aβ) peptiden, vormde de basis voor de amyloïde cascade hypothese. Deze hypothese veronderstelt dat de ophoping van toxisch Aβ peptiden in de hersenen aanleiding geeft tot AD.

State-of-the-art:

AD-gelinkte mutaties in PSEN1/2 en APP bieden een uniek model om de moleculaire mechanismen te bestuderen die opereren in de pathogenese van AD. Het is aangetoond dat deze mutaties GSEC-APP/Aβn-interacties destabiliseren tijdens de sequentiële proteolytische splitsing van APP door GSEC. Dit bevordert de productie van langere, onvolledig "verteerde" Aβ peptiden die, zoals wordt aangenomen, neurotoxiciteit opwekken.

Doelstellingen van het onderzoek:

I Opheldering van de moleculaire strategieën die GSEC-APP/Aβn stabiliseren tijdens het sequentiële klievingsproces

II Karakterisering van de moleculaire samenstelling van Aβ-profielen gegenereerd door pathogene GSEC-varianten en hun link met de aanvangsleeftijd van de eerste ziektesymptomen (AAO)

III Bepalen van het werkingsmechanisme en de bindingsplaats van GSEC-modulatoren (GSMs)

Resultaten en discussie:

I) Op basis van eerdere resultaten van onze onderzoeksgroep nemen we aan dat een extracellulaire interactie tussen het APP-substraat en GSEC verantwoordelijk is voor hun interactiestabiliteit tijdens het sequentiële klievingsproces. Geleid door de nieuwe GSEC-structuren, stelden we voor dat het NCT-ectodomein (residuen 240-245) interageert met het N-terminale deel van APP om zo het protease-substraatcomplex te stabiliseren. Onze studies demonstreren dat een interactie op korte afstand (~ 2Å) tussen het NCT-ectodomein en APP_{C99} (residu Lys28) de stabiliteit van GSEC-Aβn-assemblages kritisch beïnvloedt en daardoor de lengte van de Aβ peptiden moduleert. Deze gegevens wijzen dus op een belangrijke, actieve rol voor NCT bij de regulatie van APP-klieving en suggereren een verband tussen genetische mutaties in *NCSTN* en AD-risico.

II) De mate van destabilisatie die AD-gelinkte PSEN1 mutaties uitoefenen op het GSEC-APP/Aβn complex correleert op lineaire wijze met hun AAO. Hierdoor vermoeden we dat de veranderingen in de moleculaire samenstelling van Aβ-profielen gegenereerd door AD-veroorzakende varianten aan de basis liggen van pathogenese. Onze analyses van een reeks gekende PSEN1 FAD-mutaties, geassocieerd met een breed AAO bereik, onthullen een opmerkelijke correlatie tussen de moleculaire samenstelling van Aβ-profielen (zoals weergegeven door de Aβ(38+40)/(42+43) ratio) en AAO. Bovendien tonen onze studies aan dat deze correlatie kan worden gebruikt om de AAO van nieuwe FAD PSEN1-mutaties te voorspellen.

III) GSEC-modulatoren (GSMs) verlagen de productie van Aβ42, dewelke wordt aanzien als een van de belangrijkste boosdoeners voor AD. Ondanks hun relevantie als mogelijke therapeutica, hebben we een onduidelijk beeld van hun werkingsmechanisme en de bindingsplaats van deze moleculen in het complex. Op basis van eerder gepubliceerde studies en onze recente bevindingen, veronderstelden we dat GSMs de GSEC (NCT-PSEN)-APP interface viseren om de GSEC-APP interactie te stabiliseren. Geleid door de inzichten van de gepubliceerde GSEC atomaire structuren, hebben we een uitgebreide functionele analyse uitgevoerd in combinatie met computersimulaties

om deze hypothese te valideren. Deze studies leidde tot de identificatie van de bindingsplaats van potente GSEC-stabilisatoren en de definitie van een mogelijke bindingsmodus. Onze huidige inspanningen zijn gericht op het ophelderen van de mechanismen die ten grondslag liggen aan de modulerende effecten van de moleculen.

Conclusies:

Het werk dat in dit proefschrift is uitgevoerd, identificeerde een cruciaal extracellulair "anker" in GSEC-APP/Aβn-assemblages dat hun stabiliteit regelt en de lengte reguleert van de Aβ peptiden die worden geproduceerd. Bovendien toont het aan dat dit "anker" het doelwit is van (stabiliserende) compounds, die GSEC gemedieerde splitsing van APP moduleren op een allosterische wijze en zo de lengte van Aβ peptiden bepalen. Voorts geeft het ontdekte verband tussen de Aβ(38+40)/(42+43) ratio en de AAO van AD-gelinkte PSEN1 mutaties aan dat de omschakeling in Aβ-productie – naar de langere (≥ Aβ42) peptiden – de pathogenese van AD stimuleert. Collectief geven deze studies substantiële nieuwe inzichten in de moleculaire mechanismen die ten grondslag liggen aan de pathogenese van AD en bieden ze een solide basis voor toekomstige inspanningen gericht op het ontwikkelen van veilige therapieën om AD aan te pakken.

1 Introduction

1.1 Alzheimer's disease

"Eine eigenartige Erkrankung der Hirnrinde" (a peculiar disease of the cerebral cortex) [1] is the first-ever mentioning of the devastating, progressive neurodegenerative disorder, nowadays known as Alzheimer's disease (AD). In this seminal publication, Dr. Alois Alzheimer describes the microscopical analysis of the brain autopsy that he had performed on Auguste Deter in 1906, 5 years after she was admitted to the psychiatric hospital in Frankfurt (Germany). The autopsied brain tissue revealed the presence of abnormal extracellular and intracellular clumps and bundles of fibres, which are now known as amyloid-β (Aβ) plaques [2,3] and neurofibrillary tangles (NFTs) [4–6], respectively. Nowadays, more than 100 years later, AD represents the leading cause of dementia, with over 50 million affected people worldwide, and no disease-modifying therapy. In fact, AD is a huge social and economic problem (WHO stats) and one of the biggest challenges of modern societies [7].

Longitudinal studies of AD patients have revealed an exceptionally long preclinical (or prodromal) phase of 10 to even 20 years [8,9]. During this preclinical phase, progressive deposition of Aβ peptides occurs. This is followed by synaptic dysfunction, neuroinflammation, tau pathology and neurodegeneration [10–12] (**Figure 1.1**). A 'cellular' phase of AD [13] bridges the gap between the early biochemical phase of the disease (i.e. accumulation and spreading of the pathology) and its (late) clinical stage. The 'cellular' phase highlights the contribution of the failure of the vascular system as well as the different brain cell types (neurons, microglia, astroglia and oligodendrocytes) to the disease progression. According to this view, this phase explains the long, silent incubation period of AD as it accounts for the complex compensatory mechanisms that are able to maintain brain homeostasis for decades despite the ongoing build-up of toxic aggregates. Only when these compensatory mechanisms start to fail, irreversible pathological changes are set as a prelude for the clinical phase of the disease [13].

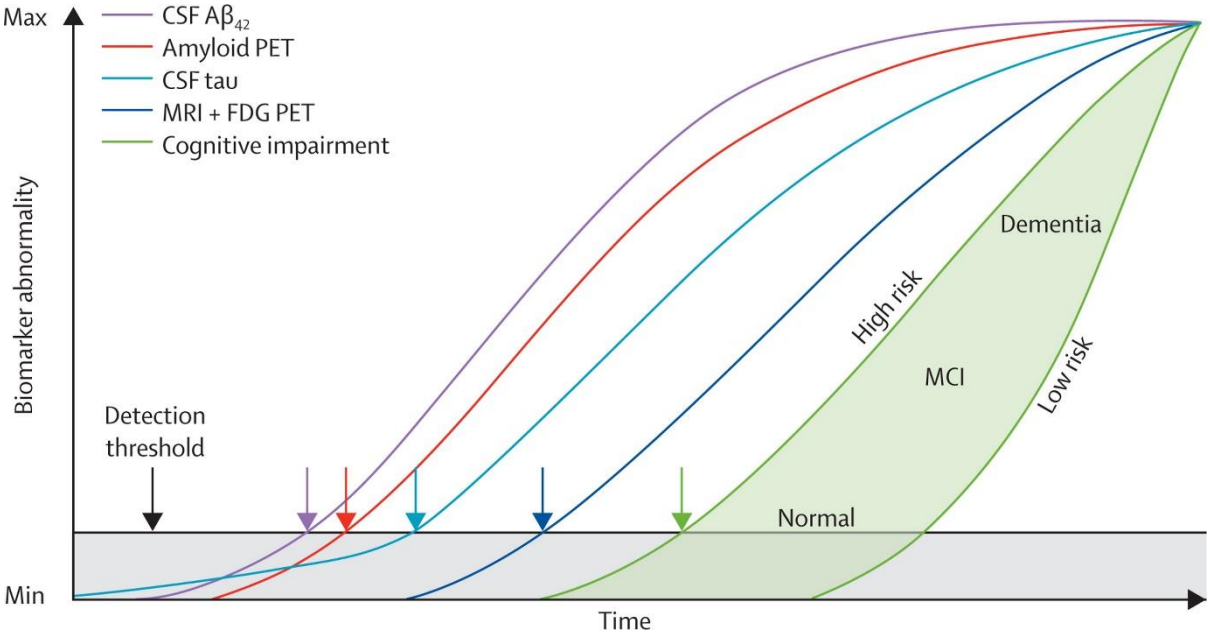

Figure 1.1 Hypothetical model of dynamic biomarkers of the Alzheimer's disease pathological cascade (adapted from [9] with permission). Up to 20 years before the first symptoms emerge, Aβ accumulation starts to ramp up in the brain of AD patients. Through a yet unidentified mechanism, this event triggers tau pathology with concomitant neuronal dysfunction and loss. Accumulation of Aβ can be followed as an early biomarker of the disease by monitoring the drop of Aβ42 levels in the cerebrospinal fluid (CSF) as well as by Positron Emission Tomography (PET) imaging of aggregated Aβ species in the brain. A couple of years before the first symptoms of the disease (mild cognitive impairment, MCI) manifest, magnetic resonance imaging (MRI) and fluorodeoxyglucose (FDG) PET inform about the ongoing process of neurodegeneration and regional deficits in cerebral metabolic rates of glucose respectively.

1.2 Sporadic AD

Although pathologically and clinically similar, two forms of AD can be distinguished. The most common form, termed sporadic AD (SAD), encompasses 99% of all AD cases. SAD is considered a multifactorial disorder, with genetic [14], lifestyle [15] and environmental [16]) factors contributing to its pathogenesis. However, the most pronounced SAD risk factor is age, with the probability of developing SAD-related dementia doubling every 5-6 years above the age of 60 [17,18]. Less than 1% of the total AD cases are caused by mutations, inherited in an autosomal dominant manner, in 3 genes: amyloid precursor protein (*APP*), presenilin 1 (*PSEN1*) and presenilin 2

(*PSEN2*). This form of the disease manifests in general before the age of 65. Familial AD (FAD) or autosomal dominant AD (ADAD), is further discussed in section 1.4.

Interestingly, SAD also has a strong genetic component. Large twin studies have predicted that the heritability of SAD (known also as late-onset AD (LOAD)) is as high as 79% [19]. The first genetic AD risk factor identified was the apolipoprotein E (*APOE*) gene polymorphism. This gene, located on chromosome 19q13, encodes 3 distinct APOE isoforms: the APOE ε4 form (population frequency: 7.5-15.6% [20]) is a major AD risk factor [21–25], the rare (6.7-10%) APOE ε2 form is a (potential) protective factor [26–29] and the most common APOE ε3 form (75.3-82.8%) is a "neutral" factor. In addition, a recent meta-analysis on AD genome-wide association studies (GWAS) have pointed to 24 other risk loci, primarily involved in APP metabolism, immunity, lipid processing and endocytosis [14] (**Figure 1.2**). Most of these loci have much smaller effect sizes (typically with odds ratios (OR) between 0.8 and 1.3) than *APOE4* (OR: ~3.3) [14]. Only, the rs75932628 (R47H) single nucleotide polymorphism (SNP) in the triggering receptor expressed on myeloid cells 2 (*TREM2*) gene has a similar OR as *APOE4*, but as it represents a rare variant, its population attributable risk is much smaller than that of the *APOE4* allele [30].

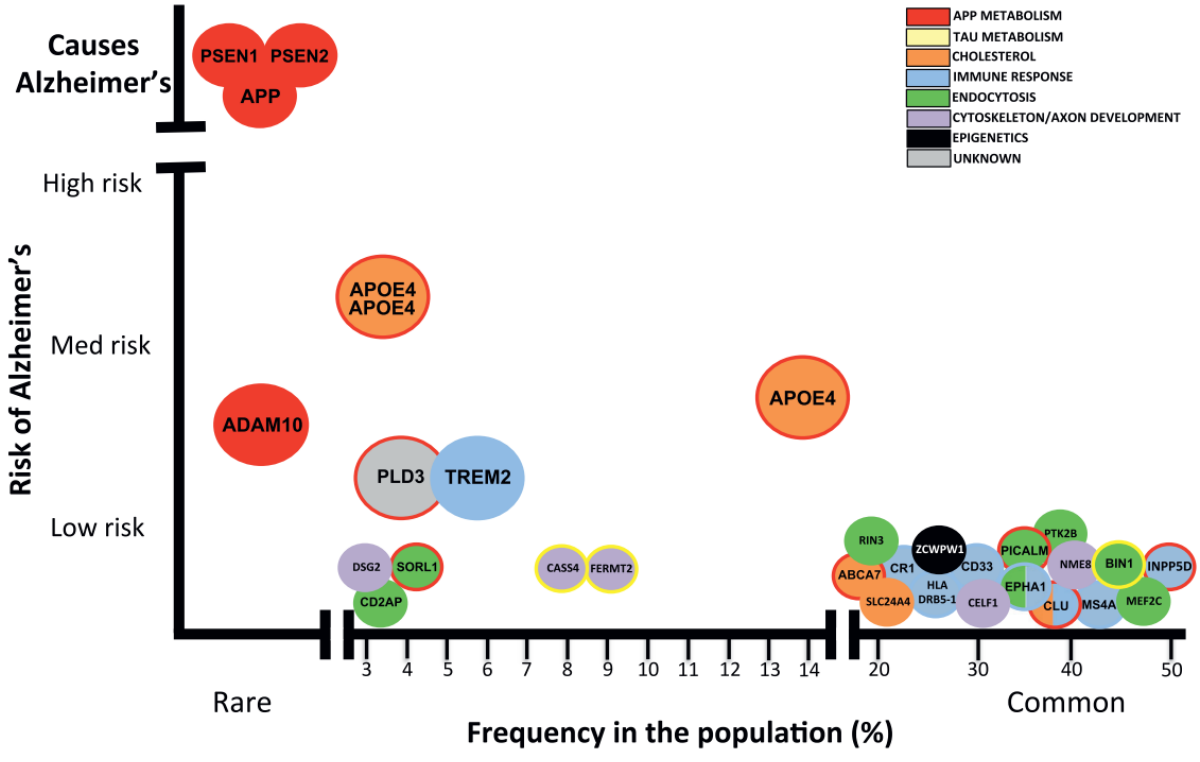

Figure 1.2 Common and rare variants contributing to AD risk. (adapted from [31] with permission). The identified risk loci for AD can be grouped into 4 major categories, based on cellular pathways: APP metabolism, lipid (cholesterol) metabolism, immune response and endocytosis. It is noteworthy that APOE serves important functions in more than one of these pathways. This provides a potential explanation of the major influence of *APOE4* on AD risk.

1.3 The "cause" of SAD: a pleiotropy of theories

Ever since its discovery, scientists have dedicated their research to establish "the" cause of AD. This has led to the proposal of multiple, non-exclusive hypotheses, each based on a certain set of observations. These include, but are not limited to, the: infection (reviewed in [32]), cholinergic [33], calcium [34], oxidative stress (reviewed in [35]), amyloid-cascade [36–38], tau (discussed in [39], vascular [40], mitochondrial-cascade [41] and damage signal [42] hypotheses. This pleiotropy of theories likely arises from the multifactorial nature and the complexity of AD.

The most widely accepted and genetically/biochemically supported hypothesis is the amyloid cascade hypothesis (ACH), which states that 'toxic' Aβ in the brain triggers a cascade of events ultimately leading to the clinical presentation of AD [36–38]. The strongest evidence for this theory stems from genetics, namely the identification of the AD-causing mutations in the genes encoding the machinery responsible for the production of Aβ peptides (discussed in section 1.4). In addition, it has been shown that APOE modulates Aβ aggregation and clearance in an isoform-dependent manner (reviewed in [43,44]). The latter provides a direct link between the high AD risk attributed to the *APOE4* allele and Aβ pathology. Of note, the link between APOE and Aβ 'toxicity' seems to extend beyond its influence on Aβ aggregation/clearance. This is evidenced by a remarkable case in which a FAD patient with pronounced Aβ pathology remained cognitively normal until her 70s due to the presence of a rare variant in the *APOE* gene [45].

According to the ACH, Aβ accumulation leads to abnormal hyperphosphorylation of tau protein which results in its deposition into NFTs [5,46]. This is supported by work in mice and cell lines showing that human tau is required for some of the Aβ-mediated neuronal damage associated with the disease. As well as by the

observations showing that mutations affecting Aβ aggregation exacerbate tau tangle formation. Of note, the inverse is not seen [47]. However, how Aβ induces tau pathology *in vivo* in the context of AD remains to be elucidated.

Despite the indisputable genetic evidence, the ACH has met considerable criticism (reviewed in [48,49]), mainly stemming from the following observations: amyloid is found in the brains of elderly people with normal cognition [50]; there is a lack of correlation between the amyloid plaque burden and disease severity [51]; AD mouse models overexpressing mutant human PSEN1 and/or APP, despite profound Aβ accumulation, do not recapitulate human AD pathology, in terms of NFTs and neuronal cell death [52] (https://www.alzforum.org/research-models/alzheimers-disease); many Aβ targeting drug clinical trials have failed (further discussed in section 1.5). However, for all these critiques counterarguments have been raised (discussed in [53]). Importantly, over the years, the ACH has received important updates based on novel findings in the field. The discovery of (water-)soluble Aβ aggregates in AD patient brains [54,55] as potently neurotoxic assemblies [56], the presence of which correlates better with AD symptoms than plaque load [57,58], led to the revision of the ACH [59,60]. The revised ACH embraces the concept that toxic Aβ oligomers trigger pathogenic cascades eventually leading to cellular degeneration and death (reviewed in [53,61]). This paradigm shift has elicited an intensive search for "the" toxic Aβ oligomer and its mechanism of toxicity (reviewed in [62,63]).

1.4 Autosomal dominant (familial) AD

Because of the complex nature of SAD, many scientists have focused their research on the autosomal dominant form of AD as it offers a genetically validated model to study the disease pathogenesis at the molecular level. Importantly, apart from the distinct age at onset (AAO), FAD and SAD are pathologically/clinically similar [64], which justifies the use of FAD models in a broad AD context. FAD was discovered in dementia-affected families that presented with rare, fully penetrant mutations leading to AD symptom onset at early stages in life (usually before the age of 65) (**Figure 1.2**). The mutations were found in the *PSEN1* and *PSEN2* genes (located on chromosome 14 and 1, respectively) [65–68], each encoding different isoforms of the catalytic subunit of the

γ-secretase complex (GSEC) [69–72]. So far, close to 300 AD-causing missense mutations have been found in *PSEN1* (clinical onset ranges from 23 to 65) and about 15 mutations in *PSEN2* (clinical onset ranges from 45 to 70) [73]. In addition, about 30 FAD-causing missense mutations have been identified in the *APP* gene (located on chromosome 21) [74,75] (clinical onset ranges from 30 to 70) [73].

The implication of APP in early-onset AD has been further revealed by the observation of AD symptoms in Down syndrome patients (trisomy 21 results in an extra copy of the *APP* gene) [2] as well as in families carrying *APP* gene duplications [76]. Furthermore, a large genetic study in cognitively healthy elderly individuals in the Icelandic population revealed the presence of an AD-protective variant in *APP* (rs63750847, A673T) [77], providing further support to the critical involvement of APP metabolism in the disease pathogenesis. The fact that AD-causing mutations have been found in GSEC and APP, respectively the protease and the substrate responsible for the generation of Aβ peptides, strongly supports the causal role of Aβ at the early stages of AD.

1.4.1 Proteolytic processing of APP

APP protein is an integral type I membrane glycoprotein with a large extracellular domain and a short cytoplasmic tail (reviewed in [78]). Research conducted in the late 1980's unravelled that alternative splicing of the APP gene results in the expression of 3 different isoforms (APP695, APP751 and APP770) [79–83]. The APP695 isoform is predominantly expressed in neurons, while the APP-751/770 ones are found mostly in peripheral tissues. The main difference between these isoforms is the lack of the domain homologous to Kunitz protease inhibitors (KPI) in the APP695 isoform [84,85]. After synthesis in the endoplasmic reticulum (ER), APP matures through N- and O-linked glycosylation, phosphorylation and sulfation [84,86] and is transported via the secretory pathway to the plasma membrane [86–88]. APP can undergo sequential proteolysis by α- and γ-secretases in the so-called non-amyloidogenic pathway. The disintegrin and metalloproteinase domain-containing protein 10 (ADAM10) is the major α-secretase in the brain, although other proteins from this family have also been described to exert α-secretase activity [89–91]. ADAM10-mediated cleavage of APP releases a soluble N-

terminal (sAPPα) and the membrane-associated C-terminal (CTFα /APP_{C83}) fragments. While sAPPα has been proposed to play a neurotrophic role [92–96] and be important for memory and neuronal survival [97,98], very little is known about the role of CTFα/APP_{C83}. In the acidic environment of endolysosomal compartments, the amyloidogenic processing of APP by β- and γ-secretases is favoured [99–104]. β-secretase shedding of APP in the brain is mediated predominantly by BACE1 [105–108]. A homologous protein called BACE2 also exerts β-secretase activity [109,110], but BACE2 is mainly expressed in the periphery [111] and is present in low amounts in the brain [112,113]. Nevertheless, recent data suggest a role of BACE2 as a dose-sensitive AD-suppressor gene [114].

β-Secretase cleavage of APP results in the release of sAPPβ and C-terminal membrane-associated APP_{C99} or APP_{C89} fragments (β-site and β'-site cleavage, respectively). Despite being only 16 amino acids shorter, sAPPβ lacks the neuroprotective properties that have been associated with sAPPα [115–117]. Instead, the sAPPβ appears to be critically involved in the pruning of synapses during neuronal development [118]. Recently, a novel function for both sAPPs has been described, in which they modulate synaptic transmission through interaction with $GABA_B$ receptor [119]. Similarly to CTFα, the functions of CTFβ are unclear. Several studies have described a toxic effect for CTFβ (reviewed in [120]). However, whether this toxicity is due to CTF itself or its proteolytically derived fragments remains to be elucidated. It is striking though that the extra 16 amino acids from the N-terminus of APP_{C99} in Aβ can result in neurotoxicity, yet can be neurotrophic when appended to the C-terminus of sAPP (i.e. sAPPα vs sAPPβ) [120].

In addition to these "canonical" pathways of APP proteolysis (Figure 1.3), "non-canonical" pathways have been described. These involve δ-secretase-, η-secretase- and mephrin-β-mediated cleavages (reviewed in [121]). The pathophysiological relevance of these cleavages is unclear, but a study by Willem et al. has indicated that the production of Aη-peptides (derived from η-secretase cleavage) could contribute to neurodegeneration [122].

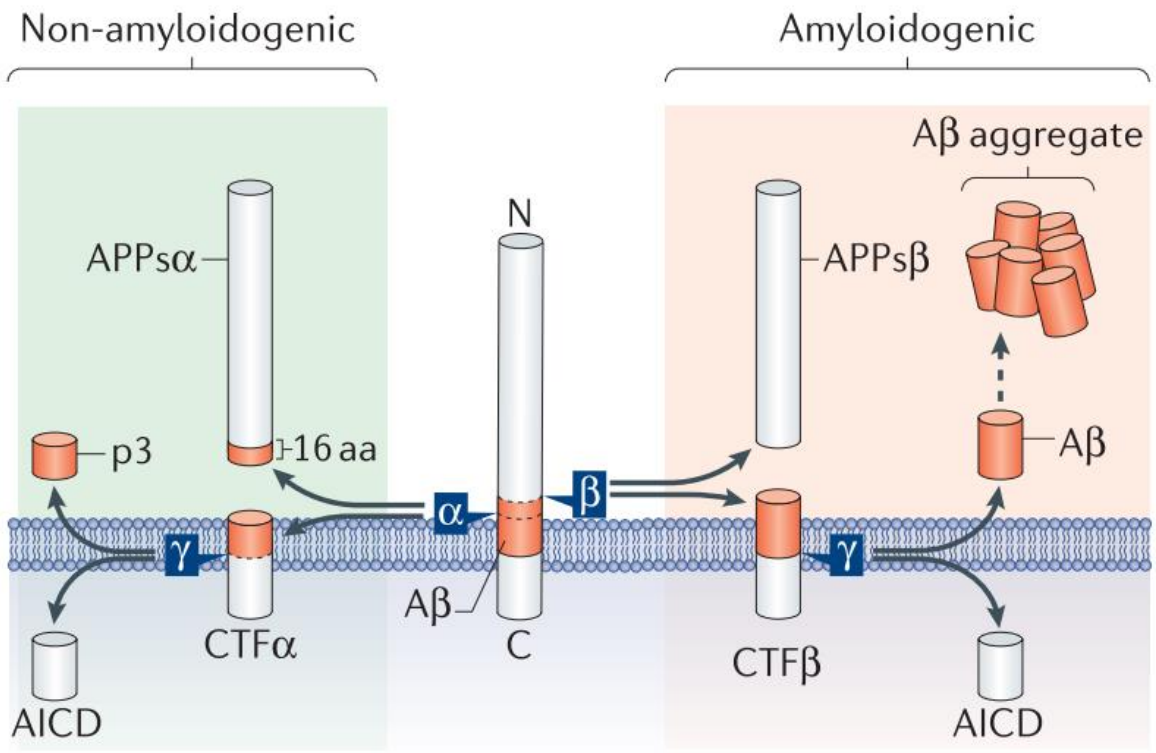

Figure 1.3 The canonical pathway of APP proteolytic processing (adapted from [78] with permission). Processing of APP along the non-amyloidogenic (green background) or amyloidogenic (orange background) pathway is dictated by the initial shedding of full-length APP by α-secretase or β-secretase, respectively. This shedding results in the release of a soluble fragment (sAPPα/sAPPβ) and a membrane-bound fragment (APP_{C83}/APP_{C99}) that is subjected to further processing by γ-secretase. This process leads to the release of the Amyloid-β (Aβ) peptides (shown in red) in the case of APP_{C99} or P3 peptides for APP_{C83} along with the production of intracellular fragments (APP intracellular domains (AICDs)).

Once APP has its ectodomain shedded, it becomes a substrate for GSEC, which further processes the membrane-bound CTFs (i.e. $APP_{C83/C99}$), yielding APP intracellular domains (AICDs) and N-terminal products of different length (P3/Aβ peptides) (**Figure 1.3**). The AICD may translocate to the nucleus to regulate transcription [123–125]. The physiological and pathophysiological role of the 3 kDa P3 peptides (i.e. Aβ17–X) is not well known. As they have been isolated from diffuse amyloid deposits in AD brains [126] and are known to contain the sequences critical for neurotoxicity, they are expected to exhibit a certain degree of toxicity. One study indeed showed that Aβ17–42 induces apoptosis in cultured cells, albeit at a lower potency than

Aβ1-42 [127]. In contrast, the Aβ(1-X) peptides have received greater interests and their production is discussed below (section 1.4.2.2) in detail.

1.4.2 The γ-secretase complex, a member of the iCLIP family

Two decades ago, a novel class of membrane-embedded proteases was discovered. These peculiar enzymes create an aqueous environment within the membrane and catalyse the hydrolysis of transmembrane domains (reviewed in [128,129]). Based on their proteolytic mechanisms, four classes of intramembrane cleaving proteases (iCLIPs) can be distinguished: zinc metalloproteases, known as Site-2-Proteases (S2Ps) [130]; serine proteases called rhomboids [131]; glutamate proteases [132] and aspartyl proteases. The latter class can be further subdivided into a GSEC (PSEN) family of aspartyl iCLIPs and a signal peptide peptidase (SPP) family (comprising the SPPs, its homologues and SPP-like (SPPL) proteases [133,134]). Both GSECs and SPPs share three conserved motifs (i.e. "Y**D**", "GXG**D**" and "PAL"), essential for their proteolytic activity, but have different active site topologies, determining distinct substrate pools (type I vs type II transmembrane proteins) (further discussed in [135]). One other crucial difference is that SPP family members function as soloists or in pairs (homodimers) [133,136,137], while GSECs/PSENs need to assemble with 3 other subunits (GSEC complex) to exert proteolytic activity.

1.4.2.1 GSEC: a dynamic multimeric complex in the membrane

GSECs are multimeric complexes consisting of PSEN1 or 2, Nicastrin (NCT), Presenilin enhancer 2 (PEN-2) and Anterior pharynx defective 1 (APH1A or B) [138–141] (**Figure 1.4**). The presence of two different genes coding for PSEN (*PSEN1* and *PSEN2*) and two genes for APH1 (*APH1A* and *APH1B*) in the human genome results in at least four different GSEC complexes in humans. These distinct GSECs are differentially present in tissues [142,143], have heterogeneous biochemical properties [144–146] and contribute differentially to Aβ production [147].

The assembly of the GSEC complex occurs in a stepwise fashion in the endoplasmatic reticulum (ER), where it is initiated by the formation of a (short-lived) NCT-APH1 subcomplex [148–150]. The next intermediary steps could involve the

individual association of PSEN and PEN-2 to the NCT-APH1 subcomplex or the preformation of a PEN-2/PSEN subcomplex [151]. The final step in the maturation process is the autocatalytic endoproteolysis of PSEN, occurring in the large cytosolic loop (between TMD6 and TMD7). The autoproteolysis generates PSEN N-terminal and C-terminal fragments (NTFs and CTFs) and results in an active pentameric complex [152]. The absence of any of the subunits results in the rapid degradation of the others or their retention in ER [153,154].

As mentioned earlier, PSEN contains the catalytic centre of the enzyme, while the other subunits of the protease serve as essential cofactors, necessary for the proper assembly, the activation, the structural stability and the trafficking of the complex [155]. PEN-2 plays a crucial role in PSEN endoproteolysis [156,157] and in the regulation of the stability and the trafficking of the complex [158,159]. The APH1 subunit serves a main role as complex stabilizer [139], but has also been suggested to exert an 'allosteric-like' role in regulating proteolytic activity [146]. Finally, the largest subunit of the complex (NCT), featured by a heavily glycosylated ectodomain, has been implicated in the recognition and the selection of substrates [160,161]. However, the role of NCT as the "substrate receptor" [160] has been challenged by functional studies [162,163]. Data generated in the context of my PhD studies provide insights into the functional role of NCT in the regulation of the GSEC-mediated cleavage [164].

Electron microscopy (EM) analysis of GSEC has offered the first snapshots of the complex architecture of the protease. Low-resolution studies have revealed that GSEC has a dynamic conformational landscape, influenced by *PSEN1* mutations and GSEC inhibitors and modulators (GSIs and GSMs) [165–167]. The elucidation of the GSEC structure at (near) atomic resolution [168–171] by milestone single-particle cryo-electron microscopy (cryo-EM) has revealed a horseshoe-like arrangement of the 20 TMDs of the GSEC subunits with the large ectodomain of NCT interacting with both ends of the horseshoe (**Figure 1.4**). The previously generated X-ray crystallography of the NCT subunit [172] has facilitated the near-atomic structural analysis.

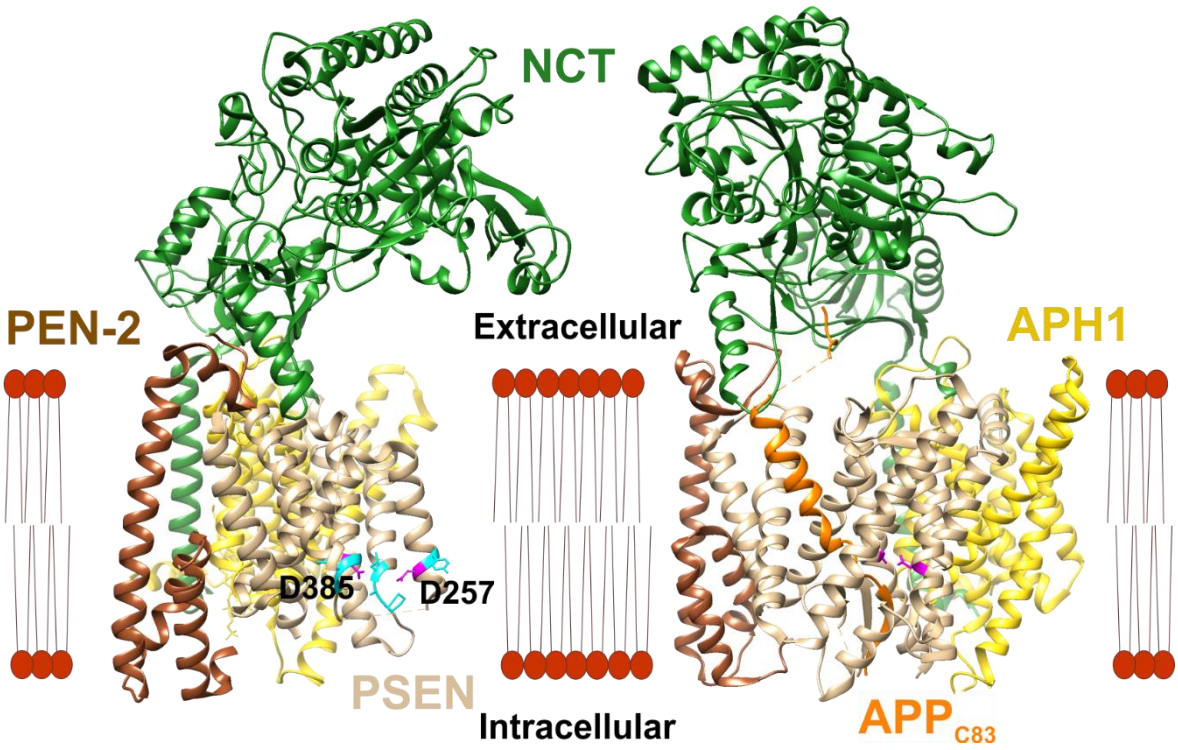

Figure 1.4: GSEC atomic structure and orientation in the membrane.
Cryo-EM resolved atomic structures of the GSEC (PSEN1/APH1A) protease. The left structure displays a side-view of the apo-form (PDB: 5A63) [170] while the right structure represents a (front-view of the) co-structure of GSEC in complex with the APP_{C83} peptide (PDB: 6IYC) [173]. Color scheme: PSEN1 is shown in tan, PEN-2 in dark brown, APH1A in gold, NCT in green and APP substrate in orange. The "YD", "GXGD" and "PAL" motifs are colored in cyan, with the catalytic residues (D257A and D385) highlighted in magenta.

In agreement with the previous studies [166,167,174], in the structural analysis, the complex, and especially the PSEN subunit, has adopted a metastable fold [171]. Interestingly, one of the resolved cryo-EM structures has presented GSEC in complex with an unidentified helical peptide, hinting at the potential location of the substrate-binding site. This site was confirmed to be the substrate-binding site by structural analysis of the GSEC in complex with Notch [175] or APP_{C83} [173]. These structures have unveiled in high resolution how GSEC and substrate engage in the initial endopeptidase 'ε E-S' complex. However, how the substrate is recruited to this site is unclear, with both experimental [176] as well as *in silico* simulation studies [177] suggesting multiple substrate entry pathways.

1.4.2.2 The complex cleavage scheme of GSEC processing of APP

The GSEC protease family exhibits broad substrate specificity with close to a hundred potential membrane-associated substrates described so far (all type I membrane proteins) [178]. An open question in the field is how GSECs select their substrates. The lack of obvious sequence homology or common motifs among substrates has led to the proposal that dynamic features in the transmembrane regions of the substrates play a key role. Previous analyses have established a short ectodomain [161,179] and a 'permissive' transmembrane and intracellular substrate domains [180] as substrate requirements for GSECs.

The large pool of substrates involves GSEC-mediated proteolysis in a wide variety of physiological processes, vital for embryonic development, normal functioning of the central nervous system (CNS) and the immune system (reviewed in [181,182]). Pathogenic mutations (in *PSEN1/2*, *NCSTN* and *PSENEN*) have also highlighted its role in at least 5 different pathologies. These include AD, frontotemporal dementia (FTD) [183], *acne inversa* – a chronic inflammatory skin disorder – [184,185], dilated cardiomyopathy [186] and breast cancer [187]. Of note, it has been proposed that PSEN may play several γ-secretase independent functions, including regulation of ER calcium homeostasis, cell signalling, lysosomal functions and autophagy (reviewed in [188]).

Nevertheless, the proteolytic function of PSEN/GSEC has received the greatest attention, with the proteolytic cleavage of APP [69] and Notch [189,190] being the most studied. In-depth characterization of the GSEC-mediated cleavage of APP has revealed a rather unique mechanism, in which sequential cuts 'digest' the transmembrane domain of the substrate [191–194] (**Figure 1.5**). The efficiency of the first endopeptidase (ε-) cleavage determines the overall GSEC activity and this ε-cut yields a membrane-bound APP-derived fragment (i.e. a 48-49 amino acid long Aβ peptide in the case of APP_{C99}) and a soluble APP intracellular domain (AICD). The long Aβ fragment undergoes further sequential GSEC carboxypeptidase-like (γ) cleavages. This processive mechanism ultimately releases an Aβ peptide to the luminal/extracellular environment. The number of sequential γ-cuts defines the length of the Aβ product.

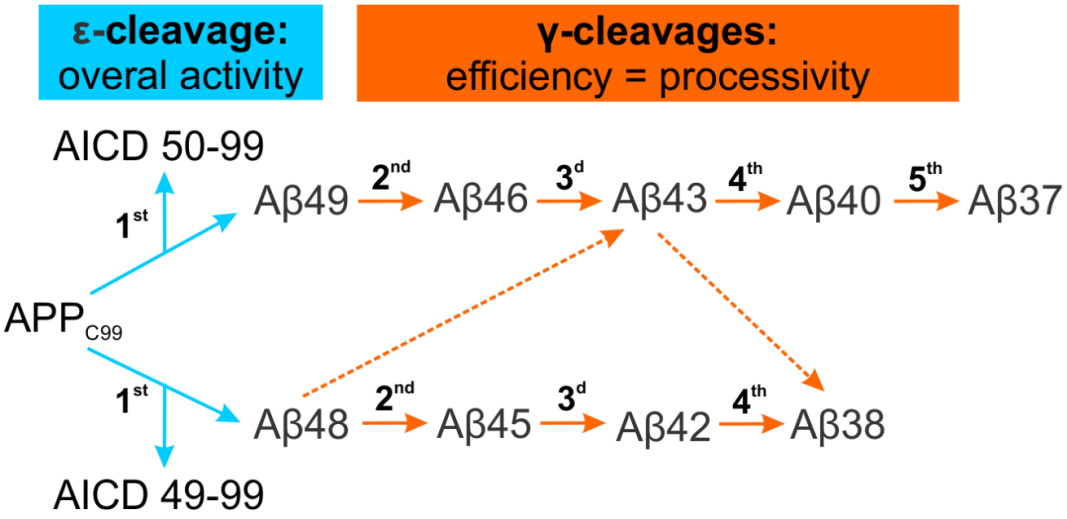

Figure 1.5: The complex cleavage scheme of APP_{C99} processing by GSEC. (Adapted from [164]). The first endopeptidase (ε-) cleavage of APP_{C99} by GSEC generates the APP intracellular domain (AICD50-99 or AICD49-99) and an Aβ substrate (Aβ48 or Aβ49, respectively) that stays bound to the protease and is subjected to sequential (γ)-cleavages along 2 dominant product lines. Work from Matsumura and colleagues has however shown that there is also some "cross-over" between them [195].

1.4.3 How do pathogenic mutations in *PSEN/APP* lead to early-onset AD?

Ever since their discovery, scientists have tried to unravel the molecular mechanisms behind the pathogenic effect of *PSEN/APP* mutations. Although the GSEC independent functions of PSEN (see section 1.4.2.2) could be contributing to AD pathogenesis, the lack of a consistent effect of *PSEN1/2* mutations on these functions speaks against a causal role [196]. In addition, considering that *APP* mutations also lead to AD, the causal mechanism is likely rooted in the impact of *PSEN* mutations on the proteolytic activity of GSEC towards APP.

The gain of "toxic" function (GOF) concept suggests that *PSEN1/2* mutations result in the increased production of Aβ42(43) species, which are highly fibrillogenic [197,198], and thus prone to aggregation. Many *in vitro* and *in vivo* FAD models [199–206], as well as studies in FAD patients [207], have demonstrated an increased Aβ42(43) production relative to Aβ40 (often illustrated by the Aβ42/40 ratio). However, several studies highlighted that an increased Aβ42/40 ratio is actually often related to a decrease in Aβ40 production rather than increased Aβ42 levels [208–213].

Alternatively, in the loss-of-function (LOF) hypothesis, impaired PSEN/GSEC function – leading to disrupted intracellular signalling pathways – is regarded as "the" disease-causing factor, with (relative) increments in Aβ42 levels dismissed as a mere bystander effect [210]. A number of observations, however, question a simple LOF mechanism. Firstly, the LOF of PSEN does not explain why *APP* mutations/duplications lead to the same disease/phenotype. Secondly, patients with hereditary forms of *acne inversa* – which present with missense/nonsense mutations in *NCSTN*, *PSENEN* or *PSEN1/2* leading to haploinsufficiency of these subunits (i.e. true LOF of GSEC) [184,185] – develop Notch related phenotypes and lack AD symptoms. Finally, carriers of *PSEN1* mutations that show the strongest reductions in GSEC activity (e.g. R278I and L435F) [214,215] present AD symptoms relatively late (please refer to Alzforum, PSEN1 mutation database).

Using the terms GOF and LOF in a sequential processing mechanism is, however, confusing as "gain" of one peptide is inevitably linked to the "loss" of another. Kinetic profiling of GSEC-mediated cleavage efficiency has shown that FAD-linked *PSEN1/2* mutations variably affect (including no effect) the initial GSEC-mediated endopeptidase (ε) cleavage, but exert a consistent impairment on the γ-cleavage efficiency (GSEC processivity) of APP [216]. This reduced processivity enriches the Aβ profiles for the production of longer (> Aβ40) species at the expense of the shorter (≤ Aβ40) forms [216,217], and has been termed as GSEC 'dysfunction' [216]. A recent study has shown that FAD-linked impaired GSEC processivity is due to the mutant-induced destabilization of GSEC-APP/Aβn (enzyme-substrate, E-S) interactions. This destabilization promotes the premature release of partially digested (i.e. longer) Aβ peptides [218].

1.4.3.1 APP mutations highlight Aβ as driver of pathogenesis

In general, we can distinguish two categories of *APP* mutations: missense variants and genomic duplications encompassing the *APP* gene. About 25 duplications of variable size have so far been described in 25 different families (http://www.molgen.vib-ua.be/ADMutations database [183]). As this type of mutations do not alter the APP protein structure nor affect APP properties, their pathogenic effect can be explained by a gene-dosage mechanism (i.e. higher expression of APP leading to

increased abundance of its derived products). In addition, considering that FAD-causing mutations in APP, such as the APPSwe (KM670-671NL) variant [219], increase APP_{C99} levels through the stimulation of BACE cleavage of APP, while the AD-protective APP (APP/Aβ A673T/A2T) variant promotes the generation of APP_{C83} [77], promotion of the amyloidogenic pathway (**Figure 1.3**) appears to be sufficient to cause AD. However, only a subset of *APP* mutations influences the steady-state levels of APP_{C99}, thus indicating that such an effect is not required for pathogenesis [196].

Alternatively, increased self-aggregation of Aβ peptides into (soluble) oligomers that convey toxicity has been commonly viewed as a potential disease-causing mechanism (reviewed in [220]). Aβ aggregation can be modulated through a direct mechanism, in which the *APP* mutations, located in the Aβ sequence, alter the biophysical properties of the Aβ peptides to favour their aggregation [221], or through an indirect mechanism, when the mutations shift the Aβ production from shorter towards longer, aggregation-prone Aβ species [218]. Our understanding of the pathogenic mechanisms of *APP* missense mutations is still incomplete. Systematic analysis of the impact of *APP* mutations on APP_{C99} proteolytic processing as well as Aβ aggregation propensity and (neuro)toxicity weighted against AAO in their carriers, will be invaluable to advance this field [196].

1.4.3.2 How does secreted Aβ trigger disease?

As its name alludes, amyloid-β peptides have the natural tendency to adopt the amyloid state. Proteins may enter the amyloid state when certain segments in its backbone get exposed, permitting them to couple into hydrogen bonds with other protein chains and leading to their assembly into fibrils adopting a cross-β-sheet conformation [222,223]. Although monomeric Aβ species are natively disordered, they display conformational fluctuations that can lead to (partially) folded states prone to self-assembly into high-order structures that create a structural and dynamic continuum [224–226]. Aβ oligomerization is considered a "nucleation-and-growth" processes, in which the formation of the nucleus or seed is the rate-limiting step [222]. After the nucleation phase, Aβ assembles into (proto)fibrils through a series of intermediate aggregation states. The soluble Aβ oligomer (AβO) intermediates are considered as the major drivers of AD

pathology (see above). However, it is still unclear what specific AβOs are toxic and through which assembly pathway they are generated. One hypothesis postulates that AβOs represent "off-pathway" species distinct from those species "on-pathway" to fibril formation [227]. Alternative hypotheses propose that toxic AβOs are mainly formed by a secondary nucleation process from monomers attaching to the surface of existing fibrils (fibril-seeded model) [228,229], or that AβOs first deposit into diffused plaques that gradually decompose into freely diffusible toxic species (amyloid plaque buffering hypothesis) [230].

With regard to how "toxic" AβOs trigger AD pathology, one straightforward mechanism of toxicity is that AβOs initiate cell damage through direct physiochemical interaction with neuronal membranes, for example by inserting in the lipid bilayer thereby disrupting its integrity. However, such a model does not account for the specificity of AβO attachment to specific cell types (i.e. selective vulnerability) and its observed binding saturability [231]. Alternatively, the receptor hypothesis regards AβOs as gain-of-function pathogenic ligands that bind adventitiously to specific proteins acting as toxin receptors (reviewed in [63]). The involvement of one or multiple high-affinity receptors became clear through experiments in which cells treated with trypsin lost their ability to bind AβOs and those showing that very low concentrations of AβOs (~ nM) are sufficient to elicit neurotoxicity [56]. A myriad of AβO receptors has so far been described, with the cellular prion protein (PrPc) being the most studied one [232]. AβO interaction with those receptors may induce a series of downstream events resulting in mitochondrial dysfunctions, tau phosphorylation and synaptic impairments (reviewed in [233]).

As research related to Aβ has mainly focused on its pathogenic role in AD (see section 1.4.3), the relevance of Aβ for normal physiology has been somewhat overshadowed. The physiological functions of Aβ have mostly been linked to preserving proper brain function through regulating synaptic function, promoting recovery from brain injury and "plugging" leaks in the blood-brain barrier (BBB) (reviewed in [234]). However, one of the first functions described for Aβ is its antimicrobial activity. Aβ has been shown to function as an antimicrobial peptide (AMP) [235,236], with Aβ oligomers having the capacity to kill invading pathogens (bacteria, viruses, fungi) by first trapping

them in a network of fibrils and subsequently disrupting their membranes or capsids (reviewed in [237]). These Aβ properties could contribute to tumour suppression. Namely, it has been proposed that Aβ may intercept oncogenic viruses, and thereby halt carcinogenesis [234].

1.5 AD clinical trials targeting Aβ: a path of failures or a road to success?

Brain Aβ begins to accumulate during the preclinical phase of AD, at least one to two decades prior to the onset of AD symptoms (**Figure 1.1**). Aβ-directed therapeutic strategies aim to either decrease total parenchymal Aβ levels or alter Aβ profiles, by lowering the production of longer and promoting the generation of shorter Aβ species. To reach these goals, two major approaches have been employed: (active/passive) immunization to promote Aβ clearance and BACE or γ-secretase inhibitors, or γ-secretase modulators to alter Aβ production.

1.5.1 Strategies targeting Aβ clearance

One strategy that has been pursued to reduce brain Aβ load is the stimulation of its clearance. The first proof of concept of the feasibility of this strategy was achieved through an active immunization paradigm. The injection of human Aβ42 "antigen" into young AD model mice has prevented the development of amyloid plaques [238]. However, human trials based on a similar paradigm have shown variable effects on Aβ clearance, no cognitive improvement [239] and have had to be stopped in a phase 2a trial as patients developed septic meningoencephalitis [240]. Currently, two active vaccination strategies are still under investigation in clinical trials (phase 3 trial for CAD106 [241] and phase 2 for ABVac40 [242]).

Passive immunization has been pursued as another promising strategy. In this case, patients are treated with infusions of monoclonal antibodies. The antibodies are proposed to bind to soluble/oligomeric Aβ in the CNS to promote its clearance. An alternative explanation of their action is provided by a 'peripheral sink hypothesis' (reviewed in [243]). This theory assumes that an equilibrium exists between plasma (peripheral) and brain Aβ and that by sequestering peripheral Aβ the antibody will lead to a compensating reduction in CNS Aβ [244]. Several monoclonal antibodies (MABs)

have been evaluated in phase 3 clinical trials. All, but one (Aducanumab), failed to meet their primary endpoints (reviewed in [245]). Aducanumab, an antibody recognizing a specific conformational epitope in Aβ [246], has been reported to slow cognitive decline in the highest dose treatment group and its manufacturer (Biogen) is currently pursuing market approval for the drug at the FDA [247]. If approved, it would be the first disease-modifying treatment for AD. The reason(s) for why Aducanumab displays an apparent therapeutic benefit while the other MABs failed to do so, might be related to its specific mechanism of action. A recent *in vitro* study revealed that out of 4 anti-Aβ MABs tested, only Aducanumab dramatically reduces the flux of AβO's through effectively inhibiting the secondary nucleation process of oligomer formation [248].

1.5.2 Strategies targeting Aβ production

Another strategy aims at decreasing Aβ production. β-Secretase (BACE) cleavage represents the rate-limiting step in Aβ production, and thus BACE has been regarded as a promising target. This has been encouraged by the initial analysis of the BACE1 KO mice showing no impaired phenotypes [249]. Several potent, small molecule BACE inhibitors have been tested in clinical trials [250]. However, the initial trials have been prematurely terminated due to liver (LY2886721), ocular (LY2811376) or cardiac (AZD-3839) toxicity (reviewed in [250]). Later studies with BACE1 inhibitors reached more advanced stages in clinical development, but none showed any functional benefit, while some actually worsened cognition (reviewed in [245,250]). It is clear now that BACE1/2 proteases process a broad range of substrates, and are involved in essential CNS functions (such as neurogenesis, axon guidance and synaptic plasticity) as well as pigmentation, muscle spindle formation and maintenance of pancreatic β-cell function (reviewed in [251,252]). Inhibition of the proteolysis of these other substrates could explain the observed adverse effects in the clinic.

Another drug target in this category is GSEC, with GSEC inhibition viewed as the most direct method to halt Aβ production. However, the outcome of the notorious Semagacestat (Eli Lilly) trial has scorched the reputation of GSEC as a drug target. Semagacestat is a general GSEC inhibitor of which the clinical development has been halted in a phase 3 trial as a result of severe side effects and a paradoxical worsening in

cognition [253]. The failure has, however, taught us valuable lessons about the highly complex nature of GSEC biology [254]. A crucial insight was that impaired Notch turnover, resulting from GSEC inhibition, induces a range of adverse effects, such as gastrointestinal problems and skin lesions [255]. The cognitive worsening could be explained by the recent discovery that Semagacestat acts as a pseudo-inhibitor that only partially inhibits GSEC, while at the same time boosts the production of longer Aβ peptides [256].

The unique, sequential APP cleavage mechanism of GSEC (**Figure 1.5**) has offered an alternative way to target Aβ production. Nearly two decades ago, a subset of non-steroidal anti-inflammatory drugs (NSAIDs) was found to selectively lower Aβ42 levels in different cellular models [257]. The observed lowering of Aβ42 has been shown to arise from a direct modulation of GSEC activity [258,259]. These so-called GSEC modulators (GSMs) offer a significant advantage over GSIs as they do not affect the overall GSEC activity (i.e. initial ε-cleavage) [260], and thereby do not affect GSEC-mediated signalling. An initial clinical trial with R-flurbiprofen (or tarenflurbil), has shown no effect on cognitive decline [261], probably due to an inadequate brain penetration of the compound and poor overall drug properties [262]. Efforts to overcome these pharmacological issues have resulted in the identification and the development of 2nd and 3rd generation GSMs with improved potency and brain penetrance (reviewed in [263]). Several of these demonstrate robust efficacy in preclinical (BPN-15606) [264] or phase 1 trials (BMS-932481 and PF-06648671) [265,266], and are evolving towards large-scale clinical trials. Although GSMs hold great promise, relatively little is known about the mechanisms underlying their function.

1.5.3 What did we learn from the clinical trials?

None of the employed strategies has met its therapeutic/preventive objectives and several led to serious side effects (reviewed in [245,267]). The failures have been viewed by some as evidence to reject the ACH [48,49]. Others have argued that they did not truly test the ACH [268,269]. The reasons for the lack of success of the past clinical trials are: **I)** the lack of the efficacy of the tested therapeutic agent (e.g. poor brain penetration, insufficient target engagement), **II)** unfavourable safety profile (i.e. occurrence of major

side effects), **III)** “incorrect” patient population. With regard to the latter, study cohorts usually consisted of patients in the late, mild and moderate stages of AD. As it is clear that Aβ accumulation in the brain starts 15-20 years before the manifestation of the first symptoms [8,9], the (potential) therapeutic solutions have been likely administered too late in the disease process. More recent clinical trials are, therefore, focused at intervening at the preclinical stage of the disease by recruiting ADAD patients (such as the Dominantly Inherited Alzheimer Network (DIAN) [270] and the Alzheimer Prevention Initiative (API) [271] cohorts) or patients with confirmed – as determined by biomarker assessment – preclinical AD [272]. Essential to the success of these (and other) trials will be to determine how we can tackle the disease process in the most efficient way. This can only be achieved by obtaining a deep mechanistic understanding of the disease pathogenesis.

2 Aims of the thesis

The main goal of this work was to advance the mechanistic understanding of AD pathogenesis in order to establish a framework for the rational development of safe and effective therapeutics.

In light of the main goal, the following milestones were set in this project:

Aim 1: Elucidation of the molecular strategies that stabilize GSEC-APP/Aβn during the sequential proteolysis

Research from the last decade has substantially advanced our understanding of how GSEC processes APP in 'healthy' and diseased states. Pathogenic mutations in *PSEN1* destabilize GSEC-APP/Aβn interactions [218], thereby inducing the premature release of partially digested (i.e. longer) Aβ peptides [213,214,216,217]. Deciphering molecular/structural underpinnings of GSEC-APP/Aβn stability would thus provide essential knowledge as to how we can prevent the production of longer, amyloidogenic (>Aβ40) peptides, believed to trigger neurotoxic cascades in AD [53]. The elucidation of the GSEC atomic structure in 2015 [170] opened a new era for the AD field as it provided a valuable template for the studies into structure-function relationships governing GSEC proteolysis. In this aim, we, therefore, took the advantage of these exciting new insights to pinpoint the molecular determinants that govern E-S interaction stability.

This work is presented in chapter 3.

Aim 2: Characterization of the molecular composition of secreted Aβ profiles generated by pathogenic GSEC variants and defining its relationship with the age of AD onset (AAO)

FAD-linked *PSEN/APP* mutations are characterized by a large heterogeneity in the age at the clinical symptom onset [73]. However, little is known about what underlies this heterogeneity. Recent mechanistic data have demonstrated that a linear relationship exists between the degree of the mutation-induced destabilization of the GSEC-APP interactions and the AAO (in cell-free conditions) [218]. This observation suggests that changes in the spectrum of Aβ peptides, arising from the destabilizing nature of pathogenic mutations, underlie AD. Previous work has mostly focused on Aβ42 and

Aβ40 peptides, mostly neglecting the contribution of other species. We aimed to provide a comprehensive analysis of the Aβ peptides produced in a physiological context, to uncover what specific changes in its molecular composition drive AD pathogenesis.
This work is presented in chapter 4.

Aim 3: Determine the mode of action and binding pocket of GSEC modulators

GSEC modulation has emerged as a new avenue to target Aβ production while avoiding undesired clinical effects related to the complex biology of the protease. Since their initial discovery, the list of compounds presenting GSEC modulatory properties has grown rapidly. Although these compounds are generally regarded to have superior safety profiles compared to the previous GSIs (reviewed in [273]), the prospect of patients having to take these drugs for a long period (i.e. decades before expected onset), allows no room for compound-related adverse effects (as with the GSIs). Therefore, it is essential to have a clear idea of how GSMs exert their effect on Aβ production and where they bind in the GSEC-APP complex, information that is currently lacking. To resolve these issues, we aimed to locate the specific binding pocket of highly potent GSMs and decipher how compound binding promotes the sequential cleavage of APP_{C99}/Aβn.
This work is presented in chapter 5 (and partially in chapter 3)

.

3 Extracellular interface between APP and Nicastrin regulates Aβ length and response to γ-secretase modulators

This chapter is based on the following published article:

Dieter Petit[1,2], Manuel Hitzenberger[3], Sam Lismont[1,2], Katarzyna Marta Zoltowska[1,2], Natalie S. Ryan[4], Marc Mercken[5], François Bischoff[5], Martin Zacharias[3], Lucía Chávez-Gutiérrez[1,2,*]

1 VIB-KU Leuven Centre for Brain & Disease Research, Leuven, Belgium
2 KU Leuven, Department of Neurosciences, Leuven Research Institute for Neuroscience and Disease (LIND), Leuven, Belgium
3 Physics Department, Theoretical Biophysics (T38), Technical University of Munich, München, Germany
4 Dementia Research Centre, UCL Queen Square Institute of Neurology, London, UK
5 Janssen Research & Development, Division of Janssen Pharmaceutica NV, 2340 Beerse, Belgium
*Corresponding author.

The EMBO Journal, June 17th 2019 (https://doi.org/10.15252/embj.2019101494)

3.1 Synopsis

γ-Secretase mediated cleavage of APP defines the length of Aβ peptides. Alzheimer's disease-causing mutations destabilize γ-secretase - APP interactions and thus promote the production of longer, amyloidogenic Aβs. Here, we investigated the molecular strategies securing γ-secretase – APP interactions.

- NCT ectodomain establishes a direct, short distance interaction with APP ectodomain
- NCT- APP interface influences the stability of γ-secretase - APP interactions and thereby modulates Aβ length
- NCT ectodomain influences the response towards compounds modulating Aβ length
- The data suggest a potential link between single-nucleotide variants in *NCSTN* and AD risk

3.2 Abstract

γ-Secretase complexes (GSECs) are multimeric membrane proteases involved in a variety of physiological processes and linked to Alzheimer's disease (AD). Presenilin (PSEN, catalytic subunit), Nicastrin (NCT), Presenilin Enhancer 2 (PEN-2), and Anterior Pharynx Defective 1 (APH1) are the essential subunits of GSECs. Mutations in *PSEN* and the Amyloid Precursor Protein (*APP*) gene cause early-onset AD. GSECs successively cut APP to generate Amyloid-β (Aβ) peptides of various lengths. AD-causing mutations destabilize GSEC-APP/$A\beta_n$ interactions and thus enhance the production of longer Aβs, which elicit neurotoxic events underlying pathogenesis.

Here, we investigated the molecular strategies that anchor GSEC and APP/$A\beta_n$ during the sequential proteolysis. Our studies reveal that a direct interaction between NCT ectodomain and APP_{C99} influences the stability of GSEC-$A\beta_n$ assemblies and thereby modulates Aβ length. The data suggest a potential link between single-nucleotide variants in *NCSTN* and AD risk. Furthermore, our work indicates that an extracellular interface between the protease (NCT, PSEN) and the substrate (APP) represents the target for compounds (GSMs) modulating Aβ length. Our findings may guide future rationale-based drug discovery efforts.

3.3 Introduction

γ-Secretase intramembrane proteases (GSECs) play multifaceted roles in physiology and disease. Of great relevance is their critical involvement in Alzheimer's disease (AD) pathogenesis, where altered cleavage of the Amyloid Precursor Protein (APP) (**Figure 3.1A**), and concomitant, relative increase in the generation of longer vs. shorter amyloid β (Aβ) peptides, has been proposed to underlie the disease [53,218]. GSEC activity is exerted by a group of heteromultimeric, membrane-embedded complexes composed of Presenilin (PSEN1 or PSEN2) [274], Nicastrin (NCT) [275], Presenilin Enhancer 2 (PEN-2) [276] and Anterior Pharynx Defective 1 (APH1A or APH1B) [276,277] in a 1:1:1:1 stoichiometric ratio [165,170,278]. PSEN bears the catalytic centre of the enzyme [69,71,72,279], while the other 'non-catalytic' subunits of the protease are required for the complex assembly, activation, structural stability/turnover and trafficking [280–284]. Once the quartet has been assembled, PSEN undergoes auto endoproteolytic cleavage, which yields an active pentameric protease complex, with the catalytic centre located at the interface between the N- and C-terminal fragments (NTF vs CTF) of PSEN [138,140,285].

In addition to the proteolytic processing of APP, the cleavage of many other type I membrane proteins, such as Notch, ErbB4, N-Cadherin, etc. (reviewed in [178]), positions GSEC activity as a regulator of several key physiological events during embryonic development, haematopoiesis, normal functioning of the nervous and immune system, as well as of disease processes, such as cancer [181,182]. Interestingly, the GSEC substrates are remarkably different in their amino acid sequences and lack any obvious common structural features [286,287]. In fact, the only known prerequisite for GSEC cleavage is the removal of protruding ectodomains (when present) from type I membrane proteins by protein sheddases [288,289]; a step that generates C-terminal transmembrane domains (TMD) with short ectodomains – the immediate GSEC substrates – that may only then undergo GSEC-mediated proteolysis.

APP_{C99} is the most studied substrate of GSECs due to its genetic and biochemical link to AD pathogenesis. Extensive research has revealed a rather unique mechanism by which APP_{C99}, the C-terminal fragment generated by β-secretase-mediated APP ectodomain shedding, is sequentially cut by GSECs [191,193,290]. The first GSEC-mediated endopeptidase (ε) cleavage releases a soluble cytosolic fragment (APP intracellular

domain, AICD) and generates a transmembrane fragment (Aβ48 or Aβ49), which is successively cut by carboxypeptidase-like (γ) cleavages, along the following product lines: Aβ49 → Aβ46 → Aβ43 → Aβ40 → Aβ37 or Aβ48 → Aβ45 → Aβ42 → Aβ38 (**Figure 3.1A**). The release of an $A\beta_n$ peptide into the luminal/extracellular environment ends the sequential process [193]. Importantly, the position of the ε-cleavage on APP_{C99} defines the type of Aβ products (product line), while the efficiency of the sequential γ-cleavages (number of cuts per substrate molecule, so-called GSEC processivity) determines the length of the N-terminal Aβ products.

Of note, mutations in both GSEC (enzyme, E) and APP (substrate, S) lead to early-onset familial AD (FAD) [74,291]. Importantly, disease-causing mutations in *PSEN1* and *PSEN2* genes consistently impair the efficiency of the γ-cleavages, shifting Aβ profiles towards the generation of longer amyloidogenic peptides [214,216,217,292]. This so-called "GSEC dysfunction" promotes – as demonstrated by the analysis of post-mortem brain samples from FAD patients [213] – the production of longer $A\beta_{\geq 42}$ peptides, which trigger neurotoxic events underlying AD [53,293]. Furthermore, many but not all FAD-causing *PSEN* variants [213,216,217] impair the initial GSEC endopeptidase (ε-) cleavage and thus may have detrimental effects on GSEC-mediated signalling cascades.

Importantly, our recent studies [218] have shown that the relative stabilities of the GSEC-APP/$A\beta_n$ (E-S) complexes, formed during the sequential cleavage of APP_{C99} by GSEC, control the efficiency of the sequential proteolysis and thereby define the length of Aβ products. In addition, they have demonstrated that pathogenic mutations in *PSEN1* and *APP* destabilize the GSEC-APP/$A\beta_n$ interactions, leading to the 'premature' release of longer, more hydrophobic Aβs [218]. Of note, a remarkable correlation between the magnitude of the mutant-induced weakening of the stability of the E-S complexes and the corresponding age of disease onset [218] places the generation of longer $A\beta_{\geq 42}$ peptides central to AD pathogenesis. The novel link between the E-S complex (structural) stability and AD pathogenicity prompted us to investigate the molecular mechanisms securing GSEC-APP/$A\beta_n$ interactions. Here, we applied a structure-based functional approach to determine the molecular strategies that anchor APP/$A\beta_n$ during GSEC-mediated proteolysis. Our analyses reveal that a direct interaction between the NCT ectodomain and APP_{C99}/$A\beta_n$ modulates the stability of GSEC-APP/$A\beta_n$ interactions and

therefore regulates Aβ product length. In fact, the data raise the intriguing possibility that AD-causing or protective single nucleotide variants (SNPs) may exist in the *NCSTN* gene. Furthermore, our analysis implicates the extracellular interface formed between GSEC (NCT, PSEN) and APP_{C99} in the regulation of the response to small compounds, referred to as GSEC modulators (GSMs). Collectively, these insights may guide future drug discovery efforts and the development of innovative strategies targeting safely and efficiently the destabilized GSEC-APP/$A\beta_n$ assemblies in AD.

3.4 Materials and methods

Antibodies and compounds

The following antibodies were used in the study: anti-FLAG M2 (F3165) from Sigma-Aldrich, anti-PSEN-CTF (MAB5232) from Merck, anti-human PSEN-NTF (MAB1563) from Millipore, anti-NCT (#612290) from BD Biosciences, horseradish peroxidase (HRP)-conjugated anti-mouse (#1721011) and anti-rabbit IgG (#1721019) from Bio-Rad, HRP-conjugated anti-rat IgG (#P0450) from Agilent, and anti-human Amyloid-beta (N) (82E1, #10323) from IBL. Anti-mouse PSEN-NTF (B19.3), -PEN-2 (B126.2), and -APP-CTF (B63) antibodies were made in-house. Antibodies used in the ELISA and GSMs were obtained through collaboration with Janssen Pharmaceutica NV (Beerse, Belgium). The ELISA capture antibodies were JRD/Aβ37/3 for Aβ37, JRF AB038 for Aβ38, JRF/cAb40/28 for Aβ40, JRF/cAb42/26 for Aβ42, and the detection antibody was JRF/AbN/25 raised against the N terminus of Aβ. Acid-based GSM I and imidazole-based GSM II and GSM III were synthesized as described previously [294,295]. GSEC inhibitor X (#565771) was purchased from Calbiochem.

Generation of stable cell lines

Ncstn$^{-/-}$ [296] and *Psen1*$^{-/-}$*Psen2*$^{-/-}$ [297] mouse embryonic fibroblasts (MEFs) were cultured in Dulbecco's Modified Eagle's Medium (DMEM)/F-12 (Life Technologies) containing 10% fetal bovine serum (FBS) (Life Technologies). *Ncstn*$^{-/-}$ MEFs were transduced with retroviruses, carrying pMSCVpuro plasmids encoding respective wild type or mutant (F239A, S240A, S240F, I241A, I241C, I241D, I241E, I241S, I241F, I241K, I241Q, I241W, N242A, N242D, N242E, N242F, N242K, N242W, N242Y,

P243A, P234F, E244A, E244D, E244F, E244K, E244Q) NCTs, using a replication-defective recombinant retroviral expression system (Clontech). Human PSEN1 MEF cell lines were generated by rescuing PSEN expression in knock-out *Psen1*$^{-/-}$*Psen2*$^{-/-}$ MEFs with either wild type human or mutant PSEN1 (V89L, L166P, R269H) variants. Briefly, retroviruses were generated by co-transfecting HEK293T cells with pMSCVpuro wild type or mutant NCT or human PSEN1 encoding plasmids and the PIK helper plasmids, as reported previously [162]. Viral particles were harvested 48h post-transfection and used to infect *Ncstn*$^{-/-}$ *or Psen1*$^{-/-}$*Psen2*$^{-/-}$ fibroblasts plated at 30–40% confluency. The culture medium was supplemented with 5 µg/ml puromycin (Sigma-Aldrich) to select clones stably expressing PSEN or NCT, which were further maintained in DMEM/F-12, 10% FBS and 3 µg/ml puromycin. NCT and PSEN1 expression levels and the reconstitution of the functional GSEC complexes in the different cell lines were analyzed by SDS-PAGE/western blot.

Transduction of MEF cell lines with adenoviruses carrying APP-encoding plasmids for cell-based activity assays

MEF cell lines were transduced with recombinant adenoviruses carrying plasmids encoding APP_{C99}, as described previously [162]. Briefly, MEF cells stably expressing either WT or mutants mNCT/hPSEN1 were plated at the density of $1x10^5$ cells/well into 12-well plates and 16h later transduced with recombinant adenoviruses Ad5/CMV-APP. 7 hours post-transduction the medium was refreshed with low-serum medium (DMEM/F-12 medium containing 0.2% serum). The cells were then incubated for 24h at 37°C or 42°C, respectively and the conditioned medium was collected for Aβ analysis [218]. When indicated the low-serum culture medium was supplemented with 0.3 µM or 1 µM GSMs (GSM I, GSM II, GSM III) or vehicle control (0.1% DMSO final concentration).

MEF electroporation with plasmids encoding wild type or mutant APP_{C99}-3xFLAG substrates

MEF cell lines were electroporated with 5 µg pSG5**APP_{C99}-3xFLAG- WT or -K28E plasmids using the NEPA21 super electroporator transfection system (Nepagene). Freshly trypsinized cells were set to a concentration of $1.5x10^6$ cells/ml in OPTI-MEM (Thermo Fisher Scientific), and 100 µl of the cell suspension was mixed with 5 µg of DNA and transferred to a Nepa 2mm gap cuvette (#EC-002S, Nepagene) for electroporation (Poring Pulse (Voltage = 140V, Length = 7.5 ms, Interval = 50 ms, # of pulses = 2, Decay rate = 10%, polarity = +), Transfer Pulse (Voltage = 20V, Length = 50 ms, Interval = 50 ms, # of pulses = 5, Decay rate = 40%, polarity = +/-)). The electroporated cells were mixed with 400 µl DMEM/F-12 medium containing 10% FBS and 3 µg/ml puromycin immediately after the electroporation and plated into 24-well plates. The medium was refreshed with low-serum medium 12h post-electroporation and collected 36 h later for the Aβ quantification.

Quantification of Aβ production by (MSD) ELISA

To determine the GSEC processivity of APP, Aβ37, Aβ38, Aβ40, Aβ42 and Aβ43 levels in conditioned medium (cell-based assays) were measured. To quantify the concentration of Aβ37, Aβ38, Aβ40 and Aβ42 peptides, Multi-Spot 96-well MSD ELISA plates pre-coated with anti-Aβ37, -Aβ38 -Aβ40, and -Aβ42 specific antibodies using the multiplex Meso Scale Discovery (MSD) technology were used. Non-specific protein binding to the plates was blocked with 150 µl/well blocking buffer (PBS supplemented with 0.1% casein) for 1.5 h at room temperature (while shaking at 600 rpm) and the blocked plates were rinsed 5 times with 150 µl/well washing buffer (PBS supplemented with 0.05% Tween-20). 25 µl of SULFO-TAG JRF/AbN/25 detection antibody diluted in blocking buffer was mixed with 25 µl of standards (synthetic human Aβ1-37, Aβ1-38, Aβ1-40, and Aβ1-42 peptides at known concentrations) or 25 µl analyzed samples, both diluted in blocking buffer, and the mix (50 µl/well) was loaded on the plate for ELISA analysis. After overnight incubation at 4°C, the plates were rinsed 5 times with washing buffer and developed by the addition of 150 µl/well of the 2x MSD Read Buffer T (Tris-based buffer containing tripropylamine). The signals were

read immediately on a Sector Imager 6000 (Meso Scale Discovery). To quantify the concentration of the Aβ43 peptide in cell-based assays, conditioned medium samples were loaded on the ELISA plates pre-coated with anti-human Aβ (1-43) rabbit IgG, supplied with the human Amyloid β (1-43) (FL) assay kit (IBL) and peptide levels were measured following the supplier's protocol.

Cross-linking in MEFs

MEF cells stably expressing either wild type of I241C mutant mouse NCT were plated into 10 cm tissue culture dishes at the density of $1.5x10^6$ cells/dish and transduced with recombinant adenovirus Ad5/CMV-APP bearing human APP_{C99}, as described above. 36 h post-transduction the cells were collected by scraping in ice-cold PBS and total membranes prepared. To induce the cross-linking between free sulfhydryl groups (i.e. cysteines), 30 µg membrane protein resuspended in 50 mM MES, 100 mM NaCl pH 6.5 was mixed with N-β-maleimidopropyl-oxysuccinimide ester (BMPS, ThermoFisher Scientific) at a final concentration of 10 µM and incubated for 2h on ice. The excess of the cross-linker was removed by washing the membrane pellets in buffer B. To promote the reaction with free-amine groups, membranes were then resuspended in 100 mM HEPES, 100 mM NaCl pH 7.5 and incubated again on ice for 2h. Cross-linked membranes were pelleted by ultracentrifugation, solubilized in 4x sample buffer (NuPAGE LDS, Thermo Fisher Scientific) supplemented with 4% β-mercaptoethanol (BME) and analyzed by SDS-PAGE/western blot. To test for the potential formation of a disulfide bridge between NCT- I241C and APP- K28C mutants, NCT- I241C MEF cell line was electroporated with 7.5 µg of pSG5**APP-C99-3xFLAG-K28C plasmid per $1x10^6$ cells. The medium was refreshed with low-serum medium containing GSEC Inhibitor X (1 µM) 12h post-electroporation and cells were harvested 24h later. Membrane fractions were prepared from the electroporated cells and resuspended in 50 mM MES, 100 mM NaCl pH 6.5. 30 µg protein (measured by Bradford protein assay) was resolved by SDS-PAGE under reducing (4% BME in sample buffer) or non-reducing (no BME in sample buffer) conditions. The presence of the cross-linked products was evaluated by western blot.

Molecular Dynamics Simulations

The NCT- I242E mutant molecular dynamics (MD) simulation conducted for this study was based on a 3000ns long simulation of the APP-derived substrate Aβ49 in complex with WT (human) GSEC, part of a computational study of GSEC- Aβn complexes [298]. The structures were based on PDB entries 5FN2 [171] (GSEC) and 2LP1 [299] (APP_{C99}). To make sure that the substrate remains in a conformation that is cleavable during the sampling, a transition state-like geometry [300] at the interface between the cleavage- (C99-V46, C99-I47) and the active site (PSEN-D257, PSEN-D385) was stabilized by the use of appropriate harmonic restraints with weak force constants (for details cf. to the previous study [298]). The complex of GSEC- I242E and Aβ49 was placed in a bilayer of 301 POPC molecules and solvated in a 0.15M KCl solution containing 53829 water molecules. Periodic boundary conditions were employed and the rectangular simulation box had a volume of approx. 2200000 $Å^3$. Lipids, water, and proteins were described by the Lipid14 [301], the TIP3P [302], and AMBER14SB [303] force fields, respectively. The target temperature was set to 303.15K by the use of the Langevin thermostat [304] with a collision frequency of $1ps^{-1}$. The desired pressure of 1.0 bar was maintained by the Monte Carlo barostat [305]. Non-bonded interactions were described up until a distance of 8Å and the particle mesh Ewald method [306] was used to describe long-range effects. To allow for 4.0 fs time steps, the SHAKE algorithm [307] and the hydrogen mass repartitioning method [308] were employed. The simulations were performed using the CUDA [309] version of PMEMD [310–312] which is part of the AMBER16 simulation package [313]. For evaluation, a 3000 ns long simulation trajectory was generated. Trajectory analysis was carried out using CPPTRAJ [314] and VMD [315], which was also utilized to render the simulation snapshots. For free energy calculations, the Molecular Mechanics Poisson-Boltzmann Surface Area (MMPBSA) [316] post-processing method as implemented in the MMPBSA.py program [317] has been employed. In order to account for the effects of the POPC bilayer, an implicit lipid model with a permittivity of $\varepsilon = 2.0$ has been used. The membrane slab was assumed to be 34 Å in thickness so that it covers the same region as the lipid tails in the explicit treatment. The head group region was assumed to be part of the aqueous layer ($\varepsilon = 80.0$) in order to ensure a realistic treatment of the electrostatics at the lipid-water interface where E242

and K28 are located (this region was populated by a high amount of water molecules - especially in the cavity region between NCT and PSEN, which is void of lipids). The implicit lipid slab was centered around the mean center of mass (COM) of the explicit bilayer in the simulation. The (internal) permittivity of the protein was assumed to be ε = 1.0 and the salt concentration was set to 0.15M. In order to estimate the influence of the I242E mutation to $\Delta\Delta G_{bind}$, 1500 frames of the simulation generated for this study were compared to the same amount of frames of the previously performed WT-GSEC - Aβ49 simulation [298]. Due to the large system sizes and the enormous computational effort involved in estimating changes of entropy upon binding, only PBSA-intrinsic solvation entropies have been considered.

Statistical analysis

All statistical analyses were performed using the GraphPad Prism 7 or 8 software. One-way ANOVA with Dunnett's post hoc test was used to test the significance of the changes between groups unless indicated otherwise. In Figure 4, an unpaired, two-tailed Student's t-test was used to test the significance between tested groups. In Figure 6, two-way ANOVA with Sidak's post hoc test was used to determine the response to the pharmacological treatments. P-value <0.05 was used as a pre-determined threshold for statistical significance. All statistical analyses are described in the corresponding figure legends.

3.5 Results

Structural data reveal a potential direct, short distance interaction between NCT and the substrate

We departed from the PDB:5FN3 high-resolution GSEC structure to investigate the structural determinants securing E-S complexes and thus controlling Aβ length. We hypothesized that this structure of GSEC (**Figure 3.1B**) [171], which contains a co-purifying helical peptide (putative substrate), depicts the interaction between GSEC and a *"de novo"* generated long Aβ substrate, just before it engages into the next catalytic turnover. In our working model, originally presented in [218] and discussed in-depth here, key interactions between GSEC and the extracellular part of the putative substrate play a critical role in the stabilization of the E-S assemblies during the sequential proteolysis of $A\beta_n$ substrates. Accordingly, we explored the presumed E-S co-structure to define interactions that could contribute directly to the regulation of the strength of the GSEC-APP/Aβ interactions.

Interestingly, we found potential contact sites between the extracellular part of the helical co-purifying peptide and the NCT ectodomain (amino acid (aa) residues 242-243 in human or 241-242 in mouse NCT (mNCT), please note that residue numbering used in this report corresponds to the sequence of mNCT unless specified otherwise) (**Figure 3.1B, zoom-in**) as well as with the first extracellular loop of PSEN1. While our recent analysis of FAD-linked PSEN1 variants [218] has demonstrated the participation of the first extracellular loop of PSEN1 in the (de)stabilization of GSEC-APP/Aβ interactions, the involvement of the ectodomain of NCT in the strength of E-S interactions has not been shown before and, if true, would provide novel insights into the roles of the 'non-catalytic' GSEC subunits in the regulation of GSEC processivity of APP (Aβ length). Therefore, we investigated the contribution of NCT ectodomain to the stability of GSEC-APP/$A\beta_n$ interactions, which defines enzyme processivity.

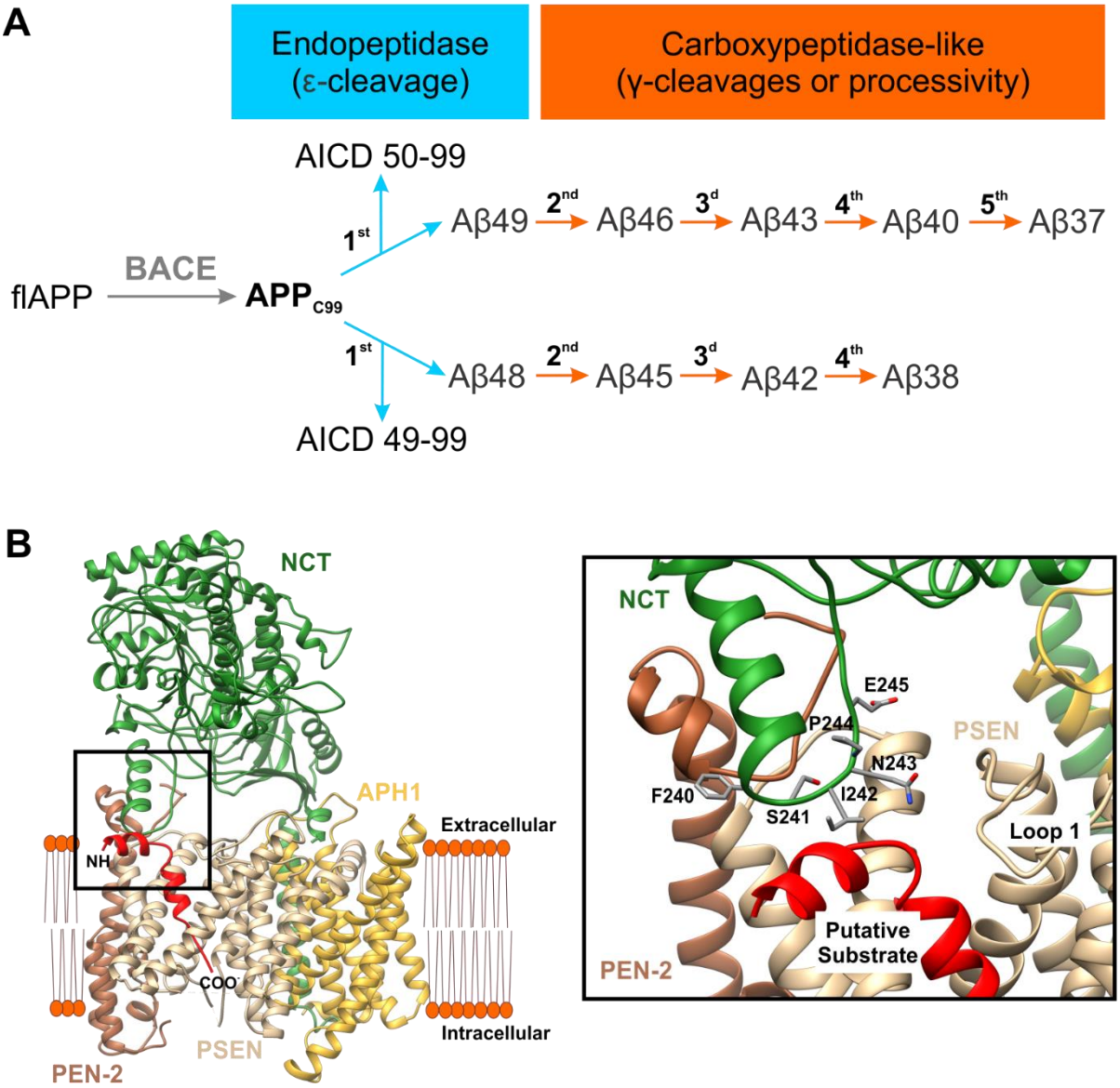

Figure 3.1. Schematic representation of APP processing and structural model (PDB: 5FN3) of the potential enzyme-substrate interface

(A) In the amyloidogenic pathway, the ectodomain shedding of the APP by BACE yields the immediate GSEC substrate, APP_{C99}. GSEC endopeptidase cleavage of APP_{C99} generates APP intracellular domain (AICD50-99 or AICD49-99) and a 'de novo generated' Aβ substrate (Aβ48 or Aβ49, respectively). While the AICDs are released, the Aβ48 and Aβ49 are subjected to subsequent GSEC proteolysis (carboxypeptidase-like γ-cleavages). **(B)** GSEC structure with co-purifying helical peptide (PDB: 5FN3) is presented. PSEN1 is shown in light brown, PEN-2 in dark brown, APH1A in gold, NCT in green and the co-purifying helical peptide in red. The topology of the helical peptide (putative GSEC substrate) is indicated by the amino and carboxyl-terminal groups. The interface between the N-terminal part of the helical peptide, the NCT ectodomain, and PSEN1 is magnified and NCT/PSEN1 side chains shown.

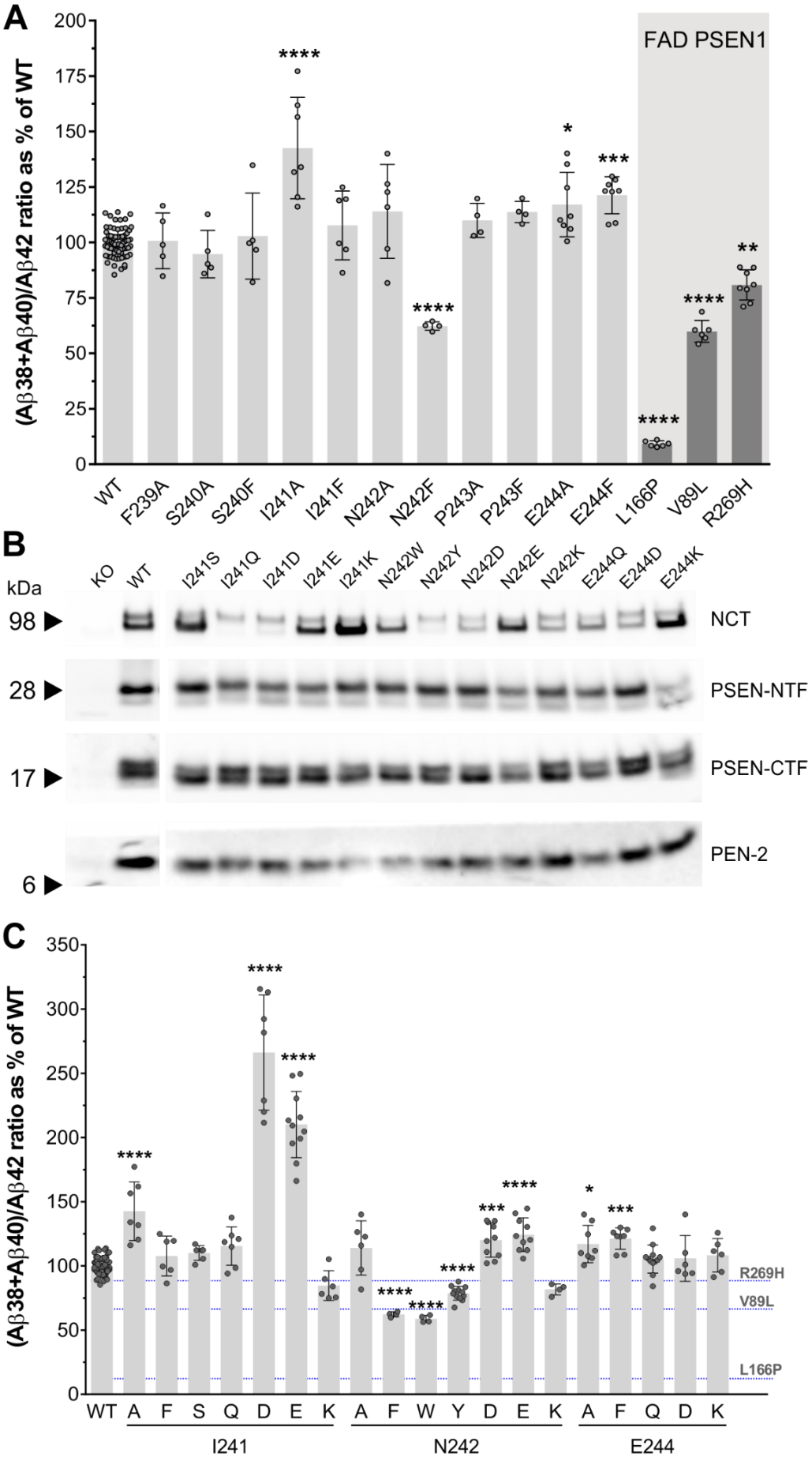
A
(Aβ38+Aβ40)/Aβ42 ratio as % of WT
FAD PSEN1
WT
F239A
S240A
S240F
I241A
I241F
N242A
N242F
P243A
P243F
E244A
E244F
L166P
V89L
R269H
B
kDa
KO
WT
I241S
I241Q
I241D
I241E
I241K
N242W
N242Y
N242D
N242E
N242K
E244Q
E244D
E244K
98
28
17
6
NCT
PSEN-NTF
PSEN-CTF
PEN-2
C
(Aβ38+Aβ40)/Aβ42 ratio as % of WT
R269H
V89L
L166P
WT A F S Q D E K A F W Y D E K A F Q D K
I241
N242
E244

Figure 3.2. NCT ectodomain regulates GSEC processivity towards APP_{C99}.
(A) Ala/Phe substitutions of aa 239-244 were introduced in the NCT ectodomain to evaluate the role of this region in the regulation of GSEC processivity. Aβ38, Aβ40, and Aβ42 levels present in the conditioned medium collected from KO NCT MEF cells rescued with WT or respective mutant NCT GSECs and transiently expressing with APP_{C99} were quantified by ELISA. Aβ(38+40)/42 ratio was calculated to determine GSEC processivity towards APP_{C99}. DKO PSEN1/PSEN2 MEFs rescued with the indicated FAD PSEN1 mutant and transduced with APP_{C99} were used as references.
(**B**) Representative SDS-PAGE/western blot analysis of CHAPSO solubilized membranes from KO NCT MEF cell lines stably expressing WT or mutant NCT subunits. The presence of mature, glycosylated NCT, N-terminal and C-terminal fragments of the endoproteolysed PSEN1 and PEN-2, compared to NCT knock-out (KO) cells, indicate that WT and mutated NCTs reconstitute GSEC complexes. Arrowheads indicate the position of molecular weight markers. (**C**) Quantification of the effects of the indicated substitutions of aa 241, 242, and 244 in NCT on GSEC processivity of APP_{C99}, estimated as indicated above by the Aβ(38+40)/42 ratio. **Figure S3.1B** shows the corresponding Aβ42/40 ratios. Data information: Data are presented as mean ± SD, N ≥ 4 independent experiments. One-way ANOVA followed by Dunnett's post-hoc test with comparison to WT was used to determine statistical significance of all tested NCT mutants; *p > 0.05, **p > 0.01, ***p > 0.001, ****p > 0.0001, F(DFn, DFd): F(27, 230) = 84,22.

NCT ectodomain –aa 241-244 – regulates GSEC processivity of APP_{C99}

To challenge the potential involvement of the NCT- 241-242 region in the regulation of the GSEC processivity of APP_{C99}, we performed Ala/Phe mutagenic scanning of the region of interest and of the two neighbouring aa on each of its side (NCT- F239A/F, S240A/F, I241A/F, N242A/F, P243A/F, and E244A/F), followed by functional evaluation of the GSEC complexes in cell-based assays. To this end, we used NCT knock-out (KO) mouse embryonic fibroblasts (MEFs) [296] stably expressing either wild type or mutant NCT and transiently expressing wild type APP_{C99} substrate. Importantly, SDS-PAGE/western blot analysis showed that all mutants restored the assembly, maturation, and activity of GSEC, as indicated by the levels of mature NCT and PEN-2, as well as the endoproteolytic generation of PSEN1-NTF and -CTF fragments (**Figure S3.1A**). To determine the effects of the tested mutant NCTs on GSEC processivity of APP, we quantified secreted Aβ38, Aβ40, and Aβ42 peptides by multi-

spot enzyme-linked immunosorbent assay (MSD-ELISA) and Aβ43 by standard ELISA.

In line with our previous studies, Aβ43 was produced at low levels relative to the other (Aβ38/Aβ40/Aβ42) peptides in wild type or mild destabilizing (such as FAD-linked V89L and R269H PSEN1) conditions [214] (**Figure S3.2**). We, therefore, used the Aβ (38+40)/42 ratio (product/substrate ratio of the 4th GSEC catalytic turnover) to estimate the overall processivity of GSEC towards APP. Importantly, we included the FAD-linked PSEN1- L166P, V89L, and R269H mutant cell lines (*Psen1*$^{-/-}$*/Psen2*$^{-/-}$ MEFs [297] stably expressing respective PSEN1 mutants) transiently expressing APP_{C99} as reference samples in the analyses. The PSEN1 pathogenic variants were selected based on their differential location in the PSEN1 structure and distinct clinical ages of disease onsets (24, 48.6, and 55 years, respectively [183]). In line with the reported detrimental effects of the FAD-linked PSEN1 mutations on GSEC processivity of APP [214,216,217], all tested pathogenic mutant GSECs lowered the Aβ(38+40)/42 ratio relative to the wild type enzyme. The results thus validate the use of the Aβ(38+40)/42 ratio for the detection of changes in the sequential GSEC-mediated cleavage of APP.

With regard to NCT, Ala/Phe substitutions of aa NCT- I241, N242, and E244 significantly altered the Aβ(38+40)/42 ratio, supporting the involvement of NCT ectodomain in the regulation of the sequential GSEC cleavage of APP (**Figure 3.2A)**. Interestingly, substitutions at these positions shifted enzyme processivity in both directions, with the NCT- I241A substitution, and to a lesser extent the E244A and E244F mutants, enhancing the efficiency of the sequential GSEC cleavages on APP, and the NCT- N242F mutation hindering the successive proteolysis. Notably, the NCT-N242F substitution reduced GSEC processivity of APP to the levels similar to those exhibited by the FAD-pathogenic PSEN1- V89L variant (**Figure 3.2A**).

Based on these data, we selected positions NCT- 241, 242, and 244 for further analysis. In the second round of site-directed mutagenesis, we replaced the hydrophobic isoleucine at the position 241 with polar aa of small-medium size (Ser, Gln), or with differentially charged side chains (Asp, Glu, and Lys). As shown in **Figure 3.2B**, all generated mutants reconstituted active GSEC complexes. Our analysis revealed that the introduction of negatively charged residues (Asp or Glu) resulted in a (mean ± SD) 2.66

± 0.45 and 2.1 ± 0.26 fold elevation in the Aβ(38+40)/42 ratio, respectively (**Figure 3.2C**), while other tested mutations at this position did not significantly alter this ratio. Furthermore, the differential effects of the I241E vs. I241Q mutants on the Aβ (38+40)/42 ratio suggest that a charge-charge interaction underlies the activation of the sequential GSEC-mediated proteolysis observed for the NCT I241E substitution. To test whether the introduction of a negative charge next to I241 would also increase GSEC processivity, we mutated NCT- N242 to Asp or Glu. To investigate further the role of position N242 on GSEC processivity of APP, we introduced bulky residues with polar (Tyr, Trp) or charged (Lys) side chains at this position, generated mutant cell lines and tested them in cell-based GSEC activity assays.

The analysis showed that all mutants at position 242 rescue GSEC complex formation (**Figure 3.2B**) and that introduction of a bulky aromatic group at position NCT- 242 is detrimental for GSEC processivity (**Figure 3.2C**). Furthermore, it revealed that the NCT- N242E/D mutations, in contrast to Asp/Glu residues at position 241, result in mild increments in the Aβ(38+40)/42 ratio, indicating that a charge-charge interaction with activating effects on GSEC processivity of APP is optimally established with negatively charged NCT residues at position 241. Of note, mutagenesis of the E244 residue did not reveal any additional substitutions affecting GSEC processivity in a significant manner. In conclusion, the data demonstrate that residues 241, 242, and to a lesser extent 244, in NCT ectodomain contribute to the mechanism(s) governing the efficiency of the successive GSEC-mediated cleavage on APP and thus modulate the length of Aβ product peptides.

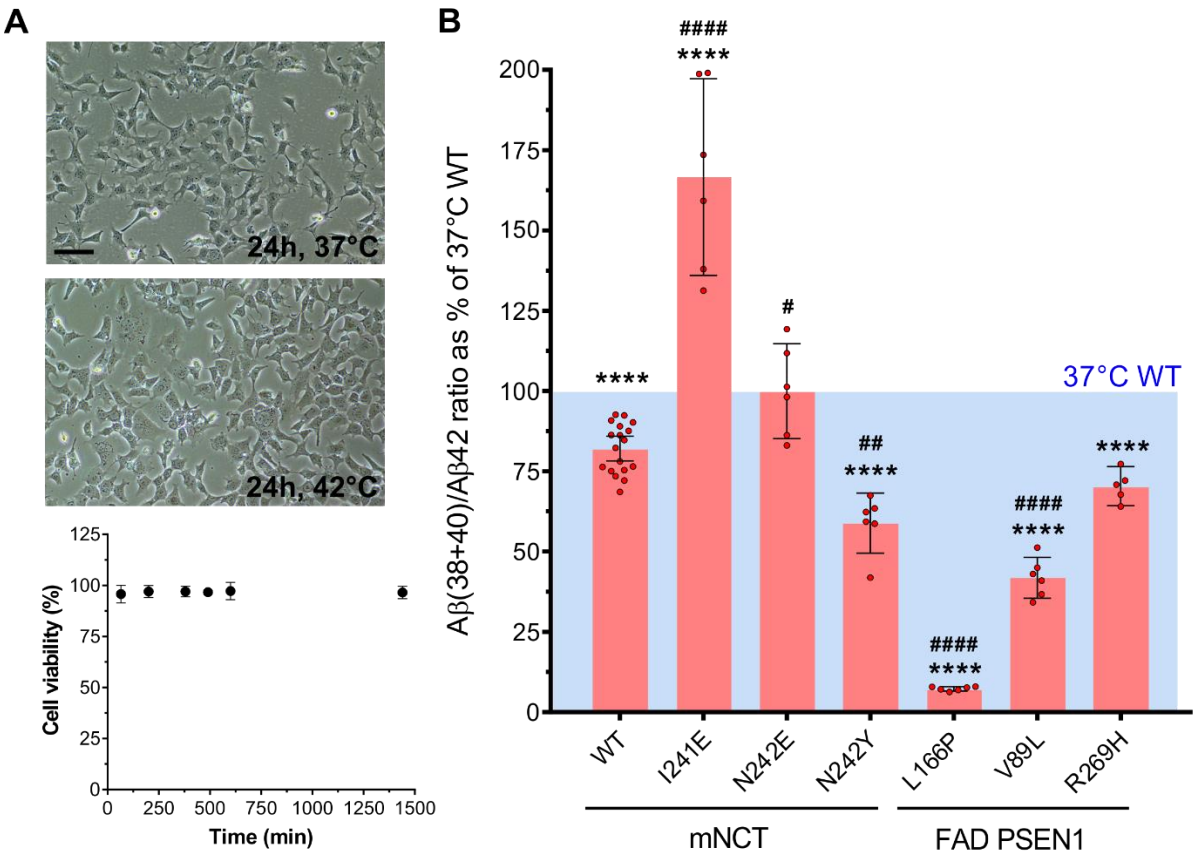

Figure 3.3. The NCT ectodomain contributes to the stability of GSEC-APP/Aβn complexes and accordingly modulate Aβ product length

(A) (Top) Representative bright-field microscopy images show MEF cells stably expressing WT or NCT mutant GSECs after 24h incubation at 37°C and 42°C. 25µm scale bar is shown. (Bottom) Cell viability determined at the indicated time points is not affected by prolonged (≥ 24h) incubation at 42°C. Data are presented as mean ± SD of 4 replicates. **(B)** Relative GSEC-APP/Aβn stabilities were assessed in cell-based GSEC thermoactivity assays, which evaluate changes in GSEC processivity (Aβ(38+40)/42 ratio) upon incubation at 42°C for 24h, relative to 37°C. Aβ peptides in the conditioned medium collected from the indicated MEF cell lines (transiently expressing APP_{C99}) were quantified and the Aβ(38+40)/42 ratios determined. The data are shown as mean ± 95% CI, as % of the WT GSEC cell line incubated at 37°C for 24h, N = 6 independent experiments. One-way ANOVA followed by Dunnett's post-hoc test with comparison to WT was used to determine the statistical significance (F(DFn, DFd): F(6, 46) = 100); ****p > 0.0001 compared to WT at 37°C, #p > 0.05, ##p>0.01, ####p>0.0001 compared to WT at 42°C. Note: Aβ profiles (including Aβ43 levels) normalized to total Aβ quantified in the cell-based thermoactivity assays with the different mNCT WT/mutants are shown in **Figure S3.2**.

Residues 241-242 in NCT ectodomain regulate the stability of GSEC-APP/Aβ interactions

We then investigated whether the observed effects of mutations at positions NCT- I241 and N242 on GSEC processivity of APP are mediated by changes in the stability of GSEC-APP/Aβ complexes. To this end, we evaluated temperature-mediated destabilization of GSEC-APP/Aβ interactions in wild type and mutant NCT MEF cell lines, transiently expressing APP_{C99} substrate, cultured at 42°C. Importantly, we first determined that prolonged incubation at 42°C does not affect cell viability of wild type MEFs (**Figure 3.3A**) and that the Aβ(38+40)/42 ratio was sensitive to detect temperature-induced changes in the stability of wild type and FAD-linked PSEN1 L166P, V89L, and R269H GSEC-APP/Aβ assemblies. Clearly, the elevated temperature significantly affected the efficiency of the 4th APP cleavage mediated by the wild type enzyme, as demonstrated by the Aβ(38+40)/42 ratio (95% CI: 78 – 86 % relative to 37°C, indicated with a blue box), and further enhanced the proven E-S destabilizing effects [218] of the FAD-linked PSEN1 mutants (**Figure 3.2C vs. 3.3B**, Aβ (38+40)/42 ratio (mean ± SD) = 9.2 ± 1.3 %, 59.9 ± 4.9 %, and 80.8 ± 6.8 % at 37°C vs. 7.3 ± 0.66 %, 41.9 ± 6.1 %, and 70.4 ± 4.9 % at 42°C for PSEN1 L166P, V89L, and R269H mutants, respectively).

These data validate the use of the cell-based GSEC thermoactivity assay to assess the (de)stabilizing nature of structural variants in the GSEC complex on the APP_{C99} sequential proteolysis. Thus, we employed this assay to evaluate the potential stabilizing or destabilizing effects of mutant NCT- I241E, N242E, or N242Y on E-S interactions. The cell-based thermoactivity assay revealed that the NCT- I241E and N242E mutants counteract the detrimental effect of temperature on the Aβ(38+40)/42 ratio, indicating that their effects on GSEC processivity are mediated by the stabilization of GSEC-APP/Aβ interactions (**Figure 3.3B**). On the contrary, the NCT- N242Y substitution, similarly to FAD-linked PSEN1 mutations, enhanced the detrimental effect of temperature on the Aβ(38+40)/42 ratio. These results demonstrate that the aa residues 241-242 within the NCT ectodomain influence Aβ generation by modulating the strength of GSEC-APP/Aβ interactions.

NCT residue 241 establishes a direct, short distance interaction with the APP/Aβ substrate

To gain insights into the structural basis underlying the (de)stabilizing effects of NCT ectodomain on GSEC-APP/Aβ interactions, we performed molecular dynamics (MD) simulations with the APP-derived Aβ49 substrate bound to human GSEC as the co-purifying peptide in the PDB:5FN3 structure (**Figure 3.4A, I**). Interestingly, the simulations suggested that human hNCT- I242 (I241 in mNCT) and APP_{C99}- K28 are in close proximity to each other (mean Cα-Cα distances of approx. 10Å during the 3 μs sampling time). A negatively charged residue present at position hNCT- 242 induced the formation of a salt bridge between hNCT- I242E (GSEC) and APP_{C99}- K28 in 34% of all sampled frames, while in 24% of all observations the two side chains were bridged by a water molecule (**Figure 3.4A, II and III**). Subsequently performed post-processing free energy calculations using the Molecular Mechanics Poisson-Boltzmann Surface Area (MMPBSA) method [316] indicated that hNCT- E242 indeed stabilizes GSEC-APP/Aβ interactions by 2.90 ± 0.13 kcal/mol (mean ± S.E.M., with N = 1500). Furthermore, the simulations supported the importance of the interactions between APP ectodomain and the first extracellular loop of PSEN1 (residues 109 to 118), a region reported previously to be involved in the substrate recognition [318] and mutated in FAD.

Based on the theoretical analysis, we speculated that the formation of a salt bridge between position 241 in mouse NCT and K28 in APP_{C99} could explain the increments in the GSEC processivity of APP observed for the NCT-I241E/D mutants (**Figures 3.2C and 3.4B, I vs. II**). To challenge this possibility experimentally, we 'inverted' the putative salt bridge between NCT-I241 and APP_{C99}- K28. If our hypothesis were correct, the 'inverted' salt bridge (NCT-I241K and K28E) would also enhance GSEC processivity. Of note, previous studies have shown that K28 in APP_{C99}/Aβ critically regulates Aβ length by an unknown mechanism [319–322], and accordingly, the single K28E APP_{C99} mutation shifted Aβ profiles (generated by the wild type GSEC) towards the generation of shorter Aβ peptides, relative to the wild type substrate (**Figure 3.4B, I vs. III**).

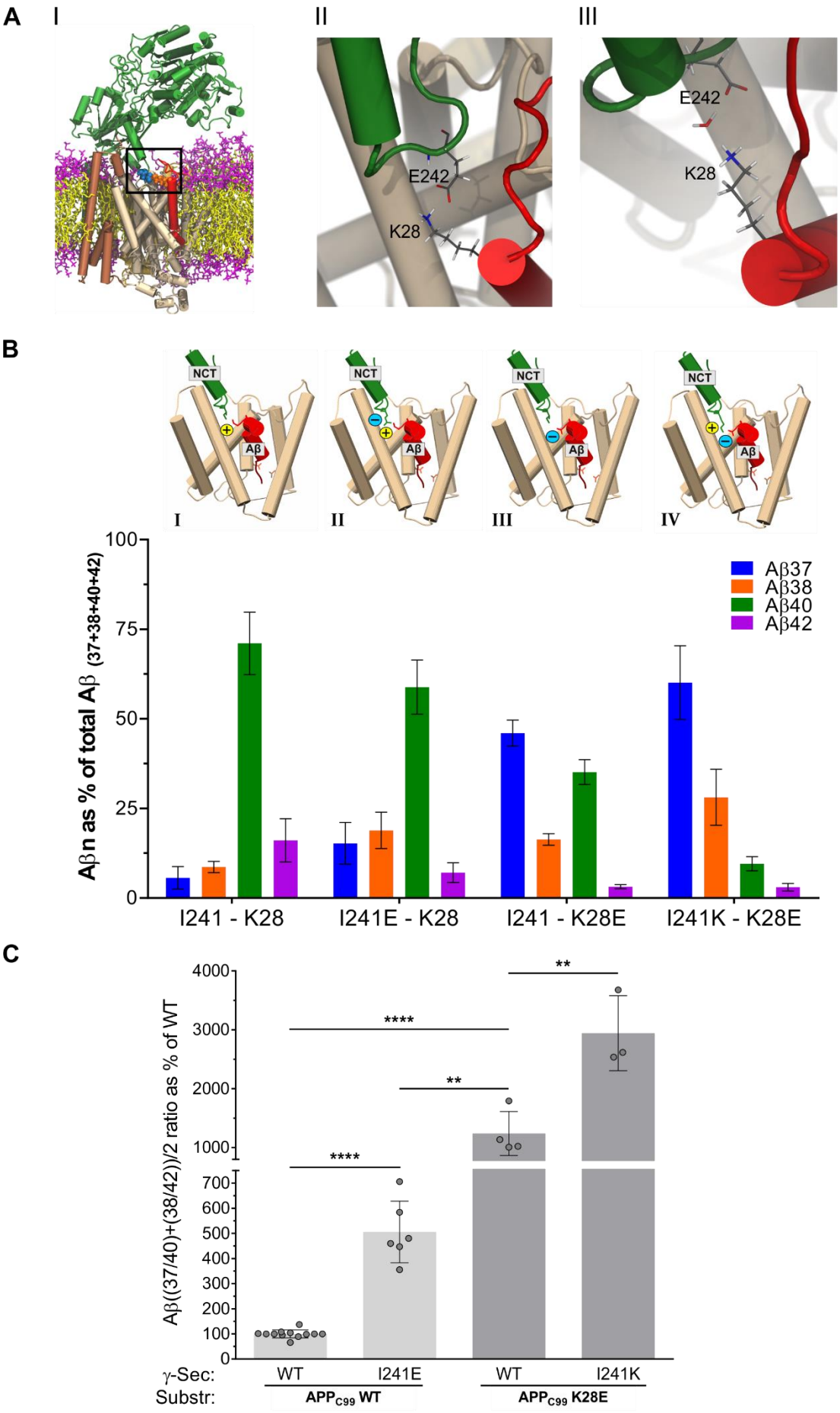
A
I
II
III
E242
K28
E242
K28
B
NCT
Aβ
I
II
III
IV
Aβn as % of total Aβ (37+38+40+42)
100
75
50
25
0
Aβ37
Aβ38
Aβ40
Aβ42
I241 - K28
I241E - K28
I241 - K28E
I241K - K28E
C
Aβ((37/40)+(38/42))/2 ratio as % of WT
4000
3000
2000
1000
700
600
500
400
300
200
100
0
****
**
****
**
γ-Sec:
WT
I241E
WT
I241K
Substr:
APPC99 WT
APPC99 K28E

Figure 3.4. Direct, short-distance interaction between positions hNCT-242 and APP/Aβ-28 regulates GSEC processivity towards APP_{C99}.
(A) Molecular dynamics simulations superimposing the cryo-EM-determined GSEC structure (PDB: 5FN3) with an NMR Aβ structure (PDB: 1IYT) on the co-purifying helical peptide (I), present hNCT-I242 and APP_{C99} -K28 at the NCT ectodomain-APP interface and modelling of the NCT I242E mutant suggests a direct (II) or indirect (bridged by H_2O, III) interaction between the NCT-E242 and the APP_{C99} -K28 side chains. **(B)** Aβ profiles (% contribution of individual Aβ37, Aβ38, Aβ40, and Aβ42 peptides to the total Aβ levels (Aβ37+38+40+42)) in the conditioned medium collected from WT or mutant (NCT) MEF cells lines co-expressing WT or mutant APP_{C99} substrates were assayed by ELISA. Schematic models of the tested GSEC-APP complexes are shown. **(C)** To account for the increased production of Aβ37 and Aβ38 at the expense of Aβ40 and Aβ42 in the tested conditions, the ratio of ((Aβ 37/40) + (Aβ 38/42))/2 was determined and used to estimate GSEC processivity of APP_{C99}. All the data are presented as mean ± SD, N ≥ 3, Unpaired, two-tailed Student's t-test was used to determine the statistical significance. **p > 0.01, ****p > 0.0001. Calculated T- and Df values were: T = 11,63; Df = 16 (I241-K28 vs I241E-K28), T = 11,37; Df = 14 (I241-K28 vs I241-K28E), T = 4,572; Df = 8 (I241E-K28 vs I241-K28E), T = 4,497; Df = 5 (I241-K28E vs I241K-K28E), T = 2,561; Df = 7.

Yet, the inclusion of the 'inverted' salt bridge (I241K – K28E) further enhanced GSEC processivity of APP_{C99} (**Figure 3.4B, III vs. IV**), supporting a stabilizing role of the ionic interaction between NCT and APP/Aβ substrates. ELISA analysis of Aβ profiles revealed a strong enhancement of the GSEC-mediated generation of Aβ37 and Aβ38, at the expense of their precursors Aβ40 and Aβ42 in mutant NCT MEFs expressing mutant APP_{C99}- K28E substrates. Therefore, we included the contribution of the Aβ37 peptide in the estimation of GSEC processivity of APP by calculating the ((Aβ37/40) + (Aβ38/42)) ratio. The results clearly showed that the GSEC processivity of the mutant APP_{C99}-K28E was further enhanced when a positive charge was introduced at the position NCT-241 (I241K) (**Figure 3.4C**, NCT-WT – APP_{C99}-K28E vs. NCT-I241K – APP_{C99}-K28E). This additive effect provides experimental evidence in support of a site-specific interaction between NCT-I241 and APP_{C99}-K28, with functional consequences on the efficiency of the sequential GSEC proteolysis.

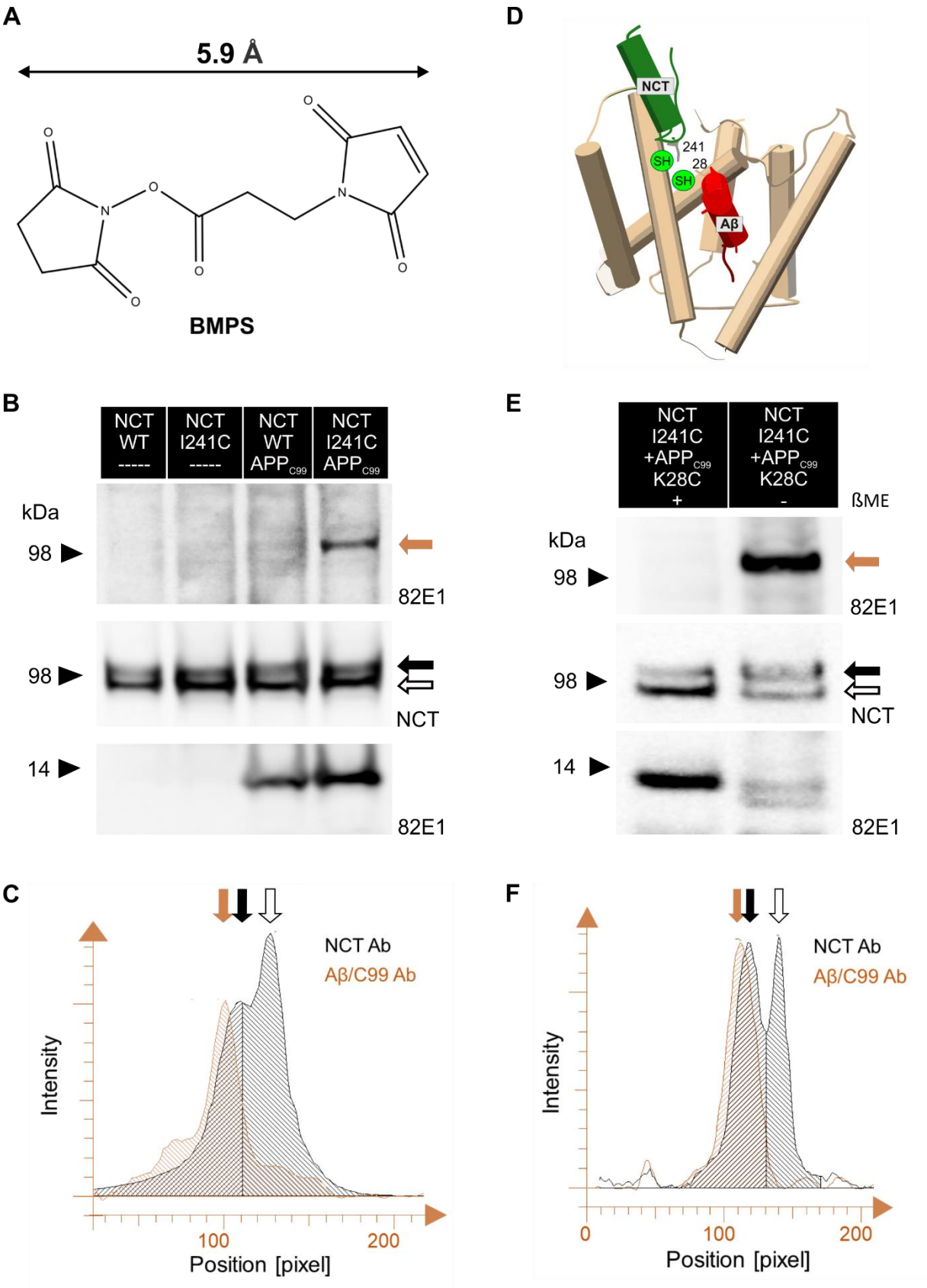
A
5.9 Å
BMPS
D
NCT
241
28
SH
SH
Aβ
B
NCT WT -----
NCT I241C -----
NCT WT APP$_{C99}$
NCT I241C APP$_{C99}$
kDa
98
82E1
98
NCT
14
82E1
E
NCT I241C +APP$_{C99}$ K28C +
NCT I241C +APP$_{C99}$ K28C -
ßME
kDa
98
82E1
98
NCT
14
82E1
C
NCT Ab
Aβ/C99 Ab
Intensity
100
200
Position [pixel]
F
NCT Ab
Aβ/C99 Ab
Intensity
0
100
200
Position [pixel]

Figure 3.5. Short distance interaction between NCT 241 and APP_{C99} K28.
(A) Chemical structure of the BMPS hetero-bifunctional (amine- and thiol-reactive groups) cross-linker. **(B)** The introduction of Cys at position 241 in NCT allows chemical cross-linking of NCT and APP_{C99} with BMPS. Representative SDS-PAGE/western blot show cross-linked NCT-APP_{C99}, NCT and APP_{C99} bands in detergent-extracted membrane proteins from BMPS cross-linker-treated membranes prepared from MEF cell lines expressing the indicated WT or mutant NCT GSEC complexes together with APP_{C99} or in the absence of the substrate. Orange, black, and white arrows indicate the NCT-APP_{C99}/Aβ crosslinked, mature NCT, and immature NCT bands, respectively. Arrowheads indicate the position of molecular weight markers. **(C)** Analysis of the western blot density profiles in panel (B) shows that the co-migration of NCT (orange arrow) with APP_{C99} shifts the cross-linked band towards a higher molecular weight than the observed for mature NCT (black arrow). Immature NCT is indicated with an open (white) arrow. Full-range molecular weight density profiles are shown in **Figure S3.3C**. **(D)** Schematic representation of the GSEC-APP_{C99} complex modified at NCT- I241 and APP-K28 by the introduction of Cys substitutions. **(E)** Representative SDS-PAGE/western blot presents NCT-APP_{C99}, NCT and APP_{C99} expression in detergent-extracted membranes prepared from MEF cell lines co-expressing the mutant NCT-I241C GSEC complex with the APP_{C99}-K28C substrate. As a negative control, the same sample was supplemented with β-mercaptoethanol (BME) to reduce all disulfide bridges. A full-range molecular weight western blot is shown in **Figure S3.3B**. Orange, black, and white arrows indicate the NCT-APP_{C99}/Aβ crosslinked, mature NCT, and immature NCT bands, respectively. Arrowheads indicate the position of molecular weight markers. **(F)** Analysis of the integrated density profiles of the respective western blot bands supports the spontaneous formation of a disulfide bond between NCT-I241C andAPP_{C99} K28C (mature and immature NCT are indicated with black and white arrows, respectively. The filled orange arrow points at the high molecular weight APP_{C99}/Aβ density (crosslinked NCT-APP_{C99}/Aβ band). Note that peak amplitudes for the cross-linked NCT-APP_{C99} and the mature NCT band were normalized to similar values for clarity purposes. Full-range molecular weight density profiles are shown in **Figure S3.3D**.

To further verify the interaction between the aa at the positions 241 in NCT and 28 in APP_{C99}, we performed chemical cross-linking experiments using the heterobifunctional cross-linker N-β-maleimidopropyl-oxysuccinimide ester (BMPS) that presents amine and thiol-reactive groups connected by a 5.9 Å spacer arm (**Figure 3.5A**). To this end, we generated mutant NCT-I241C and stably expressed it in the *Ncstn*$^{-/-}$ MEFs. SDS-PAGE/Western blot analysis of the GSEC complexes in the generated cell line showed the presence of the mature, fully glycosylated NCT as well as PEN-2 and an efficient endoproteolytic generation of PSEN1-NTF and -CTF, relative to the wild type condition (**Figure S3.3A**), indicating that the mutant NCT-I241C rescues GSEC complex formation and activity.

As next step, we expressed transiently the wild type APP_{C99} substrate in the wild type and the NCT-I241C cell lines. In addition, we included non-transduced cell lines as controls. To enhance the formation of the E-S complexes and prevent their dissociation due to proteolysis, we treated the cells overnight with 1 μM GSEC inhibitor X, a transition-state analog that halts substrate turnover but allows substrate binding to GSEC [323]. Then, we harvested the cells, prepared total membrane fractions, and subjected these fractions to a 2-step cross-linking protocol using BMPS. To evaluate the cross-linking products, we detergent-extracted membrane proteins and performed SDS-PAGE/western blot analyses using 82E1 anti-APP_{C99} (binds to the N-terminus of APP_{C99}/Aβ) and anti-NCT antibodies (**Figure 3.5B**). Immunoblotting with the anti-APP_{C99} antibody confirmed the expression of the substrate in the transduced cells (**Figure 3.5B, lanes 3 and 4, bottom panel**) and revealed the presence of a higher molecular weight band (~100 kDa) exclusively in the cross-linked extracts prepared from the NCT-I241C cell line overexpressing the APP_{C99} substrate (**Figure 3.5B, lane 4 vs. 3, top panel**). Further analysis with an anti-NCT antibody showed that the electrophoretic mobility of the "high-molecular-weight" APP_{C99}/Aβ-positive band (cross-linked NCT-APP_{C99}/Aβ complex) is slightly shifted towards a higher molecular mass, relative to the mobility of the mature, glycosylated NCT (**Figure 3.5C and S3.3C**). The observed shift supports the cross-linking of the wild type APP/Aβ substrate and mature mutant NCT-I241C and furthermore indicates that the Cys241 in NCT is at

least within 5.9 Å distance from a free amine group on the substrate, likely K28 in APP_{C99}.

Based on the apparent short distance between NCT and $APP_{C99,}$ and to confirm the involvement of K28 in the direct interaction with NCT-241, we tested the potential formation of a disulfide bond between these positions (**Figure 3.5D**). To this end, we expressed the APP_{C99}-K28C substrate in the NCT-I241C cell line, prepared total membranes and analyzed SDS-extracted membrane proteins in SDS-PAGE/western blot with anti-APP_{C99}/Aβ and anti-NCT antibodies under reducing and non-reducing conditions (**Figure 3.5E and S3.3D**). The presence of a high molecular weight APP_{C99}/Aβ-positive band (~100 kDa) under non-reducing conditions demonstrated the spontaneous formation of a disulfide bond between the NCT-I241C and APP_{C99}-K28C mutants (**Figure 3.5E and 3.5F**). Quantification of the integrated densities of the high molecular weight band corresponding to the NCT-APP_{C99}/Aβ on the anti-Aβ immunoblot revealed that ~15% (mean ± SD: 15.4 ± 5.7 %, N = 3) of the substrate got cross-linked to NCT (**Figure S3.3B**). In conclusion, our analyses demonstrate that the direct, short distance interaction between NCT-I241 and APP_{C99}-K28 modulates Aβ product profiles by stabilizing GSEC-APP/Aβ interactions.

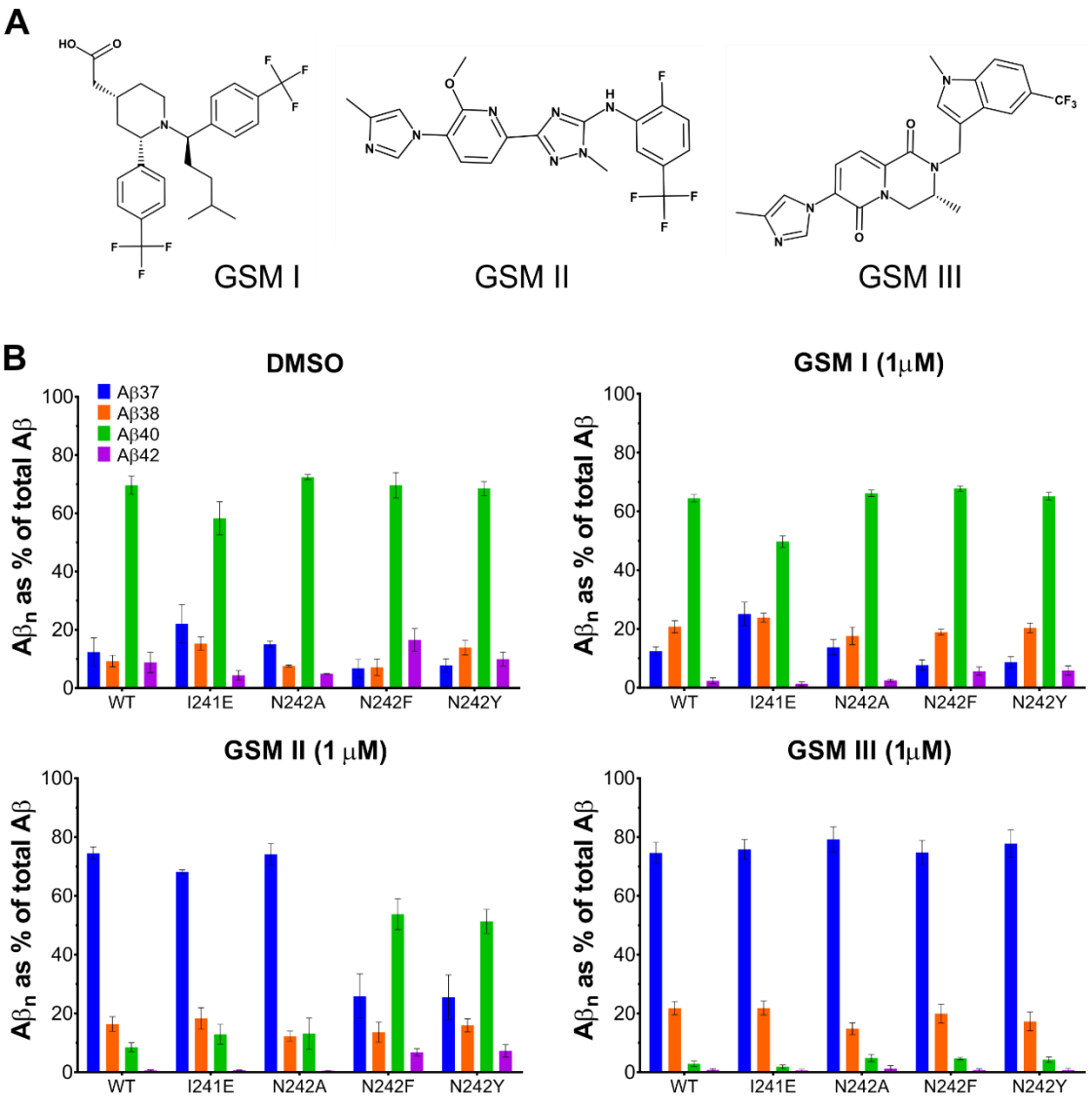

C

	Aβ 37/40			Aβ 38/42		
	DMSO vs 1 μM GSM I	DMSO vs 1 μM GSM II	DMSO vs 1 μM GSM III	DMSO vs 1 μM GSM I	DMSO vs 1 μM GSM II	DMSO vs 1 μM GSM III
WT	0.3987	<0.0001	<0.0001	<0.0001	<0.0001	<0.0001
I241E	0.5982	<0.0001	<0.0001	<0.0001	<0.0001	<0.0001
N242A	>0.9999	0.001	0.0056	0.0021	0.0023	0.0004
N242F	0.9211	0.9946	0.0001	0.0108	0.9955	0.0018
N242Y	0.9973	0.9955	<0.0001	0.0975	0.9997	0.031

Figure 3.6. GSECs destabilized by the N242F and N242Y NCT mutations do not respond to imidazole-based GSEC modulators.

(A) Chemical structures of the acidic-GSEC modulator (GSM I) and imidazole-based-GSM II and GSM III (GSM B in [218]). **(B)** Aβ profiles (% contribution of individual Aβ37, Aβ38, Aβ40, and Aβ42 peptides to the total Aβ levels (Aβ37+38+40+42)) in the conditioned medium collected from vehicle (DMSO) or GSM-treated (1 μM final concentration) MEF cells co-expressing respective WT or mutant NCT GSEC with APP_{C99} were determined by ELISA. Data generated using 0.3 μM GSM-treated MEF cells is shown in **Figure EV4**. Data are presented as mean ± SD, N ≥ 3 independent

experiments. **(C)** Aβ 37/40 and Aβ 38/42 ratios were calculated to evaluate the efficiency of the GSEC-mediated cleavage of APP_{C99} (**Figure EV4**) and statistical analysis (P values) (two-way ANOVA with Sidak's post hoc test) for the effect of GSMs on WT and mutant complexes is presented (response to GSM normalized to the corresponding vehicle condition).

NCT ectodomain (residue 242) mediates the response to imidazole-based GSEC modulators

Previous studies highlight K28 in APP_{C99} as a critical determinant of GSEC processivity of APP [319–322,324] and show that, in addition to their effects on Aβ length, mutations at this position alter the response to GSMs [321,322,324], but the underlying mechanisms remain unknown. These intriguing findings and the short distance interaction between positions 28 in APP_{C99} and 241 in NCT prompted us to test the response of mutant (de)stabilizing NCT GSEC complexes to GSMs belonging to different classes (acidic vs imidazole-based, **Figure 3.6A**). For this purpose, we transduced wild type and mutant (NCT-I241E, N242Y, and N242F) MEF cell lines with wild type APP_{C99}, as described before, and treated the cell cultures with 0.3 µM, 1 µM GSM or vehicle control (0.1% DMSO) overnight. To evaluate the response of wild type and mutant GSEC complexes towards GSMs, we collected the cell media and quantified Aβ37, Aβ38, Aβ40, and Aβ42 levels by ELISA and determined Aβ profiles (**Figure 3.6B, S3.4A**) as well as the Aβ37/Aβ40 and Aβ38/Aβ42 ratios (**Figure S3.4B and S3.4C**). The results revealed that the acidic GSM activates exclusively the Aβ42 → Aβ38 cleavage (**Figure 3.6C p_{values} for WT in columns 1 and 4**), while the imidazole-based GSMs II and III strongly activate both GSEC product lines, which is in agreement with previous findings [321,324]. The GSMs II and III thus shifted Aβ profiles towards the production of the Aβ37 and Aβ38 peptides (**blue and orange bars in Figure 3.6B**, respectively), with concomitant reduction in the Aβ40 and Aβ42 species (**green and purple bars in Figure 3.6B**, respectively).

Our analysis revealed that wild type, as well as mutant GSEC complexes, responded markedly to GSM I treatment (**right upper panel in Figure 3.6B**), with the exception of the NCT-N242Y GSEC mutant which showed a partial response (**Figure S3.4** and **Figure 3.6C, p_{values} for N242Y in column 4**). Most importantly, we observed

that the NCT-N242Y and N242F mutant GSECs did not respond to GSM II, as indicated by the Aβ profiles (**Figure 3.6B**) showing that Aβ40 (green bar) remains the major Aβ peptide produced by these mutant cell lines in the presence of 1 µM GSM II. In fact, statistical analysis on the Aβ37/Aβ40 and Aβ38/Aβ42 ratios reveals no significant differences between the processivities of the NCT-N242Y and N242F mutant cell lines treated with vehicle (DMSO) or 1 µM GSM II (**Figure 3.6C, p_{values} for N242F and N242Y in columns 2 and 5**). In contrast, the NCT-N242A GSEC mutant responded similarly to WT towards GSM II (**Figure 3.6B and 6C, p_{values} for N242A in columns 2 and 5**).

Altogether, these data demonstrate that bulky residues at the NCT-242 position not only impair the stability of GSEC-APP/Aβ assembly (and therefore enzyme processivity, as shown in **Figure 3.2C**) but also have an impact on the activation of GSEC by the imidazole-based GSM II. These results could be explained by the contribution of residue NCT-242 to the binding pocket of GSM II or to its participation in the allosteric mechanisms triggered upon GSEC-GSM interaction. We then reasoned that analysis of the mutant responses to another imidazole-based compound could enable to distinguish between these two scenarios. Interestingly, we found that the NCT-N242Y and N242F mutant GSECs did respond to GSM III, as indicated by the relative increments in Aβ37 (blue bars) in the right lower panel of **Figure 3.6B** and the significant changes in the Aβ 37/40 and Aβ 38/42 ratios for DMSO- vs. 1 µM GSM III-treated mutant cell lines (**Figure 3.6C, p_{values} for N242F and N242Y in columns 3 and 6**). These findings thus demonstrate that the mechanisms underlying GSEC processivity of APP remain intact in the mutant NCT-N242F and NCT-N242Y protease complexes, and point towards an altered binding of imidazole-based GSM II to NCT-N242Y and N242F GSECs. Furthermore, our studies also reveal a reduced response of the NCT-N242Y, N242F and N242A mutant GSEC complexes to GSM III in presence of 0.3 µM GSM III compared to the wild type protease (**Figure S3.4**). In conclusion, the differential responses of GSEC complexes bearing NCT-N242A, N242Y and N242F mutants towards imidazole-based GSM II and III (**Figure 3.6 B-C**) suggest partially distinct binding sites for these compounds. Our studies, therefore, assign a direct and active role to the ectodomain of NCT in the GSEC modulation by GSMs

3.6 Discussion

We have recently demonstrated that the stability of GSEC-APP/Aβ_n substrate interactions controls the length of Aβ product peptides, and thereby affects the risk for AD. Notably, our previous findings show that FAD-causing mutations destabilize GSEC-APP/Aβ (E-S) complexes and the magnitudes of their detrimental effects remarkably correlate with the age of disease onset [218]. The novel pathogenic link motivated us to investigate the intermolecular interactions that secure GSEC-Aβ_n assemblies during the sequential GSEC-mediated proteolysis. We departed from the high-resolution structure of GSEC in complex with a co-purifying helical peptide (PDB:5FN3, [171]). We hypothesize that this structure depicts the interaction between GSEC and the fragment generated after the initial proteolytic cleavage of the transmembrane domain of the substrate (*de novo* generated long Aβ from APP_{C99}), just before it engages into the next catalytic turnover. The putative substrate occupies the substrate-binding site, but in contrast to APP_{C83} [173], only the most N-terminal part of its transmembrane domain remains in a helical structure, while its unstructured C-terminal part extends along the substrate binding channel to reach the active site. We actually proposed that the first endopeptidase-mediated backbone break exerts a strong destabilizing effect on the helical structure of APP_{C99}, leading to this configuration. In our model further unwinding of the N-terminal helix of the substrate must occur upon each GSEC cut, in order to provide the length of the substrate to fill the S1'–S3' enzyme pockets [194] during the stepwise catalysis. The sequential unwinding of the N-terminal helix progressively destabilizes the E-S assembly, increasing the probability of its dissociation and consequent release of Aβ_n. This "unwinding model" - originally proposed in [218] - suggests that the interactions established between the N-terminal helical structure of the substrate and the protease "anchor" the E-S complex and thereby define the length of the N-terminal products (Aβ from APP). Interestingly, our analysis identified a potential contact site between the ectodomains of NCT (aa residues 241-242 in mNCT) and the co-purifying peptide (putative substrate). Accordingly, we hypothesized that the potential 'NCT-APP/Aβ' interface could directly contribute to the stability of E-S interactions, and thereby modulate the length of Aβ products. Note that the established role of the non-catalytic subunits (NCT, PEN-2, and APH1) of the

protease in PSEN/GSEC function and turnover [155,325], supports their contribution to the stability of GSEC-APP/Aβ complexes.

Our studies revealed differential contributions of residues 241-242 in NCT to GSEC-$A\beta_n$ interactions, implicating for the first time the ectodomain of NCT in the mechanisms controlling Aβ length. Interestingly, we showed that aromatic substitutions at the position NCT- 242 (N242F/W/Y) significantly reduce GSEC processivity of APP to the levels similar to those exhibited by FAD-pathogenic *PSEN1* variants (**Figures 3.2C and S3.1B**), while the presence of negatively charged residues at the position NCT- 241 promotes the production of shorter Aβ peptides. Further cell-based GSEC thermoactivity analysis demonstrated that the mutant NCT-induced shifts in Aβ profiles by influencing the stability of GSEC-APP/$A\beta_n$ interactions (**Figure 3.7**).

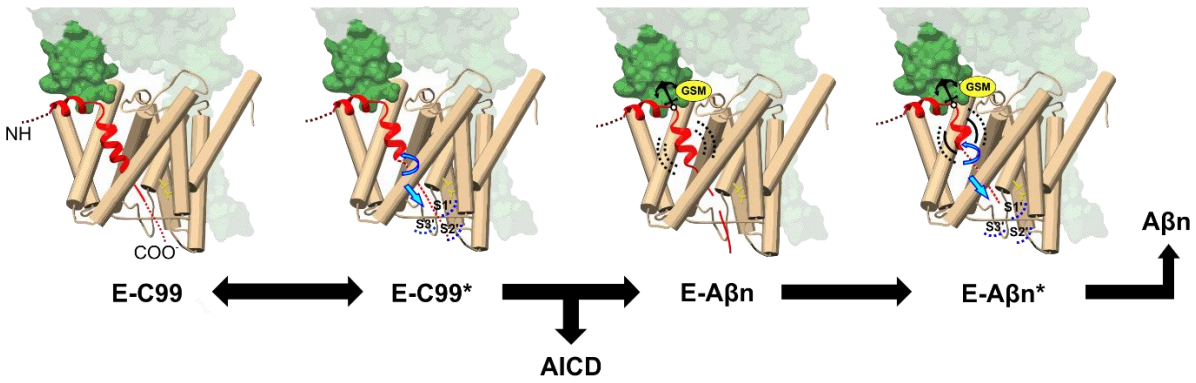

Figure 3.7. Proposed model for GSEC mediated cleavage of APP and its modulation by GSMs.
Once the E-S complex is formed, the first endopeptidase cut strongly destabilizes the helical transmembrane domain of APP_{C99}, leading to the unwinding of the most C-terminal helical part of the Aβ substrate and providing the length to the "de novo" generated Aβ substrate to reach the active site (model originally proposed in [218]). The further unwinding of the Aβ substrate with each sequential cleavage, stretches the substrate and provides the length to fill the catalytic pockets but weakens the GSEC-Aβn interaction until the eventual E-S dissociation triggers Aβ release. Here, we propose that the extracellular interface that includes NCT (241/242), APP (K28) and the first extracellular loop of PSEN1 anchors GSEC-APP/Aβn complexes during the sequential proteolytic mechanism, and the E-S interface is the target of selected imidazole-based GSMs.

The theoretical GSEC-Aβ model (developed here) pointed towards the existence of a positively charged residue in the APP substrate and suggested a direct interaction between positions I242 in hNCT and K28 in APP_{C99}, which was confirmed in cross-linking experiments. Of remark, the spontaneous formation of a disulfide bond between NCT and APP, when Cys residues were introduced at positions 241 in mNCT and 28 in APP_{C99}, defined it as a short-distance interaction surrounded by an aqueous environment, and thus likely located in the extracellular/luminal environment [326].

During the preparation of this report, the co-structures of the GSEC with the Notch or APP_{C83} substrate became available [173,175]. Interestingly, the GSEC-Notch complex shows an extracellular interface between the ectodomains of the NCT subunit and Notch, with the NCT-241-242 aa located at the E-S interface (**Figure S3.5A**). The GSEC-APP_{C83} complex shows the APP- K12 (corresponding to K28 in APP_{C99}) in the proximity to the NCT-241 residue, however, since the interface in the GSEC-APP_{C83} structure is not fully resolved, it is possible that the cross-linking of GSEC (PSEN1-Q112C) to the APP_{C83} V8C substrate affected this region in the atomic model (**Figure S3.5B**). The functional data presented here, together with the novel GSEC-substrate co-structures [173,175], suggest a conserved mechanism for the stabilization of GSEC-substrate interactions and may support the involvement of NCT ectodomain in the substrate recognition by the GSEC complex, by stabilizing the initial GSEC-substrate assembly. Of note, the ectodomain of NCT was initially proposed to act as a substrate receptor in the protease, with the anionic NCT-E333 residue and the free N-terminal amine group of the substrate interacting [160]. However, the model has been challenged by biochemical studies [162,163] and the recent E-S structural data finally disproved it. The currently accepted model for NCT function assigns to its ectodomain a rather passive role in the "substrate selection", in which it restricts -by steric hindrance- the access of substrates presenting large ectodomains [161]. Our data provide compelling evidence for additional, novel implications of the NCT ectodomain, i.e. its active role in the regulation of the GSEC processivity of APP and the modulation of the response to GSEC modulators (GSMs). Previous reports have shown that APP-K28 mutations exert profound effects on Aβ generation via an unknown mechanism [319,320] and alter the response to GSMs

[321,322,324]. Here, we demonstrate that the effects of K28 on APP processing are explained in part by its interaction with the ectodomain of NCT.

The proven direct, short distance interaction between K28 in APP_{C99} and position 241 in NCT ectodomain (**Figure 3.5**) and their shared implication in the regulation of GSEC processivity motivated us to investigate the effects of the (de)stabilizing mutations at positions NCT-241/242 on the GSEC response to GSMs. Remarkably, our data revealed that the substitutions in NCT-242 that destabilize GSEC-APP/Aβ interactions (N242F and N242Y, as demonstrated in **Figure 3.3**), also had strong deleterious effects on the response to imidazole-based GSM II in both production pathways (>90% reduction for the mutant NCT-N242F and N242Y cell lines at 1 μM GSM II relative to the wild type GSEC, **Figure S3.4**). Clearly, GSM II promoted the conversion of Aβ40 into Aβ37 and Aβ42 into Aβ38 by the wild type protease but failed to engage the NCT-N242F/Y mutant GSEC complexes on these specific cuts. The similar responses of the wild type and NCT-N242A mutant GSECs indicate that bulky substitutions at position NCT-242 not only destabilize GSEC-APP/Aβ interactions, and accordingly change Aβ product profiles, but also impair drastically the response to GSM II. The results could be explained by the contribution of residue NCT-242 to the formation of the binding pocket for GSM II or to its participation in the allosteric mechanisms triggered upon GSEC-GSM interaction. However, our studies revealed that the NCT-N242F/Y mutant GSEC complexes largely respond to GSM III. These observations support the contribution of NCT to the formation of the binding pocket for imidazole-based GSMs, rather than its participation in the mechanisms underlying the response. On this regard, the binding site of another imidazole-based GSM (ST2038, structurally similar to the GSM II) has been located to the first extracellular loop of PSEN-NTF [327], which according to structural data is in proximity to the identified NCT-APP interface. Furthermore, the novel GSEC-Notch/APP_{C83} co-structures place the substrate in between the studied NCT region and the first extracellular loop of PSEN1 (**Figure S3.5**) supporting our conclusions. Finally, a cross-competition study between the imidazole-based GSM (ST2038) and the acidic GSM I shows that pretreatment with GSM I substantially decreases the affinity-labelling of the GSEC complex by the ST2038 GSM [327], suggesting partially overlapping binding pockets for acidic and

imidazole-based GSMs. The lack of response of the mutant NCT- N242Y to GSM I observed here supports a similar conclusion.

Of potential clinical significance, the marked impact of the aa substitutions within NCT ectodomain on APP processing suggests the potential existence of AD-causing or protective single nucleotide variants (SNPs) in the *NCSTN* (i.e. NCT encoding) gene. The data specifically highlight position N242 in NCT, where a single nucleotide change – N242Y substitution – lowers GSEC processivity to the levels associated with pathogenic *PSEN1* mutations. Intriguingly, no AD-pathogenic or protective mutations have been identified so far in NCT or in any of the non-catalytic subunits of the GSEC complex. It should be noted that in clinical practice, genetic testing varies between different centres and generally involves testing specifically for known genetic causes of dementia syndromes [328]. However, a high proportion of the genetic risk for AD remains uncharacterised. Rare highly penetrant mutations in PSEN1, PSEN2, and APP are thought to account for only 5-10% of all early-onset AD (EOAD, onset <65y) cases, whilst the heritability of EOAD has been estimated to range from 92-100%, thus leaving 90-95% of the affected families with an unidentified genetic cause for the disease [329]. In late-onset AD, which has a heritability of 70-80%, five new genetic risk loci have recently been identified, with pathway analysis implicating immunity, lipid metabolism, tau binding proteins and APP metabolism [14]. Furthermore, the enrichment of rare variants in the APP metabolism in this study suggests that additional rare variants remain to be identified.

Collectively, the presented data demonstrate for the first time the existence of an extracellular NCT-APP interface implicated in the modulation of the strength of GSEC-APP/Aβ interactions (and thus Aβ length) as well as in the response of E-S complexes to GSMs (E-S stabilizers). Based on our original findings, the novel E-S structural data [173,175] and the literature, we propose that the extracellular GSEC (NCT-PSEN)-APP interface encompassing the aa region 241-242 in NCT ectodomain, K28 in APP and the first extracellular loop of PSEN plays a critical role in the stabilization of GSEC-APP/$A\beta_n$ interactions and is involved in the binding of selected imidazole-based GSMs. Notably, the idea of selectively targeting APP processing with substrate targeting compounds [330] has been raised in the past but has been abandoned due to studies showing

that potent pharmaceutics modulating Aβ length bind rather to the protease complex. Our studies may conciliate these views.

Conclusions

This study demonstrates that NCT plays an active role in the regulation of the efficiency of the sequential GSEC cleavage of APP by establishing a direct interaction with the APP/$A\beta_n$ substrate. The results of the cross-linking experiments of NCT and APP_{C99} validate the position of the co-purifying helical peptide in the PDB:5FN3 GSEC structure as the substrate-binding site for APP, and thus put this co-structure as a suitable model for the investigation of the structural-functional relationships existing within the GSEC-$A\beta_n$ complexes. Our results also suggest that an extracellular interface between GSEC and APP could be the target for GSMs (E-S stabilizers). These novel insights may conciliate different views on the location of GSM binding pocket(s) and guide future efforts to develop safe therapies targeting GSEC-APP/Aβ assemblies, i.e. the generation of GSEC stabilizing compounds (GSSC). Finally, this study raises additional considerations with potential implications for the clinic, as the remarkable involvement of NCT in the regulation of the Aβ product length suggests a potential link between single-nucleotide variants in *NCSTN* and AD risk.

3.7 Supplementary figures

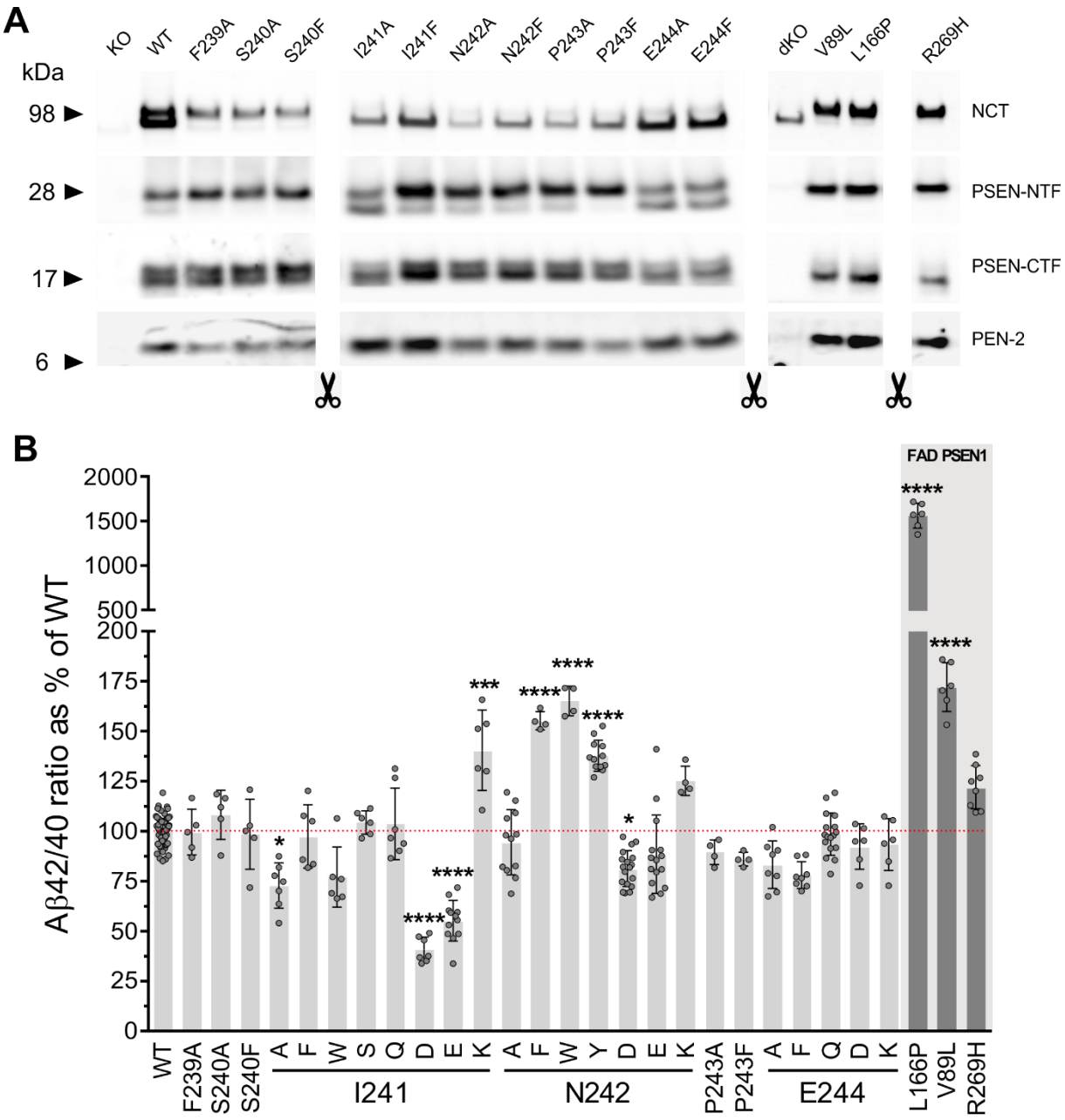

Figure S3.1. NCT ectodomain regulates the Aβ42/40 ratio

(A) Representative SDS-PAGE/western blot analysis of CHAPSO-solubilized membrane proteins from *Ncstn*$^{-/-}$ or *Psen1*$^{-/-}$/*Psen2*$^{-/-}$ MEF cell lines stably expressing WT or mutant mouse NCT/ human PSEN1 subunits (shown in Fig. 2A). The presence of mature, glycosylated NCT, N-terminal and C-terminal fragments of the endoproteolysed PSEN1 and PEN-2, compared to NCT knock-out (KO) or PSEN1/2 double KO (dKO) cells, indicate that WT and mutants reconstitute GSEC complexes. Arrowheads indicate the position of molecular weight markers. **(B)** Aβ peptides present in the extracellular media of cultured WT or mutant mNCT/hPSEN1 MEF cell lines, transiently expressing APP_{C99} substrate, were quantified by ELISA and the Aβ 42/40

ratio determined and plotted as % of the WT condition. The data are represented as mean ± SD, N ≥ 4 independent experiments. One-way ANOVA and Dunnett's post-hoc test was used to determine the statistical significance; ***p > 0.001, ****p > 0.0001 (compared to WT condition). F(DFn, DFd): F(31, 290) = 873,6.

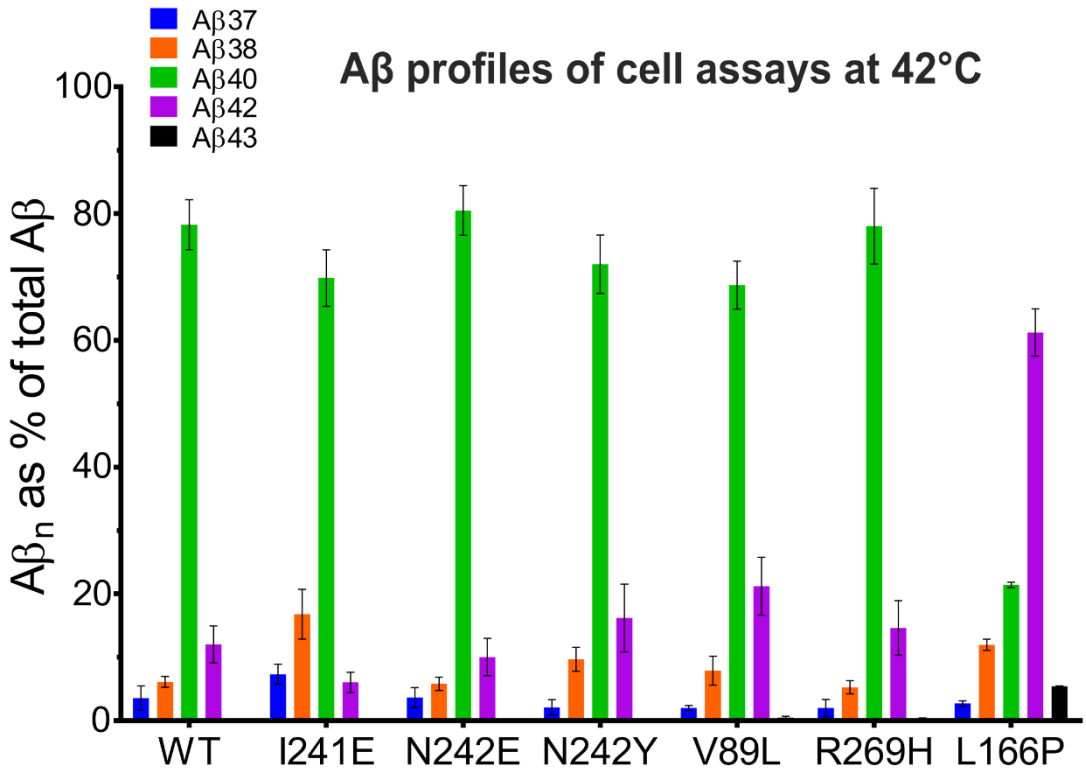

Figure S3.2. **Secreted Aβ profiles in cell-based thermoactivity assays**
Aβ profiles (% contribution of individual Aβ37, Aβ38, Aβ40, Aβ42 and Aβ43 peptides to the total Aβ levels (Aβ37+38+40+42+43)) in the conditioned medium collected from WT or mutant (NCT) MEF cells lines co-expressing WT or mutant APP_{C99} substrates, subjected to temperature challenge, were assayed by ELISA. The contribution of the Aβ43 peptides to the secreted Aβ pool is less than 1% for the WT or mildly destabilizing FAD mutants (V89L and R269H). Data are represented as mean ± SD, N ≥ 3.

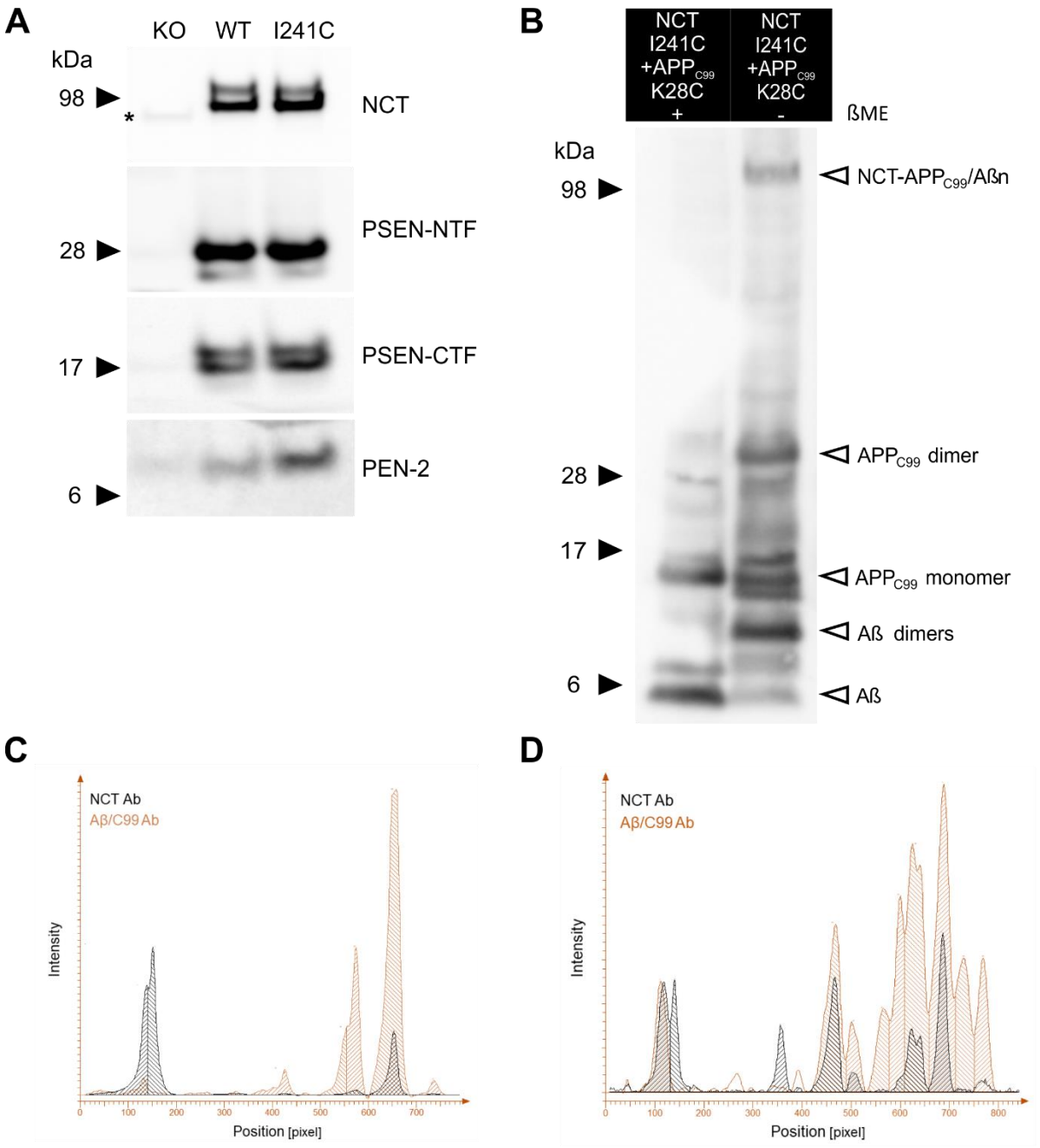

Figure S3.3. Cross-linking data demonstrates a short distance interaction between NCT 241 and APP$_{C99}$ K28

(A) Representative SDS-PAGE/western blot analysis of CHAPSO-solubilized membrane proteins extracted from Ncstn$^{-/-}$ MEF cell lines stably expressing WT or mutant mNCT- I241C subunits (shown in **Figure 3.5**). The presence of mature NCT, N-terminal and C-terminal fragments of the endoproteolysed PSEN1 as well as PEN-2, compared to NCT knock-out (KO) cells, indicate that WT and the I241C mutant reconstitute GSEC complexes. *Non-specific band. Arrowheads indicate the position of molecular weight markers. **(B)** Representative SDS-PAGE/western blot presenting NCT-APP$_{C99}$/Aβ, and APP$_{C99}$ expression (as detected by 82E1 anti-Aβ antibody) in detergent-extracted membranes prepared from MEF cell lines co-expressing respective

NCT- I241C mutant GSEC complex with APP_{C99}- K28C substrate. In the non-reduced condition (- βME) bands corresponding to APP_{C99} and/or Aβ dimers are appearing, as indicated with arrowheads. To estimate the amount of substrate cross-linked to GSEC (i.e. spontaneous disulphide bond formation between APP_{C99}/Aβ and NCT), the NCT-APP_{C99}/Aβ band was quantified and normalized to 'total APP/Aβ expression' (defined as the sum of the bands indicated with arrowheads). Mean efficiency ± SD = 15.4 ± 5.7 %, N = 3 independent experiments. Arrowheads indicate the position of molecular weight markers. **(C, D)** Analysis of the integrated density profiles on the full blots shown in **Figure 3.5B** (C) and **Figure 3.5E** (D).

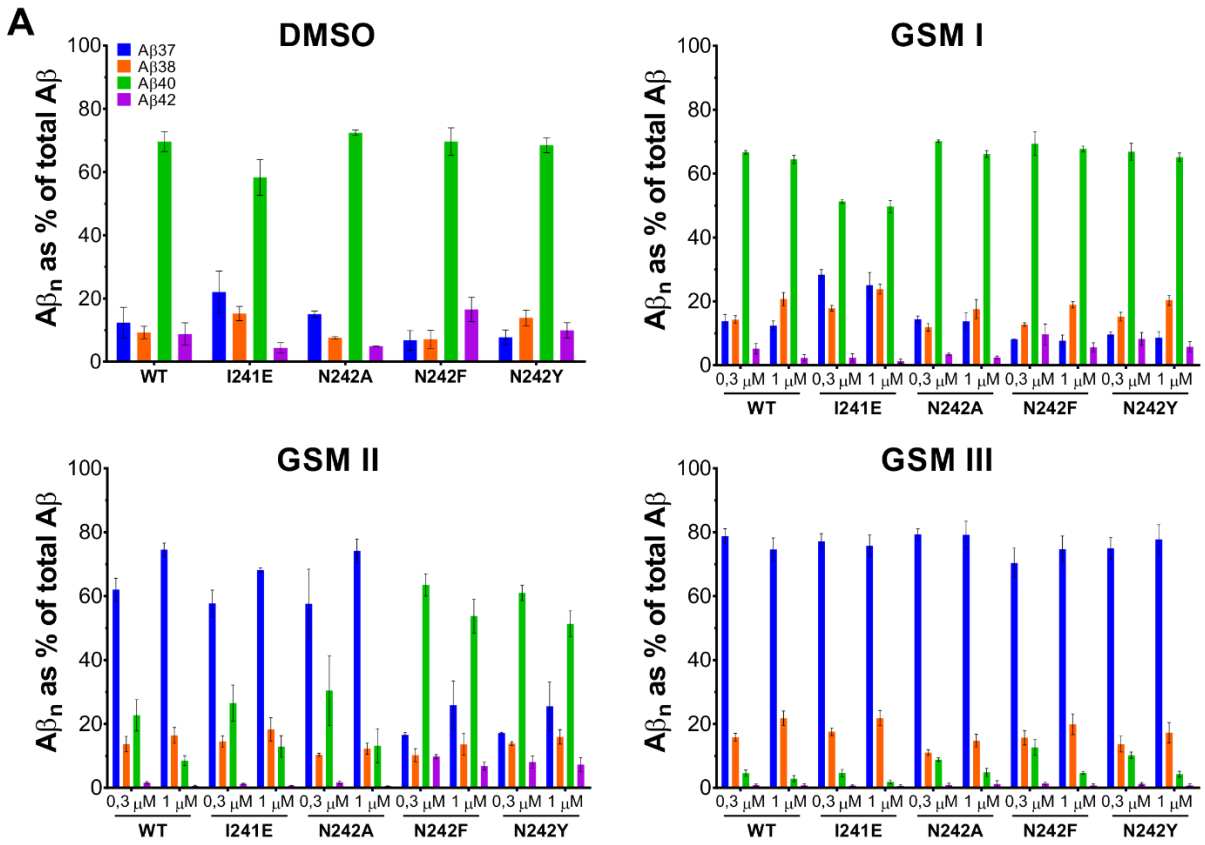

Figure S3.4. NCT ectodomain (N242) modulates the response toward imidazole-based GSEC modulators

(A) Aβ profiles generated by 0.3 and 1 μM GSM (I-II-III) or vehicle control (0.1% DMSO) treated mNCT mutant MEF cell lines (shown in **Figure 3.6**).

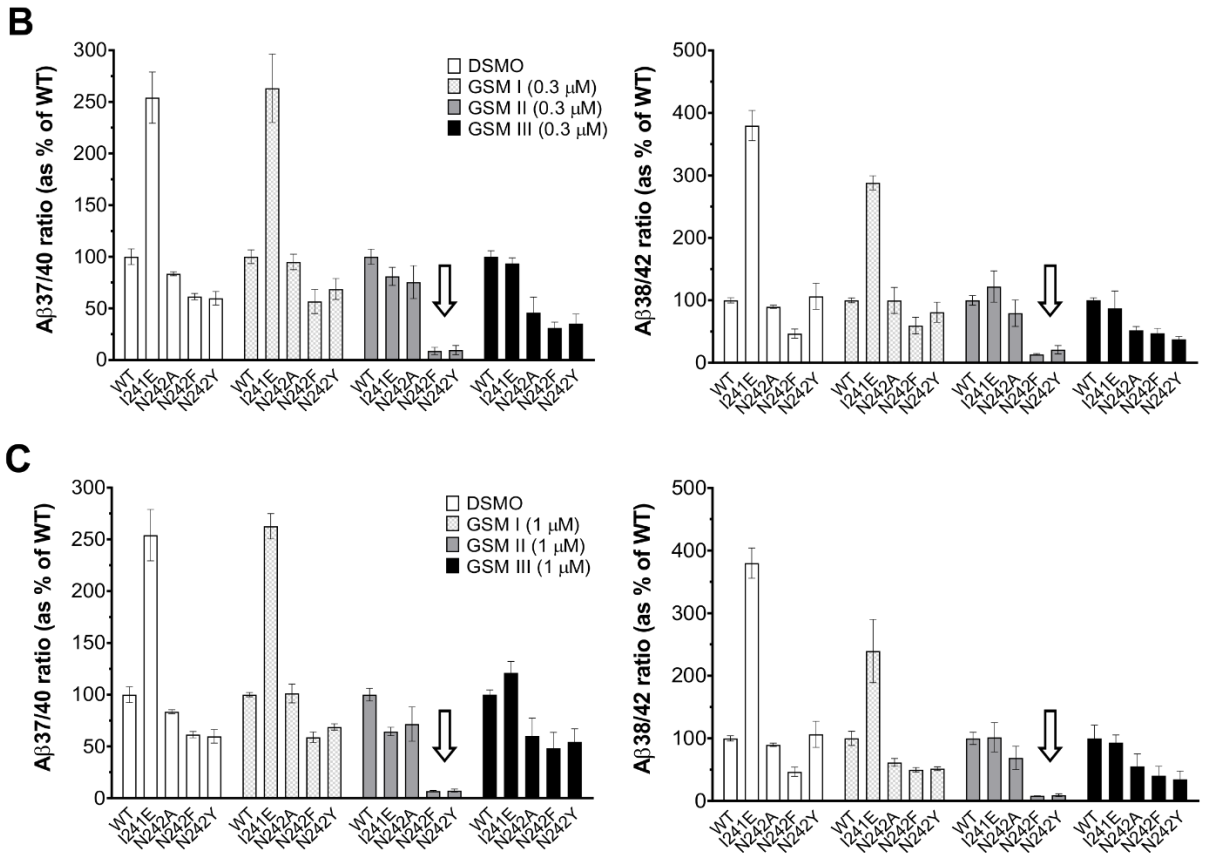

Figure S3.4. Continued

(B, C) Aβ 37/Aβ40 and Aβ 38/Aβ42 ratios were quantified to evaluate the effect of GSM 0.3 μM (B) or 1 μM (C) treatment on the processivity of different mNCT mutant GSECs (shown in **Figure 3.6**). The Aβ ratios are normalized to the response of the wild type GSEC towards vehicle (0.1% DMSO condition) or GSM treatment. The arrows indicate the lack of response to GSM II of the N242F/Y substitutions. Data information: Data are presented as mean ± SD, N ≥ 3 independent experiments.

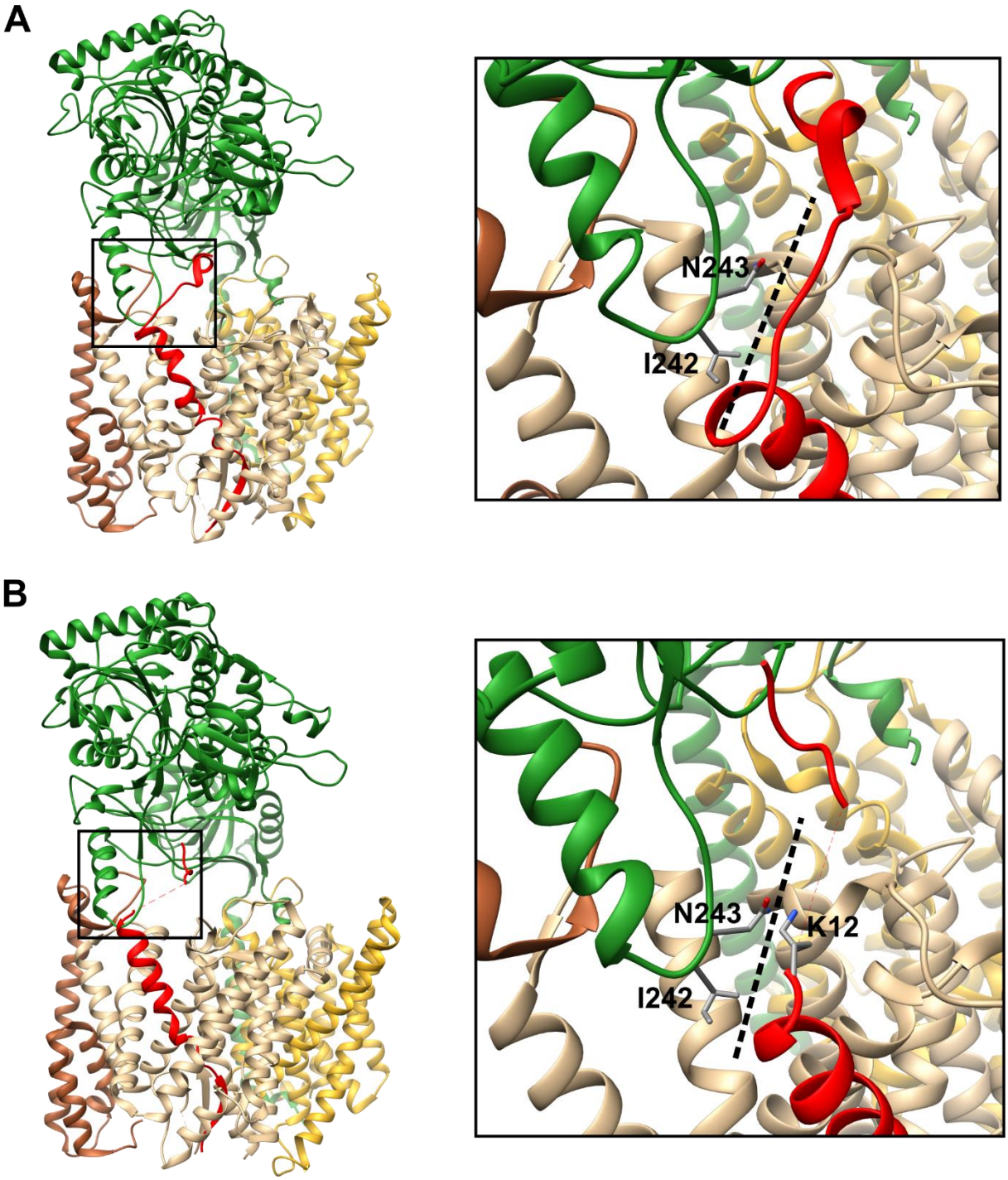

Figure S3.5. NCT–APP interface highlighted in the 6IDF and 6IYC GSEC-Substrate co-structures

(A, B) GSEC co-structure with Notch (PDB:6IDF) (A) or APP_{C83} (PDB:6IYC) (B) substrate is presented. PSEN1 is shown in light brown, PEN-2 in dark brown, APH1A in gold, NCT in green and Notch/APP_{C83} in red. The side chains of the NCT- I241 and N242 (together with K12 (corresponding to K28 in APP_{C99}) in the APP_{C83} structure) are shown and the interface between Notch/APP_{C83}, NCT ectodomain, and PSEN1 is magnified and marked with a dashed line.

3.8 Acknowledgements and author contributions

Acknowledgements:

This work was funded by the Stichting Alzheimer Onderzoek (SAO; S16013) and the KU Leuven Methusalem grant (METH/14/07). D.P. is supported by a PhD fellowship from the FWO (SB/1S23819N). N.S.R. is supported by a University of London Chadburn Lectureship in Medicine. We thank Janssen Pharmaceutica for anti-Aβ monoclonal antibodies and GSMs. We are grateful to Maria Szaruga for their critical reading of the manuscript and thank Michel Vande Kerckhove for helpful discussions.

Author Contributions:

L.C.G. designed the study, analyzed the data, supervised the research and wrote the manuscript. D.P. performed experiments and analyzed the data. S.L. performed cloning and protein purification and assisted with experiments. K.M.Z. analyzed data. N.S.R. provided input on clinically related matters. M.H. and M.Z. performed modeling and molecular dynamics simulations studies. M.M. provided Aβ ELISA antibodies and F.B. provided GSM compounds.

Conflict of interest:

D.P., M.H., S.L., K.M.Z., N.S.R, M.Z., and L.C.G. declare no competing interests. M.M. and F.B. are employees of Janssen Pharmaceutica.

4 Aβ profiles generated by Alzheimer's disease-causing *PSEN1* variants determine pathogenicity and linearly correlate with disease onset

This chapter is based on the following article that is currently in preparation:

Dieter Petit[1,2], Natalie S. Ryan[3,4], Antoinette O'Connor[3,4], Maria Szaruga[1,2], Rik Vandenberghe[5], Nick C. Fox[3,4] & Lucía Chávez-Gutiérrez[1,2,*]

1 VIB-KU Leuven Centre for Brain & Disease Research, Leuven, Belgium

2 Department of Neurosciences, Leuven Research Institute for Neuroscience and Disease (LIND), KU Leuven, Leuven, Belgium

3 UK Dementia Research Institute at UCL, London, UK

4 Dementia Research Centre, Department of Neurodegenerative Disease, UCL Queen Square Institute of Neurology, London, UK

5 Laboratory for Cognitive Neurology, Department of Neurosciences, KU Leuven, Belgium; Neurology Department, University Hospitals Leuven, 3000, Leuven, Belgium

* Corresponding author

4.1 Abstract

Increased amyloid-β (Aβ) 42 production has long been considered the key pathogenic event in autosomal dominant Alzheimer's Disease (AD), caused by mutations in Presenilin 1/2 *(PSEN1/2)* and the Amyloid Precursor Protein *(APP*) genes. However, analyses addressing the relationships between Aβ42 increments and clinical AD onset are inconsistent. This has led to reservations regarding the pathogenic role of Aβ peptides, and consideration of other potential disease-causing mechanisms. The paramount relevance of the relationship between the effects of pathogenic mutations and clinical outcome motivated us to revisit this central aspect of AD pathophysiology. We applied a mechanistically driven hypothesis that links alterations in the molecular composition of full-range Aβ profiles (beyond simply the relative proportions of Aβ42 and Aβ40) with clinical onset. Our data demonstrate that AD-causative mutation-induced changes in Aβ profiles linearly correlate with the age at symptom onset (AAO). These results offer key insights into the molecular foundation of *PSEN1* pathogenicity and provide support for therapeutic strategies set to shift Aβ profiles towards shorter and less amyloidogenic peptides.

4.2 Introduction

Alzheimer's disease (AD), the leading cause of dementia, is an inexorably progressive neurodegenerative disorder characterised by the cerebral accumulation of extracellular amyloid plaques, composed of aggregated amyloid β (Aβ) peptides; intracellular neurofibrillary tangles of the hyperphosphorylated and aggregated tau; reactive micro/astroglia; dystrophic neurites and progressive neuronal loss [13]. Genetic analysis, *in vitro* and *in vivo* biochemical data and longitudinal imaging studies strongly support the notion that altered Aβ production and/or clearance, resulting in Aβ build-up in the brain, triggers early pathogenic events leading to AD [53]. Specifically, it has been proposed that the accumulation of toxic, pathogenic Aβ42 oligomeric species in the brain precedes the onset of cognitive symptoms by more than two decades [12].

Accordingly, a number of therapeutic approaches have targeted lowering Aβ production or promoting its clearance. However, anti-Aβ clinical trials have largely been disappointing in terms of modifying the course of the disease – with the possible recent

exception of an anti-Aβ immunotherapy which is currently under review with the US FDA (https://www.alzforum.org/news/research-news/fda-accepts-aducanumab-application-priority-review). The failures have not only questioned the critical, pathogenic role assigned to Aβ, but also put AD therapeutic research and development at a critical crossroads: embracing alternative targeting strategies; continuing development of Aβ-based therapies for all disease stages; or focussing anti-amyloid therapies on treatment at a preclinical stage – ideally before amyloid deposition is established – to prevent neurodegeneration and dementia onset [331]. Of relevance, primary and secondary prevention trials are underway or planned in asymptomatic individuals at imminent risk for AD (i.e. autosomal dominant AD-linked mutant carriers or trisomy 21 patients) [332–334]

While the most common form of AD is sporadic (SAD) and characterized by a late (> 65 y) symptom onset, a rare inherited form (familial AD, FAD) is caused by autosomal dominant mutations in the Presenilin (*PSEN1/PSEN2*) [66–68,291] and the Amyloid Precursor Protein (*APP*) [74,75] genes. These autosomal dominant forms of AD are characterized by an early age at onset (AAO) – ranging from early in the 20s to late in the 50s – that is relatively consistent within families and between carriers of the same mutation. Why certain mutations cause AD symptoms several decades earlier than others is not well understood.

The FAD-causative genes are functionally related, as they encode the substrate and the catalytic subunit of the protease (γ-secretase, GSEC) involved in Aβ generation. GSECs are multimeric intramembrane proteases, with Presenilin (PSEN1 or 2) [69,71,279], Nicastrin (NCT) [335], Presenilin enhancer 2 (PEN-2) [276] and Anterior pharynx defective 1 (APH1A or B) [276,277] as essential components (**Figure 4.1A**, left panel). The GSEC-mediated proteolysis of APP_{C99} generates heterogeneous mixtures of Aβ peptides of various lengths (predominantly 37-43 aa) by a rather unique, sequential proteolytic mechanism [193]. Importantly, absolute and/or relative increments in Aβ42 levels (relative to Aβ40) have long been considered as a hallmark of FAD-linked mutations [199–206], with increments in the Aβ42/40 ratio distinguishing pathogenic PSEN1/GSEC mutants, from the wild type counterpart [209,336]. The accumulation of Aβ42 in the AD brain [337,338], together with absolute or relative (Aβ42/40 ratio) increments in this peptide in FAD

have been taken as strong evidence in support of the pathogenic role of Aβ42 [53,207]. However, a recent extensive analysis of 138 FAD-causing mutations in *PSEN1* – which failed to detect a correlation between absolute or relative (Aβ42/40 ratio) changes in the Aβ42 levels and the disease onset [339] – has challenged the notion that alterations in Aβ42 indeed underlie AD pathogenesis.

The relationship between FAD causative mutations and clinical phenotype is a fundamental question with implications for basic and clinical research as well as for therapeutic development. Recent mechanistic data demonstrate that FAD-linked mutations in *PSEN1* destabilize GSEC-APP/Aβn (Enzyme-Substrate, E-S) interactions and reveal a linear correlation between the mutation-induced destabilization of E-S interactions (in cell-free conditions) and AAO [218]; thus indicating that the destabilizing effects are central to FAD pathogenesis. This observation suggests that changes in FAD-linked Aβ peptide profiles (beyond Aβ42), arising from the destabilizing nature of pathogenic mutations, are the molecular foundation of AD pathogenicity. It is important to highlight that during the processing of APP_{C99} by GSEC several E-S complexes are generated and their stabilities progressively decay with each sequential cleavage until dissociation is favoured and shorter Aβ peptides are released. The degree of destabilization exerted by a particular pathogenic mutation dictates the type of E-S complexes that are challenged. While mildly deleterious mutations will mainly affect labile GSEC-Aβ interactions (e.g. GSEC-Aβ42, thus enhancing Aβ42 and lowering Aβ38 production levels), more destabilizing ones will promote the dissociation of more stable E-S complexes (e.g. GSEC-Aβ43, and potentially with longer Aβ peptides).

Here, we applied a mechanistically driven hypothesis that links alterations in the composition of full-range Aβ profiles (beyond simply the relative proportions of Aβ42 and Aβ40 peptides) with clinical onset. Our data demonstrate that AD-causative mutation-induced changes in the molecular composition of Aβ profiles correlate with the age at symptom onset (AAO). The findings help to clarify why certain mutations cause an onset that is decades earlier than others and most importantly support the notion that alterations in Aβ profiles are critical to FAD pathogenesis and largely determine clinical onset. Both aspects are clearly important to ongoing and future efforts aiming to delay or prevent onset in FAD, and AD more widely.

4.3 Materials and methods

Antibodies and reagents

Anti-human PSEN-CTF (MAB5232) from Merck, anti-NCT (9C3), horseradish peroxidase (HRP)-conjugated anti-mouse (#1721011) and anti-rabbit IgG (#1721019) from Bio-Rad were used in western blot analysis. Antibodies used in the Meso Scale Discovery (MSD) multispot Aβ ELISA were obtained through collaboration with Janssen Pharmaceutica NV (Beerse, Belgium). The MSD ELISA capture antibodies were JRD/Aβ37/3 for Aβ37, JRF AB038 for Aβ38, JRF/cAb40/28 for Aβ40, JRF/cAb42/26 for Aβ42, and the detection antibody was JRF/AbN/25 raised against the N terminus of Aβ. The antibodies used in the Aβ43 ELISA were anti-Aβ43 rabbit IgG (capture antibody) and anti-Aβ (N) (82E1) mouse IgG Fab' (detection antibody), both supplied with the ELISA kit (IBL).

Generation of wild type and mutant PSEN cell lines

In order to generate stable cell lines, *Psen1*$^{-/-}$*Psen2*$^{-/-}$ MEFs [340] were transduced with retroviruses, carrying pMSCVpuro plasmids encoding respective human, wild type or mutant (A79V, V89L, F105C, Ins113T (intron4), S132A, L166P, L171P, A246E, G266S, R269H, E280A, L282R, G384A, control variants: R35Q and E318G and novel pathogenic variants: V142I, G266C, L282P, T291P, V393F and P433S) hPSEN1s, using a replication-defective recombinant retroviral expression system (Clontech). Briefly, HEK293T17 cells were co-transfected with pMSCVpuro wild type or mutant human *PSEN1* encoding plasmids and a packaging vector to produce retroviruses, as reported previously [216]. Viral particles were collected at 48h post-transfection, filtered (0,45 µM pore size filter) and immediately used to transduce *Psen1*$^{-/-}$*Psen2*$^{-/-}$ MEFs cultured in Dulbecco's Modified Eagle's Medium (DMEM)/F-12 (Thermo Fisher Scientific) supplemented with 10% fetal bovine serum (FBS) (Sigma-Aldrich) at 30–40% confluency in 6-well plates. The next day, in order to select clones stably expressing hPSEN1 wild type or mutants, the culture medium of transduced MEF cells was refreshed with the DMEM- FBS medium supplemented with 5 µg/ml puromycin (Sigma-Aldrich). After three passages, puromycin concentration was reduced to 3

µg/ml. To confirm PSEN1 expression levels and reconstitution of mature and active GSEC complexes, total membranes were prepared and solubilized in 1% CHAPSO, 28 mM PIPES pH 7.4, 210 mM NaCl, 280 mM sucrose, 1.5 mM EGTA pH 8 and 1x Complete protein inhibitor mix (Roche). Total solubilized protein fractions (8 µg) were analysed in SDS-PAGE/western blot for the presence of the different GSEC subunits by means of specific antibodies (see above).

Expression of APP_{C99} in MEF cell lines

To carry out cell-based activity assays using the generated PSEN1 MEF cell lines, the cells were transduced with recombinant adenoviruses carrying plasmids encoding APP_{C99}, as described previously [164,216]. In short, MEF cells stably expressing either wild type or mutant PSEN1 were plated at the density of 25,000 cells/well into 48-well plates and 16h later transduced with recombinant adenoviruses Ad5/CMV-APP. 7 hours post-transduction the medium was refreshed with low-serum medium (DMEM/F-12 medium containing 0.2% FBS). After a further 24h incubation at 37°C or 42°C (for thermoactivity assays), the conditioned medium was collected for Aβ analysis [164].

Aβ peptide quantification in the conditioned medium by ELISA

To quantify the concentration of Aβ37, Aβ38, Aβ40 and Aβ42 peptides, Multi-Spot 96-well MSD ELISA plates pre-coated with anti-Aβ37, -Aβ38 -Aβ40, and -Aβ42 specific antibodies using the multiplex MSD technology. Non-specific protein binding to the plates was blocked with 150 µl/well blocking buffer (PBS supplemented with 0.1% casein) for 1.5 h at room temperature (while shaking at 600 rpm) and the blocked plates were rinsed 5 times with 150 µl/well washing buffer (PBS supplemented with 0.05% Tween-20). 25 µl of SULFO-TAG JRF/AbN/25 detection antibody diluted in blocking buffer was mixed with 25 µl of standards (synthetic human Aβ1-37, Aβ1-38, Aβ1-40, and Aβ1-42 peptides at known concentrations) or 25 µl analysed samples, both diluted in blocking buffer, and the mix (50 µl/well) was loaded on the plate for ELISA analysis. After overnight incubation at 4°C, the plates were rinsed 5 times with washing buffer and the signals were developed by the addition of 150 µl/well of the 2x MSD

Read Buffer T (Tris-based buffer containing tripropylamine). The signals were read immediately on a Sector Imager 6000 (Meso Scale Discovery). To quantify the concentration of the Aβ43 peptide, conditioned medium samples were loaded on the ELISA plates pre-coated with anti-human Aβ (1-43) rabbit IgG, supplied with the human Amyloid β (1-43) (FL) assay kit (IBL) and Aβ43 peptide levels were measured following the supplier's protocol.

Statistical analysis

All statistical analyses were performed using the GraphPad Prism 8 software. One-way ANOVA with Dunnett's post hoc test was used to test the significance of the changes between groups unless indicated otherwise. P-value <0.05 was used as a pre-determined threshold for statistical significance. Linear regression was used to find the best-fit value of the slope and intercept (Y= intercept + slope*X) describing a linear relationship between Y (Aβ ratios) and X (AAO) and determine R^2 (goodness of fit) and P-value. Linear interpolation was used for assigning an X value to a given Y. All statistical analyses are described in the corresponding figure legends.

4.4 Results

Molecular composition of secreted Aβ profiles informs about AD-pathogenicity of *PSEN1* variants

Our previous studies have demonstrated that pathogenic mutations destabilize GSEC-APP/Aβ interactions and that the degree of destabilization correlates with clinical onset [218]. Based on these findings, we hypothesized that mutation-induced impairments of E-S complex stability translate into the enhanced production of longer Aβs (beyond Aβ42) and the concomitant loss of shorter peptides (Aβ37, Aβ38).

To test our hypothesis, we selected *PSEN1* mutations associated with a broad range in AAO (i.e. from 24 to 60 years) and located at different positions in the 3D structure of PSEN1/GSEC. When possible, we included known pathogenic mutations occurring at the same positions as the newly identified *PSEN1* variants (see below). As non-pathogenic controls, we included two *PSEN1* variants derived from a search of the genome aggregation database (>300,000 individuals, GnomAD https://gnomad.broadinstitute.org/) filtering for *PSEN1* missense changes found three or more times in the population. According to our calculations, these aa substitutions cannot be pathogenic, otherwise, they would be commonly found in FAD patients. These criteria resulted in the selection of the FAD-linked A79V, V89L, F105C, Ins113T (intron 4), S132A, L166P, L171P, A246E, G266S, R269H, E280A, L282R and G384A *PSEN1* mutations (**Table 4.1**), and non-pathogenic R35Q and E318G *PSEN1* variants.

As the next step, we determined the effects of the pathogenic and non-pathogenic mutants on the composition of Aβ profiles. To this end, we generated stable wild type and mutant cell lines by the transduction of *Psen1*$^{-/-}$*/Psen2*$^{-/-}$ mouse embryonic fibroblasts (MEFs) [340] with retroviruses expressing the respective human *PSEN1* variants. All the tested mutations efficiently reconstituted mature and pentameric GSECs, as indicated by the levels of mature NCT and endo-proteolyzed C-terminal fragments of PSEN1 in SDS-PAGE/western blotting (**Figure S4.1A and B**). Then, we transduced wild type and mutant cell lines with human APP_{C99} expressing adenoviruses and quantified secreted (human) Aβ37, 38, 40, 42 and 43 peptides. Of note, these Aβ species comprise the vast majority of the Aβ peptides generated in a cellular context, and hence their quantitative analysis serves as a representative total of the secreted Aβ

pool. To evaluate the mutation-induced changes in the composition of Aβ profiles, and avoid potential differences in the Aβ peptide levels arising from differences in cell densities and/or APP transduction levels across experiments and cell lines, we normalized the levels of each Aβ peptide to the sum of all measured peptides (to assess relative abundances) or calculated Aβ ratios. The Aβ profile analysis demonstrated an enrichment, albeit to different extents, in the abundance of longer Aβ species (Aβ42 and/or Aβ43) relative to the shorter ones (Aβ37 and Aβ38) in the FAD-linked secreted Aβ profiles compared to the wild type reference, with the exception of the mutant S132A PSEN1 profile (**Figure 4.1B**). Furthermore, the analysis shows virtually identical Aβ profiles for the control variants and wild type cell lines, supporting a non-pathogenic nature for the R35Q and E318G *PSEN1* mutations.

PSEN1 mutant	Position	Mean AAO ± range
L166P	TMD 3	23.5 ± 0.5
G384A	TMD 7	34.0 ± 3.0
Ins113T (intron 4)	Loop 1	37.0 ± 3.0
L171P	TMD 3	38.0 ± 2.0
G266S	TMD 6	37.7 ± 2.5
L282R	IC loop	43.8 ± 6.8
E280A	IC loop	48.0 ± 1.5
V89L	TMD 1	48.7 ± 2.5
F105C	Loop 1	48.0 ± 3.0
A246E	TMD 6	50.1 ± 4.3
R269H	TMD 6	54.0 ± 4.0
A79V	TMD 1	59.3 ± 10.6
S132A	TMD 2	59.0 ± 1.0
R35Q	N-term	---
E318G	IC loop	---

Table 4.1: List of *PSEN1* mutations used as AD (non)-pathogenic references
The table summarizes the analysed set of known FAD *PSEN1* mutations, their location in the secondary structure of PSEN1/GSEC and their reported ages at onset (AAOs) ± range for AD symptoms. The AAOs associated with the tested mutations were defined according to the Alzforum *PSEN1* mutation (https://www.alzforum.org/mutations/psen-1) database, AD&FTD mutation database from the University of Antwerp (https://www.molgen.ua.ac.be/admutations), and the literature available for the tested substitutions [73]. Legend: TMD = Transmembrane Domain, IC = Intracellular, N-term = N-terminal region.

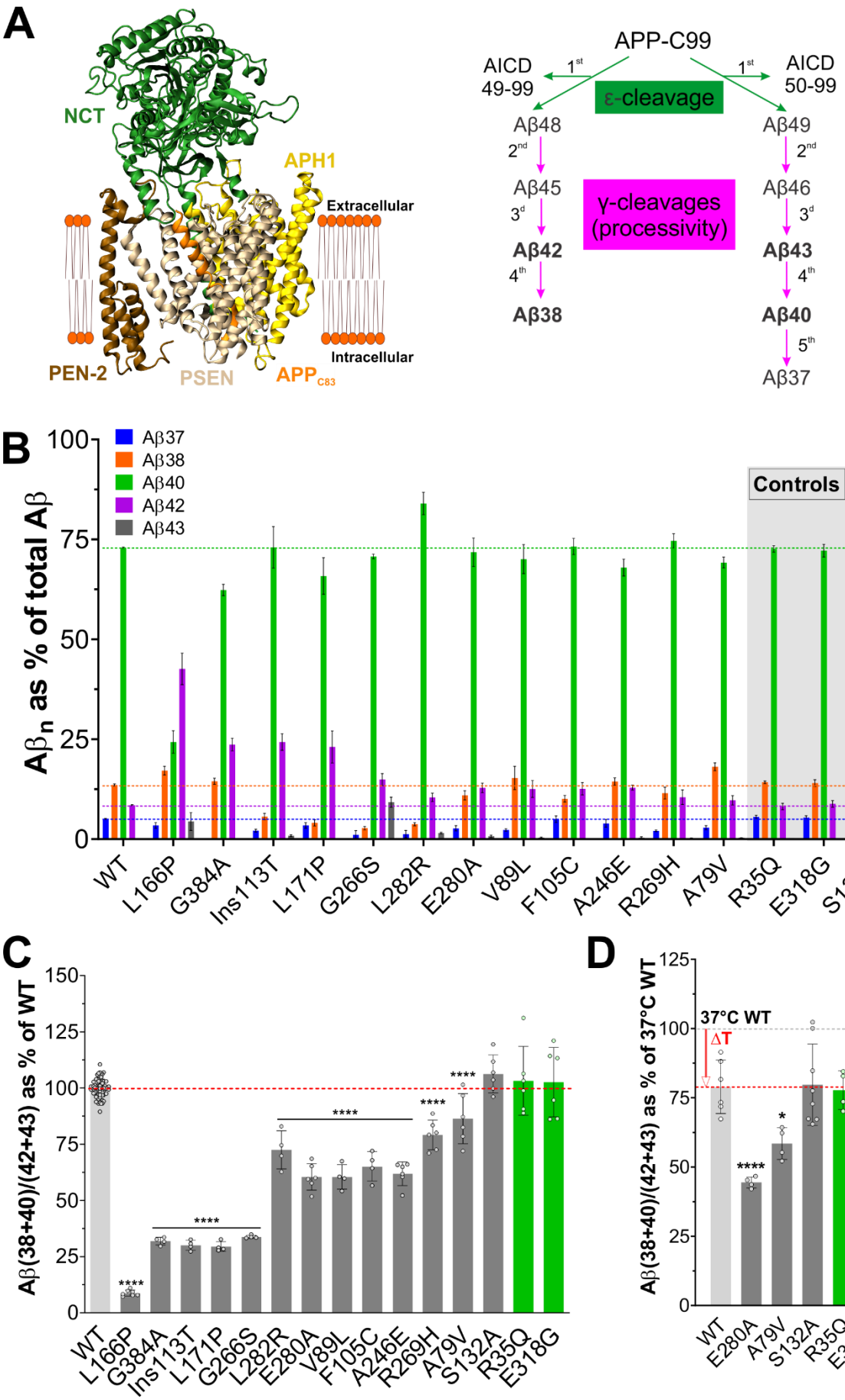
A
NCT
APH1
Extracellular
Intracellular
PEN-2
PSEN
APP C83
APP-C99
AICD 49-99
1st
ε-cleavage
AICD 50-99
Aβ48
Aβ49
2nd
Aβ45
Aβ46
3d
γ-cleavages (processivity)
Aβ42
Aβ43
4th
Aβ38
Aβ40
5th
Aβ37
B
Aβ37
Aβ38
Aβ40
Aβ42
Aβ43
Controls
Aβn as % of total Aβ
100
75
50
25
0
WT
L166P
G384A
Ins113T
L171P
G266S
L282R
E280A
V89L
F105C
A246E
R269H
A79V
R35Q
E318G
S132A
C
Aβ(38+40)/(42+43) as % of WT
150
125
100
75
50
25
0
****
WT
L166P
G384A
Ins113T
L171P
G266S
L282R
E280A
V89L
F105C
A246E
R269H
A79V
S132A
R35Q
E318G
D
Aβ(38+40)/(42+43) as % of 37°C WT
125
100
75
50
25
0
37°C WT
ΔT
****
*
WT
E280A
A79V
S132A
R35Q
E318G

Figure 4.1. Molecular composition of secreted Aβ profiles accurately informs about AD-pathogenicity of *PSEN1* variants

(A) (Left panel) GSEC co-structure with APP_{C83} (PDB: 6IYC) is presented. PSEN1 is shown in tan, PEN-2 in sienna brown, APH1A in gold, NCT in dark green and the APP substrate fragment in orange. (Right panel) The current model for the canonical cleavage of APP_{C99} by GSEC. In the first step, endopeptidase (ε-) cleavage of APP_{C99} by GSEC generates the APP intracellular domain ($AICD_{50-99}$ or $AICD_{49-99}$) and a 'de novo' Aβ substrate (Aβ48 or Aβ49, respectively). While AICDs are released into the cytosol, the membrane-bound Aβ fragments are further processed in a sequential manner through processive (γ)-cleavages. **(B)** Aβ profiles (relative abundance of the Aβ37, Aβ38, Aβ40, Aβ42 and Aβ43 peptides with respect to the total Aβ levels (Aβ37+38+40+42+43)) secreted by wild type PSEN1, 13 reported FAD mutants and 2 'control' (R35Q and E318G) substitutions. The peptides were quantified in the conditioned from the respective MEF cell lines transduced with APP_{C99} as substrate. Data are presented as mean ± 95% CI, N ≥ 4 independent experiments. **(C)** The efficiency of the 4th enzymatic turnover of APP_{C99} was quantified by calculating the Aβ(38+40)/(42+43) ratio and used as a read-out to assess the changes in the molecular composition of the Aβ profiles. Data are represented as mean ± SD, N ≥ 4 independent experiments. One-way ANOVA followed by Dunnett's post-hoc test with comparison to wild type was used to determine statistical significance; ****p > 0.0001, F(DFn, DFd): F (15, 132) = 192. **(D)** GSEC-APP/Aβn stability was evaluated in MEF cell-based GSEC thermoactivity assays (incubation of the cells at 42°C for 24h, relative to 37°C) by determining the Aβ(38+40)/(42+43) ratio. The increase in temperature reduces the processivity of the wild type GSEC complex towards APP_{C99} cleavage (ΔT) as well as that of the tested *PSEN1* substitutions. The data are shown as mean ± SD, N ≥ 4 independent experiments. One-way ANOVA followed by Dunnett's post hoc test in comparison with wild type was used to determine the statistical significance; *P > 0.05, ****P > 0.0001 compared to wild type at 37°C; F(DFn, DFd): F(5, 24)= 9.532. Note: Aβ profiles generated in cell-based thermoactivity assays by the different cell lines are shown in **Figure S4.2A**.

To quantify the mutation-induced changes in the Aβ profiles, we used the Aβ(38+40)/(42+43) ratio. This ratio weighs the levels of the products of the 4th GSEC catalytic turnover by the substrates for that 4th cleavage (APP_{C99}→49→46→**<u>43→40</u>** & APP_{C99}→48→45→**<u>42→38</u>**) (**Figure 4.1A**, right panel). This ratio considers the most abundant Aβ peptide products and provides a measure of GSEC-mediated processivity down both predominant product lines. This analysis confirmed that, in contrast to the control variants, the known FAD PSEN1 mutants consistently alter GSEC processivity

(**Figure 4.1C**). However, this was not the case for the S132A mutant, suggesting the substitution *per se* does not have a pathogenic character.

To investigate whether the S132A mutation exerts any destabilizing effects on GSEC-APP/Aβ interactions we performed cell-based thermoactivity assays (24h incubation of the APP_{C99} transduced cells at 42°C). We have previously shown that elevated temperature acts synergistically with the destabilizing effects of pathogenic PSEN1s, and accordingly, the thermoactivity assays enable us to uncover subtle, destabilizing effects associated with mild, pathogenic *PSEN1* mutations [164,218]. In this analysis, we contrasted the S132A mutant with other relatively mild (late-onset) FAD-linked A79V and E280A variants, the non-pathogenic R35Q and E318G variants and the wild type. As expected, elevated temperature lowered GSEC processivity and shifted Aβ profiles towards the production of longer forms in all tested cell lines (**Figure S4.2A**), as indicated by the reduced Aβ(38+40)/(42+43) ratio (**Figure 4.1D**). No significant differences between the wild type and the mutant cell lines were observed, demonstrating the non-destabilizing nature of the S132A variant (**Figure 4.1D)**, and strongly indicating that -like the R35Q and E318G variants- the S132A mutation is non-AD-pathogenic.

Changes in Aβ profile composition - linked to pathogenic *PSEN1* variants - correlate linearly with AAO

As next step, we evaluated whether the mutation-driven changes in the molecular composition of Aβ profiles correlate with the clinical onset of the disease symptoms. Motivated by the proven destabilizing effects of FAD causing *PSEN1* variants, we investigated the relationships between the overall impaired GSEC processivity (defined by the Aβ(38+40)/(42+43) ratio) and the AAO (mean ± range) (**Figure 4.2A**). Given the long-standing precept in the field that AD causality is intertwined with absolute or relative increments in Aβ42 levels, we also assessed the relationships between Aβ ratios that could explain relative or absolute elevations in the Aβ42 and AAO. According to the current model for the GSEC-mediated cleavage of APP_{C99} (**Figure 4.1A**) [191–194], the first GSEC endopeptidase cut defines the product line preference and thus the type of Aβ peptides that are generated.

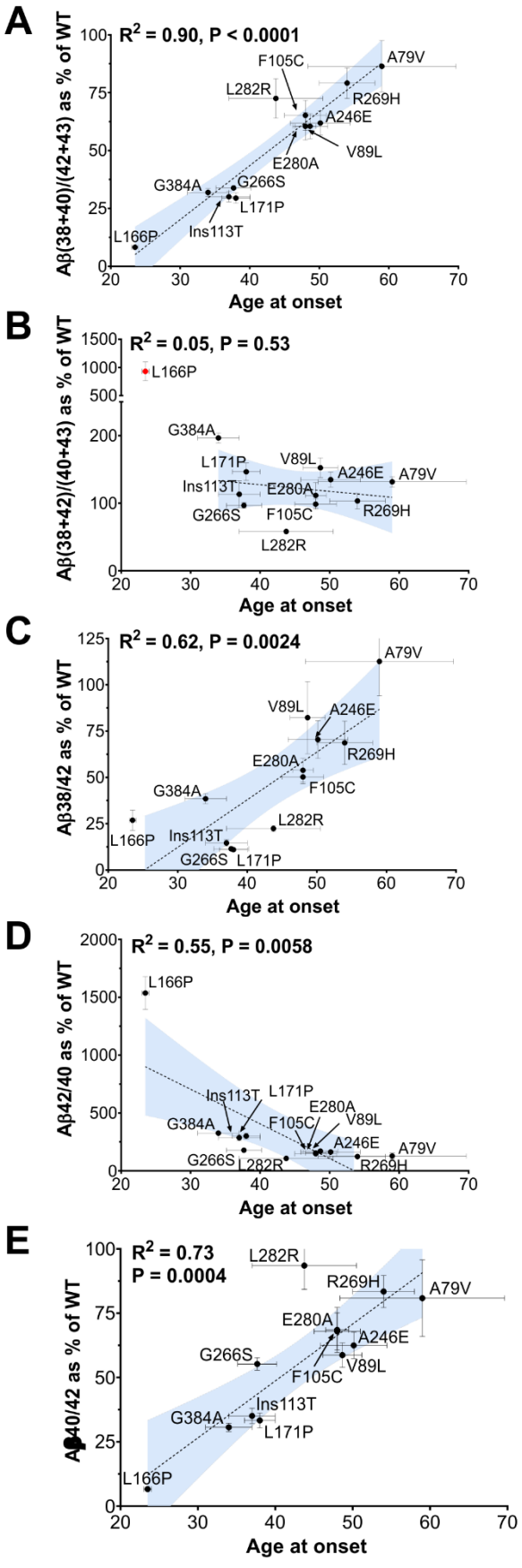

Figure 4.2. Changes in the composition of Aβ profiles linked to pathogenic PSEN1 mutants correlate linearly with AAO

(**A-F**) Linear correlations (dotted lines) between the mean age at onset (AAO) (see **Table 4.1**) of the analysed PSEN1 FAD mutants and different Aβ ratios calculated from the obtained Aβ profiles (**Figure 4.1B**). (**A**) Aβ(38+40)/(42+43) ratio (evaluates the efficiency of the 4th catalytic turnover), equation: Y = 2.332*X – 4.77.

(**B**) Aβ(38+42)/(40+43) ratio (evaluates product line preference), equation: Y = -0.9851*X + 166.8.

(**C**) Aβ38/42 (assesses the efficiency of the conversion of Aβ42 into Aβ38), equation: Y = 2.569*X – 64.81.

(**D**) Aβ42/40 and (**E**) Aβ40/42 ratios (equations: Y = -29.93*X + 1603 and Y = 2.213*X - 39.86, respectively). The 95% confidence interval (light blue surface), correlation coefficient (R^2) and statistical significance (P-value) of each correlation are shown. The L166P was identified as an outlier for the Aβ(38+42)/(40+43) ratio (Grubbs (Alpha = 0.05), G = 3.141) and Aβ42/40 ratio (Grubbs (Alpha = 0.05), G = 3.120).

We thus speculated that possible elevations in Aβ42 levels in FAD, relative to the wild type conditions, may also arise from: ***i)*** changes in the product line preference of GSEC (Aβ48 to 42/38 line rather than Aβ49 to 40/37) [216,341] and/or ***ii)*** selective impairments in the cleavage of Aβ42 → Aβ38. Accordingly, we calculated the Aβ(38+42)/(40+43) and the Aβ38/42 ratios and plotted them against the corresponding AAOs. These ratios provide estimations of the GSEC product line preference and the efficiency of the GSEC cleavage of Aβ42 into Aβ38, respectively (see **Figure 4.1A**). The regression analyses show no obvious correlation between the mutation-induced changes in the GSEC product line preference and AAO (Aβ(38+42)/(40+43), $R^2 = 0.05$, $P = 0.53$), even when excluding the L166P mutation outlier (**Figure 4.2B**); but significant linear correlations of the AAO with the Aβ(38+40)/(42+43) ($R^2 = 0.9$, $P < 0.0001$) and the Aβ38/42 ratios ($R^2 = 0.62$, $P = 0.002$) (**Figures 4.2A and 4.2C**, respectively).

Finally, we performed a similar analysis for the commonly used Aβ42/40 ratio to contrast the obtained correlative data with previous studies and approaches. The results revealed a relatively poor, but significant, correlation for the tested mutation set with a correlation coefficient of 0.55 and a P value of 0.006 (**Figure 4.2D**). Importantly, statistical analysis of the data showed the L166P mutation, (associated with a very early AAO) as an outlier (Grubbs' test with a significance level of 0.05). The extremely high Aβ42/40 ratio is, in this instance, driven by the drastic decrease in Aβ40, and large increases in Aβ42/43 levels. Statistically, the data suggest that the L166P is a 'non-representative' FAD mutation, that exerts pathogenicity through a distinct mechanism, However, our previous (thermoactivity) analysis of the L166P mutation has proven its destabilizing nature, thus supporting a common mode of action [164,218]. Therefore, we speculated that the apparent incongruence arises partially from a 'denominator problem' caused by the drastic lowering in the production of Aβ40 so that the Aβ42/40 ratio with an extremely low denominator value becomes uncertain. In connection with the linearity between Aβ and AAO observed in our data (**Figure 4.2A**), we also considered that – from a mathematic point of view – an actual linear correlation between x and y does not imply a linear correlation between x and 1/y (with a similar correlation factor, see **Figure S4.2B**). Indeed, the regression analysis of the (inverted) Aβ40/42 ratio versus

AAO resolves the issues observed for the L166P mutation and reveals a correlation factor of $R^2 = 0.73$ (P = 0.0004) (**Figure 4.2E**).

In conclusion, our data show a significant linear correlation between the changes in the composition of Aβ profiles – arising from the mutant-driven impairments of E-S stability – and disease severity (defined by the AAO). Furthermore, while the changes in the relative amounts of Aβ42 vs. Aβ40 are connected to the destabilizing effects of the *PSEN1* mutations, they do not capture in full the pathogenic PSEN1 nature.

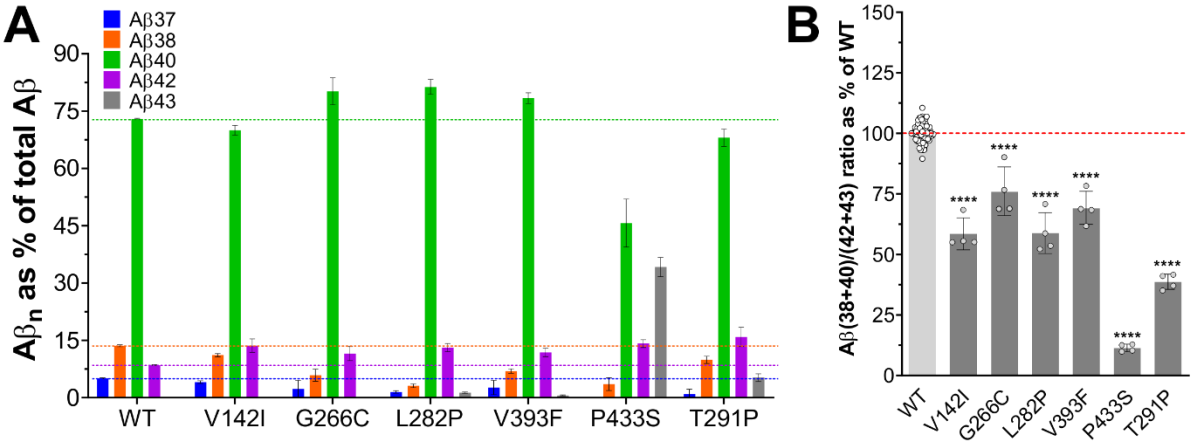

C

PSEN1 mutant	APOE genotype	Reported AAO (y)	Predicted mean AAO (y)	Lower limit (y) 95% CI	Upper limit (y) 95% CI
V142I	ε3/ε3	51.0	46.4	44.0	49.2
G266C	ε3/ε3	54.5	54.0	51.0	58.5
L282P	ε3/ε4	41.0	46.5	44.1	49.3
V393F	ε2/ε3	61.0	51.0	48.3	54.8
P433S	ε3/ε4 ε3/ε3[1]	37.0 34.0	25.9	---	30.0
T291P	ε3/ε3[2] ---	SP:33 / AD:43[2] SP:31 / AD: 35[3]	38.0	35.0	40.0

Figure 4.3. Secreted Aβ profiles enable to estimate the AD onset linked to novel and ambiguous *PSEN1* variants

(A) Aβ profiles normalized to "total" Aβ (defined as the sum of measure Aβ peptides) quantified in conditioned medium derived from wild type and respective mutant MEF cell lines transiently expressing APP_{C99}. **(B)** The efficiency of the 4th APP_{C99} turnover of the indicated PSEN1 variants quantified by the Aβ(38+40)/(42+43) ratio. One-way ANOVA followed by Dunnett's post-hoc test with comparison to wild type was used to determine statistical significance; ****p > 0.0001, F(DFn, DFd): F (6, 92) = 410. **(C)**

Table summarizing the clinical and estimated AAOs for the indicated FAD-linked *PSEN1* mutations. Superscript numbers: (1)[342], (2)[343] and (3) Chelvan et al, under revision. The 95% CI of each AAO prediction is shown as 'lower limit' and 'upper limit'. Data are presented as mean ± 95% CI, (in **A**) and mean ± SD (in **B**) of N ≥ 4 independent experiments.

Secreted Aβ profiles predict age at clinical onset for novel and ambiguous *PSEN1* variants

Advances in next-generation sequencing will lead to the wider application of genetic testing and consequent discovery of variants of unknown pathogenic significance. Although a number of algorithms help to predict pathogenicity it would be very useful to be able to assess or confirm pathogenicity biochemically and also to provide an estimate of likely AAO of novel *PSEN1* variants. This would be highly valuable in the clinical setting of an unclear (e.g. possible sporadic phenocopies) or censored family history or a *"de novo"* mutation. The strong, linear correlation between the Aβ(38+40)/(42+43) ratio and the AAO motivated us to test its predictive value in novel and/or ambiguous *PSEN1* variants. Three FAD-linked PSEN1 cases (V142I, V393F and P433S), recently disclosed by Koriath and colleagues [328], together with two novel FAD-linked *PSEN1* mutations (G266C and L282P) served as a "test cohort". Importantly, to avoid bias in our analysis, no clinical information (e.g. AAO or apolipoprotein E *(APOE)* genotype) related to the novel FAD-linked variants was provided by the clinicians involved with the cases prior to our estimations.

The V393F and P433S mutations (located in the 7th and 9th transmembrane domain (TMD) of PSEN respectively) are the first aa substitutions reported in these residues. Mutations in the other positions have already been implicated in FAD pathogenesis: V142F (TMD2) [344], G266S (located in the large intracellular (IC) loop between TMD 6-7) [345] and L282V/F/R (also part of the large IC loop) [346–348]. In addition, we evaluated the reported *PSEN1* T291P variant which has been shown to cause an atypical spastic paraplegia (SP) phenotype that precedes by several years the dementia onset (**Figure 4.3C**) [343] (Chelvan et al, under revision). We applied our novel insights to investigate what 'intrinsic' (biochemical) AD onset would be assigned to this variant.

Employing a paradigm, analogous to the cell-based assay described above, we generated the respective six PSEN1 mutant cell lines and assessed the effects of the mutations on the activity of GSEC. Western blotting analysis of the levels of mature NCT and (endo-proteolytically generated) and PSEN fragments (**Figure S4.1B**) showed that all tested mutations reconstituted mature and active GSEC complexes, with the exception of the P433S, which seems to show reduced PSEN1 endoproteolysis. In agreement, the P433S mutant substantially lowered Aβ production (**Figure S4.2C**). In addition, it elevated secreted Aβ43 levels, relative to the wild type cell line (**Figure 4.3A**).

We next calculated the Aβ(38+40)/(42+43) ratio (**Figure 4.3B**) and performed linear interpolations using the equation derived from the regression analyses presented in **Figure 4.2A** (Y = 2.332*X – 49.77). The estimated 'intrinsic' AAOs derived from the interpolation of the mutant Aβ(38+40)/(42+43) ratio are presented in **Figure 4.3C**. Comparison of the predicted AAOs with the clinical data, provided post-analysis by the involved clinicians, showed that the actual clinical ages at onset of the V142I, G266C and L282P cases were within 5, >1 and 6 years of the predicted ones, while the AAOs for the V393F and P433S variants differed from the estimated AAO by ~10 years (**Figure 4.3C**). Of relevance, the V393F case carried the APOE ε2 genotype, which has been shown to modulate AD risk and onset. We speculate that the presence of this isoforms may have contributed to a delayed AD onset, relative to the expected (see discussion). A plausible explanation for the mismatch observed for the P433S could be connected with its significant inactivating effects (see discussion). With regard to the T291P variant, the estimated, intrinsic AAO (38 y; 95% CI: 35-40) overlaps with the AD onset observed for the two identified cases (**Figure 4.3C**), indicating that altered processing of APP underlies the dementia condition, and suggesting that the earlier SP onset may arise from altered GSEC-mediated processing of (an)other, yet to be determined, GSEC substrate(s).

4.5 Discussion

Whether FAD-linked mutant-driven changes in Aβ profiles correlate with age at onset is of central importance for basic and clinical research as well as for therapeutic development. We revisited this central aspect of AD pathophysiology. In contrast to previous studies (focused on changes in Aβ42 production [206,209,339,349–352]), we applied a mechanistically-based approach that builds on the striking observation that the degree of FAD-linked PSEN1 mutant induced destabilization of the GSEC-APP/$A\beta_n$ interactions correlates with AAO [218]. These findings motivated us to characterize the spectrum of secreted Aβ profiles generated by pathogenic PSEN1/GSECs, and evaluate biologically/mechanistically meaningful relationships between the Aβ profile composition and disease severity (AAO).

The analysis of 15 previously identified mutations in *PSEN1*, consisting of substitutions linked to autosomal dominant AD as well as 2 non-pathogenic polymorphisms in *PSEN1*, in a null (*Psen1*$^{-/-}$*/Psen2*$^{-/-}$) background allowed the accurate determination of the respective secreted Aβ profiles. While the composition of secreted Aβ profiles generated by GSEC complexes bearing wild type or non-pathogenic *PSEN1* substitutions did not differ (**Figure 4.1B**), the FAD-linked Aβ profiles significantly diverged from the wild type counterpart, with the exception of the PSEN1 S132A mutant.

The assessment of the Aβ(38+40)/(42+43) ratio, an indicator of GSEC processivity, demonstrates that relative increments in the production of longer vs. shorter Aβ peptides are a consistent feature in the pathogenic-linked conditions (**Figure 4.1C**). This feature is in line with the reported impaired processivity of FAD-linked GSECs [213,214,216,217] and results from the destabilization of the GSEC-Aβn interaction [218]. Intriguingly, the S132A and wild type Aβ profiles were virtually identical, even in conditions that have proven to boost the destabilizing phenotypes of mild, pathogenic *PSEN1* variants (**Figure 4.1D**). Of note, the S132A substitution was found in one affected individual who – in addition to the *PSEN1* mutation – carried an intronic variant in the microtubule-associated protein tau (*MAPT*) gene (NM_005910.5; RefSNP: rs11872014) and an ε3/ε4 *APOE* genotype [353]. The proband presented memory problems, from age 59 years, and subsequently developed visual hallucinations,

paranoia, wandering and dyspraxia. Post-mortem brain examination revealed AD neuropathological changes as well as severe neocortical Lewy body disease [353]. Considering the biochemical analysis presented here, we speculate that *APOE4*, an established genetic risk factor for AD [25], and/or *MAPT* genotypes could have contributed to the dementia phenotype.

We next asked whether changes in the molecular composition of FAD-linked Aβ profiles, arising from the mutant destabilizing effects on E-S complexes, correlated with age at AD onset. Since absolute and/or relative increments in Aβ42 levels are widely believed to be related to AD causality, we also assessed other potential scenarios that could explain the elevations in the Aβ42 and evaluated their relationship with AD onset. We considered the following potential mechanisms: a mutation-induced shift in the product line preference of GSEC that directs APP_{C99} substrate processing through the Aβ42 product line. Of note, the Aβ40 product line constitutes the major substrate processing line, however, FAD-linked variants in *PSEN1* and *APP* often switch the position of the first GSEC epsilon cut to set the Aβ42 product line as the main one [216,341]. In addition, we tested whether the selective mutant impairment of GSEC-mediated cleavage of Aβ42 could be at the root of AD pathogenesis. Changes in the product line preference of GSEC, assessed by the Aβ(38+42)/(40+43) ratio, did not significantly correlate with AAO (**Figure 4.2B**). In contrast, the mutation-induced impairments in GSEC processivity displayed significant, linear correlations with AD onset (**Figure 4.2A and C**). Although a stronger correlation was observed for the Aβ(38+40)/(42+43) ratio than for the Aβ38/42 ratio, both correlations highlight the high pathophysiological relevance of the efficiency of the 4th GSEC proteolytic turnover on APP_{C99}.

We also compared the generated dataset with previous studies analysing the relationships between Aβ42/40 and AAO (**Figure 4.2D**). The literature in this regard is inconsistent, with studies showing no significant correlations [206,339,349,352] as well as robust correlations [209,350,351]. On one hand, the recent study by Sun and colleagues [339] revealed that relative and/or absolute increments in Aβ42 distinguish most, but not all pathogenic PSEN1/GSEC mutants, from the wild type counterpart. Specifically, ~30% of the tested pathogenic variants abrogated the generation of both Aβ42 and Aβ40 peptides. From the ~70% remaining FAD-linked mutations, ~90% lead to increments

and ~10% to decrements in the Aβ42/40 ratio. The regression analysis of the Aβ42/40 ratio and the AAO reveals no significant correlation between them (R^2 = 0.038 and P-value = 0.06), which – as concluded by the authors – stands in apparent contradiction to the amyloid hypothesis [53], and supports the possibility that AD occurs through different mechanisms. An important limitation of this study relates to the analysis of Aβ generation in detergent conditions (purified, detergent-solubilized GSEC complexes), which *per se* destabilize GSEC-APP/$Aβ_n$ interactions and thus shift Aβ profiles towards longer peptides (>Aβ42) [218]. The detergent-destabilizing conditions may explain the loss of Aβ40 and Aβ42 production and would be expected to affect the Aβ42 to Aβ40 proportions. Furthermore, the inclusion of Aβ42/40 ratios calculated from the nearly "zero activity" levels, added uncertainty to the analysis, as discussed in [354]. On the other hand, studies showing robust Aβ42/Aβ40 vs AAO correlations focused on the analysis of mutations associated with ages at onset older than 30 y. This may explain the mismatch between the reported significant correlations and the relatively poor performance of the presented analysis that includes the very early onset L166P-*PSEN1* variant.

The linear relationship between (impaired) GSEC processivity (Aβ(38+40)/(42+43), (**Figure 4.2A**)) and AAO encouraged us to test whether this correlation could help to predict age at onset of novel *PSEN1* (V142I, G266C, L282P, V393F and P433S) variants or provide insights into the AD pathogenic nature of *PSEN1* variants with atypical phenotypes (T291P). The correlative analysis assigned intrinsic AAOs within less than 6 years from the actual clinical onset for 4 out of the 6 tested cases (V142I, G266C, L282P, and T291P, **Figure 4.3C**) and intrinsic AAO values that differ by ~10y for the V393F and P433S variants. It is important to note the intrinsic error linked to the determination of the clinical ages at onset in FAD given the limited number of cases. In fact, the actual ages at onset for these mutations were each based on one individual, except for P433S for which two cases have been assessed. A small number of individuals inevitably gives a more uncertain estimate of mutation-specific onset.

The results suggest that changes in the Aβ(38+40)/(42+43) ratio largely define disease onset, but also argue that additional genetic and/or environmental factors may play a modulatory role. In the case of the – relatively mild – V393F variant carrier, we speculate that the presence of an *APOE* ε2 genotype may be a potential explanation for the mismatch between the 'intrinsic' (biochemical) and the clinical AAO. The *APOE* ε2 allele has been found to lower AD risk and delay onset [27–29]. Interestingly, genetic analysis of the world's largest FAD *PSEN1* E280A pedigree has revealed that the *APOE* ε2 allele delays AAO by ~12 years (95% CI: 8.07-15.41 y) [355]. A similar *APOE* ε2 protective behaviour would fit with the here determined intrinsic AAO for the PSEN*1* V393F mutant.

Concerning the P433S mutant, we speculate that the observed discrepancy could be explained by its extreme inhibiting effects on the global, GSEC endopeptidase activity (i.e. ~ 12% compared to the wild type, **Figure S4.2C**). Previous analysis of PSEN1 mutants displaying strong inhibitory effects on the overall GSEC activity (R278I and L435F *PSEN1*, please see Figure 3E in [218]) led us to hypothesize that extremely inactivating mutations in PSEN/GSEC silence the disease-allele and thus counteract its pathogenic effects. The delay between the intrinsic and clinical AAO observed for the P433S mutant seems to support this view. The 'silencing effect' exerted by extremely inactivating *PSEN1* variants, not only argues against a simple loss-of-function mechanism but also indicates that there is an important (Aβ) quantitative aspect in AD pathogenesis. In this regard, our analysis supports the critical involvement of the Aβ43 peptide in cellular toxicity and AD pathogenesis. Similar to the inactivating PSEN1 P433S mutation, the other extremely inactivating FAD-linked R278I and L435F *PSEN1* variants reduce the global GSEC activity and predominantly produce Aβ43 [214,356,357]. What the minimal change is in the molecular composition of the secreted Aβ pool required to initiate or delay (in therapeutic settings) disease cascade events is a critical aspect that awaits investigation.

Collectively, our results demonstrate that *PSEN1* mutant-induced destabilization of E-S interactions consistently translates into the altered composition of secreted Aβ profiles. The FAD-linked shifts in Aβ profile composition display a remarkable linear correlation with disease onset, strongly supporting the notion that Aβ profiles not only initiate pathogenic cascades but largely determine disease severity. The data also indicate that the "intrinsic" (biochemical) mutant pathogenicity is attenuated by extreme (mutation-driven) inactivating effects on the global GSEC activity or influenced by genetic factors, such as the *APOE* genotype. Finally, our data support the use of GSEC-targeting molecules securing GSEC-Aβ interactions and shifting Aβ profiles towards the short and less amyloidogenic peptides, as promising therapeutics in AD.

4.6 Supplementary figures

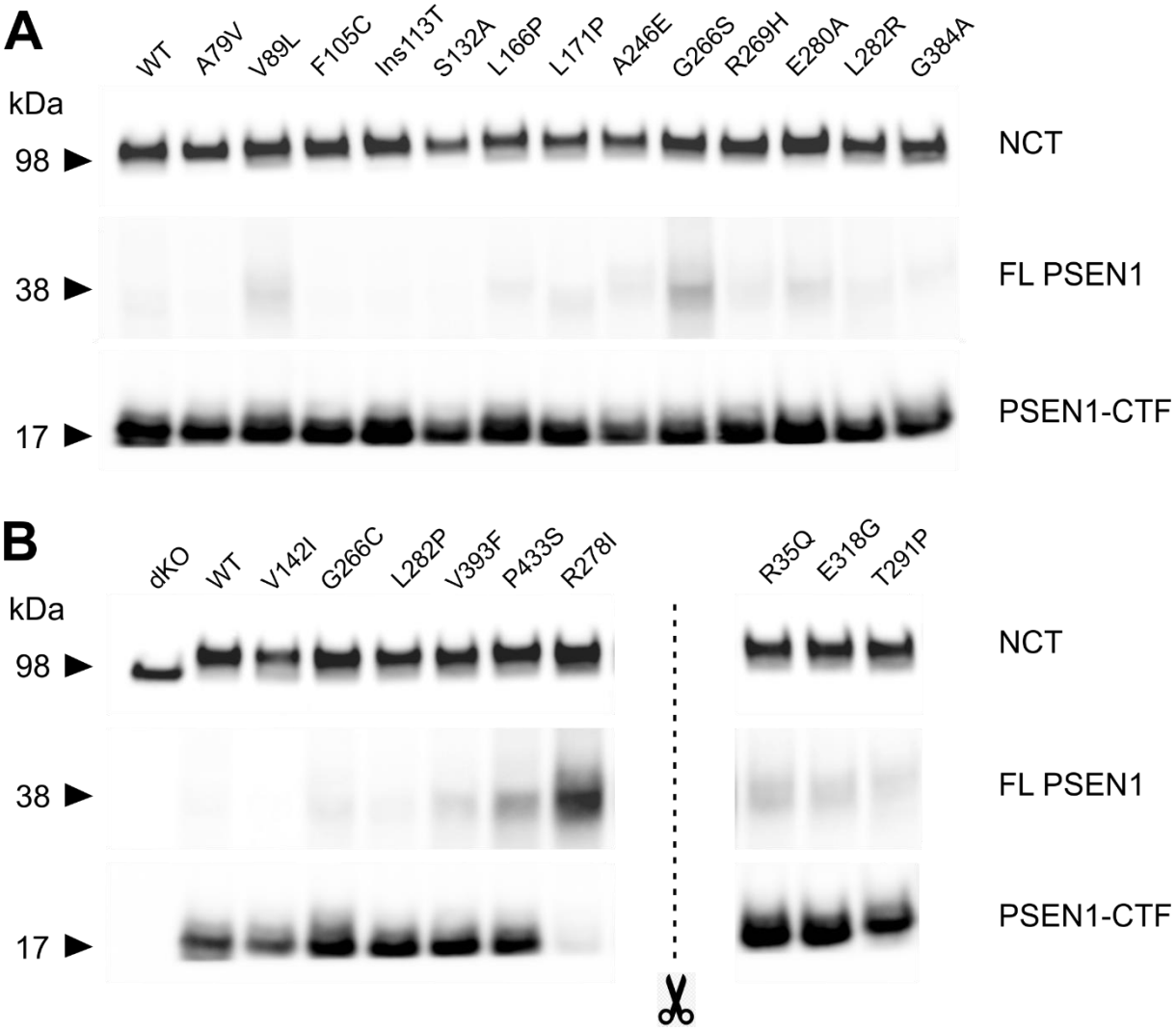

Figure S4.1. Rescue of GSEC expression in wild type/mutant PSEN1 MEF cell lines (**A-B**) Representative SDS-PAGE/western blot analysis of CHAPSO-solubilized membrane proteins from Psen1$^{-/-}$/Psen2$^{-/-}$ MEF cell lines stably expressing wild type or mutant human PSEN1 subunits. Rescue of the active GSEC complex is evidenced by the presence of mature, glycosylated NCT and the PSEN endoproteolysed C-terminal fragment (PSEN1-CTF)). Arrowheads indicate the position of molecular weight markers. (The R278I mutant was included as a reference FAD mutant displaying strong deleterious effects on PSEN1/GSEC autoactivation [214] and leading to reduced levels of PSEN-CTF and accumulation of full-length PSEN1 (FL PSEN1). The novel, inactivating P433S mutant also displays accumulation of FL PSEN1, but to a lower extent.

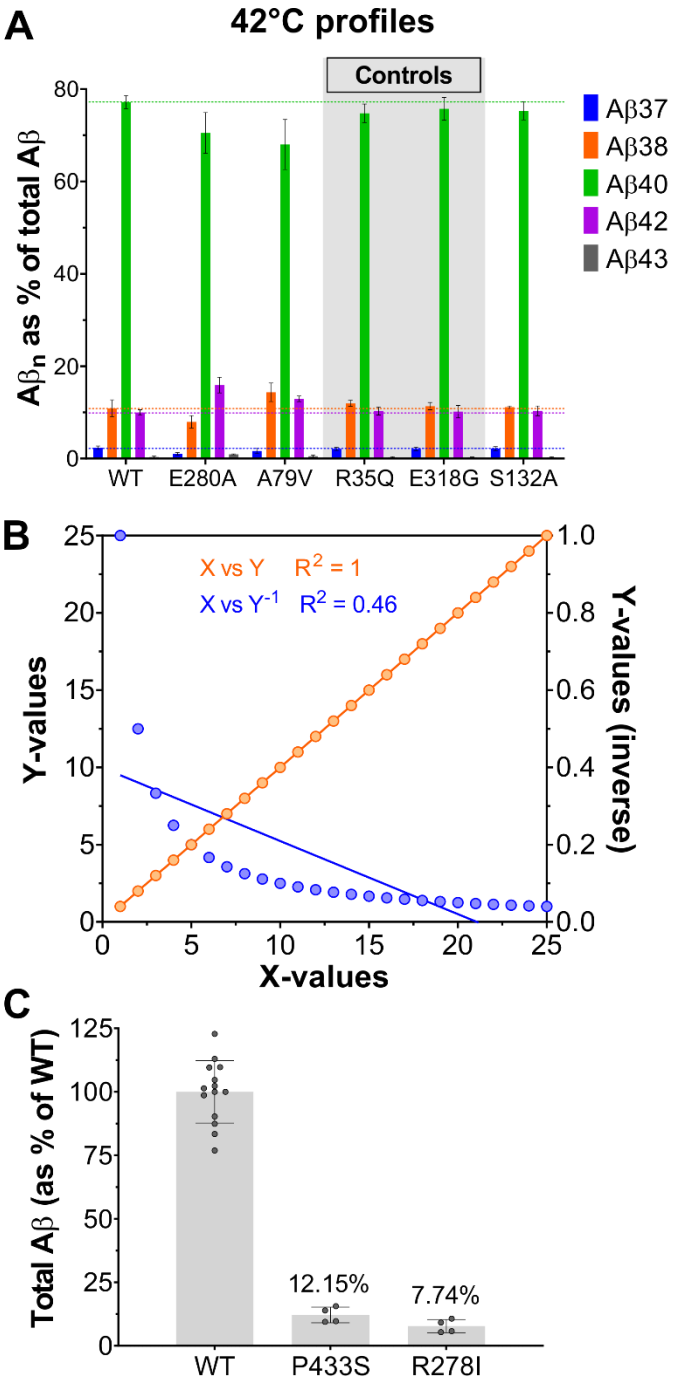

Figure S4.2. Extra data

(A) Secreted Aβ profiles normalized to total Aβ levels (Aβ37+38+40+42+43) in MEF cell-based activity assays with wild type or mutant GSECs subjected to temperature challenge (42°C). Data is represented as mean ± 95% CIs, N ≥ 4 independent experiments.

(B) A linear correlation between continuous variables X and Y does not imply a linear correlation between X and Y^{-1} with a similar correlation coefficient. Note: data represent a hypothetical data set.

(C) The levels of total Aβ production (defined as the sum of the measured peptides) of the P433S and R278I [214] inactivating PSEN1 mutants were normalized to the levels of the corresponding wild type (from each experiment).

4.7 Acknowledgements and author contributions

Acknowledgements:

This work was funded by the Stichting Alzheimer Onderzoek (SAO; S16013) and the KU Leuven Methusalem grant (METH/14/07). D.P. is supported by a PhD fellowship from the FWO (SB/1S23819N). N.S.R. is supported by a University of London Chadburn Academic Clinical Lectureship in Medicine. A.O'C is supported by an Alzheimer's Society Clinical Training Fellowship (AS-CTF-18-001) and the Rosetrees Trust charity. N.C.F. acknowledges support from Alzheimer's Research UK, the UK Dementia Research Institute and the NIHR UCLH Biomedical Research Centre. We thank Janssen Pharmaceutica NV for providing the Aβ antibodies for ELISA, Marck Mercken and Katarzyna Zoltowska for critical revision of the manuscript and Michel Vande Kerckhove for helpful discussions.

Author Contributions:

L.C.G. designed the study, analysed the data and supervised the research. D.P. performed the experiments and analysed the data. L.C.G. and D.P. wrote the manuscript with contributions from all authors. M.S. generated the T291P cell line. N.S.R., A.O'C and N.C.F. provided clinical input on the novel *PSEN1* variants. R.V. provided clinical information on the novel G266C *PSEN1* variant. All authors provided critical review and editing of the manuscript.

Conflict of interest:

D.P., N.S.R., A.O'C., M.S., R.V., and L.C.G. declare no competing interests. N.C.F reports consultancy for Roche, Biogen and Ionis, and serving on a Data Safety Monitoring Board for Biogen.

5 Characterization of the binding pocket and mode of interaction of γ-secretase stabilizers

This chapter summarizes unpublished data:

Dieter Petit[1,2], Manuel Hitzenberger[3], Matthias Koch[1,2], Sam Lismont[1,2], Katarzyna Marta Zoltowska[1,2], Marc Mercken[4], François Bischoff[4], Martin Zacharias[3], & Lucía Chávez-Gutiérrez[1,2,*]

1 VIB-KU Leuven Centre for Brain & Disease Research, Leuven, Belgium
2 Department of Neurosciences, Leuven Research Institute for Neuroscience and Disease (LIND), KU Leuven, Leuven, Belgium
3 Physics Department, Theoretical Biophysics (T38), Technical University of Munich, München, Germany
4 Janssen Research & Development, Division of Janssen Pharmaceutica NV, 2340 Beerse, Belgium
*Corresponding author.

Note: This chapter and its conclusions are written based on preliminary data.

5.1 Abstract

Recent mechanistic insights into γ-secretase (GSEC)-mediated proteolysis of the amyloid precursor protein (APP) support the stabilization of GSEC-APP (Enzyme-Substrate, E-S) interactions as a potential strategy to tackle toxic Aβ production while preserving critical GSEC roles in cell signalling. GSEC modulators (GSMs) are small molecules shown to lower Aβ42 levels by enhancing its conversion into Aβ38 while sparing the GSEC-mediated ε-cleavage, and thus the GSEC cell signalling functions. Accordingly, GSMs are considered as highly promising drugs in Alzheimer's disease (AD) therapy.

We have shown that potent GSMs modulate GSEC by stabilizing E-S interactions. However, the precise drug-target interactions and the molecular mechanisms underlying GSM action remain largely unknown. Here, we investigated the structural and kinetic bases underlying the action of potent imidazole-based GSMs. Building on the recent structural advances in the GSEC field and guided by the literature, we predicted the existence of a putative GSM-binding site at the Presenilin-Nicastrin-APP interface, a region that has been previously shown to regulate the stability of the GSEC-APP complexes. Functional *in vitro* and *in silico* analyses of the identified region strongly supported that the cavity indeed serves as the binding pocket for GSMs, and defined probable drug-target interactions. The novel insights and the generated structural models provide a valuable framework for future drug discovery efforts aimed at developing safe and effective AD therapeutics.

5.2 Introduction

Alzheimer's disease (AD) is a progressive neurodegenerative disorder and the leading cause of dementia. Seminal genetic and biochemical studies have demonstrated the central role of amyloid-β (Aβ) in AD pathogenesis which gave rise to the amyloid-cascade hypothesis (reviewed in [53]). Production of Aβ is the result of the sequential cleavage [193] of amyloid precursor protein (APP) by β-secretase (BACE) and γ-secretase (GSEC). The β-secretase (BACE1) sheds the ectodomain of APP, yielding a soluble extracellular fragment (sAPPβ) and a C-terminal membrane-embedded fragment (APP_{C99}), which is further processed in a sequential manner by the GSEC

intramembrane proteases. GSECs are multimeric complexes consisting of Presenilin (PSEN1 or 2, catalytic subunit), Nicastrin (NCT), Presenilin enhancer 2 (PEN-2) and Anterior pharynx defective 1 (APH1A or B) subunits, which together form a catalytically active complex [138–141]. Due to their involvement in Aβ generation, β- and γ-secretases have been explored as potential drug targets in AD therapy. Potent inhibitors of the enzymes have been developed, with the aim of lowering Aβ production. However, the outcomes of clinical trials with BACE (reviewed in [250]) and GSEC inhibitors (reviewed in [263]) have been disappointing. Both types of inhibitors appear ineffective in slowing down cognitive decline and lead to severe adverse effects. Limited understanding of the mechanisms underlying disease pathogenesis and the complex biology of the targeted proteases [254] are important reasons for these failures.

Intensive scientific research in the past decade focused on the effect of AD-causing mutations in *PSEN/APP* on APP processing has substantially advanced our understanding of the mechanisms underlying AD pathogenesis [216,217,358–360]. The insight that GSEC-APP/Aβn interaction stability regulates Aβ length, with pathogenic *PSEN1/2* and *APP* mutations destabilizing this interaction and priming the complex for dissociation [360], has opened a new avenue to target 'pathogenic' Aβ production. The new model proposes the use of GSEC stabilizers (GSSs), which secure Enzyme-Substrate (E-S) interactions, as potential AD therapeutics [196,360]. Notably, compounds displaying GSS features have been described before as GSEC modulators (GSMs). GSMs were identified in cell-based screening for compounds selectively lowering Aβ42 levels [257]. Initial studies demonstrated that a subset of non-steroidal anti-inflammatory drugs (NSAIDs) specifically lowers Aβ42 levels by modulating GSEC cleavage of APP [258,259]. Although the 1st generation compounds proved ineffective in the clinic [261], the development of the 2nd and the 3rd generation of GSMs has yielded molecules with significantly improved potencies and brain penetrance [361]. GSMs include acidic (NSAID-based) molecules – specifically lowering Aβ42 and elevating Aβ38 [362] – as well a range of non-acidic compounds that stimulate the production of both Aβ37 and Aβ38 at the expense of Aβ40 and Aβ42, respectively [363]. Importantly, GSMs/GSSs do not interfere with overall GSEC activity (i.e. initial endopeptidase ε-cleavage) [260]. This

feature makes GSMs less likely to cause side effects, attributed predominantly to the impaired GSEC-mediated proteolysis of other substrates (e.g. Notch).

Although potent GSMs have been developed, relatively little is known about the drug-target interactions and the mechanisms underlying their modulatory effects on APP processing. Literature, mainly relying on photoaffinity labelling (PAL) approaches using specifically designed photoprobes (reviewed in [364]), has implicated the APP substrate [330,365,366], PEN-2 [363] and PSEN N-terminal fragment (NTF) [294,327,367–370] in GSM binding. Consensus exists with regard to the mode of action of the GSMs, with both SCAM analyses [327,367] and competition experiments with active-site directed GSIs [294,368,370] showing rearrangements in the protease active site upon GSM binding, supporting an allosteric modulatory mechanism. However, different classes of GSMs (acidic vs non-acidic) display distinct effects on APP processing, and the basis of these differential effects remains unclear. Moreover, whether other (non-allosteric) mechanisms operate in the GSM-mediated modulation of Aβ production is an open question.

Here, we aimed to identify the binding pocket of imidazole-based GSMs (acting as GSSs) in order to advance our understanding of their mode of action and provide foundation for future, rational, structure-based drug discovery.

5.3 Materials and methods

Antibodies and compounds

To assess proper reconstitution of GSEC expression, the following antibodies were used: anti-human PSEN-CTF (MAB5232) from Merck, anti-human PSEN-NTF (MAB1563) from Millipore, horseradish peroxidase (HRP)-conjugated anti-mouse (#1721011), anti-rabbit IgG (#1721019) from Bio-Rad and HRP-conjugated anti-rat IgG (#P0450) from Agilent. NCT and PEN-2 were detected using in house developed Abs (9C3 for NCT and B126.2 for PEN-2). ELISA capture antibodies (JRD/Aβ37/3 for Aβ37, JRF AB038 for Aβ38, JRF/cAb40/28 for Aβ40, JRF/cAb42/26 for Aβ42), Aβ N-terminal detection antibody (JRF/AbN/25) and imidazole-based (GSM II/III) modulators (synthesis described in [295]) were obtained through collaboration with Janssen Pharmaceutica NV (Beerse, Belgium). Complete protease inhibitor (PI) tablets

and fluorogenic peptide were purchased from Sigma-Aldrich and GSEC inhibitor X (#565771) was purchased from Calbiochem.

Generation of PSEN wild type and mutant MEF cell lines

Stable MEF cell lines expressing WT or mutant PSEN1 GSEC complex were generated as described before[371]. In short, GSEC expression was rescued in *Psen1*$^{-/-}$ *Psen2*$^{-/-}$ MEFs [340] by transducing them with replication-defective, recombinant retroviruses (system described in [216]) expressing wild type, Ala/Phe PSEN1 substitutions (**Figure 5.1C**) or 'validation' PSEN1 mutants (Y106Q, Y106W, Y106W-V236W, I180Q, I180T, V236Q, V236T, V236W, V236W-Y240F, and Y240W). Cell lines were culture in Dulbecco's Modified Eagle's Medium (DMEM)/F-12 (Life Technologies) supplemented with 10% fetal bovine serum (FBS) (Sigma-Aldrich) and stably expressing clones were obtained by addition of 5 μg/ml puromycin (Sigma-Aldrich) to the culture medium 1 day after transduction. Reconstitution of active GSEC complex in the resultant cell lines was evaluated by SDS-PAGE/Western blotting for the different GSEC subunits by means of specific antibodies (see above). Briefly, cell pellets were collected for each cell line after which total membranes were prepared (by 1h ultracentrifugation at 100,000g after cell cracking) and solubilized in 1% CHAPSO, 28 mM PIPES pH 7.4, 210 mM NaCl, 280 mM sucrose, 1.5 mM EGTA pH 8 and 1x PI. Approximately 8 μg (as determined by Bradford protein assay) of CHAPSO solubilized membranes were used as input for western blot.

MEF cell-based activity assays with human APP_{C99} in different conditions

To evaluate Aβ production in the generated PSEN1 WT/variant MEF cell lines, the APP_{C99} substrate was transiently expressed in the cell lines using a recombinant adenoviral expression system as described before [162,164] with the following modifications. Freshly trypsinized cells were plated (in the morning) at the density of 12,500 cells/well into 96-well plates and transduced approximately 7h later (in the late afternoon) with Ad5/CMV-APP_{C99} adenovirus. The next morning, the culture medium was replaced with low-serum medium (DMEM/F-12 medium containing 0.2% FBS) supplemented with DMSO (0.1% for regular cell assays and 0.3% in dose-response

assays) or compounds reconstituted in DMSO (GSM II/III or L-685,458 (Inhibitor X)) at 1 µM final concentration (regular screening assay) or a concentration range (for dose-response assays). The conditioned medium was collected for Aβ analysis following a 24h incubation period at 37°C.

Quantitative analysis of secreted Aβ peptides in conditioned medium for Aβ profile determination

To quantify the concentration of Aβ37, Aβ38, Aβ40 and Aβ42 peptides in conditioned medium of compound or vehicle (DMSO) treated cell lines were subjected to ELISA. In short, single- or multi-spot 96-well MSD ELISA plates pre-coated with anti-Aβ37, -Aβ38 -Aβ40, and -Aβ42 specific antibodies (see above) using the multiplex Meso Scale Discovery (MSD) technology. Pre-coated plates were first blocked in phosphate buffer saline (PBS) supplemented with 0.1% casein to avoid non-specific protein binding by the Abs. Freshly harvested conditioned medium (from cell-based assays) or Aβ standards (synthetic human Aβ1-37, Aβ1-38, Aβ1-40, and Aβ1-42 peptides at known concentrations) were subsequently mixed (in a 1-to-1 ratio) with SULFO-TAG JRF/AbN/25 detection antibody diluted in blocking buffer and loaded on the plate (50 µl/well). Following overnight incubation at 4°C, ELISA plates were rinsed at least 5 times with washing buffer (PBS supplemented with 0.05% Tween-20) after which the MSD Gold read buffer (MSD) (150 µl/well) was added and signals were read immediately on a Sector Imager 6000 (MSD).

Molecular Dynamics Simulations

All MD simulations conducted in this study have been performed with the AMBER18 package [372], utilizing the GPU-accelerated version of pmemd [373]. For amino acids, the AMBER14SB force field [303] was used, while lipids and water have been described by the LIPID14 [301] and TIP3P [374] models, respectively. Parameters for GSM II and GSM III have been obtained with the Antechamber [375] module of AMBER18, using the GAFF2 force field [376]. Prior to obtaining RESP [377] charges (Hartree-Fock at 6-31G* level) for the ligands, their structures were optimized to a gas-phase energy minimum at the B3LYP/TZVP – level. The QM calculations have been performed with

GAUSSIAN09 [378]. All simulations have been performed at 303.15K using the Langevin thermostat [304], with a collision frequency of 1 ps^{-1}. Furthermore, the Berendsen barostat [379], with a relaxation time of 1 ps was used to sample NpT ensembles at a pressure of 1 bar. Pairwise non-bonded interactions have been calculated up to a distance of 9 Å, while long-range Coulombics were described by the particle mesh Ewald (PME) method. In the sampling phase, time steps of 4 fs were used. This was enabled by combining the SHAKE [380] algorithm with the hydrogen mass repartitioning method [308]. Periodic boundary conditions have been applied and box dimensions were approx. 109Åx117Åx194Å. Molecular docking was performed by using Autodock Vina 1.1.2 [381] with standard settings.

The starting structure of the apo-state simulation was based on the PDB structure 6IYC [173]. The structure was prepared for simulation by assigning side-chain protonation states at pH 6.5, using the PDB2PQR server [382]. The protonation state of the active site was assigned by hand, defining D257 as protonated and D385 as charged. The bilayer builder of the CHARMM-GUI server [383–385] was used to place the GSEC-APP_{C83} complex in a POPC bilayer, consisting of 304 molecules and solvated in a 0.15M KCl solution (60306 water molecules). The missing residues in the HL2 loop of PS1, as well as missing N-terminal residues of $APP_{C83,}$ have been restored (automatically by CHARMM-GUI). The N-termini of NCT and PSEN1 have been terminated by ACE, while the C-termini of APH1 and APP_{C83} were capped by NME residues. The HL2 loop was cleaved between positions M298 and A299. Next, a 7 step equilibration procedure was applied to the generated starting structure (see **Table 5.1** for details). The same procedure was also applied to all the following simulations prior to sampling. The aim was to investigate APP_{C99} instead of APP_{C83}, therefore the missing N-terminal residues were added one by one with subsequent minimizations (200 minimization cycles per step).

Table 5.1: Overview of the 7 equilibration steps performed for all simulations. The initial minimization is followed by six equilibration simulations with decreasing force constants (K) on positional restraints of amino acids (Protein, all atoms), positional restraints on lipid headgroups (Lipid, phosphorus atom) as well as restraints on the lipid dihedrals (Dihed.). Temp. = temperature, NA = not applicable.

	Steps	Time Step	K Protein	K Lipid	K Dihed.	Temp.	Pressure
min	2000	minimization	10.0	2.5	250	---	---
Eq1	125000	1fs	10.0	2.5	100	303.15K	NA
Eq2	125000	1fs	5.0	2.5	50	303.15K	NA
Eq3	125000	1fs	2.5	1.0	50	303.15K	1 bar
Eq4	250000	2fs	1.0	0.5	50	303.15K	1 bar
Eq5	250000	2fs	0.5	0.1	25	303.15K	1 bar
Eq6	250000	2fs	0.1	0.0	0	303.15K	1 bar

Statistical analysis

Statistical analysis of the data was accomplished using the GraphPad Prism 8 software. In general, one-way ANOVA with Dunnett's post hoc test was used to test the significance of the changes between groups unless indicated otherwise. P-value < 0.05 was used as a pre-determined threshold for statistical significance. All statistical analyses are described in the corresponding figure legends.

5.4 Results

Delineation of a potential (imidazole-based) GSM binding pocket

GSEC modulators (GSMs) have emerged as promising compounds in AD research due to their ability to shift Aβ production toward the generation of short and soluble Aβ peptides while keeping unaltered the first endopeptidase cleavage that has a critical role in cell signalling cascades [260]. Here, we investigated the structural basis of GSEC modulation by potent imidazole-based GSMs. We postulated that the GSM binding pocket is located at the interface between NCT, PSEN1 (loop 1) and APP. This hypothesis is supported by reports implicating NCT [164], PSEN1-NTF [294,327,367–370] and APP [330,365,366] in the interaction with GSMs. Of note, our previous studies have shown that the two FAD-linked mutations in PSEN1 (intron 4 (Ins113T) and I202F) impair the response of GSECs to imidazole-based (GSM II) and acidic (GSM I) GSMs [213]. Thus, we speculated that these PSEN1 regions contribute to protease-drug interactions. With this in mind, we examined the GSEC-APP_{C83} co-structure (PDB: 6IYC, **Figure 5.1A**) and identified a cavity that could potentially accommodate small compounds (like GSMs) (**Figure 5.1B**). This pocket is primarily shaped by residues in PSEN1 (Loop 1: aa F105-Y106 & K109-I114; TMD 3: aa F177 & I180-Y181; and TMD5: aa L232, L235-F237 & K239-Y240) and NCT (aa I242-N243) (**Figure 5.1C**). Interestingly, the GSEC-APP_{C83} co-structure demonstrates that these PSEN1 and NCT regions are in proximity to the N-terminal part of APP_{C83} (**Figure 5.1B**). Of note, previous studies have pointed at the extracellular part of APP as the GSM interaction site [330].

As the next step, we performed biochemical analyses to test experimentally the potential involvement of the identified cavity in the binding of potent imidazole-based GSMs. We selected 17 residues in PSEN1 delineating the architecture of the putative binding pocket for mutagenesis analysis (**Figure 5.1C**). We also included the FAD-linked intron 4 (Ins113T) as a control. For the purpose of these analyses, we performed an Ala/Phe scanning and generated PSEN1 wild type and mutant stable cell lines through the transduction of *Psen1*$^{-/-}$*/Psen2*$^{-/-}$ mouse embryonic fibroblasts (MEFs) with constructs expressing the respective PSEN1 mutants [340]. SDS-PAGE/western blotting for the different components of the complex indicated that all generated mutants efficiently reconstituted mature and active GSEC complexes, as judged by the

predominant expression of mature NCT and the occurrence of PSEN1 endoproteolysis (as determined by the presence of N- and C-terminal fragments of PSEN1) (**Figure S5.1**).

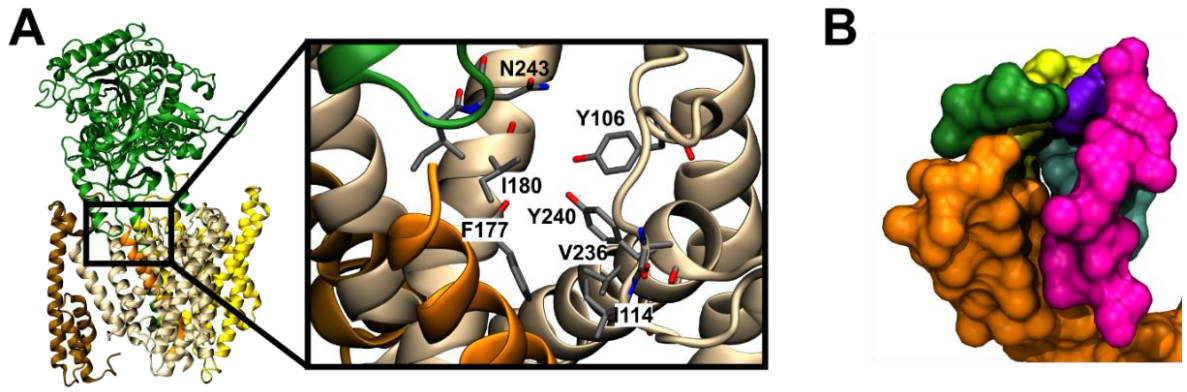

C

NCT	PSEN loop 1		PSEN TMD 3	PSEN TMD 5
I241E*	F105A	Q112A	F177A	L232A
N242A*	Y106A	Q112F	I180A	L232F
N242F*	Y106F	L113A	I180F	L235A
N242Y*	K109A	L113F	Y181A	L235F
	K109F	Ins113A	Y181F	V236A
	D110A	Ins113F		V236F
	D110F	Ins113T#		F237A
	G111A	I114A		K239A
	G111F	I114F		K239F
				Y240A
				Y240F

Figure 5.1. Delineation of a potential GSM binding pocket at the E-S interface
(A) GSEC co-structure with APP_{C83} (PDB: 6IYC) as determined by Zhou and colleagues [173] is presented. Colour scheme: PSEN1 in tan, PEN-2 in sienna brown, APH1A in gold, NCT in dark green and the APP_{C83} substrate in orange. The square shows a magnification of the PSEN-NCT-APP interface and highlights certain NCT and PSEN1 side chains. **(B)** The surface plot from the magnified region in panel A reveals the presence of a small cavity. The colours are assigned according to the table in panel C. **(C)** List of all substitutions in NCT and PSEN1 selected for the investigation of their contribution to the formation of the (imidazole-based) GSM binding pocket. The colour code matches the surface plot shown in panel B and represents the different sides of the putative pocket. # Known FAD pathogenic mutation (Ins113T: 'p.L113_I114insThr' or 'Intron 4') was used as a reference. * mouse NCT mutations of which the response to GSM II and III treatment was reported in [164].

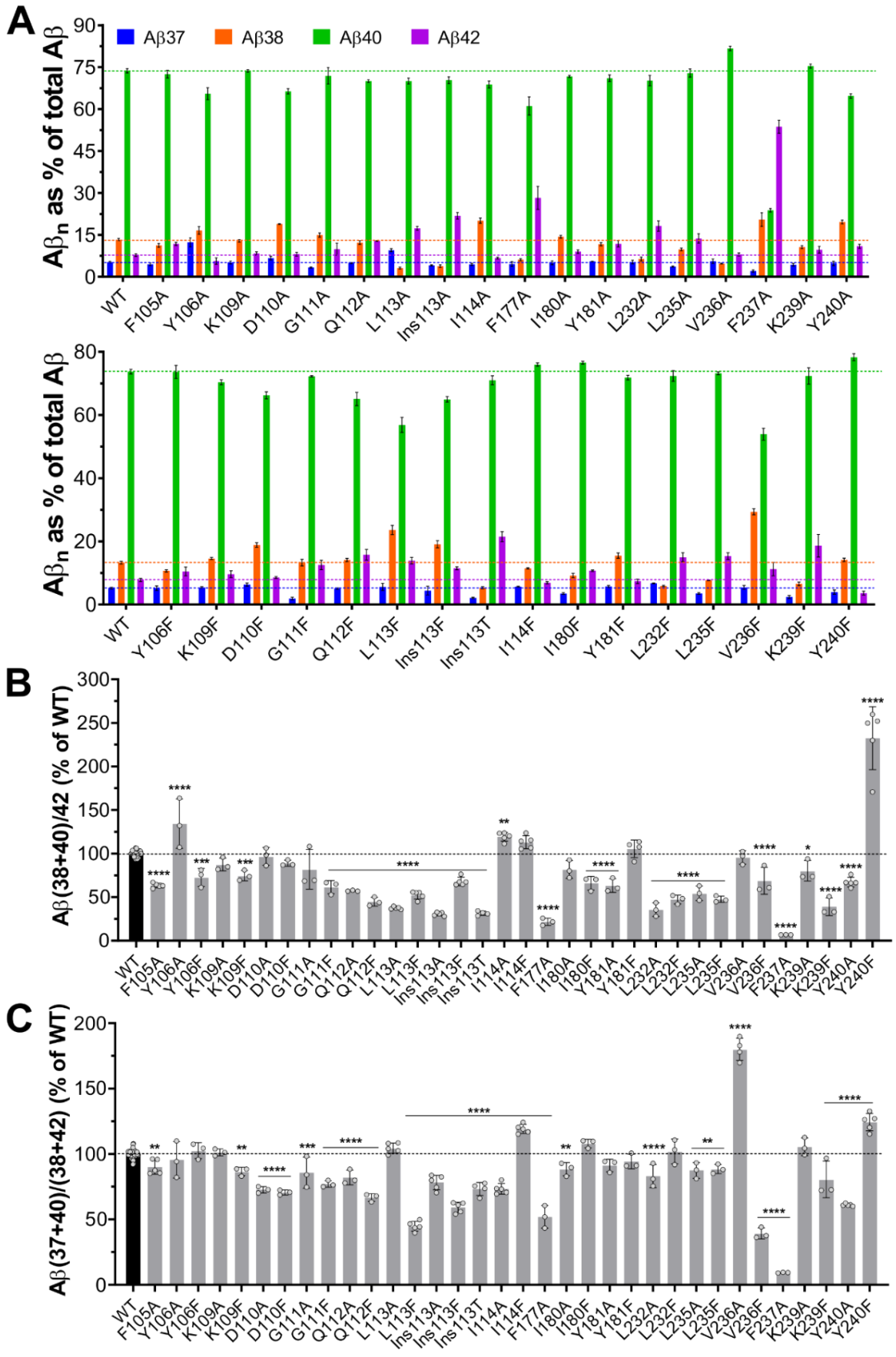
A
Aβ37
Aβ38
Aβ40
Aβ42
Aβn as % of total Aβ
WT
F105A
Y106A
K109A
D110A
G111A
Q112A
L113A
Ins113A
I114A
F177A
I180A
Y181A
L232A
L235A
V236A
F237A
K239A
Y240A
Aβn as % of total Aβ
WT
Y106F
K109F
D110F
G111F
Q112F
L113F
Ins113F
Ins113T
I114F
I180F
Y181F
L232F
L235F
V236F
K239F
Y240F
B
Aβ(38+40)/42 (% of WT)
C
Aβ(37+40)/(38+42) (% of WT)

Figure 5.2. Aβ profiles produced by PSEN1 WT or A/F mutant MEF cell lines. **(A)** Aβ profiles (% contribution of Aβ37, Aβ38, Aβ40 and Aβ42 peptides to the total Aβ pool, defined as the sum of the four peptides) secreted by PSEN1 WT or A/F mutant MEF cell lines transiently expressing human APP_{C99}. **(B)** GSEC processivity was estimated using the Aβ(38+40)/42 ratio and normalized to WT cell line. **(C)** Product line preference was assessed using the Aβ(37+40)/(38+42) ratio. Data are presented as mean ± SD, N ≥ 3 independent experiments. One-way ANOVA followed by Dunnett's post-hoc test with comparison to WT was used to determine statistical significance; *P > 0.5, **P > 0.01, ***P > 0.001, ****P > 0.0001.

We then determined how the different substitutions within PSEN1 affect APP processing. A 'baseline' level of GSEC processivity was determined by analysing Aβ profiles secreted by PSEN1 wild type and mutant cell lines transiently overexpressing human APP_{C99}. We quantified the levels of Aβ1-37, 1-38, 1-40 and 1-42 peptides in the conditioned media using multi-spot MSD ELISA (**Figure 5.2A**). These four peptides comprise the majority of Aβ peptides generated in a cellular context, and thus their analysis provides a good assessment of the total secreted Aβ pool. To assess the effects of the substitutions on the sequential processing of APP_{C99}, we estimated the Aβ(38+40)/42 ratio. Considering, that Aβ43 represents less than 1% of the total secreted Aβ pool in these conditions, the simplified (Aβ(38+40)/42 vs Aβ(38+40)/(42+43)) ratio adequately reflects the efficiency of the 4th catalytic turnover of GSEC on APP (**Figure 5.2B**). Our analysis reveals that most of the substitutions strongly reduce enzyme processivity, with the most pronounced changes observed for the Q112F, L113A/F, Ins113A, F177A, L232A/F, L235A/F, F237A and K239F substitutions. Aβ profiles generated by these mutant proteases are similar to the reference, pathogenic Ins113T (intron 4) variant, known to impair GSEC processivity [213]. The analysis also highlights the Y106A, I114A and Y240F mutations, as they significantly enhanced GSEC processivity of APP, with the Y240F mutation resulting in a 2-fold increment in the Aβ(38+40)/42 ratio (**Figure 5.2B**). In contrast, the K109A, D110A/F, G111A, I114F, I180A, Y181F and V236A mutations did not alter GSEC processivity.

Moreover, increments in the production of both Aβ38 and Aβ42 peptides by the L113F, V236F and F237A mutants suggest that these substitutions shift the product line preference of GSEC. To evaluate this, we calculated the Aβ(37+40)/(38+42) ratio,

which estimates how much Aβ peptides are derived from the Aβ49- versus the Aβ48-product lines. This analysis confirmed the initial assumptions regarding the effects of the three aforementioned substitutions. Most of the other mutations did not change or mildly altered the product line preference, except for V236A and Y240F that markedly promoted the Aβ49-46-43-40-37 pathway (**Figure 5.2C**). Intriguingly, the F237A mutant showed a nearly inversed product line preference compared to wild type. Overall, the data demonstrate that residues forming the investigated cavity in PSEN1 are strongly implicated in the regulation of GSEC processivity towards APP_{C99}.

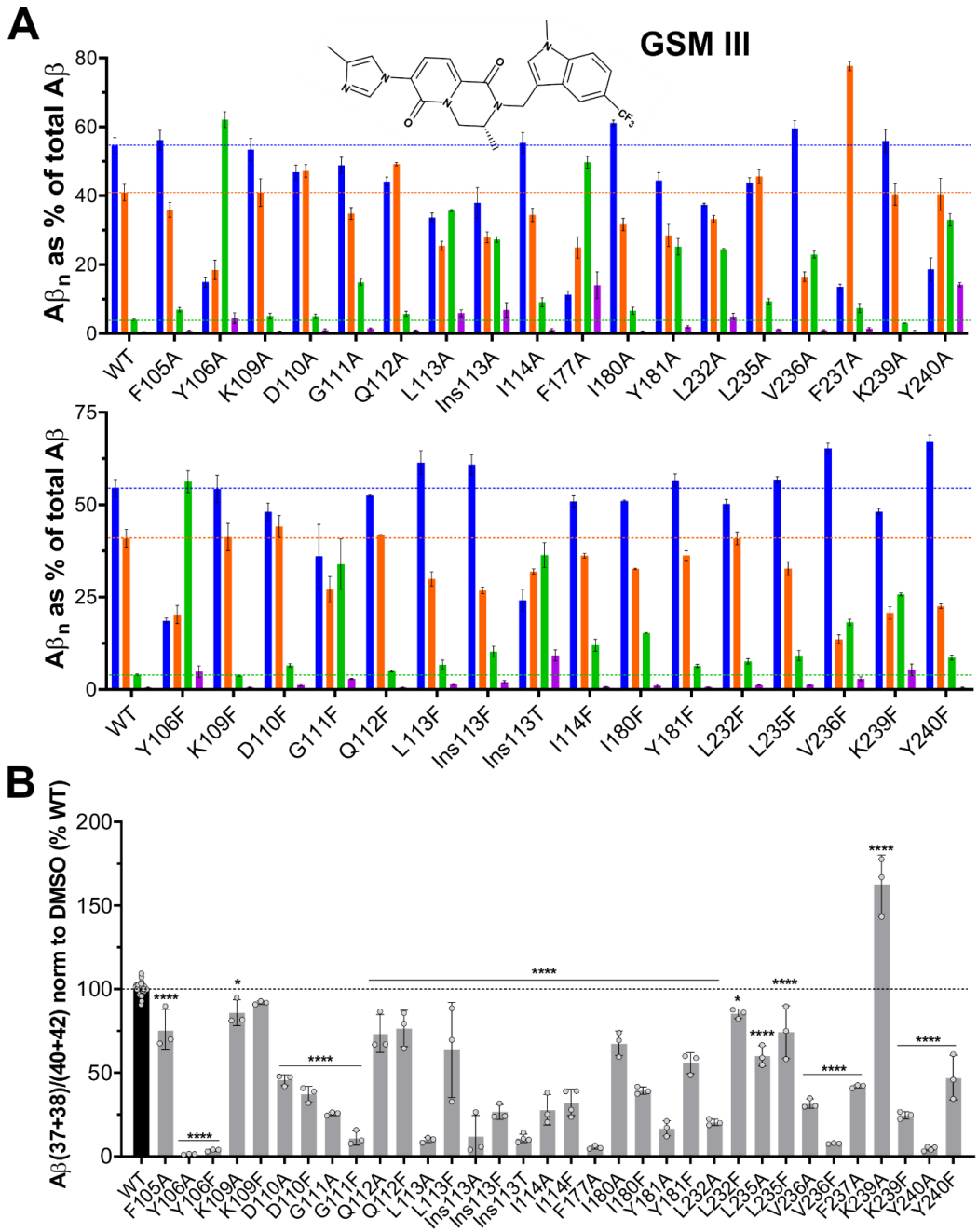

Figure 5.3. Aβ profiles produced by GSM III treated PSEN1 WT or A/F mutant MEF cell lines.

(A) Aβ profiles (cfr. **Figure 5.2**) produced by the PSEN1 WT or A/F mutant MEF cell lines treated with 1 µM GSM III. The chemical structure of GSM III is shown above the graphs. Data are presented as mean ± SD, N ≥ 3 independent experiments. **(B)** GSM response was estimated by evaluating the fold change in the Aβ(37+38)/(40+42) ratio between vehicle (DMSO) and GSM-treated cell lines and compared to the response of the WT cell line. One-way ANOVA followed by Dunnett's post-hoc test with comparison to WT was used to determine statistical significance; *P > 0.05, **P > 0.01, ***P > 0.001, ****P > 0.0001.

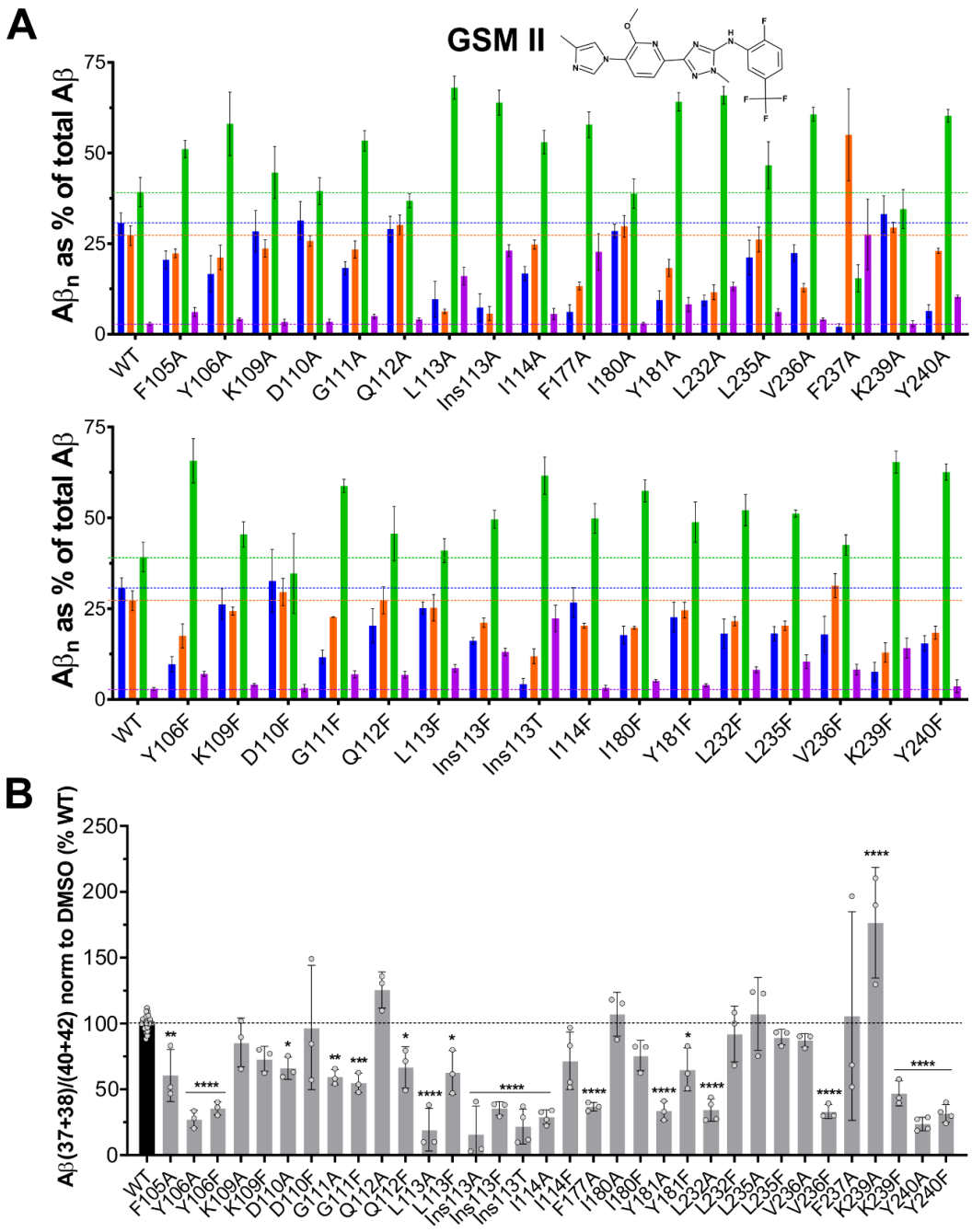

Figure 5.4. Aβ profiles produced by GSM II treated PSEN1 WT or A/F mutant MEF cell lines.
(A) Aβ profiles (cfr. **Figure 5.2**) produced by the PSEN1 WT or A/F mutant MEF cell lines treated with 1 µM GSM II. The chemical structure of GSM II is shown above the graphs. Data are presented as mean ± SD, N ≥ 3 independent experiments. **(B)** GSM response was estimated by evaluating the fold change in the Aβ(37+38)/(40+42) ratio between vehicle (DMSO) and GSM-treated cell lines and compared to the response of the WT cell line. One-way ANOVA followed by Dunnett's post-hoc test with comparison to WT was used to determine statistical significance; *P > 0.05, **P > 0.01, ***P > 0.001, ****P > 0.0001.

Structure-function analysis of GSEC identifies a cavity/pocket critical for the protease response towards imidazole-based GSMs

We then determined the effects of the Ala/Phe mutations on the response of the protease to potent imidazole-based GSMs. For these analyses, we selected two imidazole-based GSMs with different potencies (IC50 [Aβ42] 170 nM for GSM II and ~$1.4.10^{-6}$ nM for GSM III (see **Table 5.2**)). We determined Aβ profiles generated by wild type and mutant GSECs upon the respective GSM treatment (1 µM concentration) (**Figures 5.3A and 5.4A** for GSM III and II, respectively). The tested GSMs are known to promote the cleavage of Aβ40 →Aβ37 and Aβ42→ Aβ38 by stabilizing GSEC/Aβn interactions [218] and slowing down the enzyme-substrate (E-S) dissociation [386]. Accordingly, the compounds shifted the Aβ profiles generated by wild type GSEC towards the (enhanced) generation of Aβ37 and Aβ38, at the expense of Aβ40 and Aβ42 peptides. To assess the impact of the tested substitutions on the GSEC response to the GSMs, we calculated the Aβ(37+38)/(40+42) ratios. The analysis revealed impaired GSEC responses towards the more potent GSM III for the great majority of the tested mutations (**Figures 5.3B**). The K109F substitution was the only mutation that did not affect the protease response, while distinct substitutions at position 239 showed opposite effects.

The most remarkable changes were observed for the Y106A/F, G111F, L113A, F177A, V236F and Y240A substitutions that almost abolished the GSM III-induced shift in Aβ profiles. As expected [213], the pathogenic Intron 4 variant and Intron 4-like mutations all impaired the protease response toward the potent GSM III. Interestingly,

the data showed that an impaired response to GSMs is not necessarily connected with altered GSEC processivity. This is exemplified by the Y106A/F and F237A substitutions (**Figure 5.2A versus Figures 5.3A and 5.4A)**. The Y106A/F mutants exerted mild (differential) effects on GSEC processivity, still, both did not respond to the potent GSM III. Furthermore, despite a very pronounced negative impact of the F237A mutation on GSEC processivity, this mutant displayed a strong response to GSMs. Of note, the marked shift in the GSEC product line preference (favouring the Aβ42/Aβ38 production line, **Figure 5.2C**) induced by the F237A mutation resulted in the preponderant production of Aβ38 upon GSM treatment.

Comparison of the mutant's responses to GSM III versus the less potent GSM II (**Figure 5.3B vs 5.4B**) revealed a substantial overlap in the effects of the tested substitutions (18/29 or 62%). This supports the notion that both compounds bind to the same pocket in the protease. However, the tested substitutions showed in general milder effects on the GSEC responses towards GSM II. This applies to the critical Y106A/F, G111F, L113A, F177A and Y240A mutations. Interestingly, our analysis highlighted differential impacts on the GSM III- vs. GSM II-mediated shifts in Aβ profiles for the V236A and Y240A/F substitutions.

Collectively, the results show that residues forming the investigated cavity in PSEN1 are involved in the modulation of GSEC by imidazole-based GSMs. Importantly, the data indicate a clear dissociation of GSEC processivity from the protease's ability to respond to GSM treatment. The latter supports a direct effect of the substitutions on GSM binding, rather than mutant-induced conformational changes leading to an altered response to the modulators.

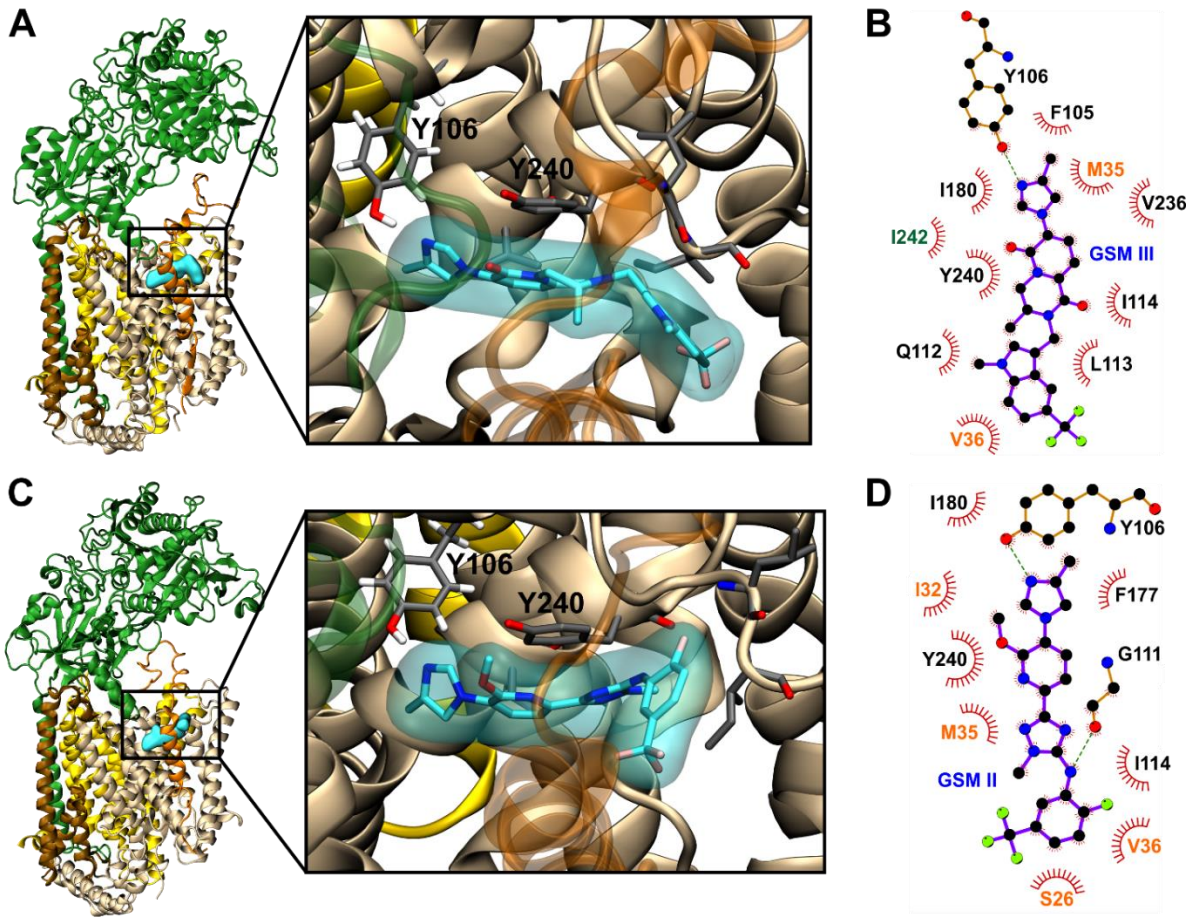

Figure 5.5. GSM binding modes proposed by MD simulations with the compounds docked into the proposed binding pocket

(A, C) Whole complex view of GSEC interaction with the GSM III (A) or GSM II (C) molecules after MD simulations with the compounds docked in the investigated pocket. The same colour scheme was used as in **Figure 5.1** for the GSEC subunits. The substrate is coloured in orange and the GSMs in cyan. The magnifications show a more detailed view of the simulated binding modes of GSM III/II. The positions of the residues (Y106 and Y240) crucial for interaction are highlighted. **(B, D)** Schematic interaction diagrams of the GSM III (B) and GSM II (D) binding modes with the GSEC-APP_{C99} complex. Hydrogen bonds are depicted in green, polar interactions in red. The plots have been generated with LigPlot^{+} [387].

In silico modelling of drug-target interactions supports the direct binding of GSMs to the identified cavity and proposes a mode of interaction for potent imidazole-based GSMs

To further investigate the potential involvement of the identified cavity in the binding of imidazole-based GSMs and explore the mechanism(s) that best explain our observations, we applied a theoretical approach. We conducted molecular dynamics

(MD) simulations modelling the binding of GSM III and II to the GSEC-APP_{C99} complex. We used the GSEC-APP_{C83} co-structure (PDB: 6IYC) [173] to build a GSEC-APP_{C99} model by performing a 3 µs long, unrestraint MD simulation of APP_{C99} in complex with GSEC. This procedure required restoration of the N-terminal APP_{C99} residues as well as the hydrophilic intracellular loop of PSEN1, as these parts are missing in the reported near-atomic structure. Initial modelling was set to track the volume of the hypothetical GSM binding cavity using the MD-Pocket software [388]. To optimize the success of the GSM docking runs, we chose a structural snapshot with a maximum-sized binding cavity as 'receptor' for compound docking analysis using the Autodock Vina software [381]. Next, the GSM III compound was docked in the 'receptor' using a combination of flexible ligand/flexible side chain and rigid docking methods to define a suitable docking pose. The initial docking model was used for a series of 400 ns MD simulations for each of the compounds (**Figure 5.5A, C**).

In the selected theoretical binding modes, GSM III (and GSM II) directly contacts PSEN1 residues that are highlighted by the functional data (**Table 5.3**). Most importantly, the model assigns a key hydrogen bond interaction between the PSEN1-Y106 residue and the conserved imidazole ring in the GSM molecule (**Figure 5.5B and 5D)**. In three independent 400 ns simulations, the Y106 hydroxyl group and the imidazole engage in hydrogen bonding in a total of 77.5% of sampled frames (with 67.3 % direct H-bonds and 10.2 % bridged by an H_2O molecule) and in 72.5% of sampled frames (29.1% H-bonds and 43.4% water bridged polar interactions) for GSM III and GSM II, respectively (**Table 5.4**). In addition, both GSMs established π-π stacking interactions with the side chain of PSEN1-Y240 residue in 94.7% and 99.2% of the simulations for GSM III and GSM II, respectively when counting all frames with a maximum angular deviation from planarity of 30° (**Table 5.4 and Figure 5.5B and 5.5D**). Furthermore, the simulations indicate that ligand binding to the GSEC-APP_{C99} complex relies mainly on hydrophobic interactions, as 66.7% of the total solvent-accessible surface area is occupied by apolar residues (i.e. 210.44 $Å^2$ of 315.76 $Å^2$ total area, **Table 5.5**).

In conclusion, the molecular modelling data support the binding of imidazole-based GSMs to the identified cavity and the direct participation of the PSEN1- F105,

Y106, I180, L113, I114, F177, I180, L232, V236 and Y240 as well as the NCT-I242 in the GSEC-GSM interactions.

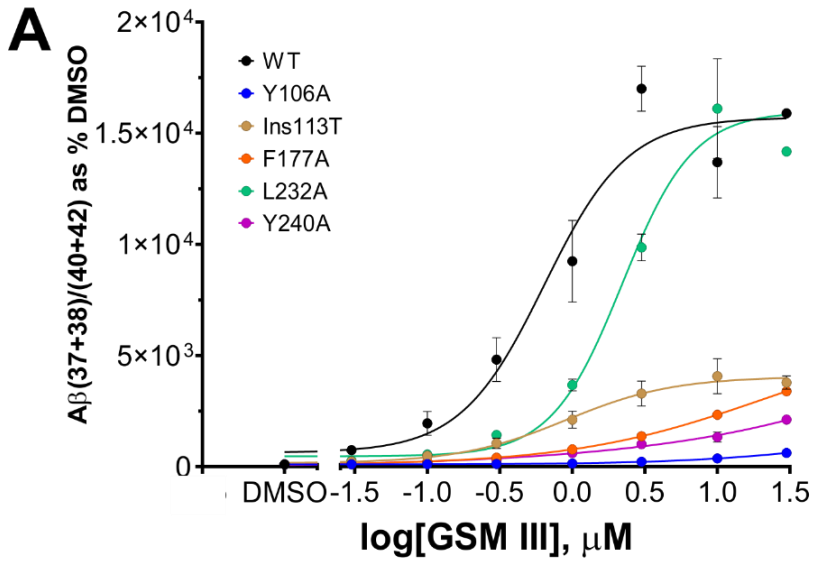

Mutant	EC50 (μM)
WT	0.64
Y106A	62.72*
Ins113T	0.91
F177A	20.65*
L232A	2.21*
Y240A	----

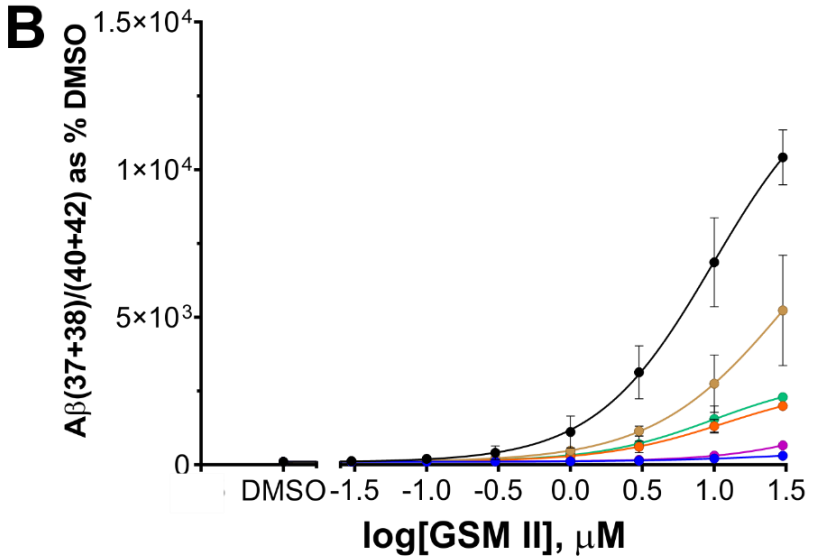

Mutant	EC50 (nM)
WT	9.81
Y106A	37.91
Ins113T	32.3
F177A	11.67
L232A	9.88
Y240A	81.13

Figure 5.6. Evaluation of WT and selected GSM low/non-responsive mutant PSEN1 variants in GSM dose-response curves.
(A, B) Evaluation of the change in the Aβ(37+38)/(40+42) ratio (as a measure of GSEC processivity for the 4th and 5th turnover) in WT and 5 PSEN1 variants (Y106A, Ins113T, F177A, L232A, Y240A) – which displayed a (strongly) impaired response to 1 μM GSM treatment – for GSM III (A) or GSM II (B) treatment, over a concentration gradient (0.03 μM - 30 μM). Data are presented as mean ± SD, N = 2 independent experiments. * No overlap in 95% CIs between the mutant's and the WT's EC50 values. CBD = cannot be determined.

Alanine substitutions of critically involved PSEN1 residues in drug-target interactions strongly reduce GSEC affinity for GSMs

As the next step, we investigated the effects of residues in PSEN1 establishing key interactions with imidazole-based GSMs -according to the theoretical model- in dose-response experiments. We selected the Y106A, F177A, L232A, Y240A as well as several substitutions at positions I180 and V236 (see below) for cellular analysis. In these studies, the GSM III and GSM II concentrations ranged from 0.03 µM up to 30 µM (**Figure S5.2**). The pathogenic Ins113T (intron 4) was tested as a reference cell line. The dose-response data for the GSM III-driven changes in the wild type Aβ profile was characterized by increases in the production of Aβ37 (**EC_{50} = 0.4 µM**, 95% CI: 0.3 - 0.5 µM) and Aβ38 (**EC_{50} = 1.3 µM**, 95% CI: 0.5 – cannot be determined (CBD) µM) and decreases in the corresponding precursor Aβ40 (IC_{50} = **0.7 µM** , 95% CI: 0.4 – 1.1 µM) and **Aβ42 (IC_{50} = 0.2 µM**, 95% CI: 2^{-8} – 0.4 µM) peptides, respectively. Clearly, the Y106A, F177A, L232A, Y240A and Ins113T mutations shifted the responses to higher inhibitory/effective **(IC_{50}/EC_{50})** concentrations (**Table 5.2**). The GSEC efficiency of the Aβ40→Aβ37 and Aβ42→Aβ38 cleavages estimated by the Aβ(37+38)/(40+42) ratio and plotted against compound concentration indicated that higher effective concentrations of GSM III are required to activate these cleavages in the PSEN1-Y106A, F177A, L232A, Y240A GSEC mutants, although the effect is not significant for the Intron4 variant (EC_{50} 95% CI wild type: 0.3 to 1.1, Y106A: 11.7 to CBD., F177A: 9 to 282, L232A: 1.6 to 3, Y240A: CBD and Ins113T: 0.5 to 1.5, **Figure 5.6A**). Inspection of the Ins113T mutant profiles shows that the mutation particularly affects the GSM III-mediated modulation of the Aβ40→Aβ37 cleavage (**Figure S5.2**), an effect that lowers the overall processivity in **Figure 5.6A**.

A similar dose-response analysis for the GSM II revealed similar mutant-driven effects, with all the tested mutations shifting the activating effects of the compounds on GSEC processivity towards higher compound concentrations (**Figures S5.2**). As expected, the GSM II treatment induced a stepwise increase in the abundance of the Aβ37/Aβ38 peptides, relative to the Aβ40/Aβ42 precursors in the wild type conditions (**Figure S5.2**). In contrast, GSM II failed to activate the processing of Aβ40 and Aβ42 in the tested GSEC mutants, as indicated by the Aβ(37+38)/(40+42) ratio. The analysis

overall evidenced consistent effects of the tested variants on the GSEC response to both GSMs (**Figure 5.6B**).

Collectively, the theoretical and functional studies support the critical involvement of the PSEN1 Y106, L113, I114, F177, L232 and Y240 positions in the binding of imidazole-based GSMs to GSEC, and indicate that all tested substitutions drastically reduce the affinity of the compounds for the GSEC and/or GSEC-APP complex.

In-depth characterization of the ligand-receptor interaction

In silico modelling showed that H-bonding between Y106 and the imidazole-ring of the investigated GSMs strongly stabilizes drug-target interactions. To further investigate the geometry of this key interaction, we introduced Gln and Trp residues at position 106 in PSEN1. Similar to Tyr, these substitutions offer a hydrogen-bonding donor group albeit at distances closer to the protein backbone (3 atoms from Cα for Trp, 4 for Gln vs 5 for Tyr). Generation of the mutant cell lines showed normal reconstitution of the mutant GSECs (**Figure S5.1**), while the functional assessment revealed no or minor impacts on the respective (Y106W and Y106Q) Aβ profiles (**Figure 5.7A)** and mutant enzyme processivities (**Figure S5.3A**).

In contrast, both substitutions exerted drastic impairments in the GSEC responses towards GSM III and II, (**Figure 5.7B**). These results imply that the relative positioning of the hydrogen bond donor group at position Y106 in PSEN1, with respect to the imidazole moiety of the GSM III/II, is critical for the drug-target interactions. To further substantiate the critical role of the Y106 side-chain, we speculated that presenting a hydrogen-bonding partner near this position would favour a polar intermolecular interaction, in detriment of the critical intermolecular bond. MD simulations suggested that the introduction of Gln or Thr at positions V236 and I180 would promote hydrogen-bonding interactions with Y106, with the Thr being less optimal in establishing the polar contact (*data not shown*). All mutant PSEN1s reconstituted active and mature GSECs (**Figure S5.1**). At the functional level, the V236Q/T mutant cell lines displayed GSEC processivities similar to the WT (vehicle-treated), while the I180Q/T substitutions exerted minor effects on Aβ profiles, as determined by the Aβ(38+40)/42 ratio (**Figure**

S5.3A). Of note, the I180Q and I180T (to a lesser extent) substitutions shifted the product line preference of GSEC towards the 42→38 line resulting in relatively increased Aβ38 and Aβ42 product levels (**Figure S5.4**).

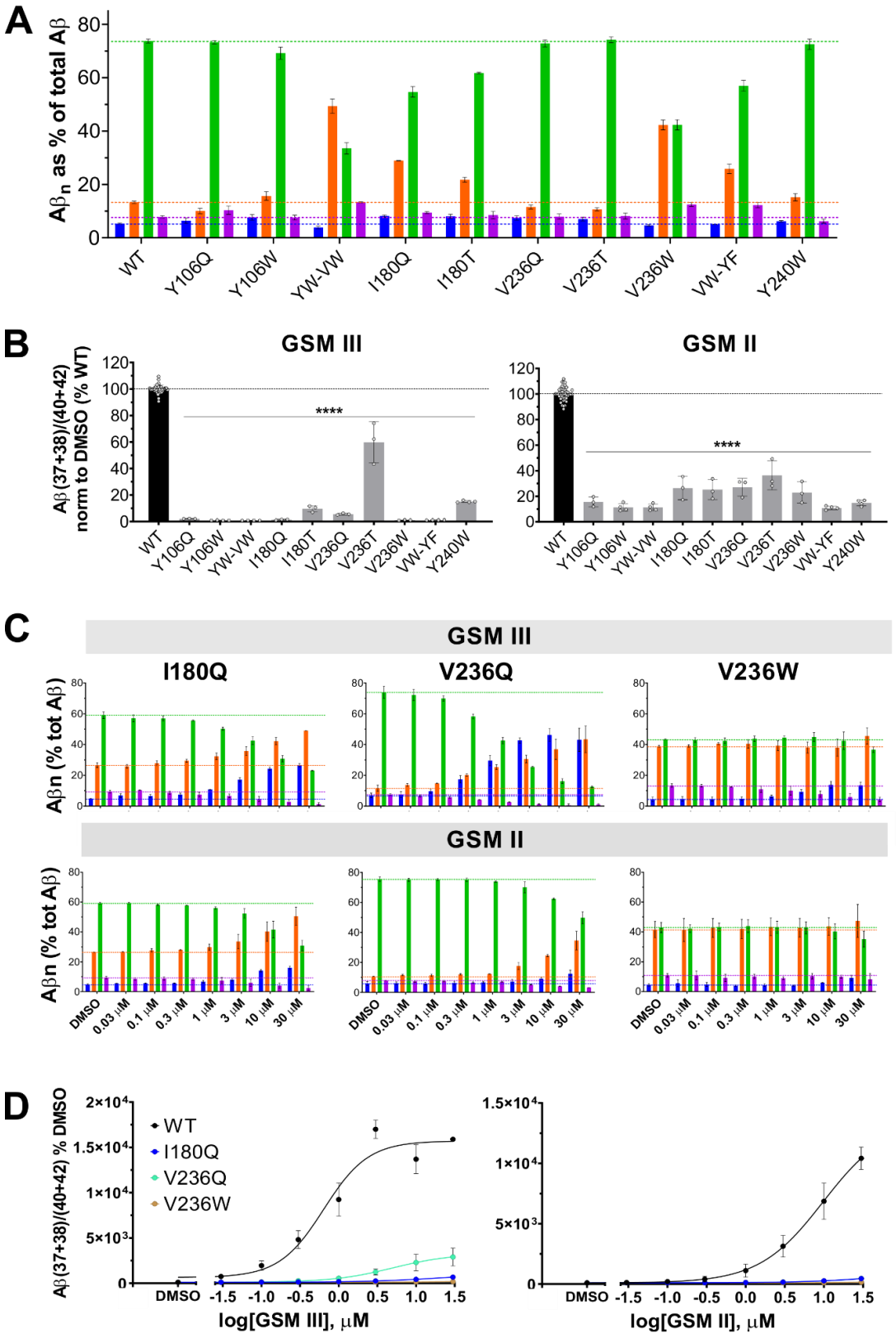

Figure 5.7. PSEN1 mutants to evaluate the proposed GSM-GSEC interaction
(A, C) Aβ profiles generated by PSEN1 WT and mutant MEF cell lines treated with vehicle (0.1% DMSO) (A), or a concentration gradient (0.03 µM - 30 µM) of GSM III/II (C). **(B)** GSM response was estimated by evaluating the fold change in the Aβ(37+38)/(40+42) ratio between vehicle (DMSO) and GSM-treated cell lines and compared to the response of the WT cell line. **(D)** Evaluation of the change in the Aβ(37+38)/(40+42) ratio (calculated based on the Aβ profiles shown in panel C, and used as a measure of GSEC processivity) in WT and the I180Q, V236Q and V236W PSEN1 variants upon treatment with GSM III or GSM II over a concentration gradient (0.03 µM - 30 µM) is presented. Data are shown as mean ± SD, N = 3 (A, B) and N = 2 (C, D) independent experiments. One-way ANOVA followed by Dunnett's post-hoc test with comparison to WT was used to determine statistical significance, ****P > 0.0001 (in panel B).

In contrast to the mild effects on enzyme processivity, Aβ profile analysis upon GSM III treatment demonstrated that all substitutions strongly impaired the GSEC response towards GSM III. In agreement with the theoretical model, the substitutions to Thr had a milder impact on the response to GSM III than the substitutions to Gln, due to a less optimal hydrogen bonding interaction with the Y106 side chain (**Figure 5.7B**). Response to GSM II appeared similarly impaired by the Gln/Thr substitutions (**Figure 5.7B**). These results support the notion that polar substitutions at positions I180 or V236 compete with the GSM's imidazole group for H-bonding with Y106. Additional dose-response experiments with the I180Q and V236Q mutant cell lines for both GSMs showed that they drastically reduced the affinity of the complex for the modulator (**Figure 5.7C, D)**.

We then hypothesized that introducing bulky residues in the pocket would sterically block GSM binding. To challenge this hypothesis, we generated the V236W, Y240W and double Y106W-V236W, V236W-Y240F mutant PSEN1 cell lines and confirmed that all mutant PSEN1s reconstituted GSEC complexes (**Figures S5.1**). These substitutions place bulky side chains centrally in the cavity of the putative pocket. Aβ profiles determined in presence of vehicle, GSM III or GSM II revealed that, in line with our hypothesis, these GSEC mutants are unresponsive to the GSMs (**Figure 5.7B**). Further dose-response experiments in the V236W PSEN1 cell line showed virtually no change in the Aβ profiles upon the treatment with GSMs at concentrations up to 10 µM

(**Figures 5.7C, D**). Strikingly, in all tested conditions, GSEC complexes containing the PSEN1 with the V236W substitution strongly preferred to cleave APP along the Aβ42 → 38 product line (**Figure S5.4**).

In conclusion, functional characterization of the proposed drug-target interactions suggested by the MD simulations strongly support a direct interaction of the GSMs with the GSEC complex in the proposed pocket.

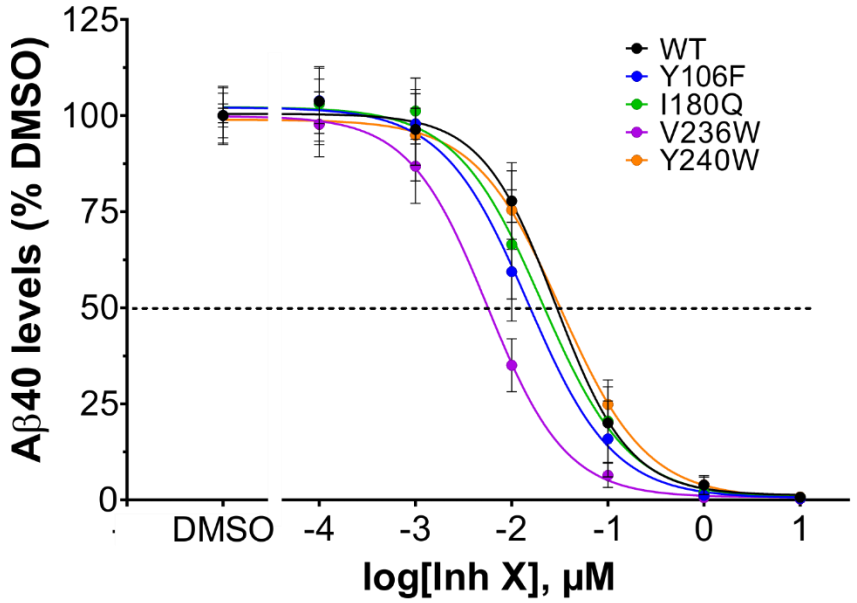

Mutant	IC50 (nM)
WT	28.63
Y106F	14.78
I180Q	20.69
V236W	5.61*
Y240W	32.42

Figure 5.8. GSM non-responsive PSEN1 variants have unaltered active site architecture

(A) Inhibitor X (Inh X, L-685,458) inhibition curves for Aβ40 production for the WT and presented mutant PSEN1 variants. The respective IC50 values are shown in a table to the right of the graph. Data are shown as mean ± SD, N = 3 independent experiments. Note: * indicates that there is no overlap in the 95% CIs between the IC50's of WT and the V236W variant.

GSM response impairing substitutions do not alter GSEC complex conformation

We proposed that the observed impairments in the GSEC responses towards GSMs arise from a direct mutant-induced alteration in the pocket architecture leading to the loss of GSEC affinity for the compounds. However, the alteration could be also explained by conformational changes in the GSEC complex that indirectly impair the response to GSMs. To determine whether GSM response impairing substitutions alter overall GSEC conformation, we probed the active site of the protease with the transition-

state analogue Inhibitor X (Inh X, L-685,458) [323]. This inhibitor has been previously used as a reporter of conformational changes on GSEC [368,370]. For this analysis, we selected 4 representative, GSM irresponsive PSEN1 mutant variants, with the substituted residues located in the distinct areas of the proposed GSM binding pocket (Y106F, I180Q, V236W and Y240W), and performed cell-based assays with Inh X, used at concentrations ranging from nM to µM. Inhibitory profiles were determined for the Aβ40 product and the derived IC50 values showed no significant differences between the PSEN1 wild type and Y106F, I180Q and Y240F mutant cell lines (**Figure 5.8**).

In contrast, the V236W substitution significantly lowered the inhibitory concentration (IC50), relative to the wild type (5.6 nM (95% CI: 4.05 – 7.64) versus 28.6 nM (95% CI: 20.73 - 40.05) for V236W and wild type conditions, respectively). The significant change indicates that the V236W substitution favours the stabilization of the transition state. The data imply that the mutation partially mimics the reported GSM-activating effects on GSEC [327]. Interestingly, MD simulations (*data not shown*) of the mutant GSEC suggest that the introduction of a Trp residue at position V236 establishes similar contacts within PSEN and with the APP_{C99} substrate as the imidazole GSMs.

Collectively, these results strongly favour a model in which imidazole-base GSMs (acting as GSS) bind to the identified pocket, and suggest that the modulator establishes direct contacts with APP at the E-S interface.

Table 5.2: Aβn EC50/IC50 values and 95% CIs for the dose-response curves of wild type (WT) and different PSEN1 mutants towards GSM III and GSM II as presented in **Figures 5.7C and S5.2**. Legend: CI = confidence interval

		GSM III dose-response			GSM II dose-response		
			95% CI (µM)			95% CI (µM)	
	Cell line	EC50 (µM)	Lower limit	Upper Limit	EC50 (µM)	Lower limit	Upper Limit
Aβ37	WT	0.02	------	------	0.38	0.26	0.54
	Y106A	1.77	------	------	~ 1594	------	------
	Ins113T	0.17	------	------	3.22	2.66	3.97

	F177A	1.09	------	------	13.65	11.73	16.95
	I180Q	1.27	------	------	5.4	3.69	13.37
	L232A	0.12	------	------	7.24	5.5	11.24
	V236W	1.02	------	------	~ 10.31	------	------
	V236Q	0.45	------	------	~ 871.0	------	------
	Y240A	0.17	------	------	5.17	4	7.24
Aβ38	WT	0.33	0.04	0.63	1.26	0.52	------
	Y106A	9.48	4.84	149.2	17.69	5.75	------
	Ins113T	0.47	0.38	0.57	4.4	3.54	5.92
	F177A	2.5	------	------	2.58	1.61	6.91
	I180Q	74.47	4.4	------	208.9	------	------
	L232A	2.16	0.8	------	2.3	1.28	10.61
	V236W	~ 30.08	------	------	------	------	------
	V236Q	5.08	0.86	------	16.74	4.77	------
	Y240A	1.1	0.37	------	------	------	------

		GSM III dose-response			**GSM II dose-response**		
			95% CI (µM)			**95% CI (µM)**	
	Cell line	**IC50 (µM)**	**Lower limit**	**Upper Limit**	**IC50 (µM)**	**Lower limit**	**Upper Limit**
Aβ40	WT	2.10^{-3}	------	0.02	0.68	0.42	1.13
	Y106A	11.94	5.61	1011	15.18	5.95	------
	Ins113T	0.33	0.2	0.5	5.68	3.62	18.77
	F177A	3.22	2.04	8.55	5.79	4.21	10
	I180Q	5.31	2.69	685.1	13.35	5.52	------
	L232A	0.28	0.26	0.31	4.58	2.91	14.22
	V236W	~ 11.98	------	------	16.71	8.7	------
	V236Q	0.95	0.81	1.12	28.86	9.18	------
	Y240A	0.38	0.23	0.54	18.16	10.35	812.7
Aβ42	WT	~ $1.42.10^{-6}$	------	------	0.17	2.10^{-8}	0.41
	Y106A	2.38	1.31	10.32	------	------	------
	Ins113T	0.12	0.04	0.19	1.3	0.91	1.95
	F177A	0.29	0.2	0.4	2.09	1.1	------
	I180Q	3.03	0.75	------	7.05	1.45	------
	L232A	0.02	------	0.08	1.1	0.5	5.87
	V236W	3.58	0.66	------	------	------	------
	V236Q	0.29	0.14	0.48	3.81	1.67	------
	Y240A	11.77	1.45	------	------	------	------

Table 5.3: Contact frequencies between GSM II or GSM III and PSEN1 residues given in % of sampled frames. Only residues with a contact frequency of at least 30% are shown. All residues with at least one atom within 3Å of the ligand were counted as contacts.

PSEN1 Residue	GSM II contact freq. (%)	PSEN1 Residue	GSM III contact freq. (%)
Y240	99.8	**I114**	99.8
F177	99.3	**V236**	99.3
V236	98.3	**Y240**	99.0
I114	96.5	**Q112**	96.8
I180	86.5	**F177**	91.0
G111	77.5	**I180**	76.7
L113	59.3	**Y106**	69.3
F105	56.0	**L232**	67.2
L232	43.7	**F105**	58.0
Y106	32.5	**L113**	56.5
		Y181	51.2

Table 5.4: Frequency of key interaction between the GSMs and PSEN1 in % of sampled frames.

Interaction	GSM II (%)	GSM III (%)
Total polar Y106 interactions	72.5	77.5
Hydrogen bond with Y106	29.1	67.3
Water bridge to Y106	43.4	10.2
Y240 π-π stacking	99.2	94.7

Table 5.5: Pocket descriptors calculated from the GSM III binding mode as obtained by Fpocket [389]. Legend: SASA = solvent accessible surface area.

Parameter	GSM pocket
Total SASA (Å^2)	315.757
Polar SASA (Å^2)	105.313
Apolar SASA (Å^2)	210.444
Volume (Å^3)	959.320

5.5 Discussion

In this study, we used a structure-based approach to identify the binding site and the molecular mechanisms of action of potent imidazole-type GSMs. Employing the insights from the literature and the recently published GSEC-Substrate co-structures [173,175], we inspected the PSEN-NCT-APP interface and identified a cavity, largely contained in PSEN1, exhibiting suitable characteristics for the accommodation of small compounds. We hypothesized that it serves as the potential binding site for GSMs. PSEN1 contributes the majority of the residues delineating this potential binding pocket, but NCT and APP (substrate) also participate (**Figure 5.1**). Of note, we have previously shown that the interaction of GSM II with the GSEC-APP complex can be blocked by introducing bulky substitutions in the residue N243 in NCT [164].

Cell-based functional evaluation of the PSEN1 implicated residues (through an A/F mutagenesis screen) showed that the cavity of interest critically regulates GSEC processivity, likely by directly impacting the stability of the GSEC-APP_{C99}/Aβn complexes [360] (**Figure 5.2**). Subsequent functional assays in the presence of two imidazole-based GSMs showed that the structural changes in this PSEN1 region drastically diminish the response towards GSMs (**Figures 5.3 and 5.4**), with substitutions at the positions Y106, G111, L113, F177, V236 and Y240 being the most impairing ones. These results are consistent with a previous report pointing at Y106 and Y240 residues as crucial interactors of a GSM II-like modulator (ST1120) [327].

Importantly, the analysis indicates that the GSEC-APP ability to respond to GSMs can be dissociated from the GSEC ability to efficiently process APP_{C99} (i.e. GSEC processivity). This is demonstrated by the F237A substitution, which strongly impairs GSEC processivity but still allows considerably efficient GSM response, and by the Y106A and Y240A variants that either do not influence or promote GSEC processivity, but severely impair the response to GSMs. These results argue against a mutant-induced disruption of the GSM mode of action, but rather support a direct (residues interact with the compound) or indirect (residues trigger complex conformational changes) effect on the GSM binding.

To investigate drug-target interactions, we performed theoretical modelling of the binding of the GSM III/II within the cavity of interest. These *in silico* studies

supported direct participation of the PSEN1 F105, I180, L113, I114, F177, I180, L232, V236 and Y240 residues as well as the NCT I242 residue in the GSEC-GSM interactions (**Figure 5.5**), overall aligning with the results of the functional screen. To further substantiate that the identified cavity represents the actual binding pocket of imidazole-based GSMs, we conducted dose-response experiments evaluating the relative affinities of the mutant GSEC complexes. All tested substitutions (PSEN1 Y106A, Ins113T, F177A, L232A and Y240A) strongly reduce GSEC affinity for the GSMs (**Figure 5.6**), further supporting the involvement of these residues in GSM binding. Intriguingly, the L232A variant showed a differential impact on the response towards the two tested modulators. The reasons for this difference should be clarified by further studies.

One of the most frequent interactions between the modulator and PSEN1 during the MD simulations is the formation of a (water-bridged) H-bond between Y106 (in PSEN1) and the imidazole-ring of the GSMs. To investigate the geometry of this key interaction, we introduced in position PSEN1 Y106 amino acids that, like Tyr, offer a hydrogen-bonding donor group (Y106Q and Y106W). In addition, based on the theoretical model, we introduced polar amino acids that bring hydrogen-bond acceptor groups within the vicinity of position Y106 (I180Q, I180T, V236Q and V236T). While these substitutions have no or mild effects on GSEC processivity, they all strongly impair the response to GSMs (**Figure 5.7**), confirming the crucial importance of this interaction in determining the stability of the GSEC-GSM complex.

As an alternative strategy to validate the location of the GSM binding pocket (as proposed by the results of the theoretical studies), we introduced bulky amino acids in the central cavity of the pocket (PSEN1 V236W, Y240W, Y106W-V236W and V236W-Y240F), with the idea that these would sterically block the GSM binding. These substitutions had mild effects on GSEC processivity, but in agreement with our hypothesis, all drastically reduced the response to the tested GSMs, and dose-response experiments with the PSEN1 V236W variant showed a complete loss of affinity for the GSM (**Figure 5.7**).

Intriguingly, the PSEN1 V236W GSEC mutant displayed an increased affinity for Inh X, indicating that the V236W substitution stabilizes the transition state conformation of the complex (**Figure 5.8**). The data imply that the mutation partially

mimics the reported GSM-induced allosteric activation of the active site, promoting GSEC processing of APP_{C99} [294,327,367,368,370]. In line with this interpretation, our MD simulations of the PSEN1 V236W mutant GSEC complex (in the absence of the GSM) revealed that PSEN1-W236 prominently interacts with APP_{C99} (contacting the same APP_{C99} residues as the modulators, *data not shown*). We speculate that the novel interactions between the PSEN1-W236 and the APP_{C99} substrate are behind the shift in the product line preference of GSEC.

We reasoned that mutant-induced alterations on the GSEC responses towards imidazole-based GSMs could be explained by direct and/or indirect mechanisms. In the first case, residues directly contribute to the GSM-binding pocket and substitutions at these positions thus alter the protease-compound binding interactions. In the second case, substitutions of residues involved in the conformational plasticity of PSEN/GSEC, and not contributing to the GSM binding pocket, induce conformational changes that alter the GSM binding pocket. These substitutions indirectly alter GSEC-compound interactions. Of note, due to the metastable structure of PSEN/GSEC [167,360,390], the protease complex is prone to go through conformational changes, and these changes correlate with alterations in the Aβ42/40 ratio [391,392]. As our results show that certain substitutions that strongly impact GSM response (Y106F and Y240W) produce very similar Aβ profiles as the wild type cell line (**Figures 5.2A and 5.7A**), it thus seems reasonable to conclude that these variants will have little impact on overall complex architecture. To substantiate this assumption, we selected 4 substitutions that (nearly) abrogate GSM response – 2 that do not change the Aβ profiles in DMSO (Y106F and Y240W) and 2 that do (I180Q and V236W) – and probed their impact on the active-site architecture, using an active-site directed GSEC inhibitor X (Inh X). Cell-based, dose-response assays show no marked changes to Inh X inhibition of Aβ40 production for 3 of these variants (**Figure 5.8**), indicating that these complexes maintain similar conformational states.

Previous studies have attributed an allosteric mode of action to different GSM classes [294,327,367–370]. In agreement, our experimental and theoretical data pinpoint the binding pocket of potent imidazole-based GSMs to a site in the protease complex that is different from the active site. Of note, the structural models show that the substrate

establishes an interface with the investigated GSMs, suggesting its potential contribution to GSM binding. In this scenario, imidazole-based GSM could have a dual mechanism of action: acting as allosteric activators and 'molecular glue' securing E-S complexes during the sequential proteolysis. In this regard, GSMs have been proposed to target the APP ectodomain [330,365,366]. These studies have actually involved a region in APP near the extracellular-membrane border, which according to our theoretical models interacts with imidazole-based GSMs. Interestingly, several reports have shown that mutations at position Lys28 in APP_{C99} enhance GSEC processivity of APP in a 'similar' manner as potent imidazole-based GSMs do [164,319–322,324]. However, the idea that GSMs target APP was challenged by studies showing that GSM photoactivable derivatives crosslink with GSEC. Our GSEC-APP-GSM model may reconcile these previous views. Whether the substrate contributes or not to the GSM binding has important implications for the mode of action of these compounds and if true may facilitate the rational design of selective compounds mainly targeting GSEC processivity of APP. These studies warrant further investigations.

Conclusions:

We have identified the binding pocket of potent imidazole-based GSMs. This cavity is located at the PSEN1-NCT-APP interface in the GSEC-APP complex and is primarily shaped by loop 1 (HL1), TMD 3 and TMD 5 residues of PSEN1. Our studies highlight PSEN1 Y106-imidazole ring H-bonding and π-π stacking interactions between the compound and the PSEN1 Y240 residue as the essential attributes of the GSEC-GSM complex. Our data support a dual-mode of action of GSMs, i.e. the direct stabilization of the GSEC-APP/Aβn interactions and the simultaneous allosteric activation of the catalytic site. The generated novel insights, together with the established models for the drug-target interactions, could pave the way for the rational design of novel GSEC-APP targeting compounds as well as for the optimization of existing ones; thus facilitating the development of safe and effective AD therapeutics.

5.6 Supplementary figures

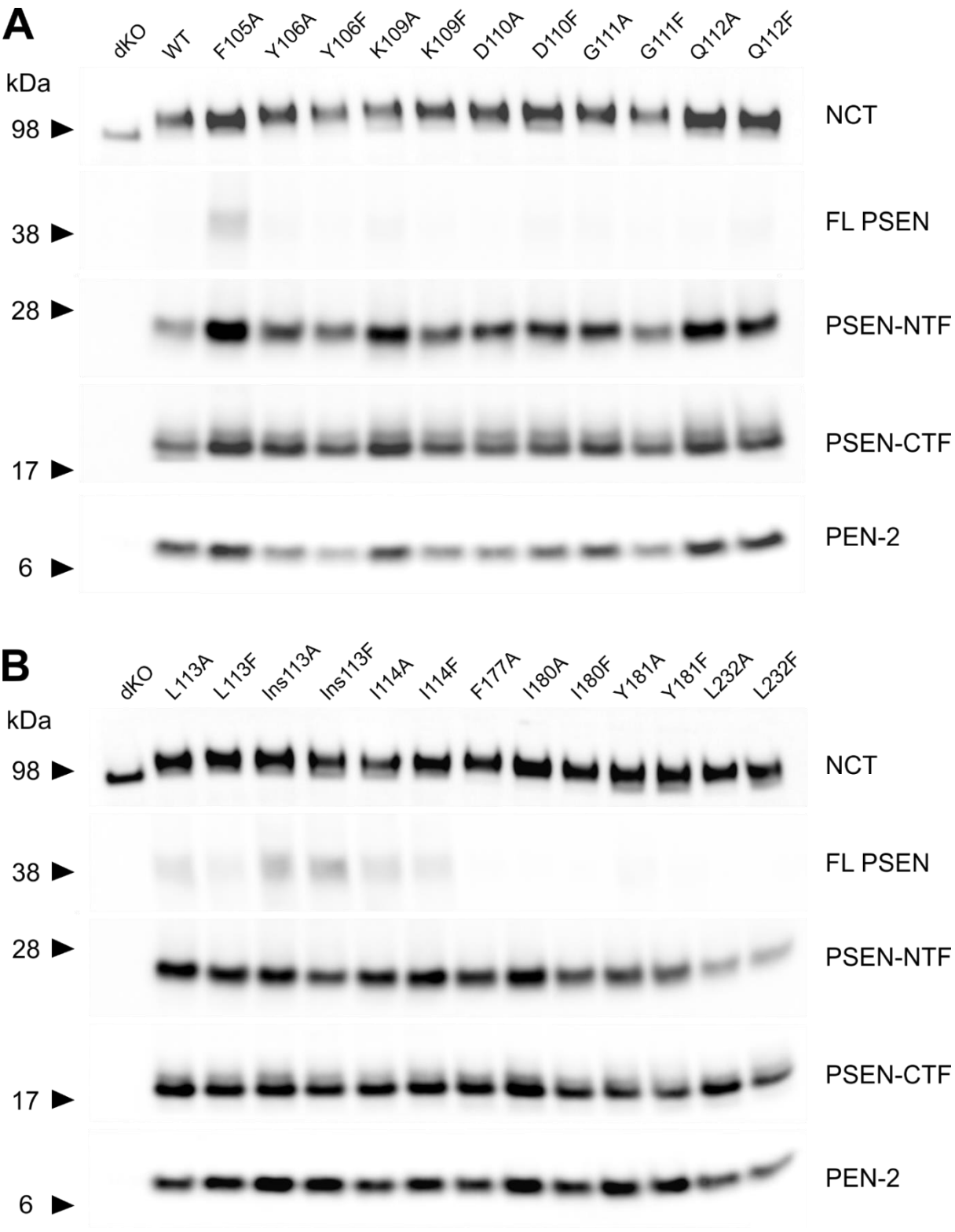

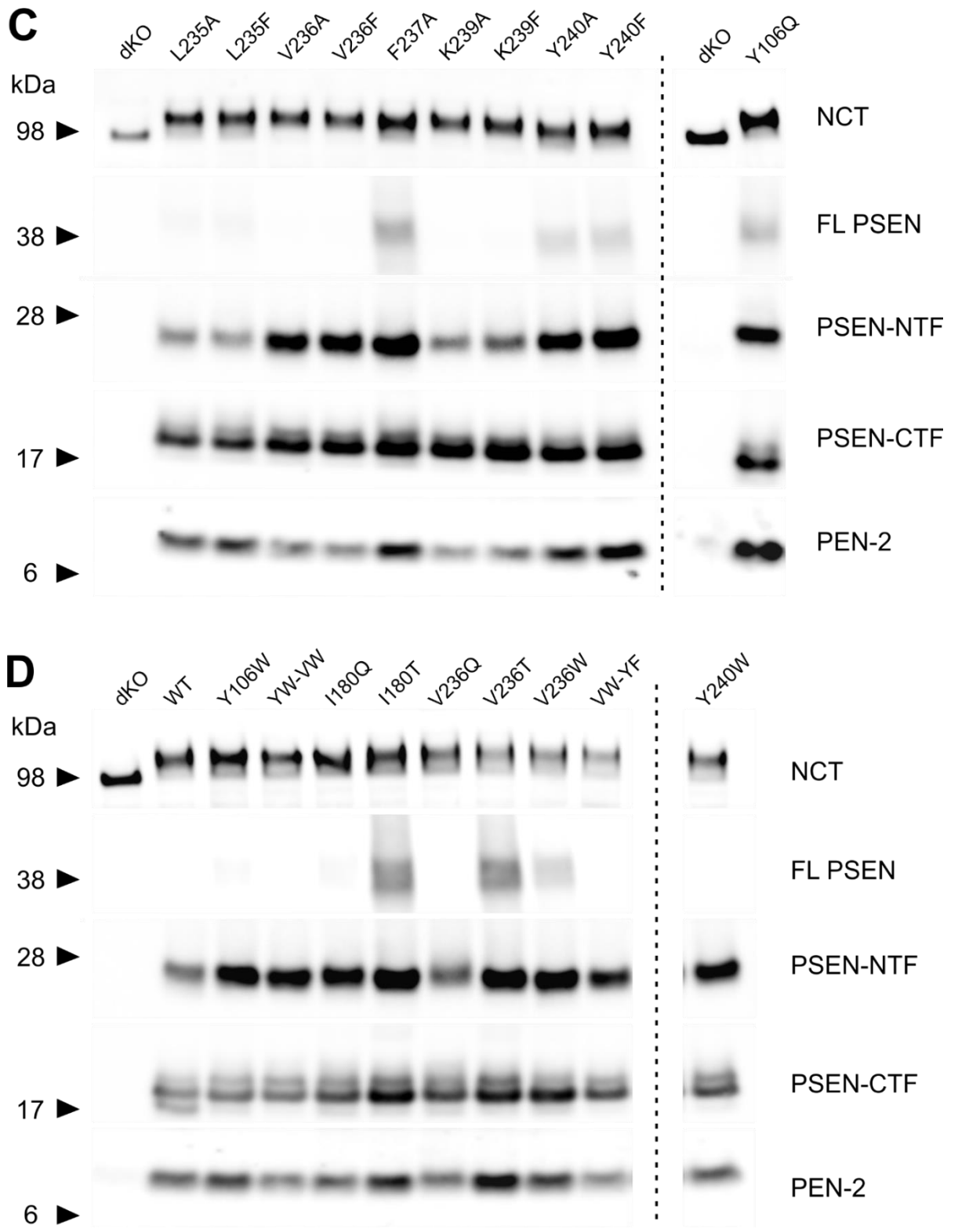

Figure S5.1. GSEC reconstitution in PSEN1 A/F screen variants

(A-D) Representative SDS-PAGE/western blot analysis of CHAPSO solubilized membranes from double knock-out (dKO) Psen1/2 MEF cell lines stably expressing WT or mutant PSEN1 subunits. Rescue of mature and active GSEC complex in the different stable lines is evidenced by the presence of mature, glycosylated NCT; the enrichment of N-terminal and C-terminal fragments (NTF/CTF) of the endoproteolysed PSEN1

over full-length uncleaved PSEN1 (FL PSEN1) and the presence of PEN-2. The position of the molecular weight markers is marked by arrowheads. Legend: YW-VW = Y106W-V236W, VW-YF = V236W-Y240F.

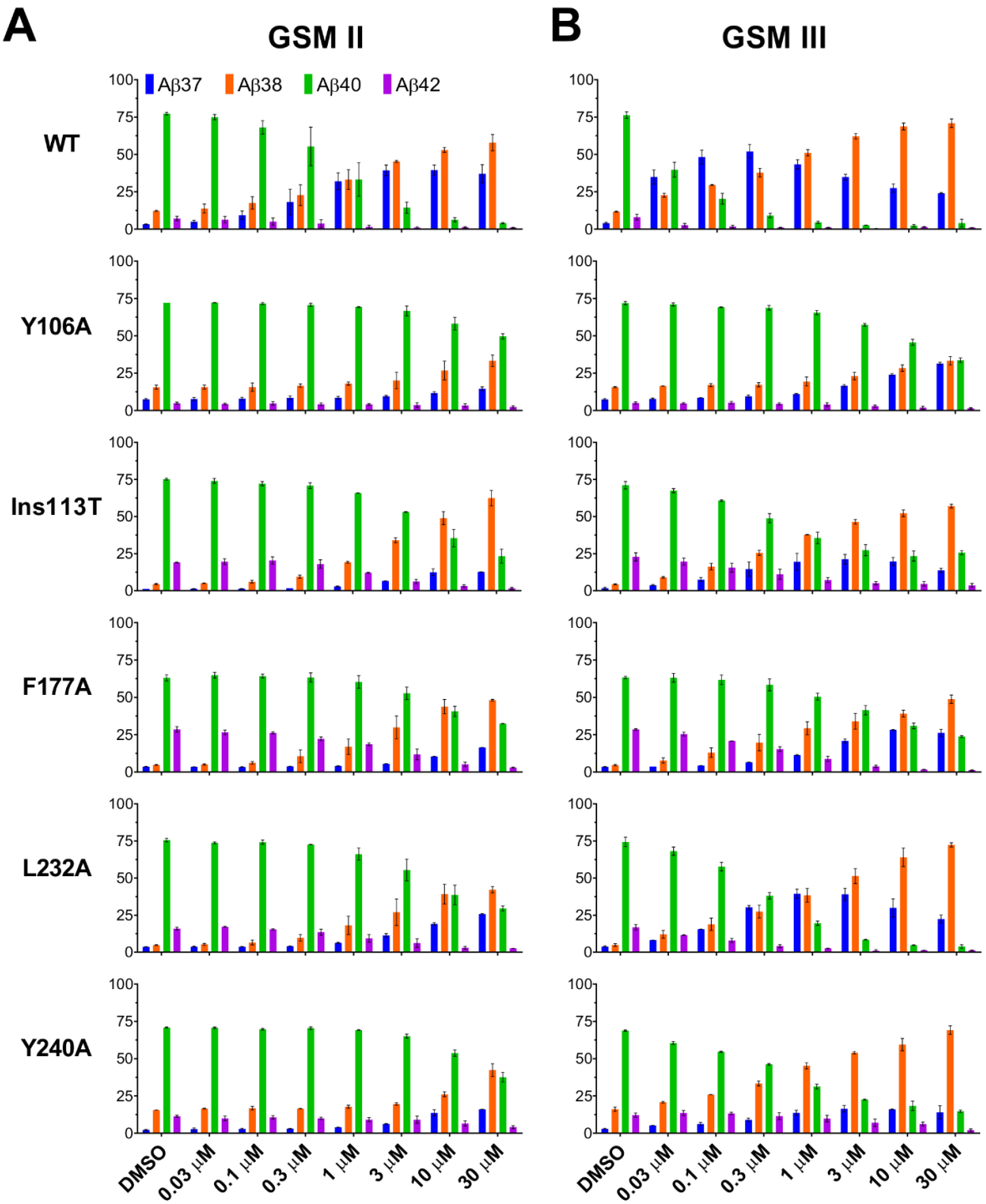

Figure S5.2. Aβ profiles of dose-response experiments with GSM II and III
(A, B) Evaluation of the change in the molecular composition of Aβ profiles in WT and 5 PSEN1 variants (Y106A, Ins113T, F177A, L232A, Y240A), which displayed a (strongly) impaired response to 1 µM GSM treatment, upon treatment with GSM II (A)

or GSM III (B) over a concentration gradient (0.03 µM - 30 µM). Data are presented as mean ± SD, N = 2 independent experiments.

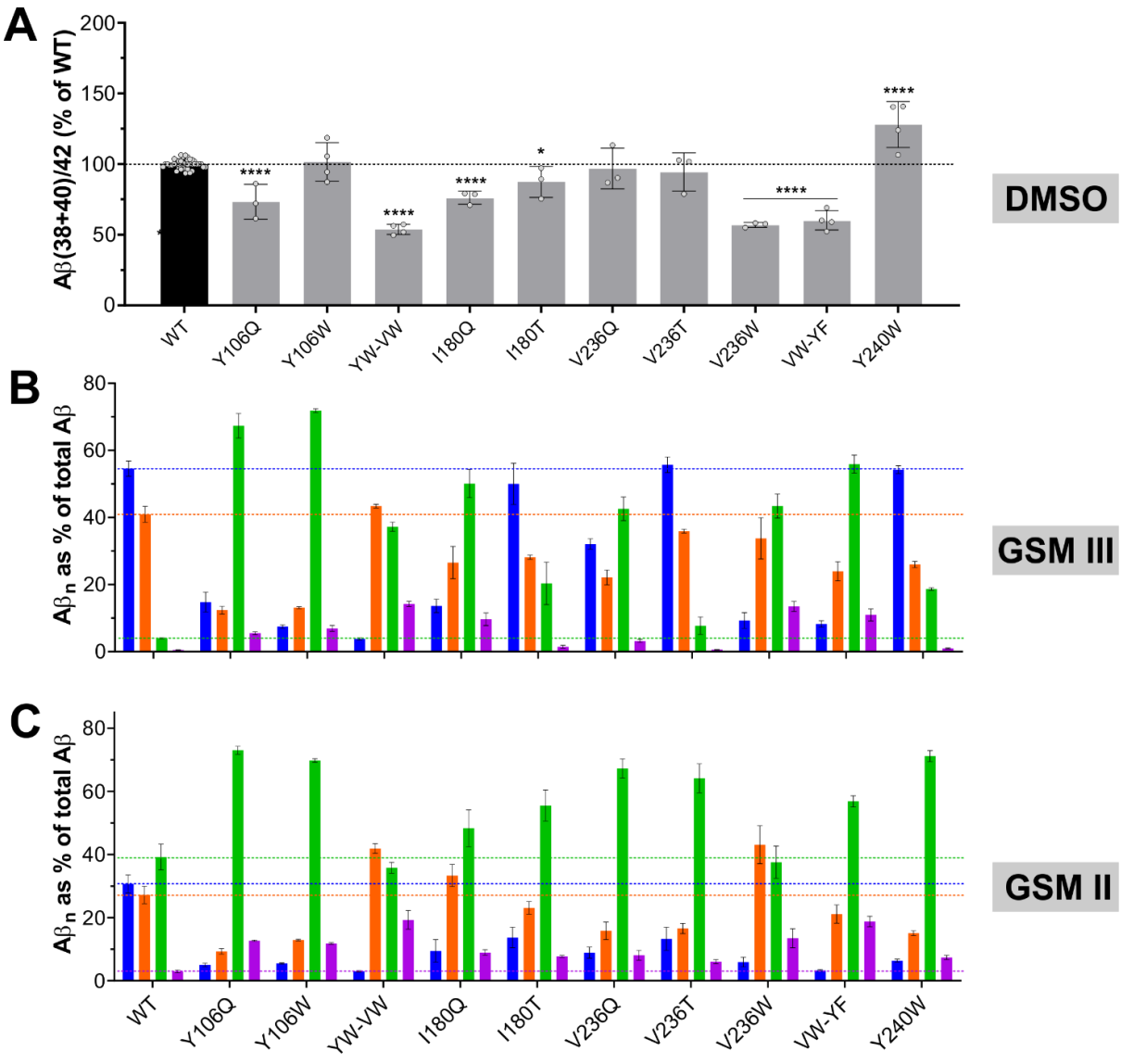

Figure S5.3. Extra PSEN1 mutations to evaluate GSM-GSEC interaction
(A) GSEC processivity was estimated using the Aβ(38+40)/42 ratio and normalized to WT cell line. **(B, C)** Aβ profiles produced by the PSEN1 WT or mutant MEF cell lines treated with 1 µM GSM III (B) or GSM II (C). Data are presented as mean ± SD, N ≥ 3 independent experiments. One-way ANOVA followed by Dunnett's post-hoc test with comparison to WT was used to determine statistical significance; *P > 0.05, ****P > 0.0001. Legend: YW-VW = Y106W-V236W, VW-YF = V236W-Y240F.

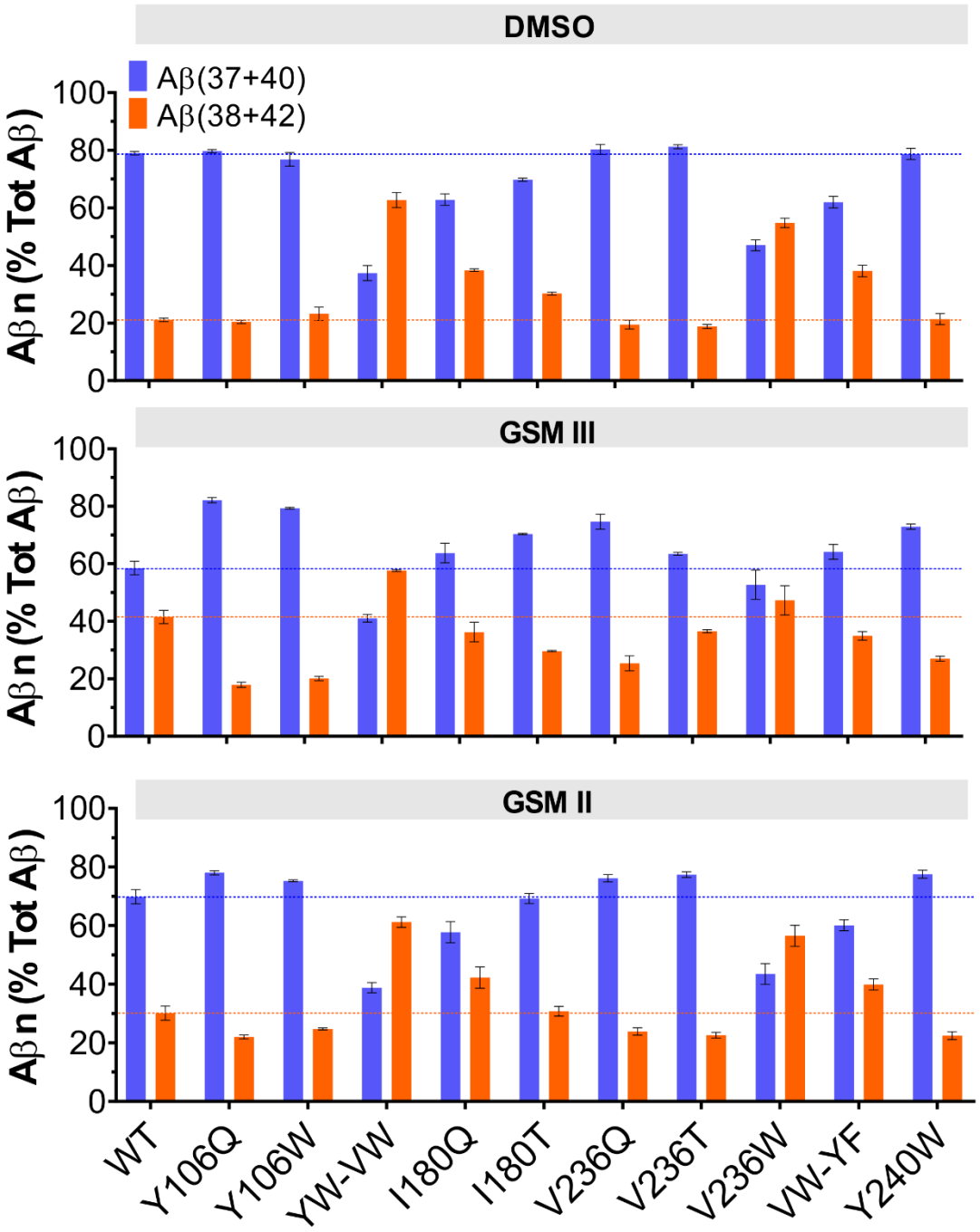

Figure S5.4. Product line preference changes in DMSO and GSM treated WT or variant PSEN1 GSECs

Comparison of the product line preferences, as calculated by contrasting Aβ37+40 with Aβ38+42 relative abundances, between the WT and PSEN1 mutant GSEC complexes. Data represent mean ± SD, N ≥ 3 independent experiments. Legend: YW-VW = Y106W-V236W, VW-YF = V236W-Y240F.

5.7 Acknowledgements and author contributions

Acknowledgements:

This work was funded by the Stichting Alzheimer Onderzoek (SAO; S16013) and the KU Leuven Methusalem grant (METH/14/07). D.P. and M.K. are supported by a PhD fellowship from the FWO ((SB/1S23819N) for D.P. and (SB/1S47020N) for M.K.). We thank Katarzyna Marta Zoltowska for critical evaluation of the results and her assistance with the writing of the manuscript.

Author Contributions:

L.C.G. designed the study, analysed the data and supervised the research. D.P. performed experiments and analysed the data. L.C.G and D.P. wrote the manuscript with the assistance of K.M.Z. who provided critical input on the results. M.K. and S.L. assisted with experiments. M.H. and M.Z. performed modelling and molecular dynamics simulations studies. M.M. provided Aβ ELISA antibodies and F.B. provided GSM compounds.

Conflict of interest:

D.P., M.H., M.K., S.L., K.M.Z., M.Z., and L.C.G. declare no competing interests. M.M. and F.B. are employees of Janssen Pharmaceutica.

6 General discussion

The lack of tangible progress and the long list of disappointing clinical trials have not only been hard for AD patients and their families but also daunted big pharma to risk investing in AD field [393]. The complex interplay between disease biology, drug mechanisms and ageing makes AD one of the most challenging medical conditions to address therapeutically. Nevertheless, our knowledge about the disease has grown exponentially in the last 30 years (see evolution in hits on PubMed for the term 'Alzheimer's disease' over the last decades), and we have also learned a lot from the failing clinical trials. Nevertheless, substantial knowledge gaps still exist, and filling these is critical for successful therapeutic development [254,394].

My doctoral studies aimed to address fundamental aspects of AD pathogenesis. I integrated mechanistic and genetic approaches to uncover the mechanisms and the structural strategies governing the GSEC-mediated proteolysis. My main goal was to unravel how Aβ production is altered in AD and how it could be intervened, in order to establish a framework for the rational development of safe and effective therapeutics.

6.1 The APP N-terminal anchor secures GSEC-APP/Aβn stability

One important milestone – accomplished at the start of my PhD studies – was the elucidation of the near-atomic structure of the GSEC complex [170]. Long-awaited, this breakthrough discovery has been made possible by technical advances in the field of single-particle cryo-EM (reviewed in [395]). At last, scientists could link the complex functionality of the protease to a structural framework. The structural data have revealed a loosely organized, 'metastable' fold, with all α-helices tilted relative to the plane of the lipid bilayer [171]. Intriguingly, rhomboid proteases also display this feature [396].

The structural metastability, together with the fact that FAD-linked *PSEN1* mutations display a scattered distribution across the protein, has led our research group to hypothesize that GSECs, and consequently the GSEC-substrate complexes, rely on a network of weak, cooperative interactions and that pathogenic mutations "destabilize" the metastable GSEC fold, thereby influencing the proteolysis. Supporting this view, GSEC thermoactivity assays have shown that thermal destabilization of the E-S

complexes mimics the effects of pathogenic mutations and that GSEC-APP/Aβn stability determines the length of Aβ peptides produced (Aβ profiles) [218].

These findings have inspired a mechanistic model for the GSEC-mediated proteolysis (updated from [218]), where the initial ε E-S complex relies on a cooperative network of interactions along the substrate TMD (global fitting). Prior to the endopeptidase cleavage, local unwinding of the substrate helix enables the accommodation of the substrate in the S1'-S3' pockets [194]. Recent E-S co-structures [173,175] have revealed that the substrate unwinding and the formation of the transition state involve conformational changes in the E and the S and the formation of a β-sheet hybrid structure. We speculated that a C-terminal 'E-S handshake' and an extracellular 'E-S anchor' grasp the substrate on both ends of the TMD during its unwinding, prior to the stabilization of the transition state (E-S*). The endoproteolytic ε-cut exerts profound destabilizing effects on the E-S complex (GSEC-Aβn), as it not only shortens the substrate but also removes the 'E-S handshake'. The cleavage triggers the local unwinding of the C-terminal part of the *de novo* generated substrate (Aβn). While the initial unwinding relies on an intriguing E-S interplay, (further) unwinding of the Aβn substrates is energetically favoured. The unwinding of the substrate extends its C-terminus towards the protease active site, enabling 'carboxypeptidase-like' proteolysis, which in turn favours further substrate unwinding, extension and proteolysis. The shortening and the destabilization of the N-terminal, remaining helix, progressively weakens the E-S assembly and confers significance to side chain- and/or backbone-dependent interactions along the shortened Aβn substrate. Our working model suggests that the interaction of GSEC with the N-terminal part of the substrates 'anchors' Aβn peptides to the enzyme during proteolysis and thereby defines Aβ length.

To uncover the structural determinants of this presumed anchor, we used the atomic structure of GSEC in complex with a co-purifying helical peptide (PDB:5FN3, [171]) as a model for γ E-S interactions. We hypothesized that this structure illustrates the interaction of GSEC with a *de novo* generated, long Aβ fragment, just before it engages into the next catalytic turnover. Exploration of the presumed γ E-S co-structure led to the identification of a short-distance interaction between GSEC and the peptide. This

potential E-S anchor implicated PSEN (the first extracellular loop, TMDs 3 and 5) and the NCT ectodomain (specifically the residues 242–243) in the stabilization of GSEC-Aβ interactions. While previous studies supported a direct interaction between PSEN1 and the substrate [176,318], our observation pointed at the potential (novel) involvement of NCT in GSEC processivity.

Structure-function analysis of the involvement of the NCT 242–243 region in APP_{C99} processing demonstrated a direct role of NCT in the stabilization of the E-S complex [164]. Of note, our studies showed that aromatic substitutions at position 242 in mouse NCT (N242F/W/Y) significantly reduced GSEC processivity of APP. In fact, these substitutions mimic 'mild' FAD-pathogenic *PSEN1* variants. In contrast, the insertion of negatively charged residues at position NCT-241 (I241E/D) shifted GSEC processivity towards the production of shorter Aβ peptides [164].

In silico modelling of the GSEC-Aβ interaction suggested that the enhanced GSEC processivity displayed by the mutants NCT-I242E/D resulted from a salt-bridge interaction between NCT E242 and APP_{695} K624 (K28 in Aβ/APP_{C99}). Experimental (mutagenic and crosslinking) analysis confirmed the E-S stabilizing interaction [164]. This data sheds new light on a previous fascinating and unexplained observation showing that substituting K28 residue in APP_{C99} (to Ala) exerts a profound effect on Aβ length [319–322,324]. We suggest that the K28 in APP_{C99} significantly contributes to the E-S anchoring mechanism, which according to our analysis is suboptimal.

Collectively, our functional data support a conserved mechanism in which the extracellular E-S interface (involving APP, NCT and PSEN) is critically involved in the stabilization of GSEC–substrate interactions and defines Aβ length (**Figure 6.1**).
The NCT ectodomain has currently been assigned a rather passive role in substrate selection, in which it restricts – by steric hindrance – the access of substrates with large ectodomains [161]. Our work highlights a novel and active role of the NCT subunit in governing APP processing and breaks with the idea of the solely 'passive' role of the GSEC non-catalytic subunits. Interestingly, the involvement of NCT in the regulation of Aβ length also suggests a potential link between, single-nucleotide variants in *NCSTN* (the NCT encoding gene) and AD risk. Here, it should be mentioned that a large

proportion of the genetic risk for early-onset AD remains uncharacterised [329] and that current genetic testing generally involves the sequencing of the known AD-linked genes *PSEN1/2* and *APP*. Our studies encourage the inclusion of the *NCSTN* gene, as well as the genes encoding the PEN-2 and APH1A/B subunits (based on the metastability of PSEN that is influenced by the other subunits), in 'standard' genetic testing of presumed FAD patients.

6.2 The molecular 'footprint' of a FAD *PSEN1* mutation: link with AD onset

Previous work of the laboratory revealed a remarkable linear correlation between the degree of FAD-linked mutant-induced destabilization of GSEC-APP/Aβn interactions and the age of AD onset (AAO) [218]. This observation places the E-S destabilization and the resulting changes in Aβ profiles, at the core of FAD pathogenesis. This study, however, did not inform about the type/length and proportions of Aβ peptides generated in pathogenic conditions. The relationship between FAD mutant-driven effects and the clinical phenotype is a fundamental aspect that remains unclear. Previous studies assessing the effects of pathogenic *PSEN1/2* and *APP* variants on APP metabolism have imposed an Aβ42-centric view. In fact, relative and/or absolute changes in Aβ42 production have been for a long time seen as the pathogenic hallmark of FAD-link variants. However, the literature in this regard is inconsistent. Analysis of the relationships between FAD mutant-driven effects on absolute and/or relative Aβ42 production levels and respective age at onset (AAO) have shown no significant correlations [339,349,352,397] as well as robust correlations [209,350,351].

We have to keep in mind though, that GSEC processing of APP_{C99} results in a complex mixture of Aβ peptides, with each distinct species having different properties with regard to hydrophobicity, aggregation propensity and toxicity. Indeed, substantial evidence exists that Aβ42 is highly (neuro)toxic. However, Aβ43, although produced at low levels, seems to be potently amyloidogenic and neurotoxic [356]. Furthermore, recent data indicate that the shorter peptides (Aβ37, Aβ38 and Aβ40) might attenuate the toxicity related to longer Aβ forms [398,399]. Indeed, mixtures with different Aβ42 to Aβ40 proportions display distinct aggregation kinetics and neurotoxic properties [400].

Accordingly, the toxic properties of "Aβ" should be considered in the context of the mixture of Aβ peptides of different lengths and proportions [220].

With this in mind, we decided to revisit how *PSEN1* FAD mutant-induced E-S destabilization affects the molecular composition of Aβ profiles in a cellular context. We quantified Aβ37, 38, 40, 42 and 43 peptides, which comprise the vast majority of the Aβ peptides generated in a cellular context. Hence, their quantitative analysis adequately represents the secreted Aβ pool. Our data showed that pathogenic *PSEN1* mutations shift the Aβ profiles towards the longer (> Aβ40) peptides at the expense of the shorter ones (≤ Aβ40), while GSECs bearing non-pathogenic *PSEN1* variants displayed profiles identical to the wild type counterpart. To provide a single number estimate of the mutation's pathogenicity, we evaluated what type of changes (compared to the wild type) in the molecular composition of Aβ profiles correlate best with the AAO (an indicator of the disease severity). For this purpose, we calculated Aβ ratios that assess different aspects of APP_{C99} processing and plotted the mutant ratios against their corresponding AAO. While there was no correlation between changes in the 'product line preference' – assessed by the calculation of the Aβ(38+42)/(40+43) ratio – and AAO, the overall efficiency of the 4th APP_{C99} turnover (illustrated by the Aβ(38+40)/(42+43) ratio) revealed a strong linear relationship with AAO ($R^2 = 0.9$, $P < 0.0001$). This data reinforces the concept that the degree of the E-S destabilization determines the AAO [218]. In this view, it is expected that both product lines are equally affected and that the consequences of the mutation will be more pronounced for the more labile E-S complexes (i.e. E-S complexes engaged in the later turnovers). In addition, we showed that the Aβ(38+40)/(42+43) ratio is the best, thus far known, predictor of the 'intrinsic' AAO of newly identified *PSEN1* mutations.

Two other important observations from our study suggest: **I**) that the 'intrinsic' (biochemical) AAO of *PSEN1* mutation carriers is subject to the influence of genetic modifiers (*APOE* genotype) and **II**) that severe, mutation-driven inactivating effects on the global GSEC activity delay the expected clinical onset (as determined by biochemical analysis).

Regarding the first point, studies on the world's largest ADAD kindred (i.e. carriers of the PSEN1 E280A, "Columbian" or "Paisa" mutation) have demonstrated that the *APOE* genotype represents an important AAO modifier in FAD. Carriers of at least one copy of the *APOE2* allele display an average AAO delay of more than 10 years [355]. Furthermore, a very recent study has shown that a carrier of the Paisa mutation and homozygous for the rare APOE Christchurch (R136S) variant [401], has an almost 30-year delay in MCI development [45]. We propose that our correlative analysis could help in the identification of genetic modifiers of AAO. Biochemical estimates will provide the "expected" onset according to the denaturing effects of the mutation and delays or acceleration in the clinical onset would suggest the presence of a modifier.

Our data also indicate that symptom onset is significantly delayed by pronounced FAD mutant-induced inactivation of the overall GSEC activity (i.e. ε-cleavage efficiency). Importantly, in FAD patients only one allele of the *PSEN1* gene is affected (except for some rare homozygous cases [402]). The other allele expresses wild type PSEN1, and thus reconstitutes a normal GSEC complex. Biochemical studies on post-mortem FAD patient and control brain samples have shown that both alleles contribute to total GSEC activity [213]. Of note, PSEN2 containing GSEC complexes also contribute to APP processing, although a recent study indicates that these complexes mainly contribute to the intracellular Aβ pool [147]. *PSEN1* mutations that strongly impact the overall GSEC activity, such as R278I, P433S and L435F [214,215,342] produce, although at very low concentrations, a pool of Aβs that is highly enriched for the longer Aβ43 species. This 'pathogenic' pool is diluted by the Aβ40 enriched profiles produced by the wild type PSEN, as is recently demonstrated for the PSEN1 L435F mutation in induced pluripotent stem cell (iPSC)-derived neurons from FAD patients [403]. The high 'intrinsic' pathogenic potential of the disease allele is thus partially silenced by its inhibitory effect on the overall Aβ production and is likely mitigated by the healthy allele. However, it is important to underline that although these strongly inactivating variants poorly contribute to the secreted Aβ production, their effects still cause AD in the '40s. Collectively, these data emphasize the importance of viewing Aβ as a complete mixture, derived in heterozygous conditions.

Our data not only links the molecular 'Aβ footprint' of a given *PSEN1* mutation to its pathogenic potential, but also to disease severity (AAO) (**Figure 6.1**), implying that the mutant-induced changes set a kind of 'alarm' for the timing of the clinical phase of the disease. The impact of newly discovered *PSEN1/2* mutations is currently often evaluated through a number of algorithms, such as Polyphen2, SIFT, CADD, etc., that have been developed to help predict their functional consequences. However, the outcomes of these different prediction algorithms do not always match with reality (as determined in an experimental setting) [404]. Therefore, the development of a method to biochemically assess the impact of mutations could work in synergy with these *in silico* analyses to achieve superior predictive capacity. Clinicians that are confronted with *PSEN1/2* mutation carriers that present with unclear or censored family history or "de novo" mutations could especially benefit from such an improved prediction method. We recognize that the applied experimental approach to determine the mutants profile is time-consuming, however, recent methodical advances – such as the novel Psen1$^{-/-}$/Psen2$^{-/-}$ N2A mouse neuroblastoma cell line model [405] – could facilitate the biochemical analysis of pathogenic *PSEN1/2* variants [336].

How do changes in the molecular 'Aβ footprint' trigger AD pathology? It is generally considered that monomeric Aβ is innocuous, but becomes neurotoxic upon self-association [406]. However, this does not necessarily mean that Aβ aggregation equals disease. A myriad of Aβ aggregates exists in the human brain, ranging from insoluble fibrillar deposits to soluble aggregates of different sizes [220]. Several studies have indicated that fibrillar Aβ assemblies (~ plaques) are not linked to AD. This is evidenced by FAD patients with the *APP* Arctic mutation presenting with very low levels of plaques [407] and cognitively normal elderly subjects with high plaque burden [50]. The latter study instead shows that these 'high pathology controls' have only low levels of soluble Aβ oligomers (AβOs) which contrasts with the high burden in actual AD subjects. The past 2 decades have been marked by an intensive search for "the" toxic Aβ oligomer and its mechanism(s) of toxicity (reviewed in [62,63]). Our data demonstrating a direct link between the molecular composition of the Aβ profiles and disease severity support the

use of relatively simple cell culture models for advanced studies into what type of 'native' AβOs are produced in a given pathogenic Aβ pool.

6.3 Stabilizing GSEC-APP/Aβn interaction: a novel strategy for AD therapy

Our work supports that the molecular Aβ 'footprint' is intimately connected to AD pathogenesis (**Figure 6.1**) and suggests that shifts in the composition of Aβ profiles towards the generation of short peptides could exert therapeutic benefits. Our previous studies have proposed the stabilization of the GSEC-APP/Aβn interactions as a novel therapeutic strategy to tackle toxic Aβ production while preserving the signalling roles of the GSEC proteases [218].

GSEC stabilizers (GSSs) are defined as molecules that ensure efficient processing of APP_{C99} along both product lines. Therefore, they stand in sharp contrast with GSEC inhibitors (GSIs) that inhibit Aβ production and suffer from a broad spectrum of adverse effects associated with the complex biology of GSECs (see section 1.5.2). Although the rationale for the use of GSSs has been established only recently, compounds stabilizing GSEC already exist and are known as GSEC modulators (GSMs). Potent GSMs stabilize E-S interactions and promote GSEC processivity [218] through slowing down E-S dissociation [386].

GSMs were identified at the start of the millennium during a screen for compounds capable of (specifically) reducing Aβ42 production [257]. While the first GSMs had very modest potency, many more compounds – with far superior potency (in the low nM range) – have been identified since then (reviewed in [361]). Apart from the triterpenoid natural product derived GSMs [408–410], we can distinguish two main classes of GSMs. The acidic (NSAID-based) GSMs specifically lower Aβ42 levels while stimulating Aβ38 production. The non-acidic GSMs – most of which contain an imidazole group – promote the production of both Aβ37 and Aβ38 from the Aβ40 and Aβ42 precursors, respectively [363]. Concerning the mode of action of GSMs, the substituted cysteine accessibility method (SCAM) [327,367], kinetic analyses [216] and competition experiments with active-site directed GSIs [294,368,370] suggest allosteric activation of the proteolytic cleavage mechanism. However, our knowledge about GSM binding and mode of action remains limited, hampering therapeutic development.

Building on recent structural and functional data, we have hypothesized that GSSs target the E-S anchoring interaction between GSEC (NCT/PSEN) and APP N-terminus. Exploration of the recent GSEC-APP_{C83} co-structure [173] led to the identification of a cavity situated at the tripartite interface between APP (N-terminus), NCT and PSEN1. Initial reports have shown that NSAIDs bind to the TMD of APP near its juxta-membrane region [330,365,366], and the K28 residue (in APP_{C99}) has been proposed to be the functional interaction partner of the carboxylic acid group [330]. However, the results of these studies have been challenged and linked to non-specific interaction between the compound and APP_{C99} aggregates [411]. Alternatively, studies have pointed to PSEN1 N-terminal fragment (NTF) as the main binding partner of non-acidic GSMs [294,327,367–370]. In addition, one study has implicated PEN-2 as the principal target of imidazole-based 2nd generation GSMs [363]. However, GSEC has been studied there in non-native conditions. Our model, arguing for a tripartite nature of the GSM binding pocket, could explain the at first glance inconsistent data in the multiple reports.

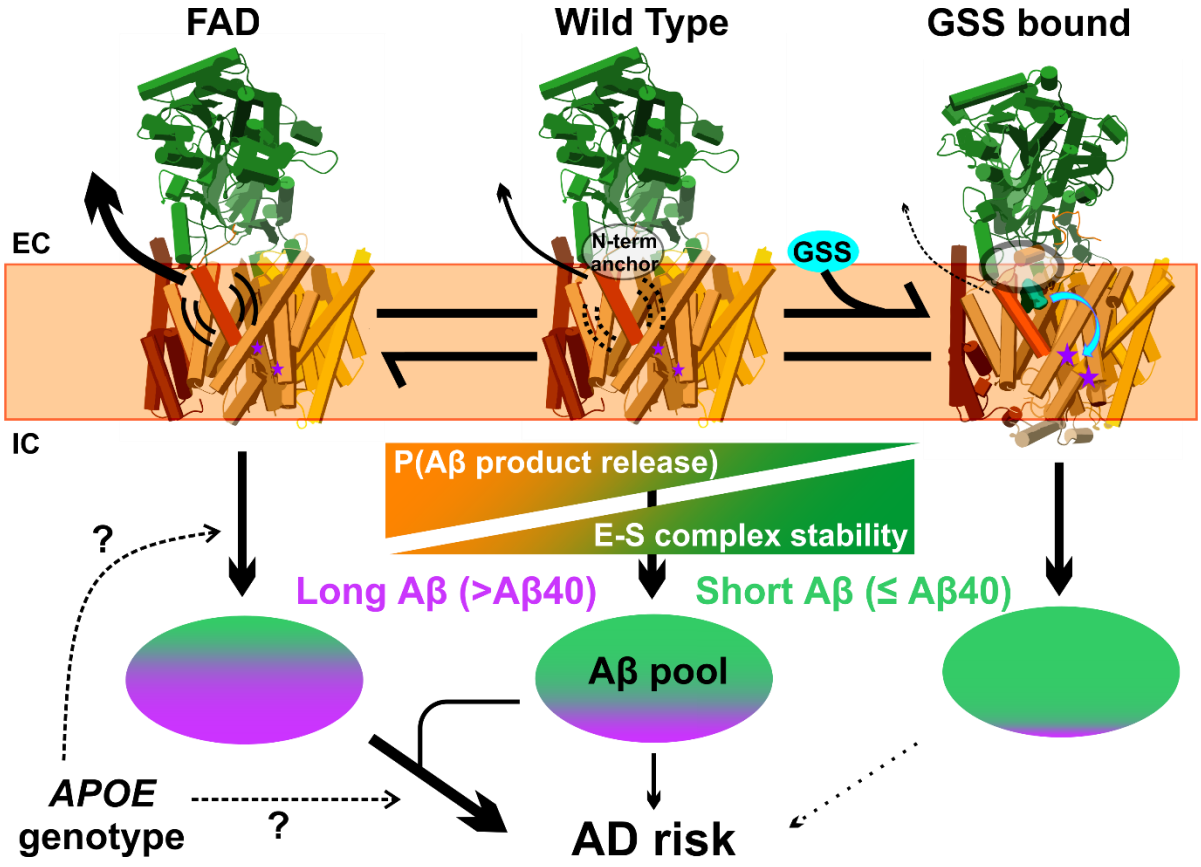

Figure 6.1 Model for how GSEC-APP/Aβn interaction stability underlies AD risk. (adapted from [164,218]). The stability of GSEC (E) – APP/Aβn (S) interaction correlates

inversely with the probability (P) of Aβ product release. Compound mediated stabilization of the interaction, occurring at the GSEC (PSEN-NCT) – APP interface, boosts the efficiency of the sequential proteolytic mechanism (in part through activation of the active site). The resulting Aβ pool is virtually devoid of the long (>Aβ40) peptides. In contrast, destabilization of the interaction, due to the presence of FAD-linked *PSEN/APP mutations*, primes the complex for premature dissociation and enriches the Aβ pool for the longer species. The composition of the Aβ pool is linked with a person's risk for developing AD, although this risk can be modified by external factors such as *APOE* genotype. Legend: GSS = GSEC stabilizer, E = Enzyme, S = Substrate, EC = extracellular, IC = intracellular.

To evaluate the involvement of the defined cavity in accommodating GSMs, we performed mutagenesis screening of all NCT and PSEN1 residues that shape the putative interaction partner. We used two imidazole-based GSMs (GSM II and III) as representative GSEC stabilizers with different potency [218]. The first, limited screen, evaluating only the contribution of residues I241 and N242 in mouse NCT, demonstrated that introducing bulky/aromatic substitutions in position 242 results in a dramatic loss of response to GSM II but not GSM III [164]. Encouraged by this data, we next focused on the contribution of PSEN1. An iterative experimental-theoretical (feedback) analysis resulted in the identification of the GSS binding pocket and the proposal of a potential binding mode. In our model, the compound situates itself between the APP N-terminus and PSEN loop 1, right at the border of the lipid bilayer. Our studies especially highlight PSEN1 Y106 H-bonding with the conserved imidazole ring of the GSMs and π-π stacking interactions of the compound with PSEN1 Y240 as essential mediators of ligand-receptor interaction. In agreement with previous work, we have shown that GSM binding allosterically activates the catalytic site. However, we speculate that the compound additionally stabilizes the GSEC-APP/Aβn interaction by acting as a molecular "glue" between the E and the S, and that both mechanisms work synergistically to enhance GSEC processivity of APP_{C99}. These detailed new insights into the binding and the action of GSMs provide a clear framework for the further, rational development of GSSs. An important goal will be to select or design compounds with better drug-like properties and excellent safety profiles [263] while maintaining sufficient potency to secure efficient APP/Aβ processing.

6.4 A critical reflection of using a FAD model to study AD pathogenesis

Due to the complex, multifactorial nature of SAD, it has proven very challenging to model it in a research context. As FAD and SAD share the same pathological and clinical hallmarks, the work conducted in the frame of this doctoral thesis has used FAD as a genetically validated model to investigate AD pathogenesis.

However, are the molecular mechanisms operating in FAD relevant for SAD pathogenesis? The indisputable genetic evidence (see section 1.4) demonstrates that altering Aβ production is sufficient to cause disease. Our work places GSEC-APP/Aβn interaction stability [218] in the foreground as the factor that dictates the profile of secreted Aβ and its inherent pathogenic potential. GSEC-APP/Aβn interaction stability is, however, not only affected by pathogenic mutations in the enzyme or the substrate but is also very sensitive to the modulation by environmental factors or compounds [218]. Consequently, in SAD brains, despite the lack of mutations in *PSEN1/2* and *APP*, the GSEC-APP/Aβn complex could still be destabilized by pathogenic, environmental factors. In this regard, it has been extensively documented that alterations in the brain lipid composition – due to ageing, genetic risk factors (i.e. *APOE*) and altered dietary lipid content – are intimately associated with AD (reviewed in [412]). Of relevance, it has been shown that the lipid environment is an important regulator of GSEC activity [413–416]. Consequently, alterations in the *de novo* generated Aβ have been observed in a subpopulation of SAD patients [213,417–420]. Although it is unknown in what percentage of cases this contributes to AD pathogenesis, the relevance of altered APP/Aβn processing clearly extends beyond the group of FAD patients.

Will the therapeutics developed based on the insights obtained by our work be applicable for SAD patients? Aβ pathology in the brain is an essential hallmark of both forms of the disease. Longitudinal studies on AD patients have demonstrated that Aβ accumulation represents one of the earliest events in the disease process (**Figure 1.1**) [8–12]. In addition, our work indicates that altered Aβ metabolism translates into increased/decreased AD severity, through its impact on the composition of the Aβ pool. Nevertheless, the critics of GSSs argue that the composition of the Aβ pool in SAD depends largely on the impaired clearance of the Aβ peptides [421]. Indeed, this is true, but given that the GSSs will reduce the production of long, toxic Aβ species, the Aβ

clearance mechanisms will no longer need to cope with these disease culprits. Therefore, the GSS-based therapeutic strategy offers a way to halt, prevent or slow down the disease process in all AD patients.

7 Conclusions

Despite on-going efforts, AD field suffers from a long history of failing clinical trials. What are the primary reasons for the lack of success? *"The real problem is that there is simply not enough underlying science to begin with. The trials are based on vague hypotheses without fundamental understanding of Alzheimer's disease itself. Too many medical trials are moonshots in the dark."* (T. Südhof, *The Washington Post*). With this in mind, this doctoral study aimed to obtain a better mechanistic understanding of AD pathogenesis to establish a framework for the rational development of safe and effective therapeutics. Overall, using a genetically and biochemically validated AD model (FAD), the research described in this thesis has contributed substantially to our understanding of the biochemical, structural and mechanistic underpinnings of AD. It has provided a strong rationale and a solid framework for the use of GSEC stabilizing compounds as a preventive therapeutic strategy to tackle AD.

In summary, the work has revealed that:

I NCT ectodomain plays an active role in regulating Aβ length

II The APP_{C99} N-terminal region (especially K28 and its surrounding amino acids) anchors the substrate to GSEC, stabilizes E-S complexes, and thereby promotes sequential proteolysis of the substrate

III FAD-causing *PSEN1* mutations produce a distinct molecular Aβ 'footprint' – enriched for long Aβ species – that defines the age at AD onset in their carriers

IV GSEC stabilizers target the GSEC (PSEN-NCT)-APP interface to secure E-S stability as well as to allosterically activate the proteolytic process

8 References

1. Alzheimer, A. Uber eine eigenartige Erkrankung der Hirnrinde. *Allg Zeitschr f Psychiatr. u Psych-Gerichtl Med* (1907). doi:10.1002/ca.980080612

2. Glenner, G. G. & Wong, C. W. Alzheimer's diease and Down syndrome: sharing of a unique cerebrovascular amyloid fibril protein. *Biochem. Biophys. Res. Commun.* **122**, 1131–1135 (1984).

3. Masters, C. L. *et al.* Amyloid plaque core protein in Alzheimer disease and Down syndrome. *Proc. Natl. Acad. Sci. U. S. A.* **82**, 4245–4249 (1985).

4. Brion, J., Heloisa, P., Jacques, N. & Jacqueline, F.-D. Mise en évidence immunologique de la protéine tau au niveau des lésions de dégénérescence neurofibrillaire de la maladie d ' Alzheimer. *Arch. Biol. Brux.* **95**, 229–235 (1985).

5. Grundke-Iqbal, I., Iqbal, K. & Tung, Y. C. Abnormal phosphorylation of the microtubule-associated protein τ (tau) in Alzheimer cytoskeletal pathology. *Proc. Natl. Acad. Sci. U. S. A.* **83**, 44913–44917 (1986).

6. Goedert, M., Wischik, C. M., Crowther, R. A., Walker, J. E. & Klug, A. Cloning and sequencing of the cDNA encoding a core protein of the paired helical filament of Alzheimer disease: Identification as the microtubule-associated protein tau. *Proc. Natl. Acad. Sci. U. S. A.* **85**, 4051–4055 (1988).

7. Weidner, W. S. & Barbarino, P. P4-443: THE STATE OF THE ART OF DEMENTIA RESEARCH: NEW FRONTIERS. *Alzheimer's Dement.* (2019). doi:10.1016/j.jalz.2019.06.4115

8. Sperling, R. A. *et al.* Toward defining the preclinical stages of Alzheimer's disease: Recommendations from the National Institute on Aging-Alzheimer's Association workgroups on diagnostic guidelines for Alzheimer's disease. *Alzheimer's Dement.* **7**, 280–292 (2011).

9. Jack, C. R. *et al.* Tracking pathophysiological processes in Alzheimer's disease: An updated hypothetical model of dynamic biomarkers. *Lancet Neurol.* **12**, 207–216 (2013).

10. Villemagne, V. L. *et al.* Amyloid β deposition, neurodegeneration, and cognitive decline in sporadic Alzheimer's disease: A prospective cohort study. *Lancet Neurol.* **12**, 357–367 (2013).

11. Gordon, B. A. *et al.* Spatial patterns of neuroimaging biomarker change in individuals from families with autosomal dominant Alzheimer's disease: a longitudinal study. *Lancet Neurol.* 241–250 (2018). doi:10.1016/S1474-4422(18)30028-0

12. Vermunt, L. *et al.* Duration of preclinical, prodromal, and dementia stages of Alzheimer's disease in relation to age, sex, and APOE genotype. *Alzheimer's Dement.* **15**, 888–898 (2019).

13. De Strooper, B. & Karran, E. The Cellular Phase of Alzheimer's Disease. *Cell*

164, 603–615 (2016).

14. Kunkle, B. W. *et al.* Genetic meta-analysis of diagnosed Alzheimer's disease identifies new risk loci and implicates Aβ, tau, immunity and lipid processing. *Nat. Genet.* **51**, 414 (2019).

15. Kivipelto, M., Mangialasche, F. & Ngandu, T. Lifestyle interventions to prevent cognitive impairment, dementia and Alzheimer disease. *Nat. Rev. Neurol.* **14**, 653–666 (2018).

16. Killin, L. O. J., Starr, J. M., Shiue, I. J. & Russ, T. C. Environmental risk factors for dementia: a systematic review. *BMC Geriatr.* **16**, 1–28 (2016).

17. Jorm, A. F. & Jolley, D. The incidence of dementia: a meta-analysis. *Neurology* **51**, 728–733 (1998).

18. Corrada, M. M., Brookmeyer, R., Paganini-Hill, A., Berlau, D. & Kawas, C. H. Dementia incidence continues to increase with age in the oldest old the 90+ study. *Ann. Neurol.* **67**, 114–121 (2010).

19. Gatz, M. *et al.* Role of genes and environments for explaining Alzheimer disease. *Arch. Gen. Psychiatry* **63**, 168–174 (2006).

20. McKay, G. J. *et al.* Variations in apolipoprotein e frequency with age in a pooled analysis of a large group of older people. *Am. J. Epidemiol.* **173**, 1357–1364 (2011).

21. Pericak-Vance, M. A. *et al.* Linkage studies in familial Alzheimer disease: Evidence for chromosome 19 linkage. *Am. J. Hum. Genet.* **48**, 1034–1050 (1991).

22. Corder, E. H. *et al.* Gene Dose of Apolipoprotein E Type 4 Allele and the Risk of Alzheimer's Disease in Late Onset Families. *Science (80-.).* **261**, 921–923 (1993).

23. Saunders, A. M. *et al.* Association of apolipoprotein E allele ε4 with late-onset sporadic Alzheimer's disease. *Neurology* **43**, 1467–1472 (1993).

24. Strittmatter, W. J. *et al.* Apolipoprotein E: High-avidity binding to β-amyloid and increased frequency of type 4 allele in late-onset familial Alzheimer disease. *Proc. Natl. Acad. Sci. U. S. A.* **90**, 1977–1981 (1993).

25. Genin, E. *et al.* APOE and Alzheimer disease: A major gene with semi-dominant inheritance. *Mol. Psychiatry* **16**, 903–907 (2011).

26. Chartier-Harlin, M.-C. *et al.* Apolipoprotein E, ε4 allele as a major risk factor for sporadic early and late-onset forms of Alzheimer's disease: analysis of the 19q13. 2 chromosomal region. *Hum. Mol. Genet.* **3**, 569–574 (1994).

27. Corder, E. *et al.* Protective effect of apolipoprotein E type 2 allele for late onset Alzheimer disease. *Nat. Genet.* **7**, 180–184 (1994).

28. Serrano-Pozo, A., Qian, J., Monsell, S. E., Betensky, R. A. & Hyman, B. T.

APOEε2 is associated with milder clinical and pathological Alzheimer disease. *Ann. Neurol.* **77**, 917–929 (2015).

29. Reiman, E. M. *et al.* Exceptionally low likelihood of Alzheimer's dementia in APOE2 homozygotes from a 5,000-person neuropathological study. *Nat. Commun.* **11**, 667 (2020).

30. Guerreiro, R. *et al. TREM2* Variants in Alzheimer's Disease. *N. Engl. J. Med.* **368**, 117–127 (2013).

31. Karch, C. M. & Goate, A. M. Alzheimer's disease risk genes and mechanisms of disease pathogenesis. *Biol. Psychiatry* **77**, 43–51 (2015).

32. Fulop, T. *et al.* Can an Infection Hypothesis Explain the Beta Amyloid Hypothesis of Alzheimer's Disease? *Front. Aging Neurosci.* **10**, 1–11 (2018).

33. Bartus, R. T., Dean, R. L., Pontecorvo, M. J. & Flicker, C. The Cholinergic Hypothesis: A Historical Overview, Current Perspective, and Future Directions. *Ann. N. Y. Acad. Sci.* **444**, 332–358 (1985).

34. Khachaturian, Z. S. Calcium Hypothesis of Alzheimer's Disease and Brain Aginga. *Ann. N. Y. Acad. Sci.* **747**, 1–11 (1994).

35. Praticò, D. Oxidative stress hypothesis in Alzheimer's disease: a reappraisal. *Trends Pharmacol. Sci.* **29**, 609–615 (2008).

36. Hardy, J. & Allsop, D. Amyloid deposition as the central event in the aetiology of Alzheimer's disease. *Trends Pharmacol. Sci.* **12**, 383–388 (1991).

37. Selkoe, D. J. The molecular pathology of Alzheimer's disease. *Neuron* **6**, 487–498 (1991).

38. Hardy, J. & Higgins, G. Alzheimer's disease: the amyloid cascade hypothesis. *Science (80-.).* **256**, 184–185 (1992).

39. Kametani, F. & Hasegawa, M. Reconsideration of amyloid hypothesis and tau hypothesis in Alzheimer's disease. *Front. Neurosci.* **12**, (2018).

40. de la Torre, J. C. & Mussivand, T. Can disturbed brain microcirculation cause Alzheimer's disease? *Neurol. Res.* **15**, 146–153 (1993).

41. Swerdlow, R. H. & Khan, S. M. A 'mitochondrial cascade hypothesis' for sporadic Alzheimer's disease. *Med. Hypotheses* **63**, 8–20 (2004).

42. Fernández, J. A., Rojo, L., Kuljis, R. O. & Maccioni, R. B. The damage signals hypothesis of Alzheimer's disease pathogenesis. *J. Alzheimer's Dis.* **14**, 329–333 (2008).

43. Yu, J.-T., Tan, L. & Hardy, J. Apolipoprotein E in Alzheimer's Disease: An Update. *Annu. Rev. Neurosci.* **37**, 79–100 (2014).

44. Yamazaki, Y., Zhao, N., Caulfield, T. R., Liu, C. C. & Bu, G. Apolipoprotein E and Alzheimer disease: pathobiology and targeting strategies. *Nat. Rev. Neurol.* **15**, 501–518 (2019).

45. Arboleda-Velasquez, J. F. *et al.* Resistance to autosomal dominant Alzheimer's disease in an APOE3 Christchurch homozygote: a case report. *Nat. Med.* **25**, 1680–1683 (2019).

46. Avila, J., Lucas, J. J., Pérez, M. & Hernández, F. Role of Tau Protein in Both Physiological and Pathological Conditions. *Physiol. Rev.* **84**, 361–384 (2004).

47. Busche, M. A. & Hyman, B. T. Synergy between amyloid-β and tau in Alzheimer's disease. *Nat. Neurosci.* (2020). doi:10.1038/s41593-020-0687-6

48. Herrup, K. The case for rejecting the amyloid cascade hypothesis. *Nat. Neurosci.* **18**, 794–799 (2015).

49. Makin, S. The amyloid hypothesis on trial. *Nature* **559**, S4–S7 (2018).

50. Esparza, T. J. *et al.* Amyloid-beta oligomerization in Alzheimer dementia versus high-pathology controls. *Ann. Neurol.* **73**, 104–119 (2013).

51. Arriagada, P. V., Growdon, J. H., Hedley-Whyte, E. T. & Hyman, B. T. Neurofibrillary tangles but not senile plaques parallel duration and severity of Alzheimer's disease. *Neurology* **42**, 631–639 (1992).

52. Bryan, K. J., Lee, H., Perry, G., Smith, M. A. & Casadesus, G. *Transgenic Mouse Models of Alzheimer's Disease: Behavioral Testing and Considerations*. *Methods of Behavior Analysis in Neuroscience* (2009).

53. Selkoe, D. J. & Hardy, J. The amyloid hypothesis of Alzheimer's disease at 25 years. *EMBO Mol. Med.* **8**, 595–608 (2016).

54. Kuo, Y. M. *et al.* Water-soluble Aβ (N-40, N-42) oligomers in normal and Alzheimer disease brains. *J. Biol. Chem.* **271**, 4077–4081 (1996).

55. Roher, A. E. *et al.* Morphology and toxicity of Aβ-(1-42) dimer derived from neuritic and vascular amyloid deposits of Alzheimer's disease. *J. Biol. Chem.* **271**, 20631–20635 (1996).

56. Lambert, M. P. *et al.* Diffusible, nonfibrillar ligands derived from Aβ1-42 are potent central nervous system neurotoxins. *Proc. Natl. Acad. Sci. U. S. A.* **95**, 6448–6453 (1998).

57. Lue, L. F. *et al.* Soluble amyloid β peptide concentration as a predictor of synaptic change in Alzheimer's disease. *Am. J. Pathol.* **155**, 853–862 (1999).

58. McLean, C. A. *et al.* Soluble pool of Aβ amyloid as a determinant of severity of neurodegeneration in Alzheimer's disease. *Ann. Neurol.* **46**, 860–866 (1999).

59. Hardy, J. & Selkoe, D. J. The amyloid hypothesis of Alzheimer's disease: Progress and problems on the road to therapeutics. *Science (80-.).* **297**, 353–356 (2002).

60. Selkoe, D. J. Alzheimer's disease is a synaptic failure. *Science (80-.).* **298**, 789–791 (2002).

61. Ferreira, S. T. & Klein, W. L. The Aβ oligomer hypothesis for synapse failure

and memory loss in Alzheimer's disease. *Neurobiol. Learn. Mem.* **96**, 529–543 (2011).

62. Viola, K. L. & Klein, W. L. Amyloid β oligomers in Alzheimer's disease pathogenesis, treatment, and diagnosis. *Acta Neuropathol.* **129**, 183–206 (2015).

63. Cline, E. N., Bicca, M. A., Viola, K. L. & Klein, W. L. The Amyloid-β Oligomer Hypothesis: Beginning of the Third Decade. *J. Alzheimer's Dis.* **64**, S567–S610 (2018).

64. Lippa, C. F. *et al.* Familial and sporadic Alzheimer's disease: Neuropathology cannot exclude a final common pathway. *Neurology* **46**, 406–412 (1996).

65. Sherrington, R. *et al.* Cloning of a gene bearing missense mutations in early-onset familial Alzheimer's disease. *Nature* **375**, 754–760 (1995).

66. Rogaev, E. I. *et al.* Familial Alzheimer's disease in kindreds with missense mutations In a gene on chromosome 1 related to the Alzheimer's disease type 3 gene. *Nature* **376**, 775–778 (1995).

67. Levy-lahad, E. *et al.* Candidate Gene for the Chromosome 1 Familial Alzheimer's Disease Locus. *Science (80-.).* **269**, 973–977 (1995).

68. Cruts, M. *et al.* Molecular genetic analysis of familial early-onset alzheimer's disease linked to chromosome 14q24.3. *Hum. Mol. Genet.* **4**, 2363–2371 (1995).

69. De Strooper, B. *et al.* Deficiency of presenilin-1 inhibits the normal cleavage of amyloid precursor protein. *Nature* **391**, 387–390 (1998).

70. Wolfe, M. S. *et al.* Two transmembrane aspartates in presenilin-1 required for presenilin endoproteolysis and gamma-secretase activity. *Nature* **398**, 513–517 (1999).

71. Steiner, H. *et al.* A Loss of Function Mutation of Presenilin-2 Interferes with Amyloid β -Peptide Production and Notch Signaling. *J. Biol. Chem.* **274**, 28669–28673 (1999).

72. Ahn, K., Shelton, C. C., Tian, Y., Zhang, X. & Gilchrist, M. L. Activation and intrinsic γ -secretase activity of presenilin 1. *Proc. Natl. Acad. Sci. U. S. A.* **107**, 21435–21440 (2010).

73. Ryman, D. C. *et al.* Symptom onset in autosomal dominant Alzheimer disease A systematic review and meta-analysis. *J. Neurol.* **83**, 253–260 (2014).

74. Goate, A. *et al.* Segregation of a missense mutation in the amyloid precursor protein gene with familial Alzheimer's disease. *Nature* **349**, 704–706 (1991).

75. Chartier-Harlin, M. C. *et al.* Early-onset Alzheimer's disease caused by mutations at codon 717 of the β-amyloid precursor protein gene. *Nature* **353**, 844–846 (1991).

76. Rovelet-Lecrux, A. *et al.* APP locus duplication causes autosomal dominant early-onset Alzheimer disease with cerebral amyloid angiopathy. *Nat. Genet.* **38**,

24–26 (2006).

77. Jonsson, T. *et al.* A mutation in APP protects against Alzheimer‘s disease and age-related cognitive decline. *Nature* **488**, 96 (2012).

78. Müller, U. C., Deller, T. & Korte, M. Not just amyloid: Physiological functions of the amyloid precursor protein family. *Nat. Rev. Neurosci.* **18**, 281–298 (2017).

79. Goldgaber, D., Lerman, M. I., McBride, O. W., Saffiotti, U. & Gajdusek, D. C. Characterization and chromosomal localization of a cDNA encoding brain amyloid of Alzheimer’s disease. *Science (80-.).* **235**, 877–880 (1987).

80. Kang, J. *et al.* The precursor of Alzheimer’s disease amyloid A4 protein resembles a cell-surface receptor. *Nature* **325**, 733–736 (1987).

81. Kitaguchi, N., Takahashi, Y., Tokushima, Y., Shiojiri, S. & Ito, H. Novel precursor of Alzheimer’s disease amyloid protein shows protease inhibitory activity. *Nature* **331**, 530–532 (1988).

82. Ponte, P. *et al.* A new A4 amyloid mRNA contains a domain homologous to serine proteinase inhibitors. *Nature* **331**, 525–527 (1988).

83. Tanzi, R. E. *et al.* Protease inhibitor domain encoded by an amyloid protein precursor mRNA associated with Alzheimer’s disease. *Nature* **331**, 528–530 (1988).

84. Oltersdorf, T. *et al.* The secreted form of the Alzheimer’s amyloid precursor protein with the Kunitz domain is protease nexin-II. *Nature* **341**, 144–147 (1989).

85. Van Nostrand, W. E. *et al.* Protease nexin-II, a potent anti-chymotrypsin, shows identity to amyloid β-protein precursor. *Nature* **341**, 546–549 (1989).

86. Weidemann, A. *et al.* Identification, biogenesis, and localization of precursors of Alzheimer’s disease A4 amyloid protein. *Cell* **57**, 115–126 (1989).

87. Haass, C. *et al.* Amyloid β-peptide is produced by cultured cells during normal metabolism. *Nature* **359**, 322–325 (1992).

88. Sisodia, S. S. β-Amyloid precursor protein cleavage by a membrane-bound protease. *Proc. Natl. Acad. Sci. U. S. A.* **89**, 6075–6079 (1992).

89. Allinson, T. M. J., Parkin, E. T., Turner, A. J. & Hooper, N. M. ADAMs Family Members As Amyloid Precursor Protein α-Secretases. *J. Neurosci. Res.* **74**, 342–352 (2003).

90. Kuhn, P. H. *et al.* ADAM10 is the physiologically relevant, constitutive α-secretase of the amyloid precursor protein in primary neurons. *EMBO J.* **29**, 3020–3032 (2010).

91. Prox, J. *et al.* Postnatal disruption of the disintegrin/metalloproteinase ADAM10 in brain causes epileptic seizures, learning deficits, altered spine morphology,

and defective synaptic functions. *J. Neurosci.* **33**, 12915–12928 (2013).

92. Saitoh, T. *et al.* Secreted form of amyloid β protein precursor is involved in the growth regulation of fibroblasts. *Cell* **58**, 615–622 (1989).

93. Araki, W. *et al.* Trophic effect of β-amyloid precursor protein on cerebral cortical neurons in culture. *Biochem. Biophys. Res. Commun.* **181**, 265–271 (1991).

94. Roch, J. M. *et al.* Increase of synaptic density and memory retention by a peptide representing the trophic domain of the amyloid β/A4 protein precursor. *Proc. Natl. Acad. Sci. U. S. A.* **91**, 7450–7454 (1994).

95. Mattson, M. P. Cellular actions of β-amyloid precursor protein and its soluble and fibrillogenic derivatives. *Physiol. Rev.* **77**, 1081–1132 (1997).

96. Meziane, H. *et al.* Memory-enhancing effects of secreted forms of the β-amyloid precursor protein in normal and amnestic mice. *Proc. Natl. Acad. Sci. U. S. A.* **95**, 12683–12688 (1998).

97. Almkvist, O. *et al.* Cerebrospinal fluid levels of α-secretase Cleaved soluble amyloid precursor protein mirror cognition in a Swedish family with Alzheimer disease and a gene mutation. *Arch. Neurol.* **54**, 641–644 (1997).

98. Anderson, J. J. *et al.* Reduced cerebrospinal fluid levels of α-secretase-cleaved amyloid precursor protein in aged rats: Correlation with spatial memory deficits. *Neuroscience* **93**, 1409–1420 (1999).

99. Cole, G. M., Huynh, T. V. & Saitoh, T. Evidence for lysosomal processing of amyloid β-protein precursor in cultured cells. *Neurochem. Res.* **14**, 933–939 (1989).

100. Golde, T. E., Estus, S., Younkin, L. H., Selkoe, D. J. & Younkin, S. G. Processing of the amyloid protein precursor to potentially amyloidogenic derivatives. *Science (80-.).* **255**, 728–730 (1992).

101. Haass, C., Koo, E. H., Mellon, A., Hung, A. Y. & Selkoe, D. J. Targeting of cell-surface β-amyloid precursor protein to lysosomes: Alternative processing into amyloid-bearing fragments. *Nature* **357**, 500–503 (1992).

102. Sannerud, R. *et al.* ADP ribosylation factor 6 (ARF6) controls amyloid precursor protein (APP) processing by mediating the endosomal sorting of BACE1. *Proc. Natl. Acad. Sci. U. S. A.* **108**, (2011).

103. Das, U. *et al.* Activity-induced convergence of app and bace-1 in acidic microdomains via an endocytosis-dependent pathway. *Neuron* **79**, 447–460 (2013).

104. Das, U. *et al.* Visualizing APP and BACE-1 approximation in neurons yields insight into the amyloidogenic pathway. *Nat. Neurosci.* **19**, 55–64 (2015).

105. Vassar, R. *et al.* β-Secretase cleavage of Alzheimer's amyloid precursor protein by the transmembrane aspartic protease BACE. *Science (80-.).* **286**, 735–741

(1999).

106. Sinha, S. *et al.* Purification and cloning of amyloid precursor protein b-secretase from human brain. *Nature* **402**, 537–540 (1999).

107. Yan, R. *et al.* Membrane-anchored aspartyl protease with Alzheimer's disease β-secretase activity. *Nature* **402**, 533–537 (1999).

108. Hussain, I. *et al.* Identification of a Novel Aspartic Protease (Asp 2) as β-Secretase. *Mol. Cell. Neurosci.* **14**, 419–427 (1999).

109. Hussain, I. *et al.* Asp1 (BACE2) cleaves the amyloid precursor protein at the β-secretase site. *Mol. Cell. Neurosci.* **16**, 609–619 (2000).

110. Farzan, M., Schnitzler, C. E., Vasilieva, N., Leung, D. & Choe, H. BACE2, a β-secretase homolog, cleaves at the β-site and within the Amyloid-β Region of the Amyloid-β Precursor Protein. *Proc. Natl. Acad. Sci. U. S. A.* **97**, 9712–9717 (2000).

111. Bennett, B. D. *et al.* Expression analysis of BACE2 in brain and peripheral tissues. *J. Biol. Chem.* **275**, 20647–20651 (2000).

112. Laird, F. M. *et al.* BACE1, a major determinant of selective vulnerability of the brain to amyloid-β amyloidogenesis, is essential for cognitive, emotional, and synaptic functions. *J. Neurosci.* **25**, 11693–11709 (2005).

113. Voytyuk, I. *et al.* BACE2 distribution in major brain cell types and identification of novel substrates. *Life Sci. Alliance* **1**, 1–14 (2018).

114. Alić, I. *et al.* Patient-specific Alzheimer-like pathology in trisomy 21 cerebral organoids reveals BACE2 as a gene dose-sensitive AD suppressor in human brain. *Mol. Psychiatry* (2020). doi:10.1038/s41380-020-0806-5

115. Mattson, M. P., Barger, S. W., Cheng, B., Lieberburg, I. & Smith-Swintosky, Virginia L Rydel, R. E. β-Amyloid precursor protein metabolites and loss of neuronal Ca2+ homeostasis in Alzheimer's disease. *Trends Neurosci.* **16**, 409–414 (1993).

116. Furukawa, K., Barger, S. W., Blalock, E. M. & Mattson, M. P. Activation of K+ channels and suppression of neuronal activity by secreted β-amyloid-precursor protein. *Nature* **379**, 74–78 (1996).

117. Furukawa, K. *et al.* Increased Activity-Regulating and Neuroprotective Efficacy of α-Secretase-Derived Secreted Amyloid Precursor Protein Conferred by a C-Terminal Heparin-Binding Domain. *J. Neurochem.* **67**, 1882–1896 (1996).

118. Nikolaev, A., McLaughlin, T., O'Leary, D. D. M. & Tessier-Lavigne, M. APP binds DR6 to trigger axon pruning and neuron death via distinct caspases. *Nature* **457**, 981–989 (2009).

119. Rice, H. C. *et al.* Secreted amyloid-b precursor protein functions as a GABA B R1a ligand to modulate synaptic transmission. *Science (80-.).* **363**, (2019).

120. Nhan, H. S., Chiang, K. & Koo, E. H. The multifaceted nature of amyloid precursor protein and its proteolytic fragments: friends and foes. *Acta Neuropathol.* **129**, 1–19 (2015).

121. Andrew, R. J., Kellett, K. A. B., Thinakaran, G. & Hooper, N. M. A Greek tragedy: The growing complexity of Alzheimer amyloid precursor protein proteolysis. *J. Biol. Chem.* **291**, 19235–19244 (2016).

122. Willem, M. *et al.* η-Secretase processing of APP inhibits neuronal activity in the hippocampus. *Nature* **526**, 443–447 (2015).

123. Kimberly, W. T., Zheng, J. B., Guénette, S. Y. & Selkoe, D. J. The Intracellular Domain of the β-Amyloid Precursor Protein Is Stabilized by Fe65 and Translocates to the Nucleus in a Notch-like Manner. *J. Biol. Chem.* **276**, 40288–40292 (2001).

124. Cao, X. & Sudhof, T. C. A transcriptively active complex of APP with Fe65 and histone acetyltransferase Tip60. *Science (80-.).* **293**, 115–120 (2001).

125. Müller, T., Meyer, H. E., Egensperger, R. & Marcus, K. The amyloid precursor protein intracellular domain (AICD) as modulator of gene expression, apoptosis, and cytoskeletal dynamics-Relevance for Alzheimer's disease. *Prog. Neurobiol.* **85**, 393–406 (2008).

126. Gowing, E. *et al.* Chemical characterization of Aβ 17-42 peptide, a component of diffuse amyloid deposits of Alzheimer disease. *J. Biol. Chem.* **269**, 10987–10990 (1994).

127. Wei, W., Norton, D. D., Wang, X. & Kusiak, J. W. Aβ17-42 in Alzheimer's disease activates JNK and caspase-8 leading to neuronal apoptosis. *Brain* **125**, 2036–2043 (2002).

128. Brown, M. S., Ye, J., Rawson, R. B. & Goldstein, J. L. Regulated intramembrane proteolysis: a control mechanism conserved from bacteria to humans. *Cell* **100**, 391–398 (2000).

129. Wolfe, M. S. Intramembrane-cleaving proteases. *J. Biol. Chem.* **284**, 13969–13973 (2009).

130. Wolfe, M. S., De Los Angeles, J., Miller, D. D., Xia, W. & Selkoe, D. J. Are presenilins intramembrane-cleaving proteases? Implications for the molecular mechanism of Alzheimer's disease. *Biochemistry* **38**, 11223–11230 (1999).

131. Urban, S., Lee, J. R. & Freeman, M. Drosophila Rhomboid-1 defines a family of putative intramembrane serine proteases. *Cell* **107**, 173–182 (2001).

132. Manolaridis, I. *et al.* Mechanism of farnesylated CAAX protein processing by the intramembrane protease Rce1. *Nature* **504**, 301–305 (2013).

133. Weihofen, A., Binns, K., Lemberg, M. K., Ashman, K. & Martoglio, B. Identification of signal peptide peptidase, a presenilin-type aspartic protease. *Science (80-.).* **296**, 2215–2218 (2002).

134. Ponting, C. P. *et al.* Identification of a novel family of presenilin homologues. *Hum. Mol. Genet.* **11**, 1037–1044 (2002).

135. Fluhrer, R., Steiner, H. & Haass, C. Intramembrane Proteolysis by signal peptide peptidases: A comparative discussion of GXGD-type aspartyl proteases. *J. Biol. Chem.* **284**, 13975–13979 (2009).

136. Nyborg, A. C. *et al.* Signal Peptide Peptidase Forms a Homodimer That Is Labeled by an Active Site-directed γ-Secretase Inhibitor. *J. Biol. Chem.* **279**, 15153–15160 (2004).

137. Fluhrer, R. *et al.* A γ-secretase-like intramembrane cleavage of TNFα by the GxGD aspartyl protease SPPL2b. *Nat. Cell Biol.* **8**, 894–896 (2006).

138. De Strooper, B. Aph-1, Pen-2, and Nicastrin with Presenilin generate an active γ-Secretase complex. *Neuron* **38**, 9–12 (2003).

139. Takasugi, N. *et al.* The role of presenilin cofactors in the γ-secretase complex. *Nature* **422**, 2114–2117 (2003).

140. Edbauer, D. *et al.* Reconstitution of γ -secretase activity. *Nat. Cell Biol.* **5**, 486–489 (2003).

141. Kimberly, W. T. *et al.* γ-Secretase is a membrane protein complex comprised of presenilin, nicastrin, aph-1, and pen-2. *Proc. Natl. Acad. Sci. U. S. A.* **100**, 6382–6387 (2003).

142. Hebert, S. S. *et al.* Coordinated and widespread expression of gamma-secretase in vivo: evidence for size and molecular heterogeneity. *Neurobiol Dis* **17**, 260–272 (2004).

143. Kumar, A. & Thakur, M. K. Presenilin 1 and 2 are expressed differentially in the cerebral cortex of mice during development. *Neurochem. Int.* **61**, 778–782 (2012).

144. Serneels, L. *et al.* γ-Secretase Heterogeneity in the Aph1 Subunit: Relevance for Alzheimer's Disease. *Science (80-.).* **324**, 639–643 (2009).

145. Frånberg, J., Svensson, A. I., Winblad, B., Karlström, H. & Frykman, S. Minor contribution of presenilin 2 for γ-secretase activity in mouse embryonic fibroblasts and adult mouse brain. *Biochem. Biophys. Res. Commun.* **404**, 564–568 (2011).

146. Acx, H. *et al.* Signature amyloid β profiles are produced by different γ-secretase complexes. *J. Biol. Chem.* **289**, 4346–4355 (2014).

147. Sannerud, R. *et al.* Restricted Location of PSEN2 /γ-Secretase Determines Substrate Specificity and Generates an Intracellular Aβ Pool. *Cell* **166**, 193–208 (2016).

148. LaVoie, M. J. *et al.* Assembly of the γ-secretase complex involves early formation of an intermediate subcomplex of Aph-1 and nicastrin. *J. Biol. Chem.* **278**, 37213–37222 (2003).

149. Gu, Y. *et al.* APH-1 interacts with mature and immature forms of presenilins and nicastrin and may play a role in maturation of presenilin·nicastrin complexes. *J. Biol. Chem.* **278**, 7374–7380 (2003).

150. Hu, Y. & Fortini, M. E. Different cofactor activities in γ-secretase assembly: Evidence for a nicastrin - Aph-1 subcomplex. *J. Cell Biol.* **161**, 685–690 (2003).

151. Fraering, P. C. *et al.* Detergent-Dependent Dissociation of Active γ-Secretase Reveals an Interaction between Pen-2 and PS1-NTF and Offers a Model for Subunit Organization within the Complex. *Biochemistry* **43**, 323–333 (2004).

152. Thinakaran, G. *et al.* Evidence that levels of presenilins (PS1 and PS2) are coordinately regulated by competition for limiting cellular factors. *J. Biol. Chem.* **272**, 28415–28422 (1997).

153. Kaether, C., Haass, C. & Steiner, H. Assembly, trafficking and function of γ-secretase. *Neurodegener. Dis.* **3**, 275–283 (2006).

154. De Strooper, B. & Annaert, W. Novel Research Horizons for Presenilins and γ-Secretases in Cell Biology and Disease. *Annu. Rev. Cell Dev. Biol.* **26**, 235–260 (2010).

155. Gertsik, N., Chiu, D. & Li, Y. M. Complex regulation of γ-secretase: From obligatory to modulatory subunits. *Front. Aging Neurosci.* **7**, 342 (2015).

156. Steiner, H. *et al.* PEN-2 is an integral component of the γ-secretase complex required for coordinated expression of presenilin and nicastrin. *J. Biol. Chem.* **277**, 39062–39065 (2002).

157. Kim, S. H. & Sisodia, S. S. Evidence that the 'NF' motif in transmembrane domain 4 of presenilin 1 is critical for binding with PEN-2. *J. Biol. Chem.* **280**, 41953–41966 (2005).

158. Mao, G., Cui, M. Z., Li, T., Jin, Y. & Xu, X. Pen-2 is dispensable for endoproteolysis of presenilin 1, and nicastrin-Aph subcomplex is important for both ??-secretase assembly and substrate recruitment. *J. Neurochem.* **123**, 837–844 (2012).

159. Holmes, O., Paturi, S., Selkoe, D. J. & Wolfe, M. S. Pen-2 is essential for γ-secretase complex stability and trafficking but partially dispensable for endoproteolysis. *Biochemistry* **53**, 4393–4406 (2014).

160. Shah, S. *et al.* Nicastrin functions as a γ-secretase-substrate receptor. *Cell* **122**, 435–447 (2005).

161. Bolduc, D. M., Montagna, D. R., Gu, Y., Selkoe, D. J. & Wolfe, M. S. Nicastrin functions to sterically hinder γ-secretase–substrate interactions driven by substrate transmembrane domain. *Proc. Natl. Acad. Sci.* **113**, E509–E518 (2016).

162. Chávez-Gutiérrez, L. *et al.* Glu332 in the nicastrin ectodomain is essential for γ-secretase complex maturation but not for its activity. *J. Biol. Chem.* **283**, 20096–

20105 (2008).

163. Zhao, G., Liu, Z., Ilagan, M. X. G. & Kopan, R. γ-Secretase Composed of PS1/Pen2/Aph1a Can Cleave Notch and Amyloid Precursor Protein in the Absence of Nicastrin. *J. Neurosci.* **30**, 1648–1656 (2010).

164. Petit, D. *et al.* Extracellular interface between APP and Nicastrin regulates Aβ length and response to γ-secretase modulators. *EMBO J.* **38**, (2019).

165. Lazarov, V. K. *et al.* Electron microscopic structure of purified, active γ-secretase reveals an aqueous intramembrane chamber and two pores. *Proc. Natl. Acad. Sci.* **103**, 6889–6894 (2006).

166. Li, Y. *et al.* Structural interactions between inhibitor and substrate docking sites give insight into mechanisms of human PS1 complexes. *Structure* **22**, 125–135 (2014).

167. Elad, N. *et al.* The dynamic conformational landscape of γ-secretase. *J. Cell Sci.* **128**, 589–598 (2015).

168. Lu, P. *et al.* Three-dimensional structure of human gamma-secretase. *Nature* **512**, 166–170 (2014).

169. Sun, L. *et al.* Structural basis of human γ-secretase assembly. *Proc. Natl. Acad. Sci.* **112**, 6003–6008 (2015).

170. Bai, X. C. *et al.* An atomic structure of human γ-secretase. *Nature* **525**, 212–217 (2015).

171. Bai, X. C., Rajendra, E., Yang, G., Shi, Y. & Scheres, S. H. W. Sampling the conformational space of the catalytic subunit of human γ-secretase. *Elife* **4**, 1–19 (2015).

172. Xie, T. *et al.* Crystal structure of the γ-secretase component nicastrin. *Proc. Natl. Acad. Sci. U. S. A.* **111**, 13349–13354 (2014).

173. Zhou, R. *et al.* Recognition of the amyloid precursor protein by human γ-secretase. *Science* **36**, eaaw0930 (2019).

174. Berezovska, O. *et al.* Familial Alzheimer's Disease Presenilin 1 Mutations Cause Alterations in the Conformation of Presenilin and Interactions with Amyloid Precursor Protein. *J. Neurosci.* **25**, 3009–3017 (2005).

175. Yang, G. *et al.* Structural basis of Notch recognition by human γ-secretase. *Nature* **565**, 192–197 (2018).

176. Fukumori, A. & Steiner, H. Substrate recruitment of γ-secretase and mechanism of clinical presenilin mutations revealed by photoaffinity mapping. *EMBO J.* **35**, 1628–43 (2016).

177. Hitzenberger, M. & Zacharias, M. Structural Modeling of γ-Secretase Aβn Complex Formation and Substrate Processing. *ACS Chem. Neurosci.* **10**, 1826–1840 (2019).

178. Haapasalo, A. & Kovacs, D. M. The many substrates of presenilin/γ-secretase. *Journal of Alzheimer's Disease* **25**, 3–28 (2011).

179. Funamoto, S. *et al.* Substrate ectodomain is critical for substrate preference and inhibition of γ-secretase. *Nat. Commun.* **4**, 1–12 (2013).

180. Hemming, M. L., Elias, J. E., Gygi, S. P. & Selkoe, D. J. Proteomic profiling of γ-secretase substrates and mapping of substrate requirements. *PLoS Biol.* **6**, 2314–2328 (2008).

181. Jurisch-Yaksi, N., Sannerud, R. & Annaert, W. A fast growing spectrum of biological functions of γ-secretase in development and disease. *Biochim. Biophys. Acta - Biomembr.* **1828**, 2815–2827 (2013).

182. McCarthy, A. J., Coleman-Vaughan, C. & McCarthy, J. V. Regulated intramembrane proteolysis: emergent role in cell signalling pathways. *Biochem. Soc. Trans.* **45**, 1185–1202 (2017).

183. Cruts, M., Theuns, J. & Van Broeckhoven, C. Locus-specific mutation databases for neurodegenerative brain diseases. *Hum. Mutat.* **33**, 1340–1344 (2012).

184. Wang, B. *et al.* Γ-Secretase Gene Mutations in Familial Acne Inversa. *Science (80-.).* **330**, 1065 (2010).

185. Pink, A. E. *et al.* PSENEN and NCSTN mutations in familial hidradenitis suppurativa (acne inversa). *J. Invest. Dermatol.* **131**, 1568–1570 (2011).

186. Li, D. *et al.* Mutations of presenilin genes in dilated cardiomyopathy and heart failure. *Am. J. Hum. Genet.* **79**, 1030–1039 (2006).

187. To, M. D. *et al.* Functional characterization of novel presenilin-2 variants identified in human breast cancers. *Oncogene* **25**, 3557–3564 (2006).

188. Duggan, S. P. & McCarthy, J. V. Beyond γ-secretase activity: The multifunctional nature of presenilins in cell signalling pathways. *Cell. Signal.* **28**, 1–11 (2016).

189. De Strooper, B. *et al.* A presenilin-1-dependent γ-secretase-like protease mediates release of notch intracellular domain. *Nature* **398**, 518–522 (1999).

190. Ray, W. J. *et al.* Cell surface presenilin-1 participates in the γ-secretase-like proteolysis of Notch. *J. Biol. Chem.* **274**, 36801–36807 (1999).

191. Qi-Takahara, Y. *et al.* Longer Forms of Amyloid-β Protein: Implications for the Mechanism of Intramembrane Cleavage by γ-Secretase. *J. Neurosci.* **25**, 436–445 (2005).

192. Yagishita, S., Morishima-Kawashima, M., Ishiura, S. & Ihara, Y. Aβ46 is processed to Aβ40 and Aβ43, but not to Aβ42, in the low density membrane domains. *J. Biol. Chem.* **283**, 733–738 (2008).

193. Takami, M. *et al.* gamma-Secretase: successive tripeptide and tetrapeptide release from the transmembrane domain of beta-carboxyl terminal fragment. *J.*

Neurosci. **29**, 13042–13052 (2009).

194. Bolduc, D. M., Montagna, D. R., Seghers, M. C., Wolfe, M. S. & Selkoe, D. J. The amyloid-beta forming tripeptide cleavage mechanism of γ-Secretase. *Elife* **5**, 1–21 (2016).

195. Matsumura, N. *et al.* γ-secretase associated with lipid rafts: Multiple interactive pathways in the stepwise processing of β-carboxylterminal fragment. *J. Biol. Chem.* **289**, 5109–5121 (2014).

196. Chávez-Gutiérrez, L. & Szaruga, M. Mechanisms of neurodegeneration — Insights from familial Alzheimer's disease. *Semin. Cell Dev. Biol.* 0–1 (2020). doi:10.1016/j.semcdb.2020.03.005

197. Jarrett, J. T., Berger, E. P. & Lansbury, P. T. The C-Terminus of the β Protein is Critical in Amyloidogenesis. *Ann. N. Y. Acad. Sci.* **695**, 144–148 (1993).

198. Jarrett, J. T., Berger, E. P. & Lansbury, P. T. The Carboxy Terminus of the β Amyloid Protein Is Critical for the Seeding of Amyloid Formation: Implications for the Pathogenesis of Alzheimer's Disease. *Biochemistry* **32**, 4693–4697 (1993).

199. Duff, K. *et al.* Increased amyloid-Aβ42(43) in brains of mice expressing mutant presenilin 1. *Nature* **383**, 710–713 (1996).

200. Borchelt, D. R. *et al.* Familial Alzheimer's Disease–Linked Presenilin 1 Variants Elevate Aβ 1–42/1–40 Ratio In Vitro and In Vivo. *Neuron* **17**, 1005–1013 (1996).

201. Scheuner, D. *et al.* Secreted amyloid β protein similar to that in the senile plaques of Alzheimer's disease is increased in vivo by the presenilin 1 and 2 and APP mutations linked to familial Alzheimer's disease. *Nat. Med.* **2**, 925–928 (1996).

202. Mann, D. M. A. *et al.* Amyloid beta Protein (Abeta) Deposition in Chromosome 14-linked Alzheimer ' s Disease : Predominance of Abeta42(43). *Am. Neurol. Assoc.* **40**, 149–156 (1996).

203. Citron, M. *et al.* Mutant presenilins of Alzheimer's disease increase production of 42-residue amyloid β-protein in both transfected cells and transgenic mice. *Nat. Med.* **3**, 67–72 (1997).

204. Xia, W. *et al.* Enhanced production and oligomerization of the 42-residue amyloid β- protein by chinese hamster ovary cells stably expressing mutant presenilins. *J. Biol. Chem.* **272**, 7977–7982 (1997).

205. Tomita, T. *et al.* The presenilin 2 mutation (N141I) linked to familial Alzheimer disease (Volga German families) increases the secretion of amyloid β protein ending at the 42nd (or 43rd) residue. *Proc. Natl. Acad. Sci. U. S. A.* **94**, 2025–2030 (1997).

206. Murayama, O. *et al.* Enhancement of amyloid β 42 secretion by 28 different

presenilin 1 mutations of familial Alzheimer's disease. *Neurosci. Lett.* (1999). doi:10.1016/S0304-3940(99)00187-1

207. Potter, R. *et al.* Increased in vivo amyloid-b42 production, exchange, and loss in presenilin mutation carriers. *Sci. Transl. Med.* **5**, 189ra77 (2013).

208. Bentahir, M. *et al.* Presenilin clinical mutations can affect γ-secretase activity by different mechanisms. *J. Neurochem.* **96**, 732–742 (2006).

209. Kumar-singh, S. *et al.* Mean Age-of-Onset of Familial Alzheimer Disease Caused by Presenilin Mutations Correlates With Both Increased Aβ42 and Decreased Aβ40. *Hum. Mutat.* **27**, 686–695 (2006).

210. Shen, J. & Kelleher, R. J. The presenilin hypothesis of Alzheimer's disease: Evidence for a loss-of-function pathogenic mechanism. *Proc. Natl. Acad. Sci. U. S. A.* **104**, 403–409 (2007).

211. Shimojo, M., Sahara, N., Murayama, M., Ichinose, H. & Takashima, A. Decreased Aβ secretion by cells expressing familial Alzheimer's disease-linked mutant presenilin 1. *Neurosci. Res.* **57**, 446–453 (2007).

212. Heilig, E. A., Xia, W., Shen, J. & Kelleher, R. J. A presenilin-1 mutation identified in familial Alzheimer disease with cotton wool plaques causes a nearly complete loss of γ-secretase activity. *J. Biol. Chem.* **285**, 22350–22359 (2010).

213. Szaruga, M. *et al.* Qualitative changes in human gamma-secretase underlie familial Alzheimer's disease. *J Exp Med* **212**, 2003–2013 (2015).

214. Veugelen, S., Saito, T., Saido, T. C., Chávez-Gutiérrez, L. & De Strooper, B. Familial Alzheimer's Disease Mutations in Presenilin Generate Amyloidogenic Aβ Peptide Seeds. *Neuron* **90**, 410–416 (2016).

215. Kretner, B. *et al.* Generation and deposition of Aβ43 by the virtually inactive presenilin-1 L435F mutant contradicts the presenilin loss-of-function hypothesis of Alzheimer's disease. *EMBO Mol. Med.* **8**, 458–465 (2016).

216. Chávez-Gutiérrez, L. *et al.* The mechanism of γ-Secretase dysfunction in familial Alzheimer disease. *EMBO J.* **31**, 2261–2274 (2012).

217. Fernandez, M. A., Klutkowski, J. A., Freret, T. & Wolfe, M. S. Alzheimer presenilin-1 mutations dramatically reduce trimming of long amyloid β-peptides (Aβ) by γ-secretase to increase 42-to-40-residue Aβ. *J. Biol. Chem.* **289**, 31043–31052 (2014).

218. Szaruga, M. *et al.* Alzheimer's-Causing Mutations Shift Aβ Length by Destabilizing γ-Secretase-Aβn Interactions. *Cell* **170**, 443-456.e14 (2017).

219. Mullan, M. *et al.* A pathogenic mutation for probable Alzheimer's disease in the APP gene at the N-terminus of β-amyloid. *Nat. Genet.* **1**, 345–347 (1992).

220. Benilova, I., Karran, E. & De Strooper, B. The toxic Aβ oligomer and Alzheimer's disease: An emperor in need of clothes. *Nat. Neurosci.* **15**, 349–357

(2012).

221. Hatami, A., Monjazeb, S., Milton, S. & Glabe, C. G. Familial Alzheimer's disease mutations within the amyloid precursor protein alter the aggregation and conformation of the amyloid-β peptide. *J. Biol. Chem.* **292**, 3172–3185 (2017).

222. Chiti, F. & Dobson, C. M. Protein misfolding, functional amyloid, and human disease. *Annu. Rev. Biochem.* **75**, 333–366 (2006).

223. Eisenberg, D. & Jucker, M. The amyloid state of proteins in human diseases. *Cell* **148**, 1188–1203 (2012).

224. Finder, V. H. & Glockshuber, R. Amyloid-β aggregation. *Neurodegener. Dis.* **4**, 13–27 (2007).

225. Miller, Y., Ma, B. & Nussinov, R. Polymorphism in alzheimer Aβ amyloid organization reflects conformational selection in a rugged energy landscape. *Chem. Rev.* **110**, 4820–4838 (2010).

226. Wu, H. & Fuxreiter, M. The Structure and Dynamics of Higher-Order Assemblies: Amyloids, Signalosomes, and Granules. *Cell* **165**, 1055–1066 (2016).

227. Matsumura, S. *et al.* Two distinct amyloid β-protein (Aβ) assembly pathways leading to oligomers and fibrils identified by combined fluorescence correlation spectroscopy, morphology, and toxicity analyses. *J. Biol. Chem.* **286**, 11555–11562 (2011).

228. Cohen, S. I. A. *et al.* Proliferation of amyloid-β42 aggregates occurs through a secondary nucleation mechanism. *Proc. Natl. Acad. Sci. U. S. A.* **110**, 9758–9763 (2013).

229. Törnquist, M. *et al.* Secondary nucleation in amyloid formation. *Chem. Commun.* **54**, 8667–8684 (2018).

230. Brody, D. L., Jiang, H., Wildburger, N. & Esparza, T. J. Non-canonical soluble amyloid-beta aggregates and plaque buffering: Controversies and future directions for target discovery in Alzheimer's disease. *Alzheimer's Res. Ther.* **9**, 1–13 (2017).

231. Lacor, P. N. *et al.* Synaptic targeting by Alzheimer's-related amyloid β oligomers. *J. Neurosci.* **24**, 10191–10200 (2004).

232. Corbett, G. T. *et al.* PrP is a central player in toxicity mediated by soluble aggregates of neurodegeneration-causing proteins. *Acta Neuropathol.* (2019). doi:10.1007/s00401-019-02114-9

233. Jarosz-Griffiths, H. H., Noble, E., Rushworth, J. V. & Hooper, N. M. Amyloid-β receptors: The good, the bad, and the prion protein. *J. Biol. Chem.* **291**, 3174–3183 (2016).

234. Brothers, H. M., Gosztyla, M. L. & Robinson, S. R. The physiological roles of amyloid-β peptide hint at new ways to treat Alzheimer's disease. *Front. Aging*

Neurosci. **10**, 1–16 (2018).

235. Soscia, S. J. *et al.* The Alzheimer's disease-associated amyloid β-protein is an antimicrobial peptide. *PLoS One* **5**, 1–10 (2010).

236. Somavarapu, A. K. & Kepp, K. P. Loss of stability and hydrophobicity of presenilin 1 mutations causing Alzheimer's disease. *J. Neurochem.* **137**, 101–111 (2016).

237. Gosztyla, M. L., Brothers, H. M. & Robinson, S. R. Alzheimer's Amyloid-β is an Antimicrobial Peptide: A Review of the Evidence. *J. Alzheimer's Dis.* **62**, 1495–1506 (2018).

238. Schenk, D. *et al.* Immunization with amyloid-β attenuates Alzheimer-disease-like pathology in the PDAPP mouse. *Nature* **400**, 173–177 (1999).

239. Holmes, C. *et al.* Long-term effects of Aβ42 immunisation in Alzheimer's disease: follow-up of a randomised, placebo-controlled phase I trial. *Lancet* **372**, 216–223 (2008).

240. Orgogozo, J. M. *et al.* Subacute meningoencephalitis in a subset of patients with AD after Aβ42 immunization. *Neurology* **61**, 46–54 (2003).

241. Vandenberghe, R. *et al.* Active Aβ immunotherapy CAD106 in Alzheimer's disease: A phase 2b study. *Alzheimer's Dement. Transl. Res. Clin. Interv.* **3**, 10–22 (2017).

242. Lacosta, A. M. *et al.* Safety, tolerability and immunogenicity of an active anti-Aβ 40 vaccine (ABvac40) in patients with Alzheimer's disease: A randomised, double-blind, placebo-controlled, phase i trial. *Alzheimer's Res. Ther.* **10**, 1–13 (2018).

243. Zhang, Y. & Lee, D. H. S. Sink hypothesis and therapeutic strategies for attenuating Aβ levels. *Neuroscientist* **17**, 163–173 (2011).

244. DeMattos, R. B. *et al.* Peripheral anti-Aβ antibody alters CNS and plasma Aβ clearance and decreases brain Aβ burden in a mouse model of Alzheimer's disease. *Proc. Natl. Acad. Sci. U. S. A.* **98**, 8850–8855 (2001).

245. Panza, F., Lozupone, M., Logroscino, G. & Imbimbo, B. P. A critical appraisal of amyloid-β-targeting therapies for Alzheimer disease. *Nat. Rev. Neurol.* **15**, 73–88 (2019).

246. Sevigny, J. *et al.* The antibody aducanumab reduces Aβ plaques in Alzheimer's disease. *Nature* **537**, 50–56 (2016).

247. Schneider, L. A resurrection of aducanumab for Alzheimer's disease. *Lancet Neurol.* **19**, 111–112 (2020).

248. Linse, S. *et al.* Kinetic fingerprints differentiate the mechanisms of action of anti-Aβ antibodies. *Nat. Struct. Mol. Biol.* 1–9 (2020). doi:10.1038/s41594-020-0505-6

249. Roberds, S. L. *et al.* BACE knockout mice are healthy despite lacking the primary β-secretase activity in brain: Implications for Alzheimer's disease therapeutics. *Hum. Mol. Genet.* **10**, 1317–1324 (2001).

250. Imbimbo, B. P. & Watling, M. Investigational BACE inhibitors for the treatment of Alzheimer's disease. *Expert Opin. Investig. Drugs* **28**, 967–975 (2019).

251. Vassar, R. *et al.* Function, therapeutic potential and cell biology of BACE proteases: Current status and future prospects. *J. Neurochem.* **130**, 4–28 (2014).

252. Yan, R. Physiological functions of the β-site amyloid precursor protein cleaving enzyme 1 and 2. *Front. Mol. Neurosci.* **10**, 1–12 (2017).

253. Doody, R. S. *et al.* A phase 3 trial of semagacestat for treatment of Alzheimer's disease. *N. Engl. J. Med.* **369**, 341–350 (2013).

254. De Strooper, B. Lessons from a failed γ-secretase Alzheimer trial. *Cell* **159**, 721–726 (2014).

255. Henley, D. B., Sundell, K. L., Sethuraman, G., Dowsett, S. A. & May, P. C. Safety profile of semagacestat, a γ-secretase inhibitor: IDENTITY trial findings. *Curr. Med. Res. Opin.* **30**, 2021–2032 (2014).

256. Tagami, S. *et al.* Semagacestat Is a Pseudo-Inhibitor of γ-Secretase. *Cell Rep.* **21**, 259–273 (2017).

257. Weggen, S. *et al.* A subset of NSAIDs lower amyloidogenic Aβ42 independently of cyclooxygenase activity. *Nature* **414**, 212–216 (2001).

258. Weggen, S. *et al.* Evidence that nonsteroidal anti-inflammatory drugs decrease amyloid-β 42 production by direct modulation of γ-secretase activity. *J. Biol. Chem.* **278**, 31831–31837 (2003).

259. Eriksen, J. L. *et al.* NSAIDs and enantiomers of flurbiprofen target γ-secretase and lower Aβ42 in vivo. *J. Clin. Invest.* **112**, 440–449 (2003).

260. Lessard, C. B. *et al.* γ-secretase modulators and APH1 isoforms modulate γ-secretase cleavage but not position of ε-cleavage of the amyloid precursor protein (APP). *PLoS One* **10**, 1–19 (2015).

261. Green, R. C., Schneider, L. S. & Amato, D. A. Effect of Tarenflurbil on Cognitive Decline. **302**, 2557–2564 (2009).

262. Imbimbo, B. P. Why did tarenflurbil fail in alzheimer's disease? *J. Alzheimer's Dis.* **17**, 757–760 (2009).

263. Golde, T. E., Koo, E. H., Felsenstein, K. M., Osborne, B. A. & Miele, L. γ-Secretase inhibitors and modulators. *Biochim. Biophys. Acta - Biomembr.* **1828**, 2898–2907 (2013).

264. Wagner, S. L. *et al.* Pharmacological and toxicological properties of the potent oral γ-secretase modulator BPN-15606. *J. Pharmacol. Exp. Ther.* **362**, 31–44 (2017).

265. Soares, H. D. *et al.* The γ-secretase modulator, BMS-932481, modulates Aβ peptides in the plasma and cerebrospinal fluid of healthy volunteerss. *J. Pharmacol. Exp. Ther.* **358**, 138–150 (2016).

266. Ahn, J. E. *et al.* Pharmacokinetic and Pharmacodynamic Effects of a γ-Secretase Modulator, PF-06648671, on CSF Amyloid-β Peptides in Randomized Phase I Studies. *Clin. Pharmacol. Ther.* **107**, 211–220 (2020).

267. Long, J. M. & Holtzman, D. M. Alzheimer Disease: An Update on Pathobiology and Treatment Strategies. *Cell* **179**, 312–339 (2019).

268. Karran, E., Mercken, M. & Strooper, B. De. The amyloid cascade hypothesis for Alzheimer's disease: An appraisal for the development of therapeutics. *Nat. Rev. Drug Discov.* **10**, 698–712 (2011).

269. Karran, E. & Hardy, J. A critique of the drug discovery and phase 3 clinical programs targeting the amyloid hypothesis for Alzheimer disease. *Ann. Neurol.* **76**, 185–205 (2014).

270. Bateman, R. J. *et al.* The DIAN-TU Next Generation Alzheimer's prevention trial: Adaptive design and disease progression model. *Alzheimer's Dement.* **13**, 8–19 (2017).

271. Reiman, E. M. *et al.* Alzheimers prevention initiative: A plan to accelerate the evaluation of presymptomatic treatments. *J. Alzheimer's Dis.* **26**, 321–329 (2011).

272. Sperling, R. A. *et al.* The A4 study: Stopping AD before symptoms begin? *Sci. Transl. Med.* **6**, 4–7 (2014).

273. Xia, W. γ-Secretase and its modulators: Twenty years and beyond. *Neurosci. Lett.* **701**, 162–169 (2019).

274. Li, Y. M. *et al.* Presenilin 1 is linked with -secretase activity in the detergent solubilized state. *Proc Natl Acad Sci U S A* **97**, 6138–6143 (2000).

275. Yu, G. *et al.* Nicastrin modulates presenilin-mediated notch/glp-1 signal transduction and βAPP processing. *Nature* **407**, 48–54 (2000).

276. Francis, R. *et al.* aph-1 and pen-2 are required for Notch pathway signaling, γ-secretase cleavage of βAPP, and presenilin protein accumulation. *Dev. Cell* **3**, 85–97 (2002).

277. Goutte, C., Tsunozaki, M., Hale, V. A. & Priess, J. R. APH-1 is a multipass membrane protein essential for the Notch signaling pathway in Caenorhabditis elegans embryos. *Proc Natl Acad Sci U S A* **99**, 775–779 (2002).

278. Sato, T. *et al.* Active γ-secretase complexes contain only one of each component. *J. Biol. Chem.* **282**, 33985–33993 (2007).

279. Wolfe, M. S. *et al.* Two transmembrane aspartates in presenilin-1 required for presenelin endoproteolysis and gamma-secretase activity. *Nature* **398**, 513–517 (1999).

280. Thinakaran, G. *et al.* Endoproteolysis of presenilin 1 and accumulation of processed derivatives in vivo. *Neuron* **17**, 181–190 (1996).

281. Takasugi, N. *et al.* The role of presenilin cofactors in the gamma-secretase complex. *Nature* **422**, 438–441 (2003).

282. Luo, W. jie *et al.* PEN-2 and APH-1 coordinately regulate proteolytic processing of presenilin 1. *J. Biol. Chem.* **278**, 7850–7854 (2003).

283. Zhang, Y. W. *et al.* Nicastrin is critical for stability and trafficking but not association of other presenilin/gamma-secretase components. *J Biol Chem* **280**, 17020–17026 (2005).

284. Kim, S., Ikeuchi, T., Yu, C. & Sisodia, S. S. Regulated Hyperaccumulation of Presenilin-1 and the " γ-Secretase " Complex. *J. Biol. Chem.* **278**, 33992–34002 (2003).

285. Selkoe, D. J. & Wolfe, M. S. Presenilin: Running with Scissors in the Membrane. *Cell* **131**, 215–221 (2007).

286. Beel, A. J. & Sanders, C. R. Substrate specificity of γ-secretase and other intramembrane proteases. *Cell. Mol. Life Sci.* **65**, 1311–1334 (2008).

287. Lleó, A. Activity of gamma-secretase on substrates other than APP. *Curr. Top. Med. Chem.* **8**, 9–16 (2008).

288. Struhl, G. & Adachi, A. Requirements for Presenilin-dependent cleavage of notch and other transmembrane proteins. *Mol. Cell* **6**, 625–636 (2000).

289. Kopan, R. & Ilagan, M. X. Gamma-secretase: proteasome of the membrane? *Nat Rev Mol Cell Biol* **5**, 499–504 (2004).

290. Yagishita, S., Morishima-Kawashima, M., Ishiura, S. & Ihara, Y. Aβ46 is processed to Aβ40 and Aβ43, but not to Aβ42, in the low density membrane domains. *J. Biol. Chem.* **283**, 733–738 (2008).

291. Sherrington, R. *et al.* Cloning of a gene bearing missense mutations in early-onset familial Alzheimer's disease. *Nature* **375**, 754–760 (1995).

292. Moore, S. *et al.* APP Metabolism Regulates Tau Proteostasis in Human Cerebral Cortex Neurons. *Cell Rep.* **11**, 689–696 (2015).

293. Karran, E. & De Strooper, B. The amyloid cascade hypothesis: are we poised for success or failure? *J. Neurochem.* **139**, 237–252 (2016).

294. Crump, C. J. *et al.* Piperidine acetic acid based γ-secretase modulators directly bind to presenilin-1. *ACS Chem. Neurosci.* **2**, 705–710 (2011).

295. Velter, A. I. *et al.* Anilinotriazoles as potent gamma secretase modulators. *Bioorganic Med. Chem. Lett.* **24**, 5805–5813 (2014).

296. Li, T., Ma, G., Cai, H., Price, D. L. & Wong, P. C. Nicastrin Is Required for Assembly of Presenilin/γ-Secretase Complexes to Mediate Notch Signaling and for Processing and Trafficking of β-Amyloid Precursor Protein in Mammals. *J.*

Neurosci. **23**, 3272–3277 (2003).

297. Nyabi, O. *et al.* No endogenous Aβ production in presenilin-deficient fibroblasts. *Nat. Cell Biol.* **4**, E164 (2002).

298. Hitzenberger, M. & Zacharias, M. Structural Modeling of γ - Secretase A β n Complex Formation and Substrate Processing. *ACS Chem. Neurosci.* **49**, (2019).

299. Barrett, P. J. *et al.* The amyloid precursor protein has a flexible transmembrane domain and binds cholesterol. *Science (80-.).* **336**, 1168–1171 (2012).

300. Singh, R., Barman, A. & Prabhakar, R. Computational insights into aspartyl protease activity of presenilin 1 (ps1) generating alzheimer amyloid β-peptides (aβ40 and aβ42). *J. Phys. Chem. B* **113**, 2990–2999 (2009).

301. Dickson, C. J. *et al.* Lipid14: The amber lipid force field. *J. Chem. Theory Comput.* **10**, 865–879 (2014).

302. Mark, P. & Nilsson, L. Structure and dynamics of the TIP3P, SPC, and SPC/E water models at 298 K. *J. Phys. Chem. A* **105**, 9954–9960 (2001).

303. Maier, J. A. *et al.* ff14SB: Improving the Accuracy of Protein Side Chain and Backbone Parameters from ff99SB. *J. Chem. Theory Comput.* **11**, 3696–3713 (2015).

304. Goga, N., Rzepiela, A. J., De Vries, A. H., Marrink, S. J. & Berendsen, H. J. C. Efficient algorithms for langevin and DPD dynamics. *J. Chem. Theory Comput.* **8**, 3637–3649 (2012).

305. Åqvist, J., Wennerström, P., Nervall, M., Bjelic, S. & Brandsdal, B. O. Molecular dynamics simulations of water and biomolecules with a Monte Carlo constant pressure algorithm. *Chem. Phys. Lett.* **384**, 288–294 (2004).

306. Darden, T., York, D. & Pedersen, L. Particle mesh Ewald: An N·log(N) method for Ewald sums in large systems. *J. Chem. Phys.* (1993). doi:10.1063/1.464397

307. Ryckaert, J. P., Ciccotti, G. & Berendsen, H. J. C. Numerical integration of the cartesian equations of motion of a system with constraints: molecular dynamics of n-alkanes. *J. Comput. Phys.* **23**, 327–341 (1977).

308. Hopkins, C. W., Le Grand, S., Walker, R. C. & Roitberg, A. E. Long-time-step molecular dynamics through hydrogen mass repartitioning. *J. Chem. Theory Comput.* **11**, 1864–1874 (2015).

309. Nickolls, J., Buck, I. A. N. & Garland, M. Scalable Parallel. in *IEEE Hot Chips 20 Symposium (HCS)* 40–53 (2008). doi:10.1145/1401132.1401152

310. Götz, A. W. *et al.* Routine microsecond molecular dynamics simulations with AMBER on GPUs. 1. generalized born. *J. Chem. Theory Comput.* **8**, 1542–1555 (2012).

311. Salomon-Ferrer, R., Götz, A. W., Poole, D., Le Grand, S. & Walker, R. C. Routine microsecond molecular dynamics simulations with AMBER on GPUs.

2. Explicit solvent particle mesh ewald. *J. Chem. Theory Comput.* **9**, 3878–3888 (2013).

312. Le Grand, S., Götz, A. W. & Walker, R. C. SPFP: Speed without compromise - A mixed precision model for GPU accelerated molecular dynamics simulations. *Comput. Phys. Commun.* **184**, 374–380 (2013).

313. Case, D. A. *et al.* AMBER 2016. *University of California, San Francisco* (2016). doi:10.1021/ct200909j

314. Roe, D. R. & Cheatham, T. E. PTRAJ and CPPTRAJ: Software for processing and analysis of molecular dynamics trajectory data. *J. Chem. Theory Comput.* **9**, 3084–3095 (2013).

315. Humphrey, W., Dalke, A. & and Schulten, K. VMD: Visual Molecular Dynamics. *J. Mol. Graph.* **7855**, 33–38 (1996).

316. Genheden, S. & Ryde, U. The MM/PBSA and MM/GBSA methods to estimate ligand-binding affinities. *Expert Opin. Drug Discov.* **10**, 449–461 (2015).

317. Miller, B. R. *et al.* MMPBSA.py: An efficient program for end-state free energy calculations. *J. Chem. Theory Comput.* **8**, 3314–3321 (2012).

318. Takagi-Niidome, S. *et al.* Cooperative Roles of Hydrophilic Loop 1 and the C-Terminus of Presenilin 1 in the Substrate-Gating Mechanism of γ-Secretase. *J. Neurosci.* **35**, 2646–2656 (2015).

319. Ren, Z., Schenk, D., Basi, G. S. & Shapiro, I. P. Amyloid β-protein precursor juxtamembrane domain regulates specificity of γ-secretase-dependent cleavages. *J. Biol. Chem.* **282**, 35350–35360 (2007).

320. Kukar, T. L. *et al.* Lysine 624 of the amyloid precursor protein (APP) is a critical determinant of amyloid β peptide length: Support for a sequential model of γ-secretase intramembrane proteolysis and regulation by the amyloid β precursor protein (APP) juxtamembrane region. *J. Biol. Chem.* **286**, 39804–39812 (2011).

321. Ousson, S. *et al.* Substrate determinants in the C99 juxtamembrane domains differentially affect ??-secretase cleavage specificity and modulator pharmacology. *J. Neurochem.* **125**, 610–619 (2013).

322. Jung, J. I. *et al.* Complex relationships between substrate sequence and sensitivity to alterations in γ-secretase processivity induced by γ-secretase modulators. *Biochemistry* **53**, 1947–1957 (2014).

323. Shearman, M. S. *et al.* L-685,458, an aspartyl protease transition state mimic, is a potent inhibitor of amyloid β-protein precursor γ-secretase activity. *Biochemistry* **39**, 8698–8704 (2000).

324. Page, R. M. *et al.* β-Amyloid precursor protein mutants respond to γ-secretase modulators. *J. Biol. Chem.* **285**, 17798–17810 (2010).

325. Carroll, C. M. & Li, Y. M. Physiological and pathological roles of the γ-

secretase complex. *Brain Res. Bull.* **126**, 199–206 (2016).

326. Rehder, D. S. & Borges, C. R. Cysteine sulfenic acid as an intermediate in disulfide bond formation and nonenzymatic protein folding. *Biochemistry* **49**, 7748–7755 (2010).

327. Takeo, K. *et al.* Allosteric regulation of γ-secretase activity by a phenylimidazole-type γ-secretase modulator. *Proc. Natl. Acad. Sci.* **111**, 10544–10549 (2014).

328. Koriath, C. *et al.* Predictors for a dementia gene mutation based on gene-panel next-generation sequencing of a large dementia referral series. *Mol. Psychiatry* 1–14 (2018). doi:10.1038/s41380-018-0224-0

329. Cacace, R., Sleegers, K. & Van Broeckhoven, C. Molecular genetics of early-onset Alzheimer's disease revisited. *Alzheimer's Dement.* **12**, 733–748 (2016).

330. Kukar, T. L. *et al.* Substrate-targeting γ-secretase modulators. *Nature* **453**, 925–929 (2008).

331. Imbimbo, B. Pietro, Ippati, S. & Watling, M. Should drug discovery scientists still embrace the amyloid hypothesis for Alzheimer's disease or should they be looking elsewhere? *Expert Opin. Drug Discov.* **0**, 1–11 (2020).

332. Bateman, R. J. *et al.* Autosomal-dominant Alzheimer's disease: A review and proposal for the prevention of Alzheimer's disease. *Alzheimer's Res. Ther.* **2**, 1–13 (2011).

333. Tariot, P. N. *et al.* The Alzheimer's Prevention Initiative Autosomal-Dominant Alzheimer's Disease Trial: A study of crenezumab versus placebo in preclinical PSEN1 E280A mutation carriers to evaluate efficacy and safety in the treatment of autosomal-dominant Alzheimer's diseas. *Alzheimer's Dement. Transl. Res. Clin. Interv.* **4**, 150–160 (2018).

334. Strydom, A. *et al.* Alzheimer's disease in Down syndrome: An overlooked population for prevention trials. *Alzheimer's Dement. Transl. Res. Clin. Interv.* **4**, 703–713 (2018).

335. Yu, G. *et al.* Nicastrin modulates presenilin-mediated notch/glp-1 signal transduction and betaAPP processing. *Nature* **407**, 48–54 (2000).

336. Hsu, S. *et al.* Systematic validation of variants of unknown significance in APP, PSEN1 and PSEN2. *Neurobiol. Dis.* **139**, 104817 (2020).

337. Iwatsubo, T., Saido, T. C., Mann, D. M. A., Lee, V. M. Y. & Trojanowski, J. Q. Full-length amyloid-β(1-42(43)) and amino-terminally modified and truncated amyloid-β42(43) deposit in diffuse plaques. *Am. J. Pathol.* **149**, 1823–1830 (1996).

338. Thal, D. R., Walter, J., Saido, T. C. & Fändrich, M. Neuropathology and biochemistry of Aβ and its aggregates in Alzheimer's disease. *Acta Neuropathol.* **129**, 167–182 (2015).

339. Sun, L., Zhou, R., Yang, G. & Shi, Y. Analysis of 138 pathogenic mutations in presenilin-1 on the in vitro production of Aβ42 and Aβ40 peptides by γ-secretase. *Proc. Natl. Acad. Sci. U. S. A.* **114**, E476–E485 (2017).

340. Herreman, A. *et al.* Total inactivation of γ-secretase activity in presenilin-deficient embryonic stem cells. *Nat. Cell Biol.* **2**, 461–462 (2000).

341. Dimitrov, M. *et al.* Alzheimers disease mutations in APP but not γ-secretase modulators affect epsilon-cleavage-dependent AICD production. *Nat. Commun.* **4**, 1–10 (2013).

342. Shen, L. *et al.* Two novel presenilin-1 mutations (I249L and P433S) in early onset Chinese Alzheimer's pedigrees and their functional characterization. *Biochem. Biophys. Res. Commun.* **516**, 264–269 (2019).

343. Dumanchin, C. *et al.* Biological effects of four PSEN1 gene mutations causing Alzheimer disease with spastic paraparesis and cotton wool plaques. *Hum. Mutat.* **27**, 1063 (2006).

344. Wang, J. C. *et al.* Genetic screening in two Iranian families with early-onset Alzheimer's disease identified a novel PSEN1 mutation. *Neurobiol. Aging* **62**, 244.e15-244.e17 (2018).

345. Matsubara-tsutsui, M. *et al.* Molecular Evidence of Presenilin 1 Mutation in Familial Early Onset Dementia. **298**, (2002).

346. Dermaut, B. *et al.* Cerebral amyloid angiopathy is a pathogenic lesion in Alzheimer's disease due to a novel presenilin 1 mutation. *Brain* **124**, 2383–2392 (2001).

347. Hamaguchi, T., Morinaga, A., Tsukie, T., Kuwano, R. & Yamada, M. A novel presenilin 1 mutation (L282F) in familial Alzheimer's disease. *J. Neurol.* **256**, 1575–1577 (2009).

348. Aldudo, J., Bullido, M. J., Arbizu, T., Oliva, R. & Valdivieso, F. Identification of a novel mutation (Leu282Arg) of the human presenilin 1 gene in Alzheimer ' s disease. *Neurosci. Lett.* **240**, 174–176 (1998).

349. Mehta, N. D. *et al.* Increased Aβ42(43) from cell lines expressing presenilin 1 mutations. *Ann. Neurol.* **43**, 256–258 (1998).

350. De Jonghe, C. *et al.* Pathogenic APP mutations near the γ-secretase cleavage site differentially affect Aβ secretion and APP C-terminal fragment stability. *Hum. Mol. Genet.* **10**, 1665–1671 (2001).

351. Duering, M., Grimm, M. O. W., Grimm, H. S., Schr, J. & Hartmann, T. Mean age of onset in familial Alzheimer's disease is determined by amyloid beta 42. *Neurobiol. Aging* **26**, 785–788 (2005).

352. Walker, E. S., Martinez, M., Brunkan, A. L. & Goate, A. Presenilin 2 familial Alzheimer ' s disease mutations result in partial loss of function and dramatic changes in Aβ42/40 ratios. *J. Neurochem.* **92**, 294–301 (2005).

353. Ryan, N. S. *et al.* Clinical phenotype and genetic associations in autosomal dominant familial Alzheimer ' s disease : a case series. **15**, (2016).

354. Tang, N. & Kepp, K. P. Aβ42/Aβ40 Ratios of Presenilin 1 Mutations Correlate with Clinical Onset of Alzheimer's Disease. *J. Alzheimer's Dis.* **66**, 939–945 (2018).

355. Vélez, J. I. *et al.* APOE*E2 allele delays age of onset in PSEN1 E280A Alzheimer's disease. *Mol. Psychiatry* **21**, 916–924 (2016).

356. Saito, T. *et al.* Potent amyloidogenicity and pathogenicity of Aβ 243. *Nat. Neurosci.* **14**, 1023–1032 (2011).

357. Trambauer, J. *et al.* Aβ43-producing PS 1 FAD mutants cause altered substrate interactions and respond to γ-secretase modulation. *EMBO Rep.* **21**, 1–13 (2020).

358. Szaruga, M. *et al.* Qualitative changes in human γ-secretase underlie familial Alzheimer's disease. *J. Exp. Med.* **212**, 2003–2013 (2015).

359. Veugelen, S., Saito, T., Saido, T. C., Chávez-Gutiérrez, L. & De Strooper, B. Familial Alzheimer's Disease Mutations in Presenilin Generate Amyloidogenic Aβ Peptide Seeds. *Neuron* **90**, 410–416 (2016).

360. Szaruga, M. *et al.* Alzheimer's-Causing Mutations Shift Aβ Length by Destabilizing γ-Secretase-Aβn Interactions. *Cell* **170**, 443–456 (2017).

361. Oehlrich, D., Berthelot, D. J. C. & Gijsen, H. J. M. γ-Secretase modulators as potential disease modifying anti-Alzheimer's drugs. *J. Med. Chem.* **54**, 669–698 (2011).

362. Page, R. M. *et al.* Generation of Aβ38 and Aβ42 is independently and differentially affected by familial Alzheimer disease-associated presenilin mutations and γ-secretase modulation. *J. Biol. Chem.* **283**, 677–683 (2008).

363. Kounnas, M. Z. *et al.* Modulation of γ-Secretase Reduces β-Amyloid Deposition in a Transgenic Mouse Model of Alzheimer's Disease. *Neuron* **67**, 769–780 (2010).

364. Nie, P., Vartak, A. & Li, Y. γ-Secretase inhibitors and modulators: Mechanistic insights into the function and regulation of γ -Secretase. *Semin. Cell Dev. Biol.* (2020). doi:10.1016/j.semcdb.2020.03.002

365. Richter, L. *et al.* Amyloid beta 42 peptide (Aβ42)-lowering compounds directly bind to Aβ and interfere with amyloid precursor protein (APP) transmembrane dimerization. *Proc. Natl. Acad. Sci.* **107**, 14597–14602 (2010).

366. Botev, A. *et al.* The amyloid precursor protein C-terminal fragment C100 occurs in monomeric and dimeric stable conformations and binds γ-secretase modulators. *Biochemistry* **50**, 828–835 (2011).

367. Ohki, Y. *et al.* Phenylpiperidine-type γ-secretase modulators target the transmembrane domain 1 of presenilin 1. *EMBO J.* **30**, 4815–4824 (2011).

368. Ebke, A. *et al.* Novel γ-secretase enzyme modulators directly target presenilin protein. *J. Biol. Chem.* **286**, 37181–37186 (2011).

369. Jumpertz, T. *et al.* Presenilin is the molecular target of acidic γ-secretase modulators in living cells. *PLoS One* **7**, 1–9 (2012).

370. Pozdnyakov, N. *et al.* γ-secretase modulator (GSM) photoaffinity probes reveal distinct allosteric binding sites on presenilin. *J. Biol. Chem.* **288**, 9710–9720 (2013).

371. Spasic, D. *et al.* Presenilin-1 maintains a nine-transmembrane topology throughout the secretory pathway. *J. Biol. Chem.* **281**, 26569–26577 (2006).

372. Case, D. *et al.* AMBER 2018. *University of California, San Francisco* (2018).

373. Salomon-Ferrer, R., Götz, A. W., Poole, D., Le Grand, S. & Walker, R. C. Routine microsecond molecular dynamics simulations with AMBER on GPUs. 2. Explicit solvent particle mesh ewald. *J. Chem. Theory Comput.* **9**, 3878–3888 (2013).

374. Jorgensen, W. L., Chandrasekhar, J., Madura, J. D., Impey, R. W. & Klein, M. L. Comparison of simple potential functions for simulating liquid water. *J. Chem. Phys.* **79**, 926–935 (1983).

375. Wang, J., Wang, W., Kollman, P. A. & Case, D. A. Automatic atom type and bond type perception in molecular mechanical calculations. *J. Mol. Graph. Model.* **25**, 247–260 (2006).

376. Wang, J., Wolf, R. M., Caldwell, J. W., Kollman, P. A. & Case, D. A. Development and Testing of a General Amber Force Field. *J. Comput. Chem.* **56531**, 1157–1174 (2004).

377. Fox, T. & Kollman, P. A. Application of the RESP methodology in the parametrization of organic solvents. *J. Phys. Chem. B* **102**, 8070–8079 (1998).

378. Frisch, M. J. *et al.* Gaussian 09 Revision A.1. *Gaussian Inc. Wallingford CT* (2009).

379. Berendsen, H. J. C., Postma, J. P. M., Van Gunsteren, W. F., Dinola, A. & Haak, J. R. Molecular dynamics with coupling to an external bath. *J. Chem. Phys.* **81**, 3684–3690 (1984).

380. Andersen, H. C. Rattle: A 'velocity' version of the shake algorithm for molecular dynamics calculations. *J. Comput. Phys.* **52**, 24–34 (1983).

381. Trott, O. & Olson, A. J. AutoDock Vina: improving the speed and accuracy of docking with a new scoring function, efficient optimization, and multithreading. *J. Comput. Chem.* **31**, 455–461 (2010).

382. Dolinsky, T. J., Nielsen, J. E., McCammon, J. A. & Baker, N. A. PDB2PQR: An automated pipeline for the setup of Poisson-Boltzmann electrostatics calculations. *Nucleic Acids Res.* **32**, 665–667 (2004).

383. Jo, S., Kim, T., Iyer, V. G. & Im, W. CHARMM-GUI: a web-based graphical user interface for CHARMM. *J. Comput. Chem.* **29**, 1859–1865 (2008).

384. Wu, E. L. *et al.* CHARMM-GUI membrane builder toward realistic biological membrane simulations. *J. Comput. Chem.* **35**, 1997–2004 (2014).

385. Lee, J. *et al.* CHARMM-GUI supports the Amber force fields. *J. Chem. Phys.* **153**, (2020).

386. Okochi, M. *et al.* γ-Secretase Modulators and Presenilin 1 Mutants Act Differently on Presenilin/γ-Secretase Function to Cleave Aβ42 and Aβ43. *Cell Rep.* **3**, 42–51 (2013).

387. Wallace, A. C., Laskowski, R. A. & Thornton, J. M. LIGPLOT: a program to generate schematic diagrams of protein-ligand interactions The LIGPLOT program automatically generates schematic 2-D representations of protein-ligand complexes from standard Protein Data Bank file input. *Protein Eng.* **8**, 127–134 (1995).

388. Schmidtke, P., Le Guilloux, V., Maupetit, J. & Tufféry, P. fpocket: Online tools for protein ensemble pocket detection and tracking. *Nucleic Acids Res.* **38**, 582–589 (2010).

389. Le Guilloux, V., Schmidtke, P. & Tuffery, P. Fpocket: An open source platform for ligand pocket detection. *BMC Bioinformatics* **10**, 1–11 (2009).

390. Bai, X. C., Rajendra, E., Yang, G., Shi, Y. & Scheres, S. H. Sampling the conformational space of the catalytic subunit of human gamma-secretase. *Elife* **4**, e11182 (2015).

391. Uemura, K. *et al.* Allosteric modulation of PS1/γ-secretase conformation correlates with amyloid β42/40 ratio. *PLoS One* **4**, (2009).

392. Zoltowska, K. M., Maesako, M. & Berezovska, O. Interrelationship between changes in the amyloid β 42/40 ratio and presenilin 1 conformation. *Mol. Med.* **22**, 329–337 (2016).

393. Hawkes, N. Pfizer abandons research into Alzheimer's and Parkinson's diseases. *BMJ* **360**, k122 (2018).

394. De Strooper, B. & Chávez Gutiérrez, L. Learning by Failing: Ideas and Concepts to Tackle γ-Secretases in Alzheimer's Disease and Beyond. *Annu. Rev. Pharmacol. Toxicol.* **55**, 419–437 (2014).

395. Cheng, Y. Single-particle cryo-EM-How did it get here and where will it go. *Science (80-.).* **361**, 876–880 (2018).

396. Baker, R. P. & Urban, S. Architectural and thermodynamic principles underlying intramembrane protease function. *Nat. Chem. Biol.* **8**, 759–768 (2012).

397. Murayama, O. *et al.* Enhancement of amyloid β 42 secretion by 28 different presenilin 1 mutations of familial Alzheimer's disease. *Neurosci. Lett.* **265**, 61–

63 (1999).

398. Kim, J. *et al.* Aβ40 Inhibits Amyloid Deposition In Vivo. *J. Neurosci.* **27**, 627–633 (2007).

399. Moore, B. D. *et al.* Short Aβ peptides attenuate Aβ42 toxicity in vivo. *J. Exp. Med.* **215**, 283–301 (2018).

400. Kuperstein, I. *et al.* Neurotoxicity of Alzheimer's disease Aβ peptides is induced by small changes in the Aβ42 to Aβ40 ratio. *EMBO J.* **29**, 3408–3420 (2010).

401. Wardell, M. R., Brennan, S. O., Janus, E. D., Fraser, R. & Carrell, R. W. Apolipoprotein E2-Christchurch (136 Arg----Ser). New variant of human apolipoprotein E in a patient with type III hyperlipoproteinemia. *J. Clin. Invest.* **80**, 483–490 (1987).

402. Kosik, K. S. *et al.* Homozygosity of the autosomal dominant alzheimer disease presenilin 1 E280A mutation. *Neurology* **84**, 206–208 (2014).

403. Oakley, D. H. *et al.* The Alzheimer Disease-Causing Presenilin-1 L435F Mutation Causes Increased Production of Soluble Aβ43 Species in Patient-Derived iPSC-Neurons, Closely Mimicking Matched Patient Brain Tissue. *J. Neuropathol. Exp. Neurol.* **79**, 592–604 (2020).

404. Miosge, L. A. *et al.* Comparison of predicted and actual consequences of missense mutations. *Proc. Natl. Acad. Sci. U. S. A.* **112**, E5189–E5198 (2015).

405. Pimenova, A. A. & Goate, A. M. Novel presenilin 1 and 2 double knock-out cell line for in vitro validation of PSEN1 and PSEN2 mutations. *Neurobiol. Dis.* **138**, 104785 (2020).

406. Walsh, D. M. & Selkoe, D. J. Aβ oligomers - A decade of discovery. *J. Neurochem.* **101**, 1172–1184 (2007).

407. Schöll, M. *et al.* Low PiB PET retention in presence of pathologic CSF biomarkers in Arctic APP mutation carriers. *Neurology* **79**, 229–236 (2012).

408. Hubbs, J. L. *et al.* Optimization of a natural product-based class of gamma-secretase modulators. *J. Med. Chem.* **55**, 9270–9282 (2012).

409. Loureiro, R. M. *et al.* Efficacy of SPI-1865, a novel gamma-secretase modulator, in multiple rodent models. *Alzheimer's Res. Ther.* **5**, 19 (2013).

410. Jung, J. I. *et al.* Cholestenoic acid, an endogenous cholesterol metabolite, is a potent γ-secretase modulator. *Mol. Neurodegener.* **10**, 1–15 (2015).

411. Beel, A. J. *et al.* Nonspecificity of binding of γ-secretase modulators to the amyloid precursor protein. *Biochemistry* **48**, 11837–11839 (2009).

412. Kao, Y., Ho, P., Tu, Y., Jou, I. & Tsai, K. Lipids and Alzheimer ' s Disease. *Int. J. Mol. Sci.* **21**, 1505–1541 (2020).

413. Osenkowski, P., Ye, W., Wang, R., Wolfe, M. S. & Selkoe, D. J. Direct and potent regulation of γ-secretase by its lipid microenvironment. *J. Biol. Chem.*

283, 22529–22540 (2008).

414. Holmes, O., Paturi, S., Ye, W., Wolfe, M. S. & Selkoe, D. J. Effects of membrane lipids on the activity and processivity of purified γ-secretase. *Biochemistry* **51**, 3565–3575 (2012).

415. Winkler, E. *et al.* Generation of Alzheimer disease-associated amyloid β 42/43 peptide by γ-secretase can be inhibited directly by modulation of membrane thickness. *J. Biol. Chem.* **287**, 21326–21334 (2012).

416. Ayciriex, S. *et al.* The lipidome associated with the γ-secretase complex is required for its integrity and activity. *Biochem. J.* **473**, 321–334 (2016).

417. Hata, S. *et al.* Alternative processing of γ-secretase substrates in common forms of mild cognitive impairment and alzheimer's disease: Evidence for γ-secretase dysfunction. *Ann. Neurol.* **69**, 1026–1031 (2011).

418. Hata, S. *et al.* Multiple γ -secretase product peptides are coordinately increased in concentration in the cerebrospinal fluid of a subpopulation of sporadic Alzheimer ' s disease subjects. *Mol. Neurodegener.* **7**, 1–12 (2012).

419. Kakuda, N. *et al.* Altered γ-secretase activity in mild cognitive impairment and Alzheimer's disease. *EMBO Mol. Med.* **4**, 344–352 (2012).

420. Mattsson, N. *et al.* Increased amyloidogenic APP processing in APOE ε4-negative individuals with cerebral β-amyloidosis. *Nat. Commun.* **7**, 1–7 (2016).

421. Mawuenyega, K. G. *et al.* Decreased clearance of CNS β-amyloid in Alzheimer's disease. *Science (80-.).* **330**, 1774 (2010).

9 Acknowledgements, Personal Contribution and Conflict of Interest statements

9.1 Scientific acknowledgements

Petit et al, EMBO J, 2019; Extracellular interface between APP and Nicastrin regulates Aβ length and response to γ-secretase modulators.

We thank Janssen Pharmaceutica for anti-Aβ monoclonal antibodies and GSMs. We are grateful to Maria Szaruga for their critical reading of the manuscript and thank Michel Vande Kerckhove for helpful discussions. This work was funded by the Stichting Alzheimer Onderzoek (SAO; S16013) and the KU Leuven Methusalem grant (METH/14/07). D.P. is supported by a PhD fellowship from the FWO (SB/1S23819N). N.S.R. is supported by a University of London Chadburn Lectureship in Medicine.

Petit et al, in preparation, 2020; Aβ profiles generated by Alzheimer's disease-causing PSEN1 variants determine pathogenicity and linearly correlate with disease onset.

We thank Janssen Pharmaceutica for providing the Aβ antibodies for ELISA, Marck Mercken and Katarzyna Zoltowska for critical revision of the manuscript and Michel Vande Kerckhove for helpful discussions. This work was funded by the Stichting Alzheimer Onderzoek (SAO; S16013) and the KU Leuven Methusalem grant (METH/14/07). D.P. is supported by a PhD fellowship from the FWO (SB/1S23819N). N.S.R. is supported by a University of London Chadburn Academic Clinical Lectureship in Medicine. A.O'C is supported by an Alzheimer's Society Clinical Training Fellowship (AS-CTF-18-001) and the Rosetrees Trust charity. N.C.F. acknowledges support from Alzheimer's Research UK, the UK Dementia Research Institute and the NIHR UCLH Biomedical Research Centre.

Petit et al, unpublished, 2020; Characterization of the binding pocket and mode of interaction of γ-secretase stabilizers.

This work was funded by the Stichting Alzheimer Onderzoek (SAO; S16013) and the KU Leuven Methusalem grant (METH/14/07). D.P. and M.K. are supported by a PhD fellowship from the FWO ((SB/1S23819N) for D.P. and (SB/1S47020N) for

M.K.). We thank Katarzyna Marta Zoltowska for critical evaluation of the results and her assistance with the writing of the manuscript.

9.2 Personal contributions

Petit et al, EMBO J, 2019; Extracellular interface between APP and Nicastrin regulates Aβ length and response to γ-secretase modulators.

In this study, I was responsible for: I) the generation of all tested stable MEF cell lines and validating proper GSEC reconstitution in the different lines by means of SDS/PAGE Western blotting. II) Cell-based activity assays with APP_{C99} (wild type or mutant) on the generated cell lines with concomitant Aβ quantifications via MSD ELISA. III) Cross-linking experiments on MEF cell-derived samples. Moreover, I performed all related data analysis, participated in the interpretation of the results and assisted in the writing of the manuscript. Sam Lismont cloned the pSG5 APP_{C99}-3xFLAG WT vector and assisted in some experiments. Manuel Hitzenberger conducted all modelling and molecular dynamics simulations studies and the associated data analysis.

Petit et al, in preparation, 2020; Aβ profiles generated by Alzheimer's disease-causing PSEN1 variants determine pathogenicity and linearly correlate with disease onset.

In this study, I was responsible for: I) the generation and validation of all tested stable MEF cell lines except the MEF hPSEN1 T291P line which was generated by Maria Szaruga. II) Cell-based activity assays with APP_{C99} on the generated cell lines with concomitant Aβ quantifications via (MSD) ELISA. Moreover, I performed all data analysis, participated in the interpretation of the results and wrote the manuscript together with my supervisor (Prof. Chávez-Gutiérrez)

Petit et al, unpublished, 2020; Characterization of the binding pocket and mode of interaction of γ-secretase stabilizers.

In this study, I was responsible for all experiments presented in the study, except for the theoretical studies involving *in silico* docking experiments and additional MD simulations (which were performed and analysed by Manuel Hitzenberger). Sam

Lismont assisted during the GSM II/III dose-response experiments with selected mutant MEF cell lines, while Matthias Koch assisted with the Inh X dose-response experiments. Moreover, I performed all data analysis, participated in the interpretation of the results and wrote the chapter draft together with my supervisor and with the assistance of Katarzyna Marta Zoltowska.

9.3 Conflict of interest

Petit et al, EMBO J, 2019; Extracellular interface between APP and Nicastrin regulates Aβ length and response to γ-secretase modulators.

D.P., M.H., S.L., K.M.Z., N.S.R, M.Z., and L.C.G. declare no competing interests. M.M. and F.B. are employees of Janssen Pharmaceutica.

Petit et al, in preparation, 2020; Aβ profiles generated by Alzheimer's disease-causing PSEN1 variants determine pathogenicity and linearly correlate with disease onset.

D.P., N.S.R., A.O'C., M.S., R.V., and L.C.G. declare no competing interests. N.C.F reports consultancy for Roche, Biogen and Ionis, and serving on a Data Safety Monitoring Board for Biogen.

Petit et al, unpublished, 2020; Characterization of the binding pocket and mode of interaction of γ-secretase stabilizers.

D.P., M.H., M.K., S.L., K.M.Z., M.Z., and L.C.G. declare no competing interests. M.M. and F.B. are employees of Janssen Pharmaceutica.

10 Curriculum Vitae

Dieter Petit

Date and place of birth: 09/05/1992, Wilrijk (Belgium)
Current address: Winksele, Belgium
E-mail: dieter.petit@kuleuven.vib.be, phone (work): +32 16 37 43 88

EDUCATION

09/2015 – 12/2020 expected PhD student, Laboratory of proteolytic mechanisms mediating neurodegeneration, KU Leuven/VIB Center for Brain and Disease Research, Belgium, **Project: 'Mechanistic insights into the foundations of Alzheimer's disease pathogenesis and its value for therapeutic development'**, Promotor: Prof. Lucía Chávez-Gutiérrez

09/2013 - 06/2015 University of Antwerp, **Master of Science** in Biochemistry and Biotechnology: Molecular and Cellular Gene biotechnology, Grade: Magna cum laude

09/2010 - 06/2013 University of Antwerp, **Bachelor of Science** in Biochemistry and Biotechnology, Grade: Magna cum laude

PUBLICATIONS

05/2019 – Petit, Dieter, et al. "Extracellular interface between APP and Nicastrin regulates Aβ length and response to γ-secretase modulators." The EMBO journal (2019): e101494.

PERSONAL AWARDS

Travel award to attend the 11th General Meeting of the International Proteolysis Society (IPS) "Interfaces in Proteolysis" 29 Sep - 4 Oct 2019, Czech Republic Mariánské Lázně (Awarded September 2019)

Bursary award to attend the Molecular Neurodegeneration course (UK, 2019) (Awarded November 2018)

Holder of an SB PhD fellowship of the FWO (Fonds Wetenschappelijk Onderzoek), Flanders, Belgium
(Awarded December 2016, Extended in July 2018)

Price of the faculty "Pharmaceutical, Biomedical and Veterinary Sciences" for the "Bachelor Biochemistry and Biotechnology who distinguished himself the most during his bachelor education" (Awarded September 2013)

CONFERENCES

09-10/2019 – 11th General Meeting of the International Proteolysis Society (IPS) "Interfaces in Proteolysis", Mariánské Lázně (Czech Republic)

- ***Poster presentation:*** "Aβ profiles inform on pathogenicity and predict the ages of symptom onset of novel pathogenic *PSEN1* variants"

01/2019 – **Molecular Neurodegeneration course**, Wellcome Genome Campus, Hinxton, Cambridge, (United Kingdom)

- ***Poster presentation:*** "Nicastrin – APP interaction modulates the length of Aβ peptides by regulating the stability of γ-secretase – substrate interactions"

09/2018 – **Meeting of the GBM Study Group "Molecular Neurobiology": Dynamics of the Nervous System in Health and Disease**, Marburg (Germany)

- ***Oral presentation and Poster:*** "An emerging role for the Nicastrin (NCT) ectodomain in the modulation of γ-secretase processivity through direct interaction with the APP substrate"

09/2018 – **EMBO at Basel life: Molecules in biology and medicine**, Basel (Switzerland)

09/2017 – **VIBes in Biosciences PhD Symposium,** Gent (Belgium)

09/2016 – **The Brain Mosaic: Cellular heterogeneity in the CNS**, Leuven (Belgium)

PRESENTATIONS AT INTERNAL EVENTS (VIB/KU LEUVEN)

05/2019 – VIB Center for Brain and Disease (CBD) Science day, Thor Central (Genk, Belgium)

- ***Poster presentation:*** "Extracellular interface between APP and Nicastrin regulates Aβ length and response to γ-secretase modulators"

03/2019 – Internal VIB (public) seminar, ON4 building Gasthuisberg (Leuven, Belgium)

- ***Oral presentation:*** "Extracellular interface between APP and Nicastrin regulates Aβ length and response to γ-secretase modulators"

10/2018 – 7th VIB CBD-NERF PhD week, ON4 building Gasthuisberg (Leuven, Belgium)

- ***Poster presentation:*** "An emerging role for the NCT ectodomain in the modulation of Aβ length through direct interaction with APP"

05/2018 – VIB Center for Brain and Disease (CBD) Science day, Lamot Conference Center (Mechelen, Belgium)

- ***Poster presentation:*** "An emerging role for the NCT ectodomain in the modulation of γ-secretase processivity through direct interaction with the APP substrate"

10/2017 – 6th VIB CBD-NERF PhD week, ON4 building Gasthuisberg and IMEC tower (Leuven, Belgium)

- ***Poster presentation:*** " γ-secretase conformational flexibility: functional relevance for the NCT-PSEN1-PEN-2 interface"

01/2017 – VIB Center for Brain and Disease (CBD) department day, De Ark, (Antwerpen, Belgium)

- ***Poster presentation:*** "Investigating the structural determinants and the mechanisms of γ-secretase (dys)function"

09/2016 – 5th VIB CBD-NERF PhD week, ON4 building Gasthuisberg and IMEC tower (Leuven, Belgium)

- ***Poster presentation:*** "Probing γ-secretase (GS) conformational flexibility and its relevance in Alzheimer's disease (AD)"

LICENCES

Federation of European Laboratory Animal Science Associations (FELASA) Category C 'Animal Experiment Leader (Feb 2015)

EXPERIENCE

01/2015 – 05/2015 **Masterthesis**, VIB Department of Molecular Genetics, Antwerp
Promotor: Prof. Dr. Marc Cruts, Subject: Investigating possible genetic modifiers for onset age in FTLD patients caused by a mutation in the granulin gene.

11/2014 - 12/2014 **Internship**, MULTIPLICOM NV, NIEL
Promotor: Prof. Dr. Jurgen Del-Favero, Supervisor: Dr. Hans Wils, Internship as part of the master program at the University of Antwerp, Subject: Stability testing for two different MASTR™ assays

03/2014 - 04/2014 **Bachelor Thesis**, VIB Department of Molecular Genetics, Antwerp
Promotor: Prof. Dr. Vincent Timmerman, Subject: Research on the expression of specific NOD-like receptors in peripheral nerves because of acute damage to the nerve